Multimodality Imaging

in colorectal cancer

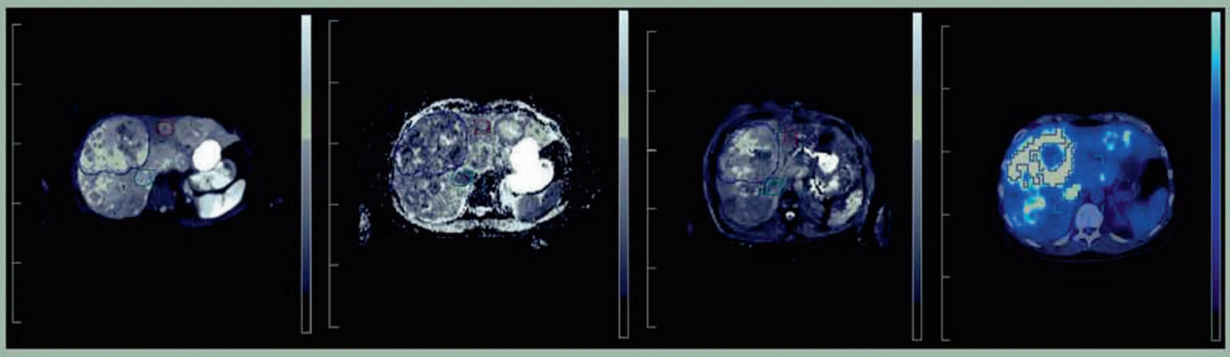

Linda Heijmen

Multimodality Imaging in Colorectal Cancer

Linda Heijmen

The research described in this thesis was performed at the department of Medical Oncology and the department Radiology and Nuclear Medicine of the Radboud University Medical Center and was supported by a grant of the Dutch Cancer Society (Grant number KUN 2008-4098).

Printing of this thesis was financially supported by the Radboud University Nijmegen.

ISBN: 978-94-6108-826-0

Multimodality Imaging in Colorectal Cancer

Proefschrift

ter verkrijging van de graad van doctor
aan de Radboud Universiteit Nijmegen
op gezag van de rector magnificus prof. dr. Th.L.M. Engelen,
volgens besluit van het college van decanen
in het openbaar te verdedigen op maandag 1 december 2014
om 14.30 uur precies

door

Linda Heijmen

geboren op 11 april 1985
te Zevenaar

Promotoren

Prof. dr. C.J.A. Punt (UvA)
Prof. dr. A. Heerschap

Copromotoren

Prof. dr. H.W.M. van Laarhoven (UvA)
Prof. dr. L.F. de Geus- Oei (UT)

Manuscriptcommissie

Prof. dr. J.H.A.M. Kaanders (voorzitter)
Prof. dr. I.D. Nagtegaal
Prof. dr. O.S. Hoekstra (VUmc)

Table of contents

1

General introduction and outline of the thesis

Rationale

Colorectal cancer is the third most common malignancy in the Netherlands and the second most common cause of cancer related death. Almost half of the patients with colorectal cancer will eventually present with metastatic disease, primarily in the liver [1]. Patient with oligometastatic disease are treated with resection and chance of cure. However, the majority of patients rely on palliative systemic therapy for treatment [2].
The outcome of palliative systemic therapy has improved in recent years by the addition of targeted agents to cytotoxic treatment regimens. Bevacizumab, which targets the vascular endothelial growth factor (VEGF) and thereby inhibits formation of new vessels, has been added to first line therapy. The addition of anti-VEGF and anti-EGFR antibodies to standard chemotherapy regimen has resulted in a significant benefit in progression free survival and sometimes overall survival [3].
However, despite the improved treatment a substantial percentage of patients (5.4%- 14.4%) has no disease stabilization after start of chemotherapy [4, 5]. Unnecessary toxicity could be prevented and costs reduced when response to treatment could be predicted prior to start of treatment or at earlier time points than with conventional treatment monitoring.

Currently, oncologists mainly rely on measurement of tumor size to monitor disease progression and treatment effects. However, recent progress in imaging techniques provides the opportunity to examine additional tumor properties, such as vascular supply of the tumor, hypoxia, glucose metabolism and cell density. These techniques are also referred to as functional and molecular imaging techniques for they visualize and measure functional or molecular properties and characteristics rather than anatomy [6].
Targeted therapies often have a more direct effect on these tumor properties than on tumor size [7]. Especially targeted therapies may have cytostatic effects or lead to cavitation rather than a reduction in tumor size. Tumor size may not be an optimal way to evaluate effectiveness of targeted therapies, including bevacizumab. Furthermore, continuation of bevacizumab after tumor progression to first line prolongs survival in patients and thus, still exhibits efficacy. Thus, targeted treatment may affect tumor physiology and biology before volumetric changes are evident or even without volumetric changes occur. Therefore, functional and molecular imaging techniques have the potential to monitor response to therapy more accurately and at earlier time points than conventional imaging techniques [8]. However, since changes in functional and molecular imaging parameters early after start of treatment might be subtle, it is important to determine which changes could be confidently detected in an individual patient. To validate the functional and molecular imaging techniques the repeatability of its parameters have to be assessed. The repeatability of a technique defines which differences can be due to normal variation and which changes can

be confidently attributed to real biological changes in the tumor. If changes within a tumor are greater than can be attributed to normal variation, it can be assumed that this is due to treatment effect.
Additionally, functional and molecular imaging techniques may reveal tumor properties that are prerequisites for a response to treatment. Factors that may determine treatment response are: delivery of the drugs via the vascular system of the tumor, cellular uptake, retention and metabolism, and intrinsic sensitivity of the tumor to the anticancer agent. Assessment of these tumor properties using functional and molecular imaging, therefore may predict treatment response.

In this thesis, the validation of functional and molecular imaging techniques to measure tumor properties of colorectal liver metastases is assessed. Early response monitoring and response prediction using functional and molecular imaging is evaluated in patients with advanced stage colorectal cancer starting first line systemic treatment. Furthermore, the effect of bevacizumab on functional and molecular imaging parameters in an animal colorectal cancer model is studied.

Functional and molecular imaging techniques

A wide variety of functional and molecular imaging techniques is available. The imaging techniques in this thesis have been selected for their potential for response monitoring and the experiences with the techniques within our center. All functional and molecular imaging techniques described in this thesis and the biological properties they assess are described below.

Diffusion weighted imaging (DWI) is an MR technique sensitive to random water movement. From diffusion weighted images apparent diffusion coefficients (ADC), values for the magnitude of the diffusion of water molecules, can be calculated. An example of an ADC map showing a colorectal liver metastasis is shown in figure 1.
The water movement is inhibited by cell structures, like membranes. Therefore, the ADC value is inversely correlated to cell density [9]. Low ADC values are often associated with malignant tissue, and within malignant lesions are associated with poorer differentiation grade [10-13]. High ADC values are also indicative of necrosis [14, 15] and could therefore also indicate hypoxic, therapy resistant areas, which are most times in close proximity of necrotic areas. The ADC value could be predictive of response, by assessment of these tumor characteristics. When treatment reduces cell density by cytotoxic and cytostatic effects, the ADC value should rise. Consequently, ADC values may also be effective for (early) response monitoring.

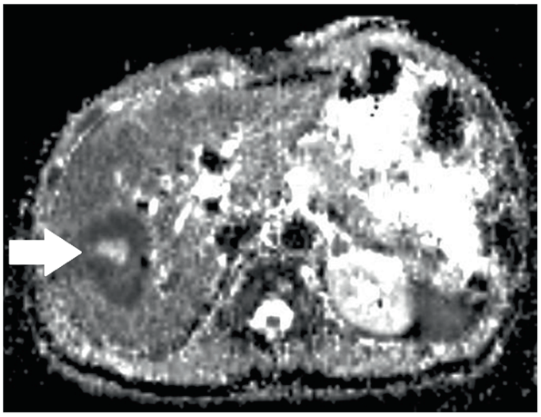

Figure 1. *ADC map calculated from diffusion weighted images showing a tumor (arrow) with cell dense tissue in the dark rim and central necrosis (white centre).*

Tumor vascularity can be assessed by dynamic contrast enhanced magnetic resonance imaging (DCE-MRI). It requires repetitive in vivo imaging following the intravenous injection of a contrast agent. Several studies showed that microcirculation as assessed with DCE-MRI might predict outcome. High vascular permeability seems to favor a favorable treatment outcome [16-18]. Bevacizumab, the targeted agent against VEGF, influences the vasculature and bevacizumab effectiveness might be monitored using DCE-MRI [19]. Besides monitoring the effects of antiangiogenic or antivascular drugs, previous studies suggest that conventional cytotoxic agents may also have an effect on tumor vascularity and DCE-MRI parameters [14, 20, 21].

T2* MRI can also be used to assess vascular properties, however, without the requirement for the administration of contrast agents. T2* MR contrast arises from local inhomogeneities of the magnetic field mainly due to the tissue level of blood deoxyhemoglobin [22]. Therefore, T2* measurements are dependent on hypoxia, blood flow, and blood volume [23] and may be sensitive to bevacizumab-induced changes in tumor vasculature. An example of a T2* map showing a liver metastasis is given in figure 2.

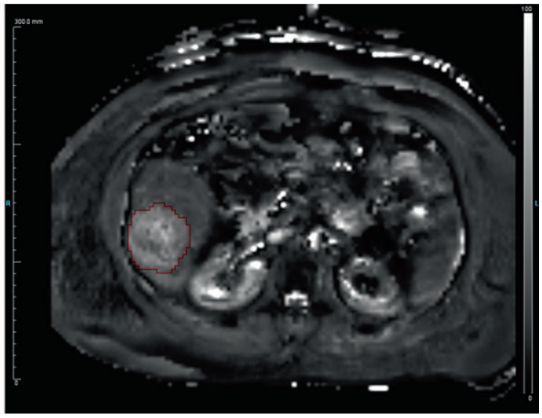

Figure 2. *T2* map showing the delineated colorectal liver metastasis in red.*

Fluorine-18-Fluorodeoxyglucose positron emission tomography (FDG-PET) is sensitive to determine glucose uptake in tissues. FDG is a glucose analogue which accumulates via glucose transporters in cells requiring glucose. In the cell, phosphorylation of FDG to FDG-6-phosphate results in intracellular trapping as the metabolite cannot be metabolized any further [24]. In this way cells with a high glucose metabolism can be detected. An FDG-PET/CT of a colorectal liver metastasis with central necrosis is shown in figure 3.

Most tumors mainly depend on anaerobic glycolysis for their energy supply. Anaerobic glycolysis is an unproductive process yielding only 2 molecules of ATP per glucose molecule, while subsequent oxidative phosphorylation can deliver 36 ATP. Tumors may have a high glycolytic rate even when oxygen is abundant, the so-called Warburg effect [25].

Tumor FDG uptake can change due to treatment effects. FDG-PET in colorectal cancer is suggested to be a sensitive technique for response monitoring. In a systematic review, four out of five studies in advanced colorectal cancer showed changes in standardized uptake values (SUV) of FDG PET 72 hours to 2 months after start of systemic treatment [26]. FDG-PET also seems sensitive to therapies with a predominantly cytostatic effect [24]. With the increasing number of available effective targeted therapies and their cytostatic effects, FDG-PET may be a an important technique for monitoring the response to therapy.

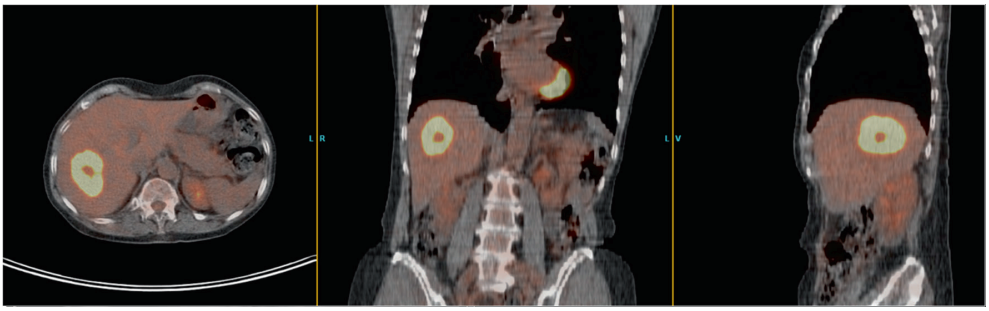

Figure 3. *FDG PET with low dose CT showing a high FDG uptake in the solitary liver metastases, with central necrosis.*

When the uptake of FDG is monitored over time, so called dynamic FDG-PET, the vascular supply of FDG can be followed. Furthermore since the FDG concentration in the blood pool can be monitored, correction for competitive uptake, for example uptake in the muscles or other tumor sites, is possible. Since dynamic FDG starts when FDG is injected there is no variation in the injection-scan interval. For these reasons dynamic FDG-PET may be better reproducible compared to conventional static FDG PET technique, while maintaining sensitivity for metabolic changes.

In addition to the semi-quantitative parameters (SUV) of static PET, quantitative parameters can be calculated. These quantitative parameters include the metabolic rate of glucose (in $nmol \cdot mL^{-1} \cdot min^{-1}$), transport constant k1 that describes the delivery and extraction of the tracer into the tissue pool, k2 that describes the rate of the transport of FDG back from tissue to plasma, and k3 that describes the rate for the phosphorylation of FDG in the tissue [27]. Pretreatment metabolic rate and change in metabolic rate after 3 cycles of chemotherapy was predictive of survival in patients with colorectal cancer metastases [28].

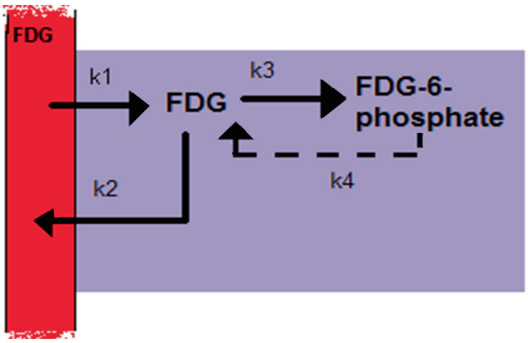

Figure 4. *A two compartment model showing the rate constant k1 describing the uptake of FDG in the cells (purple) from the plasma (red), k2 describes the transfer rate of FDG back into the plasma, k3 describes the phosphorylation rate of FDG to PDG-6-phosphate by hexokinase, k4 describes the dephosphorylation rate.*

Outline of the thesis

This thesis investigates the potential of the abovementioned functional and molecular imaging techniques to predict response to treatment in metastatic colorectal cancer.
In **chapter 2** the use of diffusion weighted imaging for tumor response prediction is discussed more extensively. An overview of the current results of diffusion weighted imaging of cancer in literature is presented.
Chapter 3, 4, 5, 6 and 7 describe the validation studies of the above described functional and molecular imaging techniques. Repeatability and correlations with histopathology of DWI and T2* are described in **chapter 3 and 4**.
Chapter 5 describes the repeatability of static FDG-PET in colorectal liver metastases and correlates the results to histopathology. Since several parameters, such as the interval between injection and scanning and vascular supply of the tracer, might negatively influence repeatability of static FDG PET, the repeatability of dynamic FDG may be better, while maintaining sensitive to tumor metabolism. Therefore also the repeatability of dynamic FDG-PET is determined and described in **chapter 6**.

Chapter 7 and 8 describe the potential of various imaging techniques to measure the effect of the anti-angiogenic agent bevacizumab. In the first study, the effect of bevacizumab monotherapy is measured with functional and molecular imaging and correlated with histopathology results. In the second study, the effect of bevacizumab after disease progression on combined chemotherapy and bevacizumab is assessed.
In **chapter 9** the potential of FDG-PET, DWI and T2* for early response prediction, was assessed. Patients with colorectal liver metastases starting first line palliative systemic therapy (including bevacizumab) underwent PET and MRI before and one week after start of treatment. Therapy induced parameter changes were correlated to response and final outcome.

Reference List

[1] IKNL. http://cijfersoverkanker.nl/.

[2] Manfredi S, Lepage C, Hatem C, Coatmeur O, Faivre J, Bouvier AM. Epidemiology and management of liver metastases from colorectal cancer. AnnSurg. 2006;244:254-9.

[3] Tol J, Punt CJ. Monoclonal antibodies in the treatment of metastatic colorectal cancer: a review. Clinical therapeutics. 2010;32:437-53.

[4] Tol J, Koopman M, Cats A, Rodenburg CJ, Creemers GJ, Schrama JG, et al. Chemotherapy, bevacizumab, and cetuximab in metastatic colorectal cancer. N Engl J Med. 2009;360:563-72.

[5] Sobrero A, Ackland S, Clarke S, Perez-Carrion R, Chiara S, Gapski J, et al. Phase IV study of bevacizumab in combination with infusional fluorouracil, leucovorin and irinotecan (FOLFIRI) in first-line metastatic colorectal cancer. Oncology. 2009;77:113-9.

[6] Marcus CD, Ladam-Marcus V, Cucu C, Bouche O, Lucas L, Hoeffel C. Imaging techniques to evaluate the response to treatment in oncology: current standards and perspectives. Crit Rev Oncol Hematol. 2009;72:217-38.

[7] Tunariu N, Kaye SB, Desouza NM. Functional imaging: what evidence is there for its utility in clinical trials of targeted therapies? Br J Cancer. 2012;106:619-28.

[8] Desar IM, van Herpen CM, van Laarhoven HW, Barentsz JO, Oyen WJ, van der Graaf WT. Beyond RECIST: molecular and functional imaging techniques for evaluation of response to targeted therapy. Cancer treatment reviews. 2009;35:309-21.

[9] Koh DM, Collins DJ. Diffusion-weighted MRI in the body: applications and challenges in oncology. AJR Am J Roentgenol. 2007;188:1622-35.

[10] Nakajo M, Kajiya Y, Tani A, Yoneda S, Shirahama H, Higashi M, et al. (1)(8)FDG PET for grading malignancy in thymic epithelial tumors: significant differences in (1)(8)FDG uptake and expression of glucose transporter-1 and hexokinase II between low and high-risk tumors: preliminary study. Eur J Radiol. 2012;81:146-51.

[11] Costantini M, Belli P, Rinaldi P, Bufi E, Giardina G, Franceschini G, et al. Diffusion-weighted imaging in breast cancer: relationship between apparent diffusion coefficient and tumour aggressiveness. Clin Radiol. 2010;65:1005-12.

[12] Hambrock T, Somford DM, Huisman HJ, van Oort IM, Witjes JA, Hulsbergen-van de Kaa CA, et al. Relationship between Apparent Diffusion Coefficients at 3.0-T MR Imaging and Gleason Grade in Peripheral Zone Prostate Cancer. Radiology. 2011.

[13] Takeuchi M, Matsuzaki K, Nishitani H. Diffusion-weighted magnetic resonance imaging of endometrial cancer: differentiation from benign endometrial lesions and preoperative assessment of myometrial invasion. Acta radiologica. 2009;50:947-53.

[14] Uhl M, Saueressig U, van Buiren M, Kontny U, Niemeyer C, Kohler G, et al. Osteosarcoma: preliminary results of in vivo assessment of tumor necrosis after chemotherapy with diffusion- and perfusion-weighted magnetic resonance imaging. Investigative radiology. 2006;41:618-23.

[15] Kamel IR, Bluemke DA, Ramsey D, Abusedera M, Torbenson M, Eng J, et al. Role of diffusion-weighted imaging in estimating tumor necrosis after chemoembolization of hepatocellular carcinoma. AJR Am J Roentgenol. 2003;181:708-10.

[16] Mayr NA, Hawighorst H, Yuh WT, Essig M, Magnotta VA, Knopp MV. MR microcirculation assessment in cervical cancer: correlations with histomorphological tumor markers and clinical outcome. Journal of magnetic resonance imaging: JMRI. 1999;10:267-76.

[17] Devries AF, Griebel J, Kremser C, Judmaier W, Gneiting T, Kreczy A, et al. Tumor microcirculation evaluated by dynamic magnetic resonance imaging predicts therapy outcome for primary rectal carcinoma. Cancer research. 2001;61:2513-6.

[18] George ML, Dzik-Jurasz AS, Padhani AR, Brown G, Tait DM, Eccles SA, et al. Non-invasive methods of assessing angiogenesis and their value in predicting response to treatment in colorectal cancer. The British journal of surgery. 2001;88:1628-36.

[19] Hirashima Y, Yamada Y, Tateishi U, Kato K, Miyake M, Horita Y, et al. Pharmacokinetic parameters from 3-Tesla DCE-MRI as surrogate biomarkers of antitumor effects of bevacizumab plus FOLFIRI in colorectal cancer with liver metastasis. Int J Cancer. 2011.

[20] DeVries AF, Kremser C, Hein PA, Griebel J, Krezcy A, Ofner D, et al. Tumor microcirculation and diffusion predict therapy outcome for primary rectal carcinoma. Int J Radiat Oncol Biol Phys. 2003;56:958-65.

[21] Manton DJ, Chaturvedi A, Hubbard A, Lind MJ, Lowry M, Maraveyas A, et al. Neoadjuvant chemotherapy in breast cancer: early response prediction with quantitative MR imaging and spectroscopy. Br J Cancer. 2006;94:427-35.

[22] Chavhan GB, Babyn PS, Thomas B, Shroff MM, Haacke EM. Principles, techniques, and applications of T2*-based MR imaging and its special applications. Radiographics. 2009;29:1433-49.

[23] Howe FA, Robinson SP, McIntyre DJ, Stubbs M, Griffiths JR. Issues in flow and oxygenation dependent contrast (FLOOD) imaging of tumours. NMR Biomed. 2001;14:497-506.

[24] Contractor KB, Aboagye EO. Monitoring predominantly cytostatic treatment response with 18F-FDG PET. Journal of nuclear medicine: official publication, Society of Nuclear Medicine. 2009;50 Suppl 1:97S-105S.

[25] Warburg O. On the origin of cancer cells. Science. 1956;123:309-14.

[26] de Geus-Oei LF, Vriens D, van Laarhoven HW, Van Der Graaf WT, Oyen WJ. Monitoring and predicting response to therapy with 18F-FDG PET in colorectal cancer: a systematic review. J NuclMed. 2009;50 Suppl 1:43S-54S.

[27] Patlak CS, Blasberg RG, Fenstermacher JD. Graphical evaluation of blood-to-brain transfer constants from multiple-time uptake data. Journal of cerebral blood flow and metabolism: official journal of the International Society of Cerebral Blood Flow and Metabolism. 1983;3:1-7.

[28] Vriens D, van Laarhoven HW, van Asten JJ, Krabbe PF, Visser EP, Heerschap A, et al. Chemotherapy response monitoring of colorectal liver metastases by dynamic Gd-DTPA-enhanced MRI perfusion parameters and 18F-FDG PET metabolic rate. Journal of nuclear medicine: official publication, Society of Nuclear Medicine. 2009;50:1777-84.

2

Tumor response prediction by diffusion weighted MR imaging: ready for clinical use?

Abstract

Background: The efficacy of anticancer therapy is usually evaluated by anatomical imaging. However, this method may be suboptimal for the evaluation of novel treatment modalities, such as targeted therapy. Theoretically, functional assessment of tumor response by diffusion weighted imaging (DWI) is an attractive tool for this purpose and may allow an early prediction of response. The optimal use of this method has still to be determined.

Method: We reviewed the published literature on clinical DWI in the prediction of response to anticancer therapy, especially targeted therapy. Studies investigating the role of DWI in patients with cancer either for response prediction and/ or response monitoring were selected for this analysis.

Results: We identified 24 studies that met our criteria. Most studies showed a significant correlation between (changes in) apparent diffusion coefficient (ADC) values and treatment response. However, in different tumors and studies, both high and low pretreatment ADC were found to be associated with response rate. In the course of treatment, an increase in ADC was associated with response in most cases.

Conclusion: The potential of DWI for (early) response monitoring of anticancer therapies has been demonstrated. However, validation is hampered by the lack of repeatability and standardization. We recommend that these issues should be properly addressed prior to further testing the clinical use of DWI in the assessment of treatments.

Introduction

With the increased use of targeted therapies in patients with advanced cancer, it has become clear that the standard anatomical methods of response evaluation (i.e. assessment of lesion size on CT scans) are of limited value to assess the efficacy of these new treatment modalities. Targeted therapies induce necrosis and cavitation, which means that effective treatment does not necessarily result in a reduction of tumor diameter. This has increased the interest in applications of functional imaging techniques for response prediction, such as dynamic contrast enhanced MRI (DCE-MRI) [1]. DCE-MRI is a non-invasive imaging technique that can be used to measure properties of tissue microvasculature. It is widely explored in research and a favored technique to evaluate tumors with respect to their state of microcirculation [2]. In the last decade, diffusion weighted imaging (DWI), another functional MR imaging modality, has been the subject of research with promising results. Preclinical studies comparing DCE-MRI and DWI suggest that both perform well in early response monitoring after anti-vascular therapy. Both imaging modalities showed changes in their parameters hours to days after treatment [3-6]. In this review, we will focus on clinical studies to assess the potential of DWI for predicting response to cancer therapy and discuss the additional value of DWI compared to functional imaging with DCE-MRI.
As some technical background is indispensable for understanding the study results, we will start with a description of the basic principles of DWI.

1 Diffusion-weighted MR Imaging

Although MR methods for measuring molecular diffusion were already developed in the 1960s [7], only in the last decade has measurement of water diffusion received increased attention in biomedical studies [8-11]. Diffusion results from random thermal motion of molecules, known as Brownian motion. It can be restricted by cell structures, such as cell membranes. Therefore, measurement of water diffusion may reflect cellularity. The diffusion of water at this microscopic level can be quantitatively measured with MRI. In DWI, the rate of water diffusion within tissues is measured by movement probing field gradients, that de- and refocus the signal of the water molecules. The dephasing gradient leads to a phase shift of water proton spins that is compensated by a rephasing gradient if a water molecule remains at the same location. However, if the water molecule has moved to another position between these two gradients, this leads to incomplete re-phasing (figure 1). Therefore, all moving water molecules result in a certain loss of the water signal. The greater the movement of the water molecules, the lower the signal will be, so the magnitude of this loss reflects the mobility of water.

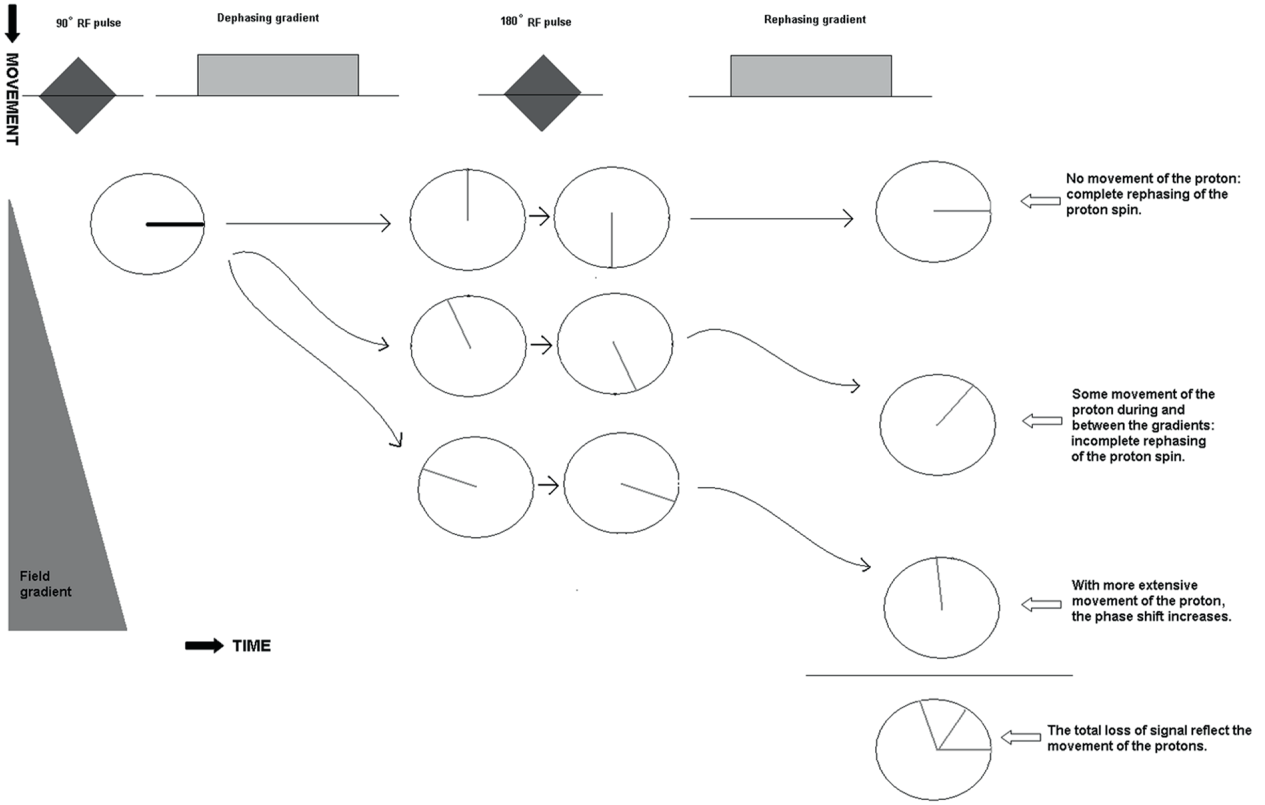

Figure 1. *MR diffusion measurement with a spin echo sequence and two movement probing gradients. Proton spins that are in phase after a 90° radiofrequency pulse, shift in phase due to the dephasing gradient. This degree of the phase shift is dependent of the gradient strength that the protons experience. After an interval and a 180° pulse, a rephasing gradient is given. Protons that have moved during and in the time between the two gradients, do not return to their initial state because they experience a different field (gradient) strength and therefore a different phase shift. The final phase shift is larger if the movement in the direction of the field strength is larger. In total the extend of the signal loss reflects the water movement. The figure does not take chemical shift, dipolar coupling and MR relaxation during the pulses and between pulses into account, but technical aspects of the experiment (not shown in the figure) can diminish and account for those effects.*

By using different gradient durations and amplitudes, combined in *b*-values, the rate of the diffusion of microscopic water within tissues can be measured. The b-value is proportional to the square of the gradient strength (G) and the diffusion time interval (Δ): $b \sim G^2 \cdot \Delta$. A diffusion coefficient is calculated using the equation: $ADC = -b \ln(S_B/S_0)$, in which the signal intensity with a certain b-value (S_B) is divided by the signal intensity when the b-value is zero (S_0) [12]. The calculated diffusion coefficient is called apparent diffusion coefficient (ADC). The word "apparent" is added because other factors than random diffusion may influence the mobility of water. The ADC is an average of the water mobility in all directions (if the experiment takes all 3 spatial axes into account) and is therefore influenced by the presence of structures such as cellular membranes and the extracellular matrix: a relatively high cellularity will give a relatively low ADC value (figure 2 and 3). Obviously, diffusion weighted imaging is also sensitive to other types of motion, such as perfusion, cardiac and respiratory motion. Diffusion weighted images can be evaluated by visual inspection: however, the signal intensity in the image does not only reflect diffusion but also the T2 value of the tissue. This so-called T2 shine-through effect is countered by using an apparent diffusion coefficient map with high *b*-values.

Most early DWI research was performed in the brain, because of little tissue movement, in addition to other advantages such as good magnetic field homogeneity and high signal to noise ratios [8]. Due to stronger cardiac and respiratory motion, DWI of the abdomen and especially of the liver, is much more difficult to perform adequately.

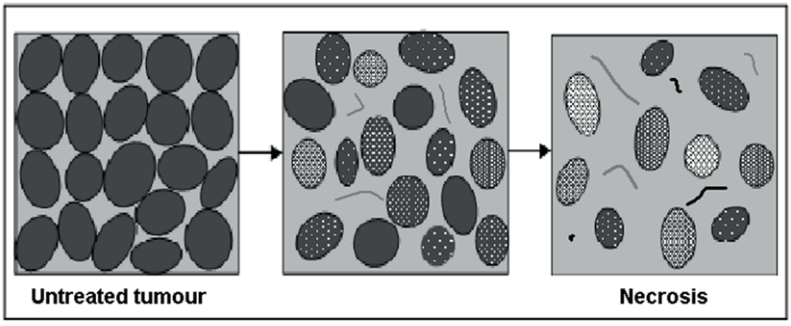

Figure 2. *Schematic view of the decrease in cellularity in an effectively treated tumor. Since in necrotic tissue there are fewer intact cell membranes to restrain the water movement, this results in a higher apparent diffusion coefficient (ADC).*

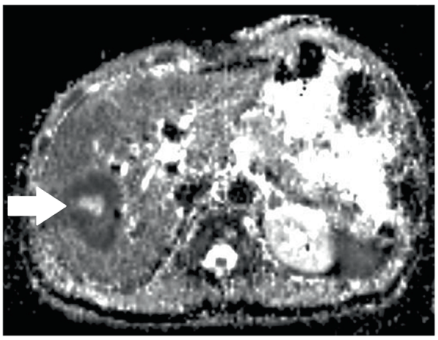

Figure 3. *Example of an diffusion map image of a solitary liver metastasis before treatment. A high ADC value (white) is seen in the centre of the tumor, caused by central necrosis. The active rim, with high cellularity has a low ADC value (dark).*

2 Role of DWI in tissue characterization

In principal, DWI could characterize specific tissue properties, rendering invasive biopsies unnecessary if a highly negative predictive value could be reached.

This could be particularly useful in lesions that are difficult to access and in patients that are at risk for complications of a biopsy procedure. Since ADC-values from DWI measurements reflect cellularity, the mean ADC-value could be a tool to distinguish benign from malignant lesions, and to differentiate between different grades of malignancy, assuming a difference in cellularity.

Several studies have evaluated DWI for this purpose in patients with suspicious breast lesions. Significantly lower mean ADC-values were observed in invasive breast cancer and DCIS compared with benign breast lesions. DWI was able to differentiate with a specificity and sensitivity of over 80 percent. However, in order to reach the necessary high sensitivity, specificity dropped to 55-67%. DWI can reach a high negative predictive value and prevent biopsy in a subpopulation of the women with benign breast lesions [13-16]. Furthermore, lower ADC-values in breast cancer lesions were independently associated with higher histological grade, nodal status and vascular invasion [17;18].

DWI has also shown to discriminate malignant ovarian lesions and endometrial cancer from benign lesions with lower ADC scores. Especially for endometrial lesions, DWI demonstrated promising results with very high sensitivity (96%) and specificity (95%) [19;20]. In addition, in prostate cancer a negative correlation was demonstrated between ADC and Gleason score, with a lower mean ADC for increasing Gleason scores. However, prostate tumors with lower Gleason scores are often not visible with DWI and this technique alone does not appear ready to replace prostate biopsies, but has complementary diagnostic potential [21;22].

Not all studies showed a correlation between histopathology and ADC values. In hepatocellular carcinoma, no significant relationship between ADC and histopathalogic grade was observed. Well, moderately and poorly differentiated tumors had overlapping ADC-values, with a mean of 1.45, 1.46, and 1.36 x 10(-3) mm(2)/s, respectively [23].

DWI may be of specific value to detect tumor necrosis, since necrosis increases ADC-values. This is of clinical importance since necrosis corresponds with therapy effect, especially in osteosarcoma where necrosis-rate corresponds with response and prognosis [24;25]. This concept was confirmed in a small series of 8 osteosarcoma patients. A higher ADC was measured in necrotic compared to viable tissue, assessed by macroscopic evaluation [26]. Similar results were found in 18 patients with osteo- and Ewing sarcoma after chemotherapy and in a small study of 8 patients with hepatocellular carcinoma. The latter study showed a strong correlation between ADC and degree of tumor necrosis ($r=0.95$; $p=<0.05$) after chemoembolization [27;28]. However, in retrospectively reviewed data of 28 patients with brain tumors, no correlation was observed between ADC and cellularity in histological samples (correlation coefficient −0.278; $p=0.54$) [29].

The divergent results in the abovementioned studies suggest that the value of DWI for tissue characterization may depend on tumor type. Furthermore, studies with negative results might be underrepresented, since they are less likely to be published. Also technical issues, such as instrument setting and composing *b*-values, may play a role in the divergent results. Higher *b*-values give a stronger diffusion weighing, and when low *b*-values are used in the ADC calculation, the ADC can be corrupted by perfusion effects. The selection of *b*-values can affect the measured ADC considerably, as shown in studies in breast, cervical and vaginal cancer [30;31]. Furthermore, the interpretation of DWI in biological terms is complex. For instance, (minor) necrosis in the tumor may increase the mean ADC-values of the tumor in such a way that it becomes more difficult to differentiate from benign lesions. The ADC values of tumors may differ dependent on the size of the necrotic lesions [32]. Also, macromolecules may have an effect. In the cavity of brain abscesses, the main biologic parameter causing restriction in ADC was viable cell density, but additionally a negative correlation between extracellular protein concentration and mean restricted ADC-value was observed. This suggests that, like cell structures, macromolecules restrict random water movement [33]. Theoretically, the interpretation of DWI for tissue characterization may be facilitated by histogram analyses. Histogram analyses of the ADC allow for segmentation of tissue [10], and might therefore give more detailed insight into ADC distribution in tumor tissue.

3 Role of DWI in response prediction: pretreatment ADC

Necrotic areas in tumors are often surrounded by hypoxic, but viable cells. This is of clinical importance, since hypoxic tumors are less sensitive to ionizing radiation [34], are more prone to aggressive behaviour and may be less sensitive to cytotoxic agents [35]. Therefore, it may be hypothesized that patients with necrotic areas in their tumors, and thus high pretreatment ADCs, would have a worse treatment outcome. Several studies have indeed shown a relation between pretreatment ADC and treatment outcome (Table 1).

Study	Location of tumor	N	b-values (s/mm²)	Treatment	Correlation ADC and response	Significance
Cui et al, 2008	Colorectal or gastric hepatic metastases	23/ 87 metastases	b-value: 0-800, 1.5T	New chemotherapy schedule	Negative correlation: higher ADC in non-responders group	P=0.003
Koh et al, 2007	Colorectal hepatic metastases	20/48 metastases	b-value: 0-150-500, 1.5T	Neoadjuvant chemotherapy	Negative correlation: high ADC gives less response	$p < 0.002$ for higher mean ADC
Kim et al, 2009	Locally advanced rectal cancer	40	b-value: 0-1000, 1.5T	Neoadjuvant chemo-radiation	Positive correlation: higher ADC in complete responders group	P < 0.0001
DeVries et al, 2003	Rectal cancer	34	b-value: 30,-300,-1100, 1.5T	Neoadjuvant chemo-radiation	No correlation	P=0.825
Nilsen et al, 2010	Locally advanced breast cancer	25	b-value: 100-250-800, 1.5T	Neoadjuvant chemotherapy	No correlation	P=0.816: 4 cycles P=0.620: before surgery
Harry et al, 2008	Advanced cervical cancer	20	b-value: 0-1000, 1.5T	External beam radiotherapy	No correlation	p=0.98~ MR p=0.19~ clinical response
Dzik-Jurasz et al, 2002	Advanced rectal cancer	14	b-value: 0-345, 1.5T	Chemotherapy or Chemo-radiation	Negative correlation: higher ADC gives less response (/size reduction)	P=0.01 for chemotherapy p=0.001 for chemoradiation
Mardor et al, 2004	Brain tumors	12	b-value: 5 en 1000, 0.5T	Fractionated radiation therapy	Negative correlation: A lower ADC was found in the group with the best response.	P<0.02 for ADC P<0.001 for diffusion index

Table 1. *Response prediction with pretreatment ADC.*

Most studies show that the ADC-value prior to treatment is inversely correlated to the response to treatment, supporting the abovementioned theory. Already in 2002, ADC's were measured in 14 patients with clinically advanced rectal cancer before chemotherapy and chemoradiation. A strong negative correlation between mean pretreatment tumor ADC and percentage size change of tumors after chemotherapy and chemoradiation was observed [36]. Three more studies showed a negative relation between ADC-values and treatment

response. One of these studies was performed in 48 colorectal hepatic metastases (in 20 patients) treated with neoadjuvant chemotherapy. Responding lesions, defined by RECIST criteria, had significantly lower pretreatment mean ADC's (1.15 x 10(-3) mm(2)/s) than non-responding lesions (1.91 x 10(-3) mm(2)/s). Linear regression showed a significant relation between percentage reduction and pretreatment mean ADC [37]. Also, it was shown in 23 patients with 87 liver metastases of colorectal and gastric cancer that pretreatment mean ADC was significantly lower in responding compared to non-responding lesions according to RECIST criteria. Weak but significant correlations were observed between final tumor size reduction and mean pretreatment ADC [38]. These results were demonstrated again in 12 patients with brain tumors treated with radiation therapy. A positive correlation was shown for ADC pretreatment and relative change in tumor volume measured by T1 weighted MRI at day 46 [39].

However, not all studies endorse the hypothesis. Studies in rectal, cervical and breast cancer patients, treated with respectively chemoradiation or chemotherapy, did not report any correlation between pretreatment ADC and treatment response [40-42]. Another study presented ADC data of 40 patients with locally advanced rectal cancer and a significantly higher pretreatment ADC was observed in patients who had a complete pathologic response on combined chemoradiotherapy compared to those who had not. However, these ADC-values were measured *after* chemoradiation and therefore could reflect treatment effect [43].

In conclusion, in some studies a significant association between pretreatment ADC's and treatment outcome has been observed. Since the current studies use different protocols with various *b*-values and different calculations for ADC, the ADC values and cut-off values observed in these studies cannot be compared and are impossible to translate to the clinic. Also sensitivity and specificity observed in the studies cannot be translated to a general clinical setting.

4 Role of DWI in response evaluation

Supposing that systemic anti-tumor treatment decreases tumor cellularity, treatment should increase ADC-values. Decreases in tumor cellularity will ultimately lead to reduction in tumor size. This reduction in tumor size can be expected after 2 – 3 cycles of systemic treatment, which usually is between 6 and 12 weeks after start of treatment. This has become the conventional time of response evaluation. First we will discuss the role of ADC measurements at the conventional time of treatment response evaluation. Early response evaluation is discussed in the next section. All response monitoring studies are summarized in table 2.

Time of monitoring	Study	Tumor	N (pat/ lesions)	b-values	Therapy	Correlation ADC and response	P
Before and after treatment	Kim et al., 2010	Locally advanced rectal cancer	76	b-value: 0-600-1000	Neoadjuvant chemo-radiation	***Positive:*** higher ADC in complete responders	<0.0001
Before treatment and early in treatment (3 weeks)	Hamstra et al, 2008	high grade glioma	34 and 60	b-value: 0-1000, 1.5T	Radiotherapy and/ or surgery ± chemo-therapy	***Positive:*** more changes in ADC at functional diffusion map in non progressive tumors	< 0.001
Before and early in treatment (day 4,11 and 39)	Theilmann et al, 2004	Liver metastases of breast cancer	13/ 60	b-value: 0-150-300-450, 1.5T	Start of (a new) chemo-therapy regimen	***Positive:*** a higher increase in ADC in responders	
Before and 1-5 months after therapy	Song et al, 2010	Prostate cancer	49	b-value: 0-1000, 3T	Radiotherapy	***Positive:*** ADC was increased after treatment	0.001
Before and after chemotherapy treatment	Koh et al., 2007	Metastases of colorectal cancer	20/ 48	b-value: 0-150-500, 1.5T	Neoadjuvant chemo-therapy	***Positive:*** after chemotherapy, responding lesions significantly increased in mean ADC-values.	0.025
Before and after treatment (2-4 weeks)	Tomura et al 2006	Brain tumors	39	b-value: 0-1000, 1.5T	Stereotactic irradiation	***Positive:*** ADC rose after treatment. A higher normalized ADC was found in lesions without recurrence.	P< 0.05: after STI .
Before and early in treatment (2-4 weeks)	Vandecaveye et al, 2010	squamous cell carcinoma of the head and neck	30	b-value: 0- 50-100-500- 750-1000 1.5T	Chemo-radiation	***Positive:*** The ΔADC in tumors and metastases, 2 and 4 weeks after treatment was lower in lesions with post-CRT recurrence than in lesions with CR	P<0.001: ΔADC recurrence vs CR P<0.001: ΔADC, locoregional controle
Before and after treatment (after 4 cycles and before surgery)	Nilsen et al, 2010	Locally advanced breast cancer	25	b-value: 100-250-800, 1.5T	Neoadjuvant chemo-therapy	***None***: there was no correlation between individual pretreatment breast tumor ADC and MR response measured after four cycles or prior to surgery	P=0.018: increase ADC
Before and early in treatment (2 weeks)	Harry et al, 2008	Advanced cervical cancer	20	b-value: 0-1000, 1.5T	Chemo-radiation	***Positive:*** ADC values after 2 weeks of therapy showed a significant correlation with eventual MR response and clinical response	P=0.048 ADC at 2 weeks P=0.009 for ΔADC

Before and 3 weeks into treatment	Moffat et al, 2005	Brain tumors	20	b-value: 0-1000, 1.5T	Chemo- and/or radiotherapy	***Positive***: responding lesions had a higher percentage with increase in ADC-values.	
Before and after treatment	Okuma et al, 2009	irresectable lung tumor	17/ 20	1.5T	RFA	***Positive:*** after treatment the ADC was higher. The ADC post-RFA was higher in no-progression than local progression groups	P<0.05
Before and after chemotherapy treatment	Hayashida et al, 2006	Osteo- and Ewing sarcoma	18	b-value: 0-1000, 1.5T	Neoadjuvant chemo-therapy followed by surgery	***Positive***: change in the ADC value was statistically greater in those with >90% necrosis .	P=0.003: ADC change
Early in treatment (after first and second cycle) compared to before treatment	Pickles et al, 2006	Breast cancer	10	b-value: 0-700, 1.5T	Neoadjuvant chemo-therapy	***Positive:*** ADC increased after first and second chemotherapy cycle	P=0.005: first cycle P=.004: second cycle
Before and 1 week after treatment	Mardor et al, 2003	Brain tumors	8/ 10	b-value: 5-1000, 0.5T	Radiotherapy	***Postive:*** 3 of 6 responding lesions showed increase in ADC. The 4 nonresponding lesions all showed stable or decreasing ADC-values.	-
Before treatment and 2-3 and 4 weeks into treatment	Hein et al, 2003	Locally advanced rectal cancer	9	b-value: 30-300-1100, 1.5T	Neoadjuvant chemo-radiation	***Negative:*** the tumor ADC showed a decrease at the 2nd 3rd and 4th week of chemoradiation treatment compared to pretreatment value.	P=0.028 (2nd week) P=0.012 (3rd week) P=0.008 (4th week)

Table 2. *Response monitoring with DWI.*

Most studies indeed showed an increase in ADC in responding tumors. In osteosarcomas and Ewing sarcomas (N=18), a significantly higher median change of ADC after treatment was observed in the group with ≥ 90% histological necrosis compared to the group with <90% necrosis, while no significant difference in the change of tumor volume between the groups was observed [27]. An increase in mean ADC was also found in colorectal hepatic metastases that responded to chemotherapy (as defined by RECIST criteria). The responding lesions showed a significant increase in mean ADC, while no change was observed in non-responding metastatic lesions or normal liver parenchyma [37]. Comparable results were observed in brain tumors after radiation therapy [44], and for patients who underwent radiofrequency ablation for an irresectable lung tumor. ADC-values after treatment were shown to be significantly higher in patients who did not have local progression later on [45]. ADC in prostate cancer also rose after radiotherapy. In lesions in which the ADC-value did not increase, no locoregional control was achieved with radiotherapy [46].

Only two studies reported contrasting results of a decrease in ADC-value after chemo- or chemoradiotherapy. One showed that ADC was associated with response to chemotherapy of rectal cancer. In the tumors responding to chemotherapy, low ADC values prior and during treatment were associated with response [36]. In patients undergoing neoadjuvant chemoradiotherapy for rectal cancer, all 9 patients showed a decrease in mean ADC-value 4 weeks after start of treatment, including the 4 with tumor down staging. They attributed this effect to the development of intratumoral radiation-induced fibrosis and cytotoxic edema due to a shift of water from the extracellular to the intracellular space, as found in pathohistological observation. This results in restrained free diffusion, due to the limiting effect of fibres or cell swelling on water movement, respectively [47]. However, both could still be a coincidence since the number of patients in the studies was very small. In a recent study, in a much larger cohort of rectal cancer patients (n=76), neoadjuvant chemoradiotherapy caused a significant increase in ADC-values. Furthermore, patients with complete response after therapy had a higher posttherapy mean ADC than those with non-complete response [48].

As stated above, changes in ADC may precede changes in tumor size, since early after start of treatment changes in cellularity and necrosis may already occur. Thus it seems plausible that DWI can provide an early marker for treatment efficacy. This hypothesis is based on the finding that DWI can be used in the diagnosis of acute stroke, before conventional imaging techniques show abnormalities [49;50]. This also implicates that the timing of imaging is of crucial importance: changes in ADC could precede changes in tumor size and may even disappear after a certain time because of repair mechanisms [51]. Systemic treatment results in a response in only a subset of patients and is, also in non-responding patients, accompanied by adverse effects and costs. Therefore, preferably treatment efficacy is determined at an early stage.

This was shown in a study of 10 breast cancer patients treated with neoadjuvant chemotherapy. The longest tumor diameter (as measured by conventional anatomical MRI) and ADC-values were recorded prior to and after the first and second chemotherapy cycle. Significant alterations from the baseline value were noted for ADC at the first chemotherapy cycle (ADC increased from 1.00 to 1.14) and the second chemotherapy cycle (ADC increased from 1.00 to 1.27). While changes in the measurement of the longest diameter only achieved a borderline significance compared to baseline at the second time point (size decreased from 1.00 to 0.80) and no significance at the first time point. These data confirm that changes in tumor biology may precede changes in tumor size [52].

Similar results were obtained during chemotherapy in 13 patients with 60 liver metastases of breast cancer. ADC changes as early as 4 days after start of treatment and correlated with objective clinical response on day 39, which was determined by lesion volume measurement on MRI. In responders, a significant change in ADC at day 11 was found, whereas in non-responders, there was no change. According to the authors, these results suggested that diffusion can be useful to predict the response of liver metastases to effective chemotherapy [53].

Several studies in patients with malignant brain tumors showed marked increases in ADC early after start of radiation and/or chemotherapy [54-56]. In 2 studies, patients with brain tumors showed prolonged survival if they had a higher percentage of voxels with an increased ADC 3 weeks after start of treatment [55;57]. Both studies used functional diffusion mapping (fDM), which implies that not the mean ADC-value was calculated but an ADC-value per voxel. The pretreatment and posttreatment ADC per voxel are expressed in a scatter plot, resulting in a functional diffusion map. Changes over 0.55 10(-3) mm(2)/s (two times the standard deviation) were considered to be real biological changes. One of these studies showed an association between percentage of the voxels with increased diffusion at functional diffusion maps and one year survival in patients with high grade gliomas treated with chemoradiation or radiotherapy. Patients with over 4.7 percent of their tumor showing increase in ADC-value at 3 weeks had a longer median survival (52.6 versus 10.9 months; log rank, $p<0.003$). Anatomical response (volume changes measured with T1 contrast enhanced MRI) at 10 weeks had similar predictive value (median survival 31.6 versus 10.9 months; log rank $p<0.0007$), indicating that DWI probably can predict survival several weeks earlier than anatomical imaging with MRI. Combining anatomical response measurements and functional diffusion mapping predicted survival even better: median overall survival in the worst responding group, intermediate responding group and best responding group were 8.1, 14.4 and 52.6 months respectively ($P<0.001$) [57]. In the second study it was shown that fDM is also predictive of survival in a group with different types of brain tumors [55]. In a study on the predictive value of DWI in squamous cell carcinoma of the head and neck, 30 patients underwent DWI and anatomical MRI at baseline, 2 weeks and 4 weeks after start of

chemoradiotherapy. Patients without recurrence had a significantly higher difference in ADC after 2 and 4 weeks of treatment than patients with recurrence ($p<0.001$). Although there was some overlap in the complete remission and recurrence group, differences in ADC were far more sensitive and specific than measured volumetric changes to predict locoregional control [58].

Also in patients in whom pretreatment ADC-values did not correlate with response, changes in ADC-value did: in neoadjuvant treated cervical cancer patients changes in ADC just 2 weeks after treatment correlated with response. In breast cancer patient ADC changes measured after 4 cycles of chemotherapy correlated with response [41;42].

The abovementioned studies suggest a relationship between ADC's measured early after start of treatment and treatment outcome (based on tumor recurrence and survival). The relation between early ADC changes and clinical outcome seems more lucid than ADC changes after a longer treatment period. This may be due to tissue repair mechanisms such as decrease of edema and organization of necrosis. In fact, in a study of kidney tumors an increase in ADC after 3 days of treatment with the tyrosine kinase inhibitor sunitinib was observed, while ADC values decreased back to the starting value after 10 days [51]. Thus, DWI seems to be useful for early evaluation of clinical response, although the optimal timing for imaging for each tumor type remains uncertain.

Although a relation has been shown between changes in ADC after treatment and response to treatment according to conventional anatomical imaging, the direction of these changes were equivocal as both increases [27;37;44;59] and decreases in ADC's [36;47] were observed.

Since the number of participants was limited in most studies, future studies should include power calculations to indicate how many patients or lesions should be included in the imaging study to provide clinically meaningful results. Although some studies included a larger number of patients, it remains unclear whether the observed statistically significant differences were clinically relevant. Also, the repeatability of DWI measurements should be assessed to determine what percentage change in ADC-value could be considered a real change and what would be due to normal variation. This could help to determine which changes are relevant for the individual patient. Assessment of the repeatability would be more useful if protocols can be exchanged between clinics. Otherwise each clinic should examine the repeatability of its own protocols.

5 Comparison of DWI and DCE-MRI

DCE-MRI appears to be a favored functional imaging technique in many studies. In DCE-MRI, the tissue uptake of an MR contrast agent is monitored over time. Essentially, DCE-MRI is sensitive to a combination of vascular flow, volume and permeability. In tumor tissue this combination_may have acquired typical properties due to angiogenesis. Therefore, these may be used as biomarkers to identify tumor tissue and to assess tumor response [7;60-62].

The dynamic uptake of a contrast agent in the extravascular extracellular space of tumors, which occurs typically within a few minutes after intravenous application, is measured by T1 weighted MR imaging. From the signal changes reflecting this uptake, the rate constant k_{ep} (describing the exchange rate of the contrast agent between vascular and extravascular space) and the volume transfer constant K^{trans} (describing the volume transfer of the contrast agent) are commonly calculated (figure 4). These parameters represent microvessel perfusion, permeability, and the extracellular leakage space.

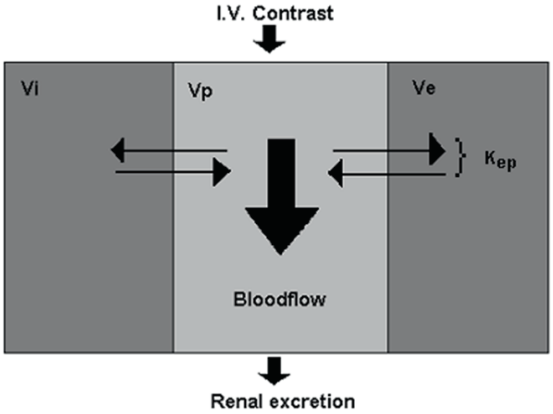

Figure 4. *Schematic view on the body compartments assessed by DCE-MRI. Vi= interstitial space of healthy tissue; Vp= blood plasma volume; v_e= tumor interstitial space; k_{ep}= rate constant in exchange between interstitial space and blood plasma; K^{trans}= volume transfer constant in exchange between interstitial space and blood plasma. $K^{trans}= v_e * k_{ep}$.*

Especially functional imaging studies of response to antivascular treatment are most often performed with DCE-MRI, whereas studies on response prediction with DWI where most often performed in patients treated with chemo- or radiation therapy. However, treatment changes caused by antivascular therapy may also have an effect on DWI-parameters, while chemo- and radiotherapy could have an effect on DCE-parameters [63;64]. Therefore, the question arises whether DCE-MRI and DWI for response evaluation, can be used interchangeably or whether one technique is superior to the other for a specific treatment modality.

A study, performed in 2003, where DCE-MRI and DWI were applied before onset of treatment in 34 patients with primary rectal cancer undergoing preoperative chemoradiation, showed more promising results for DCE-MRI. Perfusion indices separated responders from non-responders, whereas ADC-values could not (mean ADC responders 0.648 vs non-responders 0.657; p=0.825). Perfusion indices were higher in non-responders vs. responders (10.7 ± 2.7 mL/min/100 g vs. 7.5 ±1.5 mL/min/100 g; p<0.001). No posttherapy imaging was conducted in this study [40].

Three studies have shown similar results for DWI and DCE-MRI in the early prediction of outcome. In a study with 11 patients treated with neoadjuvant chemotherapy for breast cancer DWI and DCE-MRI were performed before and after 4 cycles of chemotherapy. K^{trans} reduction ($p<0.04$) and delta ADC ($p<0.05$) were both sensitive to longitudinal changes in breast tumor status [65]. A study with 16 patients with glioblastoma treated with AZD2171, an antiangiogenic agent, a significant change in both diffusion and perfusion parameters one day after treatment compared to pretreatment values was observed, although perfusion parameters seemed to change more in the same period [63]. A third study with similar results for DWI and DCE-MRI was performed in 8 patients with osteosarcoma treated with standard chemotherapy. Imaging was performed after 5 cycles. ADC, slopes and time-to-peak-values were significantly different between necrotic areas and viable tumor (based on histology after resection). Again, DCE-MRI parameters showed a larger difference than DWI-parameters [26]. A fourth study, in 13 patients with hepatocellular carcinoma treated with yttrium-90-labeled microspheres, DCE-MRI and DWI were performed before and after one month of treatment. A significant decrease in enhancement (22% less arterial enhancement; $p=0.013$) and increase in ADC were found (17% increase in ADC; $p<0.01$). Unfortunately, no relation with treatment effect, defined as reduction of tumor size, was assessed [66].

In contrast, in a study of 40 patients with primary inoperable breast cancer no predictive value for tumor volume decrease after neoadjuvant chemotherapy for both DWI and DCE-MRI was shown, after two cycles of neoadjuvant chemotherapy. The negative results for DCE-MRI are in contrast with results of other studies and as the authors suggested the negative results for DWI in their study could be a result of imaging after two cycles of chemotherapy rather than one, like the positive studies did. Perhaps due to repair or resistance mechanisms, the ADC could decrease again after a longer treatment time [67]. Yet, this study was performed in a larger number of patients than most other studies. Negative results were also obtained in 41 patients with glioblastoma treated with chemoradiation. The only two parameters measured at 21-28 days after therapy, which significantly anticipated tumor progression, were T1 largest diameter and T2 size variation. Perfusion and diffusion were no significant predictors of progression free survival. However, no measurements early after start of therapy were performed [68].

The great advantage of DWI over DCE-MRI is that administration of a contrast agent is not required. Although gadolinium-based contrast agents are relatively safe, intravenous access is required and a risk of allergic reactions and renal toxicity remains. Both DWI and DCE-MRI measurements require calibration, for individual variation, that may not be trivial to perform. The calculated parameters are based on kinetic models with certain assumptions, for example the arterial input function (AIF) in case of DCE-MRI, which may differ per patient [69-71]. In conclusion, at the moment there is no clear evidence to prefer either DWI or DCE-MRI for response monitoring of the diverse anti-cancer treatments.

6 Conclusions

DWI may be regarded as a promising imaging tool for the prediction of response to treatment. Based on the results thus far, in the clinic DWI seems to perform as well as DCE-MRI and it may be suitable for a broader range of therapies. In fact, DWI can be used both in the evaluation of conventional cytotoxic treatment and anti-vascular therapy.

However, an important question is whether this new imaging technology is ready to be implemented in clinical practice. DWI adds to conventional imaging, since differences or early changes in cellularity can be measured, which gives the opportunity for early response prediction. However, at this moment the repeatability of DWI of tumors is insufficiently investigated. Repeatability studies are necessary to ascertain the magnitude of the ADC changes that can be confidently detected and which are possibly the result of normal variation. In addition, the cut-off values to determine response vary between different tumor types and treatments and depends on the ADC measurement technique. A guideline to determine response, like RECIST for anatomical evaluation and PERCIST to evaluate metabolic response in FDG-PET, is needed before DWI could be implemented in clinical practice [72;73]. In fact, at present, there is not sufficient standardization nor evidence to abandon anatomical assessment of tumor burden [74]. Therefore, we think it is crucial that further research is performed to standardize and validate DWI for obtaining data and marker quantification. Extensive recommendations towards the use of DWI in the clinic recently have been described by Padhani et al. [10]. Furthermore, this standardized way to monitor response with DWI should be researched extensively to determine how it relates to RECIST criteria and clinical outcome.

We believe that further research into the potential of DWI may result in a new powerful tool for response evaluation. A major advantage for the individual patient would be the availability of early response evaluation, which may spare non-responding patients the toxicity (and expenses) of these treatments.

Reference List

[1] Padhani AR: MRI for assessing antivascular cancer treatments. Br J Radiol 2003;76 Spec No 1:S60-S80.

[2] Padhani AR, Leach MO: Antivascular cancer treatments: functional assessments by dynamic contrast-enhanced magnetic resonance imaging. Abdom Imaging 2005;30:324-341.

[3] Cheng HL, Haider MA, Il-Macky MJ, Sweet JM, Trachtenberg J, Gertner MR: MRI and contrast-enhanced ultrasound monitoring of prostate microwave focal thermal therapy: an in vivo canine study. J Magn Reson Imaging 2008;28:136-143.

[4] Jordan BF, Runquist M, Raghunand N, Baker A, Williams R, Kirkpatrick L, Powis G, Gillies RJ: Dynamic contrast-enhanced and diffusion MRI show rapid and dramatic changes in tumor microenvironment in response to inhibition of HIF-1alpha using PX-478. Neoplasia 2005;7:475-485.

[5] Thoeny HC, De KF, Vandecaveye V, Chen F, Sun X, Bosmans H, Hermans R, Verbeken EK, Boesch C, Marchal G, Landuyt W, Ni Y: Effect of vascular targeting agent in rat tumor model: dynamic contrast-enhanced versus diffusion-weighted MR imaging. Radiology 2005;237:492-499.

[6] Vogel-Claussen J, Gimi B, Artemov D, Bhujwalla ZM: Diffusion-weighted and macromolecular contrast enhanced MRI of tumor response to antivascular therapy with ZD6126. Cancer Biol Ther 2007;6:1469-1475.

[7] Stejskal EO, Tanner J: Spin diffusion measurements: spinechoes in the presence of a time-dependent field gradient. Journal of Chemicals Physics 1965;42:288-292.

[8] Special Issue: Progress in Diffusion-Weighted Imaging: Concepts, Techniques, and Applications to the Central Nervous System. NMR in Biomedicine 2010; 23[7]:659-904.

[9] Koh DM, Collins DJ: Diffusion-weighted MRI in the body: applications and challenges in oncology. AJR Am J Roentgenol 2007;188:1622-1635.

[10] Padhani AR, Liu G, Mu-Koh D, Chenevert TL, Thoeny HC, Takahara T, Dzik-Jurasz A, Ross BD, Van CM, Collins D, Hammoud DA, Rustin GJ, Taouli B, Choyke PL: Diffusion-weighted magnetic resonance imaging as a cancer biomarker: consensus and recommendations. Neoplasia 2009;11:102-125.

[11] Bammer R, Holdsworth SJ, Veldhuis WB, Skare ST: New methods in diffusion-weighted and diffusion tensor imaging. Magn Reson Imaging Clin N Am 2009;17:175-204.

[12] Hagmann P, Jonasson L, Maeder P, Thiran JP, Wedeen VJ, Meuli R: Understanding diffusion MR imaging techniques: from scalar diffusion-weighted imaging to diffusion tensor imaging and beyond. Radiographics 2006;26 Suppl 1:S205-S223.

[13] Kuroki Y, Nasu K, Kuroki S, Murakami K, Hayashi T, Sekiguchi R, Nawano S: Diffusion-weighted imaging of breast cancer with the sensitivity encoding technique: analysis of the apparent diffusion coefficient value. Magn Reson Med Sci 2004;3:79-85.

[14] Marini C, Iacconi C, Giannelli M, Cilotti A, Moretti M, Bartolozzi C: Quantitative diffusion-weighted MR imaging in the differential diagnosis of breast lesion. Eur Radiol 2007;17:2646-2655.

[15] Partridge SC, Demartini WB, Kurland BF, Eby PR, White SW, Lehman CD: Differential diagnosis of mammographically and clinically occult breast lesions on diffusion-weighted MRI. J Magn Reson Imaging 2010;31:562-570.

[16] Rubesova E, Grell AS, De M, V, Metens T, Chao SL, Lemort M: Quantitative diffusion imaging in breast cancer: a clinical prospective study. J Magn Reson Imaging 2006;24:319-324.

[17] Nakajo M, Kajiya Y, Kaneko T, Kaneko Y, Takasaki T, Tani A, Ueno M, Koriyama C, Nakajo M: FDG PET/CT and diffusion-weighted imaging for breast cancer: prognostic value of maximum standardized uptake values and apparent diffusion coefficient values of the primary lesion. Eur J Nucl Med Mol 2010;37:2011-2020.

[18] Costantini M, Belli P, Rinaldi P, Bufi E, Giardina G, Franceschini G, Petrone G, Bonomo L: Diffusion-weighted imaging in breast cancer: relationship between apparent diffusion coefficient and tumour aggressiveness. Clin Radiol 2010;65:1005-1012.

[19] Takeuchi M, Matsuzaki K, Nishitani H: Diffusion-weighted magnetic resonance imaging of endometrial cancer: differentiation from benign endometrial lesions and preoperative assessment of myometrial invasion. Acta Radiol 2009;50:947-953.

[20] Takeuchi M, Matsuzaki K, Nishitani H: Diffusion-weighted magnetic resonance imaging of ovarian tumors: differentiation of benign and malignant solid components of ovarian masses. J Comput Assist Tomogr 2010;34:173-176.

[21] Woodfield CA, Tung GA, Grand DJ, Pezzullo JA, Machan JT, Renzulli JF: Diffusion-weighted MRI of peripheral zone prostate cancer: comparison of tumor apparent diffusion coefficient with Gleason score and percentage of tumor on core biopsy. AJR Am J Roentgenol 2010;194:W316-W322.

[22] Hambrock T, Somford DM, Huisman HJ, van O, I, Witjes JA, Hulsbergen-van de Kaa CA, Scheenen T, Barentsz JO: Relationship between Apparent Diffusion Coefficients at 3.0-T MR Imaging and Gleason Grade in Peripheral Zone Prostate Cancer. Radiology 2011;259:453-461.

[23] Nasu K, Kuroki Y, Tsukamoto T, Nakajima H, Mori K, Minami M: Diffusion-weighted imaging of surgically resected hepatocellular carcinoma: imaging characteristics and relationship among signal intensity, apparent diffusion coefficient, and histopathologic grade. AJR Am J Roentgenol 2009;193:438-444.

[24] Bacci G, Ferrari S, Bertoni F, Ruggieri P, Picci P, Longhi A, Casadei R, Fabbri N, Forni C, Versari M, Campanacci M: Long-term outcome for patients with nonmetastatic osteosarcoma of the extremity treated at the istituto ortopedico rizzoli according to the istituto ortopedico rizzoli/osteosarcoma-2 protocol: an updated report. J Clin Oncol 2000;18:4016-4027.

[25] Bielack SS, Kempf-Bielack B, Delling G, Exner GU, Flege S, Helmke K, Kotz R, Salzer-Kuntschik M, Werner M, Winkelmann W, Zoubek A, Jurgens H, Winkler K: Prognostic factors in high-grade osteosarcoma of the extremities or trunk: an analysis of 1,702 patients treated on neoadjuvant cooperative osteosarcoma study group protocols. J Clin Oncol 2002;20:776-790.

[26] Uhl M, Saueressig U, van BM, Kontny U, Niemeyer C, Kohler G, Ilyasov K, Langer M: Osteosarcoma: preliminary results of in vivo assessment of tumor necrosis after chemotherapy with diffusion- and perfusion-weighted magnetic resonance imaging. Invest Radiol 2006;41:618-623.

[27] Hayashida Y, Yakushiji T, Awai K, Katahira K, Nakayama Y, Shimomura O, Kitajima M, Hirai T, Yamashita Y, Mizuta H: Monitoring therapeutic responses of primary bone tumors by diffusion-weighted image: Initial results. Eur Radiol 2006;16:2637-2643.

[28] Kamel IR, Bluemke DA, Ramsey D, Abusedera M, Torbenson M, Eng J, Szarf G, Geschwind JF: Role of diffusion-weighted imaging in estimating tumor necrosis after chemoembolization of hepatocellular carcinoma. AJR Am J Roentgenol 2003;181:708-710.

[29] Guo AC, Cummings TJ, Dash RC, Provenzale JM: Lymphomas and high-grade astrocytomas: comparison of water diffusibility and histologic characteristics. Radiology 2002;224:177-183.

[30] Kallehauge JF, Tanderup K, Haack S, Nielsen T, Muren LP, Fokdal L, Lindegaard JC, Pedersen EM: Apparent Diffusion Coefficient (ADC) as a quantitative parameter in diffusion weighted MR imaging in gynecologic cancer: Dependence on b-values used. Acta Oncol 2010;49:1017-1022.

[31] Peters NH, Vincken KL, van den Bosch MA, Luijten PR, Mali WP, Bartels LW: Quantitative diffusion weighted imaging for differentiation of benign and malignant breast lesions: the influence of the choice of b-values. J Magn Reson Imaging 2010;31:1100-1105.

[32] Lyng H, Haraldseth O, Rofstad EK: Measurement of cell density and necrotic fraction in human melanoma xenografts by diffusion weighted magnetic resonance imaging. Magn Reson Med 2000;43:828-836.

[33] Mishra AM, Gupta RK, Saksena S, Prasad KN, Pandey CM, Rathore D, Purwar A, Rathore RK, Husain N, Jha DK, Jaggi RS, Husain M: Biological correlates of diffusivity in brain abscess. Magn Reson Med 2005;54:878-885.

[34] Rockwell S, Dobrucki IT, Kim EY, Marrison ST, Vu VT: Hypoxia and radiation therapy: past history, ongoing research, and future promise. Curr Mol Med 2009;9:442-458.

[35] Vaupel P, Mayer A: Hypoxia in cancer: significance and impact on clinical outcome. Cancer Metastasis Rev 2007;26:225-239.

[36] Dzik-Jurasz A, Domenig C, George M, Wolber J, Padhani A, Brown G, Doran S: Diffusion MRI for prediction of response of rectal cancer to chemoradiation. Lancet 2002;360:307-308.

[37] Koh DM, Scurr E, Collins D, Kanber B, Norman A, Leach MO, Husband JE: Predicting response of colorectal hepatic metastasis: value of pretreatment apparent diffusion coefficients. AJR Am J Roentgenol 2007;188:1001-1008.

[38] Cui Y, Zhang XP, Sun YS, Tang L, Shen L: Apparent diffusion coefficient: potential imaging biomarker for prediction and early detection of response to chemotherapy in hepatic metastases. Radiology 2008;248:894-900.

[39] Mardor Y, Roth Y, Ochershvilli A, Spiegelmann R, Tichler T, Daniels D, Maier SE, Nissim O, Ram Z, Baram J, Orenstein A, Pfeffer R: Pretreatment prediction of brain tumors' response to radiation therapy using high b-value diffusion-weighted MRI. Neoplasia 2004;6:136-142.

[40] DeVries AF, Kremser C, Hein PA, Griebel J, Krezcy A, Ofner D, Pfeiffer KP, Lukas P, Judmaier W: Tumor microcirculation and diffusion predict therapy outcome for primary rectal carcinoma. Int J Radiat Oncol Biol Phys 2003;56:958-965.

[41] Harry VN, Semple SI, Gilbert FJ, Parkin DE: Diffusion-weighted magnetic resonance imaging in the early detection of response to chemoradiation in cervical cancer. Gynecol Oncol 2008;111:213-220.

[42] Nilsen L, Fangberget A, Geier O, Olsen DR, Seierstad T: Diffusion-weighted magnetic resonance imaging for pretreatment prediction and monitoring of treatment response of patients with locally advanced breast cancer undergoing neoadjuvant chemotherapy. Acta Oncol 2010;49:354-360.

[43] Kim SH, Lee JM, Hong SH, Kim GH, Lee JY, Han JK, Choi BI: Locally advanced rectal cancer: added value of diffusion-weighted MR imaging in the evaluation of tumor response to neoadjuvant chemo- and radiation therapy. Radiology 2009;253:116-125.

[44] Tomura N, Narita K, Izumi J, Suzuki A, Anbai A, Otani T, Sakuma I, Takahashi S, Mizoi K, Watarai J: Diffusion changes in a tumor and peritumoral tissue after stereotactic irradiation for brain tumors: possible prediction of treatment response. J Comput Assist Tomogr 2006;30:496-500.

[45] Okuma T, Matsuoka T, Yamamoto A, Hamamoto S, Nakamura K, Inoue Y: Assessment of early treatment response after CT-guided radiofrequency ablation of unresectable lung tumours by diffusion-weighted MRI: a pilot study. Br J Radiol 2009;82:989-994.

[46] Song I, Kim CK, Park BK, Park W: Assessment of response to radiotherapy for prostate cancer: value of diffusion-weighted MRI at 3 T. AJR Am J Roentgenol 2010;194:W477-W482.

[47] Hein PA, Kremser C, Judmaier W, Griebel J, Pfeiffer KP, Kreczy A, Hug EB, Lukas P, DeVries AF: Diffusion-weighted magnetic resonance imaging for monitoring diffusion changes in rectal carcinoma during combined, preoperative chemoradiation: preliminary results of a prospective study. Eur J Radiol 2003;45:214-222.

[48] Kim SH, Lee JY, Lee JM, Han JK, Choi BI: Apparent diffusion coefficient for evaluating tumour response to neoadjuvant chemoradiation therapy for locally advanced rectal cancer. Eur Radiol 2011;21:987-995.

[49] Warach S, Chien D, Li W, Ronthal M, Edelman RR: Fast magnetic resonance diffusion-weighted imaging of acute human stroke. Neurology 1992;42:1717-1723.

[50] Warach S, Gaa J, Siewert B, Wielopolski P, Edelman RR: Acute human stroke studied by whole brain echo planar diffusion-weighted magnetic resonance imaging. Ann Neurol 1995;37:231-241.

[51] Desar IM, van Laarhoven HW, Hambrok T, Ter Voert E, Van Der Graaf WT, Van Spronzen D, Barentsz JO, Heerschap A, van Herpen CM. Assessment of early vascular effects of the angiogenesis inhibitor sunitinib (SU) in renal cell carcinoma (RCC) by dynamic contrast enhanced MRI (DCE-MRI) and diffusion weight MRI (DWI) at 3 tesla (T). ASCO 2010.

[52] Pickles MD, Gibbs P, Lowry M, Turnbull LW: Diffusion changes precede size reduction in neoadjuvant treatment of breast cancer. Magn Reson Imaging 2006;24:843-847.

[53] Theilmann RJ, Borders R, Trouard TP, Xia G, Outwater E, Ranger-Moore J, Gillies RJ, Stopeck A: Changes in water mobility measured by diffusion MRI predict response of metastatic breast cancer to chemotherapy. Neoplasia 2004;6:831-837.

[54] Mardor Y, Pfeffer R, Spiegelmann R, Roth Y, Maier SE, Nissim O, Berger R, Glicksman A, Baram J, Orenstein A, Cohen JS, Tichler T: Early detection of response to radiation therapy in patients with brain malignancies using conventional and high b-value diffusion-weighted magnetic resonance imaging. J Clin Oncol 2003;21:1094-1100.

[55] Hamstra DA, Chenevert TL, Moffat BA, Johnson TD, Meyer CR, Mukherji SK, Quint DJ, Gebarski SS, Fan X, Tsien CI, Lawrence TS, Junck L, Rehemtulla A, Ross BD: Evaluation of the functional diffusion map as an early biomarker of time-to-progression and overall survival in high-grade glioma. Proc Natl Acad Sci U S A 2005;102:16759-16764.

[56] Moffat BA, Chenevert TL, Lawrence TS, Meyer CR, Johnson TD, Dong Q, Tsien C, Mukherji S, Quint DJ, Gebarski SS, Robertson PL, Junck LR, Rehemtulla A, Ross BD: Functional diffusion map: a noninvasive MRI biomarker for early stratification of clinical brain tumor response. Proc Natl Acad Sci U S A 2005;102:5524-5529.

[57] Hamstra DA, Galban CJ, Meyer CR, Johnson TD, Sundgren PC, Tsien C, Lawrence TS, Junck L, Ross DJ, Rehemtulla A, Ross BD, Chenevert TL: Functional diffusion map as an early imaging biomarker for high-grade glioma: correlation with conventional radiologic response and overall survival. J Clin Oncol 2008;26:3387-3394.

[58] Vandecaveye V, Dirix P, De KF, Op de BK, Vander P, V, Roebben I, Nuyts S, Hermans R: Predictive value of diffusion-weighted magnetic resonance imaging during chemoradiotherapy for head and neck squamous cell carcinoma. Eur Radiol 2010;20:1703-1714.

[59] Hylton N: Dynamic contrast-enhanced magnetic resonance imaging as an imaging biomarker. J Clin Oncol 2006;24:3293-3298.

[60] van Laarhoven HW, Klomp DW, Rijpkema M, Kamm YL, Wagener DJ, Barentsz JO, Punt CJ, Heerschap A: Prediction of chemotherapeutic response of colorectal liver metastases with dynamic gadolinium-DTPA-enhanced MRI and localized 19F MRS pharmacokinetic studies of 5-fluorouracil. NMR Biomed 2007;20:128-140.

[61] Vriens D, Geus-Oei L, Heerschap A, van Laarhoven HW, Oyen WJ: Vascular and metabolic response to bevacizumab-containing regimens in two patients with colorectal liver metastases measured by dynamic contrast enhanced MRI and dynamic 18F-FDG PET. Clinical Colorectal Cancer 2010;10:E1-E5.

[62] Batchelor TT, Sorensen AG, di TE, Zhang WT, Duda DG, Cohen KS, Kozak KR, Cahill DP, Chen PJ, Zhu M, Ancukiewicz M, Mrugala MM, Plotkin S, Drappatz J, Louis DN, Ivy P, Scadden DT, Benner T, Loeffler JS, Wen PY, Jain RK: AZD2171, a pan-VEGF receptor tyrosine kinase inhibitor, normalizes tumor vasculature and alleviates edema in glioblastoma patients. Cancer Cell 2007;11:83-95.

[63] Davis TW, O'Neal JM, Pagel MD, Zweifel BS, Mehta PP, Heuvelman DM, Masferrer JL: Synergy between celecoxib and radiotherapy results from inhibition of cyclooxygenase-2-derived prostaglandin E2, a survival factor for tumor and associated vasculature. Cancer Res 2004;64:279-285.

[64] Yankeelov TE, Lepage M, Chakravarthy A, Broome EE, Niermann KJ, Kelley MC, Meszoely I, Mayer IA, Herman CR, McManus K, Price RR, Gore JC: Integration of quantitative DCE-MRI and ADC mapping to monitor treatment response in human breast cancer: initial results. Magn Reson Imaging 2007;25:1-13.

[65] Kamel IR, Reyes DK, Liapi E, Bluemke DA, Geschwind JF: Functional MR imaging assessment of tumor response after 90Y microsphere treatment in patients with unresectable hepatocellular carcinoma. J Vasc Interv Radiol 2007;18:49-56.

[66] Manton DJ, Chaturvedi A, Hubbard A, Lind MJ, Lowry M, Maraveyas A, Pickles MD, Tozer DJ, Turnbull LW: Neoadjuvant chemotherapy in breast cancer: early response prediction with quantitative MR imaging and spectroscopy. Br J Cancer 2006;94:427-435.

[67] Leimgruber A, Ostermann S, Yeon EJ, Buff E, Maeder PP, Stupp R, Meuli RA: Perfusion and diffusion MRI of glioblastoma progression in a four-year prospective temozolomide clinical trial. Int J Radiat Oncol Biol Phys 2006;64:869-875.

[68] Rijpkema M, Kaanders JH, Joosten FB, van der Kogel AJ, Heerschap A: Method for quantitative mapping of dynamic MRI contrast agent uptake in human tumors. J Magn Reson Imaging 2001;14:457-463.

[69] Tofts PS, Brix G, Buckley DL, Evelhoch JL, Henderson E, Knopp MV, Larsson HB, Lee TY, Mayr NA, Parker GJ, Port RE, Taylor J, Weisskoff RM: Estimating kinetic parameters from dynamic contrast-enhanced T(1)-weighted MRI of a diffusable tracer: standardized quantities and symbols. J Magn Reson Imaging 1999;10:223-232.

[70] van Laarhoven HW, Rijpkema M, Punt CJ, Ruers TJ, Hendriks JC, Barentsz JO, Heerschap A: Method for quantitation of dynamic MRI contrast agent uptake in colorectal liver metastases. J Magn Reson Imaging 2003;18:315-320.

[71] van Dorsten FA, van der GM, Engelbrecht MR, van Leenders GJ, Verhofstad A, Rijpkema M, de la Rosette JJ, Barentsz JO, Heerschap A: Combined quantitative dynamic contrast-enhanced MR imaging and (1)H MR spectroscopic imaging of human prostate cancer. J Magn Reson Imaging 2004;20:279-287.

[72] Wahl RL, Jacene H, Kasamon Y, Lodge MA: From RECIST to PERCIST: Evolving Considerations for PET response criteria in solid tumors. J Nucl Med 2009;50 Suppl 1:122S-150S.

[73] Therasse P, Eisenhauer EA, Verweij J: RECIST revisited: a review of validation studies on tumour assessment. Eur J Cancer 2006;42:1031-1039.

[74] Eisenhauer EA, Therasse P, Bogaerts J, Schwartz LH, Sargent D, Ford R, Dancey J, Arbuck S, Gwyther S, Mooney M, Rubinstein L, Shankar L, Dodd L, Kaplan R, Lacombe D, Verweij J: New response evaluation criteria in solid tumours: revised RECIST guideline (version 1.1). Eur J Cancer 2009;45:228-247.

3

Diffusion weighted MR imaging in liver metastases of colorectal cancer: repeatability and biological validation

Abstract

Background: Before diffusion weighted imaging can be implemented in standard clinical practice for response monitoring, data on repeatability are needed to assess which differences outside the range of normal variation can be detected in an individual patient. In this study we assessed the repeatability of the apparent diffusion coefficient (ADC) values in colorectal liver metastases. To provide a biological basis for these values, their relation with histopathology was assessed.

Methods: Diffusion weighted imaging was performed twice in 1 week in patients scheduled for metastasectomy of colorectal liver metastases. Correlation between ADC values and apoptosis marker p53, anti-apoptotic protein BCL-2, proliferation marker Ki67 and serum vascular endothelial growth factor (VEGF) concentration were assessed.

Results: A good repeatability coefficient of the mean ADC (coefficient of repeatability 0.20 $*10^{-3}$ mm^2/s) was observed in colorectal liver metastases (n=21). The ADC value was related to the proliferation index and BCL-2 expression of the metastases. Furthermore, in metastases recently treated with systemic therapy, the ADC was significantly higher (1.27 $*10^{-3}$ mm^2/s vs. 1.05 $*10^{-3}$ mm^2/s, P=0.02).

Conclusion: The good repeatability, correlation with histopathology and implied sensitivity for systemic treatment-induced antitumor effects suggest that DWI might be an excellent tool to monitor response in metastatic colorectal cancer.

Introduction

Colorectal cancer is the second leading cause of cancer-related death in Europe [1] and despite improved treatment, almost half of patients with colorectal cancer will develop distant metastases, primarily in the liver. Only a small percentage of the patients with liver metastases can be treated by metastasectomy with curative intent [2]. Palliative systemic therapy prolongs the median overall survival, but only approximately 50% of patients respond to this potentially toxic and expensive treatment [3]. Response evaluation is commonly performed after 8–9 weeks of treatment. A tool to monitor therapy response early is therefore desirable, as this would prevent unnecessary toxicity and costs.

Assessment of cancer and their metastases with functional imaging may lead to improved diagnosis and early knowledge of treatment efficacy. Diffusion weighted MR imaging (DWI) is a promising functional imaging tool for tissue characterization, response prediction and response evaluation in cancer [4; 5]. From DW MR images an apparent diffusion coefficient (ADC) can be calculated, which is a measure of water mobility. A high apparent diffusion coefficient implies that water can move freely, for instance when few intact cell structures, such as membranes, are present [6]. Cellular processes, like apoptosis and proliferation influence cell density and thus the ADC value. In a study of animals with a colorectal cancer graft a correlation between ADC and both apoptotic index and proliferation index was observed [7].

Several clinical studies show that a higher pretreatment ADC value is associated with a poorer response to chemo- and/or radiotherapy [8; 9; 5; 10]. High ADC values indicate there are necrotic areas with poor vascular supply, which might explain detrimental treatment outcome [8; 11; 12]. Poor vascular supply with hypoxia leads to upregulated serum vascular endothelial growth factor (VEGF), which is associated with advanced disease stage and unfavorable outcome [13; 14].

In most tumors, including liver metastases of colorectal cancer, an increase in ADC after the start of treatment occurs in response to treatment, reflecting treatment-induced cell death [8; 15-19]. However, timing is essential to witness this response to treatment: in later stages of treatment, tissue reorganization results in the formation of fibrosis, which could alter ADC values again [20].

Before diffusion weighted imaging can be implemented in standard clinical practice, data on repeatability are needed to assess which differences outside the range of normal variation can be detected in an individual patient. Previously, in malignant hepatic tumors, mainly hepatocellular carcinoma, it has been shown that limits of agreement of the mean ADC value in repeated DWI ranged between 28.5% and 31.3% [21]. However, repeatability could depend on the specific type of tumor and its heterogeneity. In this study we assessed the repeatability of the mean tumor ADC value, as well as the repeatability of the distribution

of ADC values, using a histogram analysis. To provide a biological basis for these ADC values, we also assessed the relation between apoptosis marker p53, anti-apoptotic protein BCL-2, proliferation marker Ki67 and serum VEGF levels.

Materials and methods

Patients

Between August 2009 and January 2011, patients with liver metastases of colorectal cancer who were scheduled for metastasectomy were approached for participation in this study. Patients with a contra-indication to MRI (claustrophobia, MRI-incompatible implants, pacemaker) were excluded. Previous systemic treatment was allowed and patients received chemotherapy up until 1 month before study participation. No chemotherapy or other anti-tumor therapy was administered between the two DWI examinations. A total of 19 patients were included. This study had institutional review board approval (CMO region Arnhem-Nijmegen). All patients read and signed informed consent before entering the study.

DWI

Respiratory triggered diffusion weighted imaging was performed twice within a week. All patients underwent surgery within 3 weeks of the last measurement. Measurements were performed on a 1.5-Tesla whole body MR system (Magnetom Avanto, Siemens Medical Solutions, Erlangen, Germany) using the body coil for excitation and a six-channel body matrix coil combined with a 24- channel spine matrix coil for signal reception. DWI was performed with an EPI (echo planar imaging) sequence and diffusion weighted images were obtained in three orthogonal directions with *b*-values of 50, 300 and 600 s/mm^2. 2D-PACE (prospective acquisition correction) navigator triggering was applied to reduce breathing motion by synchronizing the measurement with the patient's breathing cycle. Parallel imaging combined with GRAPPA (generalised autocalibrating partially parallel acquisition) and an acceleration factor of 2 allowed increased imaging speeds, to further reduce motion artifacts. To suppress the fat signal, SPAIR (spectrally adiabatic inversion recovery) was included. Other imaging parameters were as follows: TR 2000 ms; TE 82 ms; 30 transversal slices of 6.0-mm thickness separated by 1.2 mm; field of view 400x400 mm; matrix size 192x192; bandwidth 1736 Hz/px; three averages; anterior–posterior phase encoding direction. The ADC images were calculated automatically by the Syngo VB17 software using a noise level of 10.

On all slices with visible tumor a region of interest (ROI) was drawn around the tumor. The ROI was drawn on the *b*_50 image for optimal contrast between tumor and background. Given the high contrast between the liver and the tumor on the low b-value images, no problems occurred drawing the regions of interest. Furthermore, of all patients recent FDG PET were available, which was used to eliminate any uncertainty whether a lesion could be

for example a cyst (with also high contrast) instead of a liver metastasis. ROIs on test and retest images were drawn in the same session by the same reader (a researcher with 2 years' experience) using Inveon Research Workplace (IRW 3.0, Siemens Healthcare). This software overlays the ADC map on the b-50 images. By adjusting the transparency of both layers the ROI can now be drawn in the exact right position in both layers at the same time. The ROI is therefore automatically in the exact right position on the ADC map. Afterwards all voxel ADC values in the ROI were exported to an Microsoft excel file. No voxel values were excluded from the analyses. The mean ADC, 10^{th}, 25^{th}, 50^{th}, 75^{th} and 90^{th} percentiles of all voxel ADC values in the tumor ROI were calculated.

Immunohistochemistry

Of 19 colorectal cancer patients who participated in the study histological material of 21 different liver metastases (from 17 different patients) was available for analysis. Immunohistochemistry of consecutive 5-µm paraffin-embedded sections was performed for Ki67 (proliferation), p53 and BCL-2 (anti-apoptosis). Sections were mounted on a SuperFrost slide and dried overnight at 37°C. Sections were deparaffinised in histosafe and rehydrated in graded ethanol solutions before staining. Sections were incubated in citrate buffer (pH 6.0). Staining was performed with commercially available antibodies. Ki67 was stained with a primary monoclonal mouse antibody MIB-1 (Dako, the Netherlands), p53 with mouse monoclonal p53 antibody clone DO-7 (Neomarkers, Fremont, CA, USA) and BCL-2 with monoclonal mouse BCL-2 antibody clone 124 (Dako, the Netherlands). For detection an anti-mouse polymer detection kit (PowerVision, Richmond, VA, USA) was used. Diaminobenzidine (DAB) was used as chromogen and hematoxylin was used as counterstaining.

BCL-2 staining was scored as negative or focally positive by an experienced pathologist. Other sections were digitalised using a light microscope (DM6000 Leica, Wetzlar, Germany; objective of 10× at 100× magnification) using a Macintosh computer running IPLab for Macintosh (Scanalytics Inc., Fairfax, VA, USA), which controlled this motorized system and generated 24-bit color composite images (pixel size 1.8 µm) as described previously by Rademakers et al [22]. An ROI was drawn around the tumor area, excluding evident necrosis. Necroses often gives aspecific staining results, and only a few data including necrotic areas were available for analyses. For all slices the optimal threshold for positive staining was determined. The fraction of positive staining in the tumor area and fraction of positive cells (labeling index) were determined using Image J software [22]. From the p53 and Ki67 sections the fraction-positive haematoxylin nuclear staining was determined and averaged. The positive nuclear fraction was used as a surrogate marker of cell density.

ELISA

Before imaging EDTA blood samples were taken from all 19 patients. Samples were kept on ice until centrifugation, 10 min 2000 rounds/min at 4°C. The plasma was frozen and stored at -80°C until further analysis. Plasma levels of VEGF-A and were determined in duplicate using an in-house available enzyme linked immunosorbent assay (ELISA). Mean concentrations per patient are reported in nanograms per millilitre (ng/L).

Statistics

A lesion-by-lesion analysis was performed to assess the intra-observer repeatability, by the use of a Bland–Altman analysis [23]. Because differences between the two acquisitions were not proportional to the mean ADC value, we expressed standard deviation, coefficient of repeatability and limits of agreement as absolute numbers instead of a percentage. Mean, standard deviation and coefficient of repeatability were calculated. Coefficient of repeatability was calculated using the formula: CR= 1.96*SD. The SD was calculated by squaring all the differences, adding them up, dividing them by the number of measurements and taking the square root [23]. The coefficient of repeatability describes -within the paired ADC measurements- the difference that is smaller in 95% of the pairs. Therefore, the coefficient of repeatability could also be viewed as a boundary: changes smaller than the coefficient of repeatability could come from measurement errors and normal variation, while larger changes can be considered real biological changes.

The limits of agreement were calculated by adding (upper limit) or subtracting (lower limit) the coefficient of repeatability from the mean difference. The coefficient of variation was calculated by dividing the standard deviation by the average of the mean ADC values.

As the mean ADC values of liver metastases were normally distributed, Student's t test was performed to assess whether the mean ADC values of tumors treated with systemic therapy before inclusion in the study differed from untreated tumors and to compare ADC values between BCL-2-positive and -negative tumors. A Pearson correlation coefficient was calculated between the fractions of positive staining and mean ADC values, measured on both examinations.

Results

Patients

Nineteen patients were included in this study. Because of illness, one patient did not complete the second MR examination. In total, 23 metastases were detected on DWI in 19 patients. The average size of the metastases was 31.3 cm^3 (range 0.7–130.4 cm^3), 18 metastases were located in the right liver lobe and 5 in the left liver lobe. Three patients who had completed both MRIs did not undergo the planned metastasectomy; one metastasectomy was converted to

radiofrequent ablation and two patients had unresectable metastases. Therefore, histological data were available for 16 patients. Most patients had received systemic treatment before inclusion in the study. An overview of the patients' characteristics is given in Table 1.

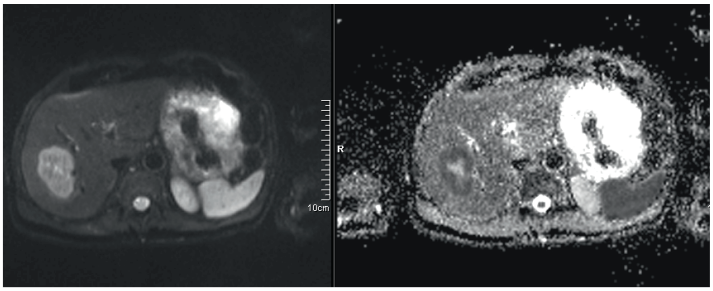

Figure 1. *Left: a b_50 weighted image. The contrast between metastasis and surrounding liver tissue is very clear. Right: the ADC map of the same metastasis showing a dark cell-dense rim and a light necrotic centre.*

Repeatability of DWI

Liver metastases were commonly visible on ADC maps as hypointense lesions (Fig. 1). Histogram analysis of the ADC values within the liver metastasis showed that the distribution did not follow a Gaussian distribution pattern, but has a positive skew (Fig. 2).

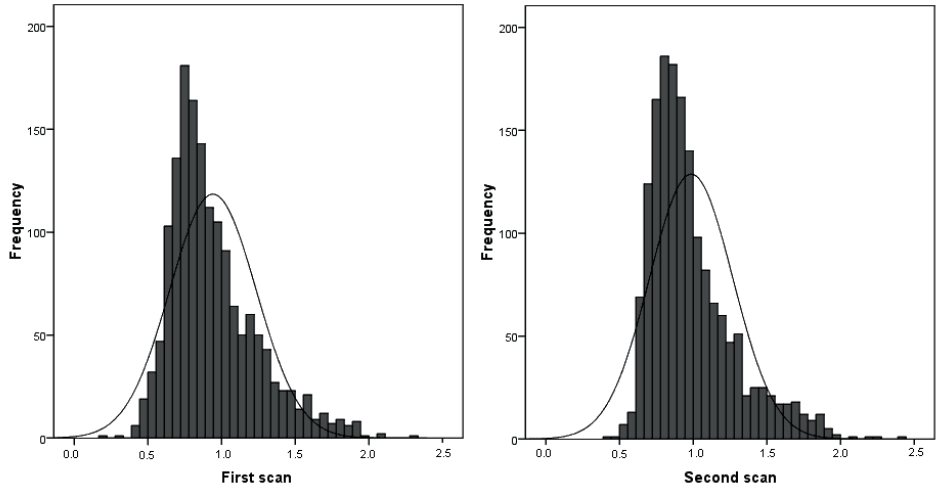

Figure 2. *Histograms of the ADC values of the metastasis obtained from the first and second DWI scan of the patient of which the images are shown in figure 1. A Gaussian distribution is represented by the black curve.*

	Gender	Age	Location primary tumor	DWI 1	DWI 2	Previous systemic therapy	Liver metastases
1	M	60	Rectum	complete	complete	Yes (Neoadjuvant)	Resected
2	F	50	Rectum	complete	complete	Yes (Neoadjuvant)	Unresectable
3	M	79	Caecum	complete	complete	Yes (Neoadjuvant)	Resected
4	A	56	Sigmoid	complete	complete	Yes (>1 year before study participation)	Resected
5	M	62	Sigmoid	complete	complete	Yes (>1 year before study participation)	Resected
6	F	48	Rectum	complete	complete	Yes (>1 year before study participation)	Resected
7	F	71	Sigmoid	complete	complete	Yes (7 months before study participation)	Resected
8	M	64	Caecum	complete	complete	Yes (> 1 year before study participation)	Conversion to RFA
9	M	59	Rectum	complete	complete	Yes (Neoadjuvant)	Resected
10	M	72	Sigmoid	complete	complete	Yes (2 months before study participation)	Resected
11	F	56	Sigmoid	complete	complete	Yes (>1 year before study participation)	Resected
12	M	69	Caecum	complete	- (felt unwell)	No	Unresectable
13	F	72	Rectum	complete	complete	Yes (>1 year before study participation)	Resected
14	M	61	Sigmoid	complete	complete	Yes (Neoadjuvant)	Resected
15	M	61	Sigmoid	complete	complete	No	Resected
16	M	76	Rectum	complete	complete	No	Resected
17	F	67	Caecum	complete	complete	Yes (Neoadjuvant)	Resected
18	M	61	Caecum	complete	complete	No	Resected
19	M	59	Rectum	complete	complete	No	Resected

Table 1. *Characteristics of all participating patients.*

The mean ADC value in all liver metastases was 1.17 (± 0.11) *10^{-3} mm^2/s. The coefficient of repeatability for the mean ADC value of the tumor, assessed by a lesion-by-lesion analyses of 21 metastases that were imaged twice, was 0.20 *10^{-3} mm^2/s. The limits of agreement were -0.22 and 0.19 *10^{-3} mm^2/s. The coefficient of variation was 8.9%.

Percentile	Mean (*10^{-3} mm^2/s)	Coefficient of repeatability (*10^{-3} mm^2/s)	Lower limit of agreement (*10^{-3} mm^2/s)	Upper limit of agreement (*10^{-3} mm^2/s)
Mean	1.17	0.20	-0.22	0.19
P10	0.76	0.26	-0.28	0.24
P25	0.95	0.25	-0.25	0.25
P50	1.16	0.22	-0.21	0.22
P75	1.37	0.22	-0.24	0.20
P90	1.72	0.28	-0.30	0.26

Table 2. *Mean, coefficient of repeatability and limits of agreement of the mean ADC, 10^{th}, 25^{th}, 50^{th}, 75^{th} and 90^{th} percentiles*

For all percentiles in the Bland–Altman analysis the distribution of differences versus the mean of all liver lesions showed that the difference in ADC values between the first and second examinations did not depend on the mean ADC value (Fig. 3).

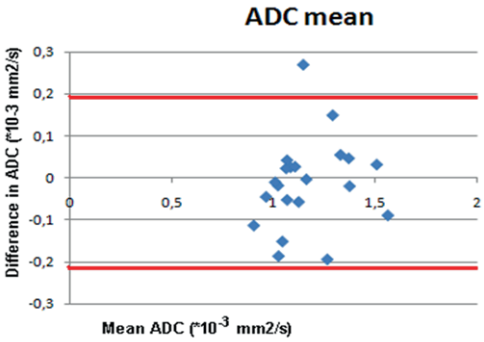

Figure 3. *Bland Altman plots of the mean ADC values of each metastasis showing the difference between the first and second scan on the y-axis and the mean ADC value on the x-axis. The red lines show the limits of agreement. The difference is not proportional to the mean ADC value.*

Furthermore, the repeatability of the ADC mean did not depend on the volume of the metastases, previous treatment or the location in the right or left liver lobe. Compared with the repeatability of the mean ADC value, the repeatability was slightly worse at the other points of the distribution. Nevertheless, for all percentiles the coefficient of repeatability was below 0.30 *10^{-3} mm^2/s (Table 2).

Apparent diffusion coefficient and previous treatment

The mean ADC value of the lesions in patients pretreated with systemic therapy was higher compared with the ADC of untreated lesions. The higher ADC values were more prominent in the most recently treated patients: metastases in patients who had received their last systemic treatment within 3 months of the first DWI had a mean ADC of 1.27 $*10^{-3}$ mm^2/s compared with 1.05 $*10^{-3}$ mm^2/s in previously untreated tumors (P=0.02) (Fig. 4).

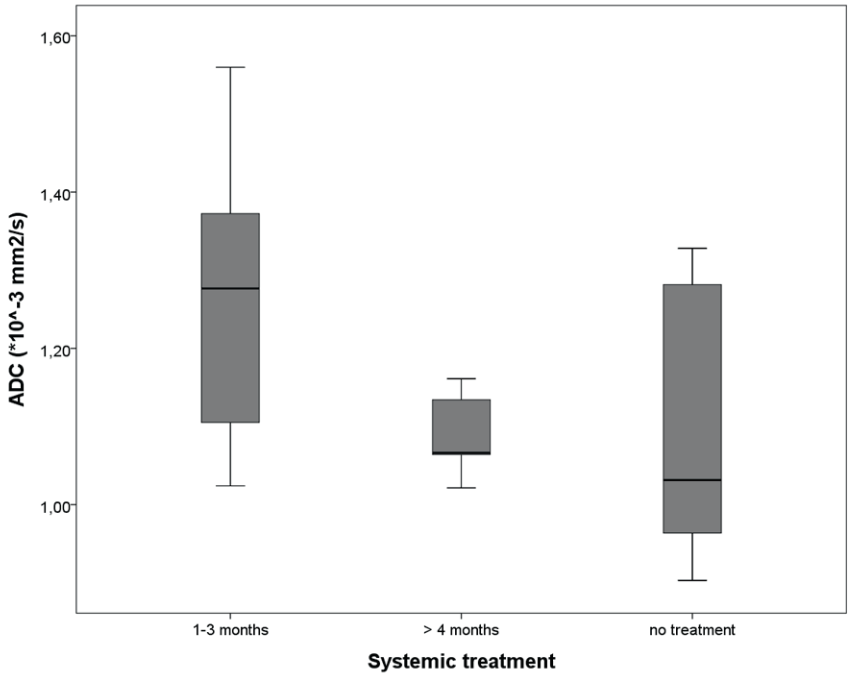

Figure 4. *Box plot of the mean ADC-values, showing a higher mean ADC-value in the recently treated tumor metastases. The mean ADC in recently treated metastases was 1.27 $*10^{-3}$ mm^2/s versus 1.05 $*10^{-3}$ mm^2/s in untreated tumors (p=0.02).*

Apoptosis and proliferation

The anti-apoptotic biomarker BCL-2 was expressed in 6 metastases. The mean ADC value of BCL-2-expressing metastases was significantly lower than the mean ADC of BCL-2-negative metastases (1.24 $*10^{-3}$ vs. 1.03 $*10^{-3}$ mm/s^2, P<0.01). Both the BCL-2-negative and focally positive group contained recently treated and chemotherapy-naive metastases.

p53 was expressed in most tumors. In 15 out of 21 tumors p53 was expressed in more than 1% of the nuclei. The other tumors had a very low expression of p53. The average labeling index of p53 was 0.20 (range 0.00–0.61). However, p53- expression did not correlate with the ADC value.

The average labeling index of the proliferation marker Ki67 was 0.13 (range 0.00–0.34). Ki67 significantly correlated with ADC values. The lower the ADC value the higher the proliferation index (r=-0.61, *P*=0.006). Both ADC and Ki67 labeling index correlated with nuclear density, which was used as a surrogate marker for cell density. A strong positive correlation was observed between Ki67 expression and the nuclear density (r=0.74, *P*<0.001), while a negative correlation between ADC and nuclear density was observed (r=-0.56, *P*=0.017) (Figs. 5, 6).

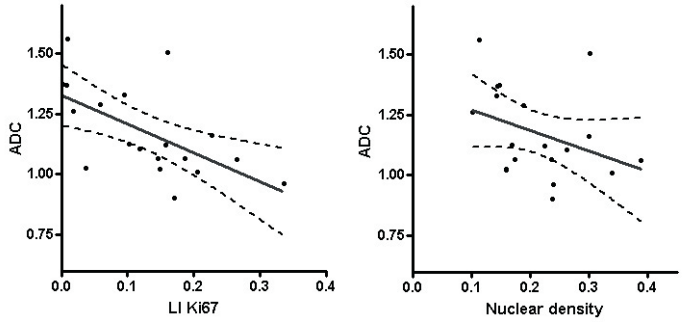

Figure 5. *A scatter plot (A) of the KI67 labeling index(x-axis) and mean ADC value (y-axis) shows a significant negative correlation, r=-0.61 p<0.01. The mean ADC value is negatively correlated to the nuclear density, the surrogate marker for cell density, r=-0.56 y p=0.02 (plot B).*

As the Ki67 expression and BCL-2 expression was only determined in vital tumor tissue, represented by the lower ADC values, we evaluated the relation between the 10th, 25th and 90th percentiles and the immunohistochemical results. The 90th percentile did not correlate with the labeling index of Ki67 (r=-0.16, *P*=0.52) and did not differ in BCL-2-negative or focally positive tumors (1.77 *10^{-3} vs. 1.75 *10^{-3} mm/s^2, *P*=0.92). However, for the 10th and 25th percentile ADC values a correlation with Ki67 was observed (r=-0.64, *P*=0.003 and-0.68, *P*=0.002, respectively). The 10th and 25th percentile ADC values were also significantly lower in BCL-2 focally positive tumors (0.64 *10^{-3} vs. 0.85 *10^{-3} mm/s^2, *P*=0.02 and 0.77 *10^{-3} vs. 1.02 *10^{-3} mm/s^2, *P*=0.008, respectively).

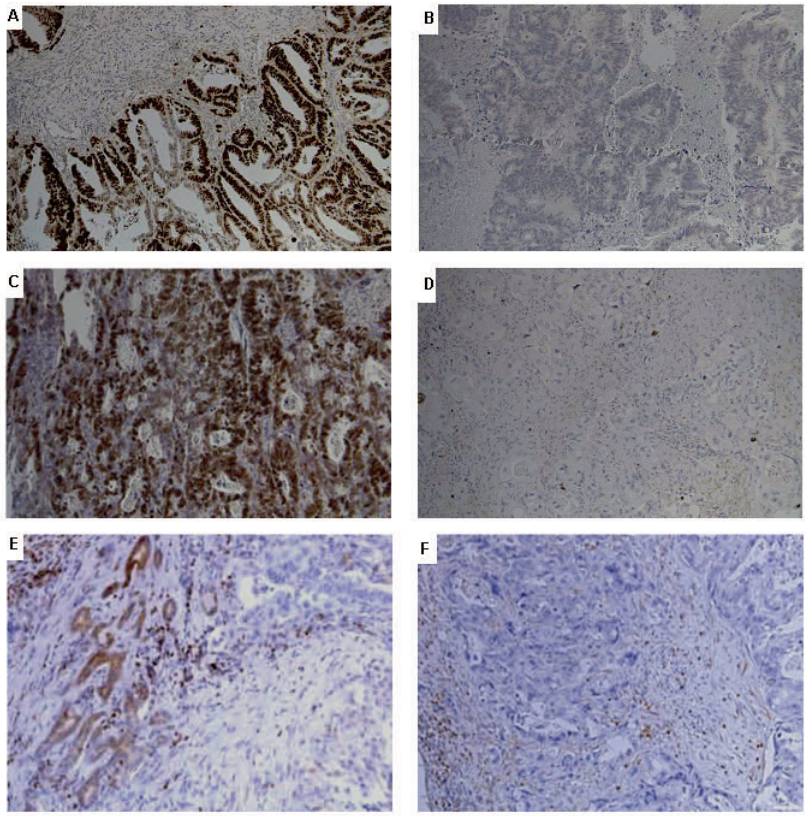

Figure 6. *Example of a tumor with a high (labeling index: 0.61) (A) and a tumor with low (labeling index: 0.00) (B) expression of p53 and an example of a tumor with high (labeling index: 0.34) (C) and low (labeling index: 0.00) (D) KI 67 expression, and an example of a tumor with focally positive BCL-2 staining(VD:124/mm^2) (E) and a tumor with no BCL-2 staining (F).*

VEGF

The average VEGF-A concentration in the serum was 4.0 ng/mL. VEGF concentration correlated with the mean ADC value in lesion(s) (r=0.59, *P*=0.004). We observed a higher VEGF-A concentration in sera of patients pretreated with systemic therapy: VEGF-A was 8.2 (± 2.5) ng/mL in patients pretreated with bevacizumab-containing neoadjuvant chemotherapy vs. 2.0 (± 1.1) ng/mL in all other patients (*P*<0.001) (Fig. 7).

Discussion

The mean findings of this study are a mean ADC in colorectal liver metastases of 1.17 *10^{-3} mm^2/s with a coefficient of repeatability of 0.20 *10^{-3} mm^2/s. The mean ADC value correlated with the expression of proliferation marker Ki67 and anti-apoptotic marker BCL-2.

Diffusion weighted imaging in liver metastases showed excellent repeatability, both compared with other imaging techniques and compared with other repeatability data from the DWI application. For instance, a previous study assessing repeatability of k_{ep} in liver metastases measured with dynamic contrast enhanced MRI observed a coefficient of repeatability of 0.009 with a mean value of 0.033 (27%) [24]. Moreover, the repeatability of oesophageal and breast cancer measured with FDG and FLT-PET was approximately 30% [25]. The repeatability was also better compared with primary liver tumors measured with DWI [21]. Good repeatability may be (partly) due to the use of respiratory triggering, minimizing the negative effects of breathing movement.

However, the most important question remains whether the repeatability is sufficient to use DWI for (early) response monitoring. Cui et al showed that the mean ADC of average liver metastases responding to chemotherapy increased by 0.22 after 1 week of treatment, while non-responding lesions did not change significantly [8]. Koh et al [16] measured liver metastases before and after chemotherapy and found that the responding lesion (measured with b-values 150–500) increased from a mean of 1.15 $*10^{-3}$ mm^2/s before treatment to 1.41 $*10^{-3}$ mm^2/s at the end of treatment. According to the repeatability established in our study, these reported changes can be detected confidently by our measurement technique.

Although histopathology only represents a small vital tumor area and the ADC value represents the entire tumor, the mean ADC showed an excellent correlation with histopathological data, as did the 10^{th} and 25^{th} percentiles. Conversely, the high ADC values (90^{th} percentile) did not correlate with histopathology, suggesting that the low ADC values, which represent vital tumor tissue, correlate better with histopathology than the high ADC values, which represent the excluded necrotic and non-vital areas. Mean ADC was significantly lower in BCL-2-expressing tumors, which could be explained by the anti-apoptotic effect of this protein. By prevention of apoptosis more cell membranes will remain intact, and therefore promote a low mean ADC value. However, the labeling index of p53 did not correlate with the mean ADC value. The effect of p53 expression and p53-regulated apoptosis on cell density and thus ADC value may not be straightforward. Accumulation of p53, as detected by immunohistochemistry, does not necessarily imply the presence of mutated, inactive p53. Furthermore, the absence of p53 accumulation does not always mean that functional p53 is present, for instance when p53 is deleted [26].

The ADC value was inversely correlated with the proliferation index, measured by Ki67 expression. This is probably due to the influence of proliferation on the cell density of the tissue. We used the fraction of positive haematoxylin staining in the tumor area as a surrogate marker of cell density and observed a correlation of both Ki67 with cell density as well as a correlation of ADC values with cell density. Of course the fraction of the tumor with positive staining for nuclei depends not only on cell density, but also on the size of the nuclei and number of nuclei per cell.

Finally, the ADC values correlated with the VEGF concentrations in the plasma of patients. Metastases treated with bevacizumab-containing regimens had a higher ADC value, and higher VEGF levels in their plasma. An increased (bound) VEGF level in the serum after bevacizumab administration has been observed in several studies [27]. A possible explanation is that the clearance of VEGF bound to bevacizumab is lower than that of free VEGF. As a result, the total VEGF level may rise while the free (functional) VEGF levels may decrease during bevacizumab treatment [28]. However, VEGF is also known to increase vascular permeability [29]. Therefore, VEGF levels could also have a direct impact on ADC values, which could also explain the correlation between ADC and VEGF level.

In conclusion, we observed an excellent repeatability coefficient of the mean ADC in colorectal liver metastases. The ADC value was related to the proliferation index and BCL-2 expression of the metastases. Furthermore, in recently treated metastases the ADC value was notably higher. The very good repeatability, the correlation with histopathology and the implied sensitivity for systemic treatment-induced antitumor effects suggest that DWI might be an adequate tool for response monitoring in metastatic colorectal cancer.

Reference List

[1] Malvezzi M, Bertuccio P, Levi F, La Vecchia C, Negri E (2012) European cancer mortality predictions for the year 2012. Ann Oncol 23:1044-1052

[2] Manfredi S, Lepage C, Hatem C, Coatmeur O, Faivre J, Bouvier AM (2006) Epidemiology and management of liver metastases from colorectal cancer. Ann Surg 244:254-259

[3] Tol J, Koopman M, Cats A, et al. (2009) Chemotherapy, bevacizumab, and cetuximab in metastatic colorectal cancer. N Engl J Med 360:563-572

[4] Heijmen L, Verstappen MC, Ter Voert EE, et al. (2012) Tumour response prediction by diffusion-weighted MR imaging: Ready for clinical use? Crit Rev Oncol Hematol doi:10.1016/j.critrevonc.2011.12.008

[5] Koh DM, Collins DJ (2007) Diffusion-weighted MRI in the body: applications and challenges in oncology. AJR Am J Roentgenol 188:1622-1635

[6] Yablonskiy DA, Sukstanskii AL (2010)Theoretical models of the diffusion weighted MR signal. NMR Biomed 23:661-681

[7] Zhang XY, Sun YS, Tang L, Xue WC, Zhang XP (2011) Correlation of diffusion-weighted imaging data with apoptotic and proliferation indexes in CT26 colorectal tumor homografts in balb/c mouse. J Magn Reson Imaging 33:1171-1176

[8] Cui Y, Zhang XP, Sun YS, Tang L, Shen L (2008) Apparent diffusion coefficient: potential imaging biomarker for prediction and early detection of response to chemotherapy in hepatic metastases. Radiology 248:894-900

[9] Dzik-Jurasz A, Domenig C, George M, et al. (2002) Diffusion MRI for prediction of response of rectal cancer to chemoradiation. Lancet 360:307-308

[10] Mardor Y, Roth Y, Ochershvilli A, et al. (2004) Pretreatment prediction of brain tumors' response to radiation therapy using high b-value diffusion-weighted MRI. Neoplasia 6:136-142

[11] Herneth AM, Guccione S, Bednarski M (2003) Apparent diffusion coefficient: a quantitative parameter for in vivo tumor characterization. Eur J Radiol 45:208-213

[12] Uhl M, Saueressig U, van Buiren M, et al. (2006) Osteosarcoma: preliminary results of in vivo assessment of tumor necrosis after chemotherapy with diffusion- and perfusion-weighted magnetic resonance imaging. Invest Radiol 41:618-623

[13] De Vita F, Orditura M, Lieto E, et al. (2004) Elevated perioperative serum vascular endothelial growth factor levels in patients with colon carcinoma. Cancer 100:270-278

[14] Galizia G, Lieto E, Ferraraccio F, et al. (2004) Determination of molecular marker expression can predict clinical outcome in colon carcinomas. Clin Cancer Res 10:3490-3499

[15] Hamstra DA, Galban CJ, Meyer CR, et al. (2008) Functional diffusion map as an early imaging biomarker for high-grade glioma: correlation with conventional radiologic response and overall survival. J Clin Oncol 26:3387-3394

[16] Kim SH, Lee JY, Lee JM, Han JK, Choi BI (2011) Apparent diffusion coefficient for evaluating tumour response to neoadjuvant chemoradiation therapy for locally advanced rectal cancer. Eur Radiol

[17] Koh DM, Scurr E, Collins D, et al. (2007) Predicting response of colorectal hepatic metastasis: value of pretreatment apparent diffusion coefficients. AJR Am J Roentgenol 188:1001-1008

[18] Mardor Y, Pfeffer R, Spiegelmann R, et al. (2003) Early detection of response to radiation therapy in patients with brain malignancies using conventional and high b-value diffusion-weighted magnetic resonance imaging. J Clin Oncol 21(6):1094-1100

[19] Song I, Kim CK, Park BK, Park W (2010) Assessment of response to radiotherapy for prostate cancer: value of diffusion-weighted MRI at 3 T. AJR Am J Roentgenol 194:W477-W482

[20] Desar IM, van Laarhoven HW, Hambrok T, et al. (2010) Assessment of early vascular effects of the angiogenesis inhibitor sunitinib (SU) in renal cell carcinoma (RCC) by dynamic contrast enhanced MRI (DCE-MRI) and diffusion weight MRI (DWI) at 3 tesla (T). ASCO (abstract)

[21] Kim SY, Lee SS, Byun JH, et al. (2010) Malignant hepatic tumors: short-term repeatability of apparent diffusion coefficients with breath-hold and respiratory-triggered diffusion-weighted MR imaging. Radiology 255:815-823

[22] Rademakers SE, Rijken PF, Peeters WJ, et al. (2011) Parametric mapping of immunohistochemically stained tissue sections; a method to quantify the colocalization of tumor markers. Cell Oncol (Dordr) 34:119-129

[23] Bland JM, Altman DG (1986) Statistical methods for assessing agreement between two methods of clinical measurement. Lancet 1:307-310

[24] van Laarhoven HW, Rijpkema M, Punt CJ, et al. (2003) Method for quantitation of dynamic MRI contrast agent uptake in colorectal liver metastases. J Magn Reson Imaging 18:315-320

[25] Hatt M, Cheze-Le Rest C, Aboagye EO, et al. (2010) Repeatability of 18F-FDG and 3'-deoxy-3'-18F-fluorothymidine PET tumor volume measurements. J Nucl Med 51:1368-1376

[26] Munro AJ, Lain S, Lane DP (2005) P53 abnormalities and outcomes in colorectal cancer: a systematic review. Br J Cancer 92:434-444

[27] Stefanini MO, Wu FT, Mac Gabhann F, Popel AS (2010) Increase of plasma VEGF after intravenous administration of bevacizumab is predicted by a pharmacokinetic model. Cancer Res 70:9886-9894

[28] Hsei V, Deguzman GG, Nixon A, Gaudreault J (2002) Complexation of VEGF with bevacizumab decreases VEGF clearance in rats. Pharm Res 19:1753-1756

[29] Nagy JA, Benjamin L, Zeng H, Dvorak AM, Dvorak HF (2008) Vascular permeability, vascular hyperpermeability and angiogenesis. Angiogenesis 11:109-119

4

Repeatability and biological basis of in vivo T_2^* magnetic resonance imaging of liver metastasis of colorectal cancer

Abstract

In this study the repeatability of T_2* MR imaging in colorectal liver metastases was assessed and T_2* values were correlated with the expression of the hypoxia related markers GLUT-1 and CA-IX as well as the relative vascular area, and the vessel density in resected tumors. The repeatability of T_2* was analyzed in 18 patients with in total 22 colorectal liver metastases using the Bland & Altman method for the 16^{th} , 50^{th}, and 84^{th} percentile values. Immunohistochemical staining was performed on 17 resected tumors obtained from 16 patients. The median T_2* of all liver metastases was 25.0 ± 5.6 ms vs. 23.0 ± 4.1 ms (median ± st.dev.) in normal liver. The coefficient of repeatability was 11.2 ms and the limits of agreement were -13.2 ms and 9.1 ms for median T_2* values. On average T_2* showed fair repeatability. No correlations between T_2* values, hypoxia and vascularity related markers were observed.

Introduction

In colorectal cancer about 50% of the patients develop distant metastasis, mainly in the liver (1–3). Resection of colorectal metastases can only be performed in few patients with metastatic disease. Currently, non resectable metastatic disease is treated with cytotoxic drugs like 5-fluorouracil, capecitabine, oxaliplatin and/or irinotecan, often combined with bevacizumab, an antibody against vascular endothelial growth factor. In standard clinical practice, approximately six to nine weeks after start of treatment, computed tomography is performed and tumor size is assessed to evaluate treatment. Monitoring response at an earlier stage is desirable, as only a subset of patients receiving chemotherapy responds to this potentially toxic and expensive therapy. Therefore, predictive markers are needed to determine treatment efficacy at an early stage.

Changes in tumor size can also be imaged with magnetic resonance (MRI), which in addition offers the potential to acquire functional information, for example, dynamic contrast enhanced MRI (DCE-MRI) to measure tumor vascularity (4). There is an increasing interest in MR to image T_2*, also known as R_2* (=1/T_2*), intrinsic susceptibility-weighted or blood oxygenation level dependent (BOLD) MRI, as an alternative for DCE-MRI as this circumvents the need for contrast agent administration (5–10). The transverse magnetization relaxation T_2* is a combination of spin-spin relaxation and magnetic field inhomogeneity (11). A major factor affecting T_2* relaxation is deoxygenated hemoglobin in blood. When hemoglobin is oxygenated, it is diamagnetic, but when deoxygenated, it becomes paramagnetic (12,13). Paramagnetic deoxyhemoglobin affects the local magnetic field sensed by nearby water protons in blood and surrounding tissues, which leads to a decrease in the T_2* time. Specific parameters that may influence T_2* in tissue are blood oxygen saturation, hematocrit, blood flow, and blood volume (14). In vessels near hypoxic tissue, it is likely that more oxygen is released from hemoglobin. If blood flow remains the same this will result in a higher deoxyhemoglobin level and therefore the T_2* relaxation time in and near the vessel will decrease. This is of clinical importance, since hypoxic tumors are likely to have an increased resistance to radiation therapy and chemotherapy (15,16).

Tumor hypoxia may result from poor vascularity in solid tumors and is associated with a higher uptake of glucose by glucose transporters (GLUT1) and increased H^+ ion production. Intracellular H^+ and HCO^{3-} ions can form H_2O and CO_2 which can freely diffuse through the cell membrane. Once outside the cell, membrane-bound carbonic anhydrase IX (CA-IX) catalyzes the reverse process. Next, the HCO^{3-} ions are transported back into the cell thereby trapping the H^+ ions in the extracellular space. Therefore, in hypoxic conditions, GLUT1 and CA-IX are up-regulated and can be used as surrogate measures of hypoxia in tumors (17).

To predict treatment outcome or monitor therapy, differences in T_2* should reflect true differences in tumor biology and not variations in the MR system or body physiology.

Knowledge of repeatability is of special relevance in early response monitoring. Therefore, this study aimed to assess the repeatability of T_2* MRI in colorectal liver metastases next to normal appearing liver. As T_2* is expected to be governed by tumor hypoxia and tissue vascularity we also investigated the correlation of T_2* with the expression of the hypoxia related markers GLUT-1 and CA-IX as well as the relative vascular area (RVA), and vessel density (VD) as measures of vascularity in metastases.

Methods

Patients

Between August 2009 and January 2011 twenty patients with liver metastases of histologically proven colorectal cancer, who were scheduled for metastasectomy were included. Prior to surgery, patients underwent two MRI examinations to assess repeatability. Two of these patients did not complete the MR part of the study. The remaining eighteen patients, eleven males and seven females, were analyzed in this study. Median age was 61 years (range 48 – 79). All measurements were carried out after approval of the local institutional medical ethics committee and written informed consent was obtained from each patient.

Magnetic resonance imaging

All MRI examinations were performed on a 1.5T whole body MR system (Magnetom Avanto, Siemens Healthcare, Erlangen, Germany) using the body coil for excitation and a six channel body matrix coil combined with a twenty-four channel spine matrix coil for signal reception. After conventional T_1- and T_2-weighted imaging, T_2* imaging was performed using a spoiled gradient-recalled echo, FLASH 2D, sequence. Every image slice was obtained with a TR of 225 ms, and multiple TE values (4.76, 9.53, 14.29, 19.06, 23.82, 28.58, 33.35, 38.11, 42.88, 47.64, 52.40 ms). Other scan parameters were: flip angle: 25 degrees, field of view: 400 mm, slice thickness: 6.0 mm, matrix size: 128x128. Parallel acquisition (GRAPPA) with an acceleration factor of 2 was used. Patients continued normal shallow breathing during the scans, no breath-hold or respiratory gating was applied. T_2* imaging was followed by diffusion weighted MRI (DWI) as colorectal liver metastasis are usually clearly visible on these images. DWI was performed with respiratory triggered echo planar imaging (EPI) sequence and b-values 50-300-600 s/mm^2 in three orthogonal directions. The measurement protocol was repeated after 2-8 days (median: 4 days).

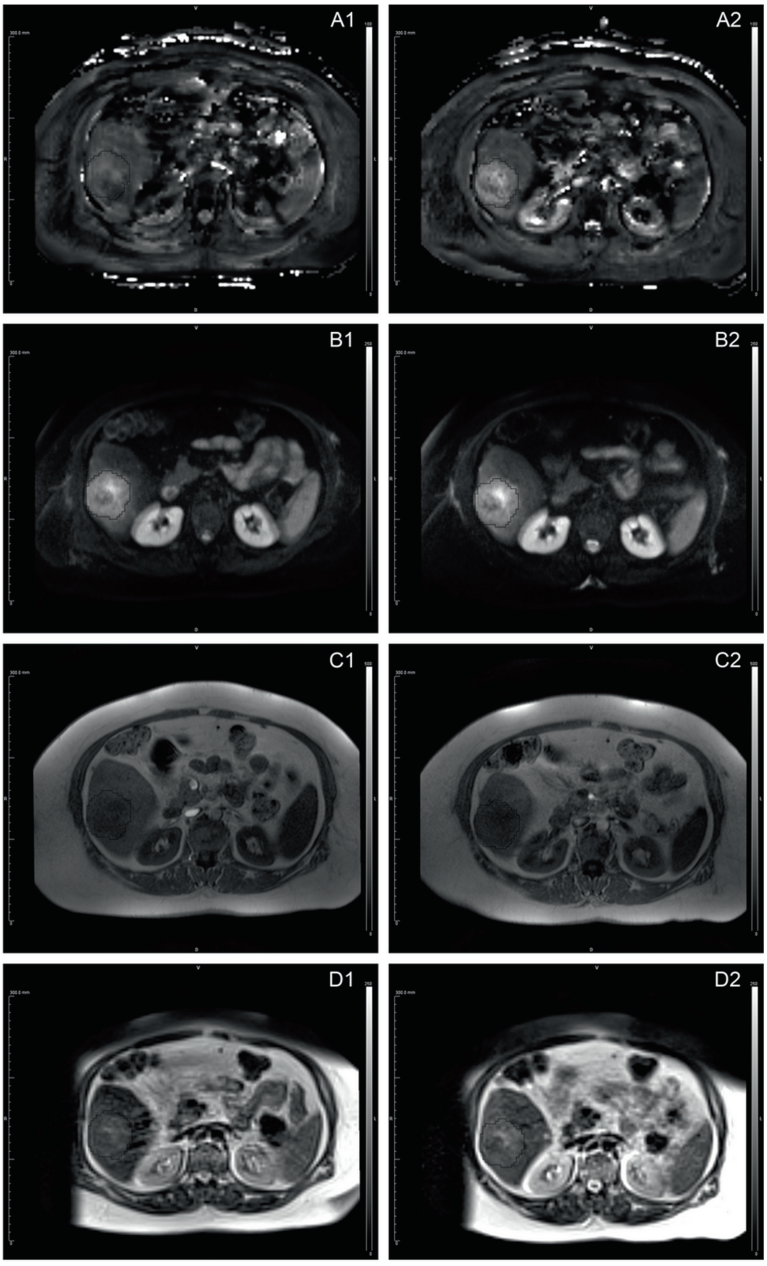

Figure 1. *Example of a T_2* map (A), a diffusion weighted b=50 s/mm^2 image (B), a T_1 (C) and a T_2 weighted image (D), at the same location, in the same patient. Images on the left are obtained on scan day one, images on the right on scan day two.*

MR post processing

T_2* maps were generated using in-house built software based on Matlab (MathWorks, Natick, MA, USA). The echo time data was fitted pixel by pixel to a mono-exponential curve $SI = A\ \rho\ exp(- TE / T_2^*) + B$ where ρ is the proton density, TE is the echo time, and the parameter of interest T_2*, the relaxation time. An arbitrary scale factor A, and a baseline B, were added to incorporate scanner dependencies.

Software allowed to overlay the DWI (b=50 s/mm^2) images, the T_1 and T_2 weighted images on the calculated T_2* maps. By adjusting the transparency of the different layers, 3D regions of interest (ROIs) could be drawn in the exact right position in all layers at the same time using the information from all the different imaging techniques. To compare the repeatability of the lesions with that of normal liver tissue, additional 3D ROIs with the same volume and in the same liver region as the lesions were drawn in normal appearing liver tissue excluding large blood vessels and bile ducts. Datasets obtained on scan day one and scan day two were processed in the same session to be able to draw the liver ROIs in both datasets in the same position. In addition, all ROIs were drawn by same reader (a researcher with 4 years' experience). Voxel values inside the ROIs were extracted and analyzed in a histogram, which provided additional information on the distribution of T_2* values within the lesion or normal appearing liver tissue.

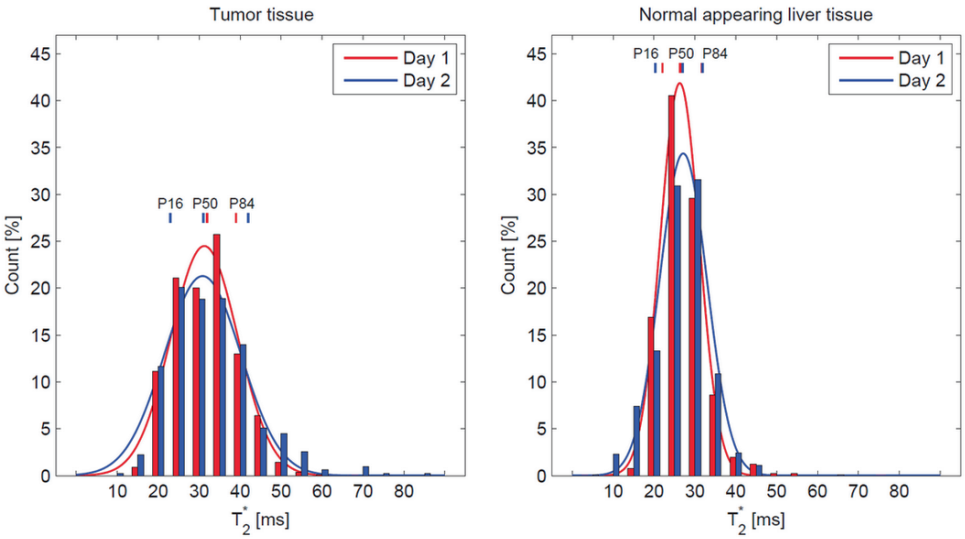

Figure 2. *Example of the histogram distribution of T_2* values in a tumor ROI (left) and in a size matched normal appearing liver ROI (right). The bars indicate the counts on scan day one (red) and two (blue), the Gaussian shaped curves in the background are fitted normal distributions for scan day one (red) and two (blue). The vertical lines above the bars indicate the 16th, 50th and 84th percentile values in the measured data for scan day one (red) and two (blue).*

An example of a ROI drawn on a calculated T_2* map, together with a diffusion weighted b=50 s/mm^2 image and conventional T_1 and T_2 weighted images is shown in figure 1. Figure 2 shows an example of the histogram distribution of T_2* values in a tumor ROI and in a size matched normal appearing liver ROI.

Immunohistochemistry

Immunohistochemical staining was performed on 17 resected tumors obtained from 16 patients to assess the relation between T_2*, hypoxia and tumor vascularity. Expressions of GLUT-1 and CA-IX were investigated as hypoxia related markers, and the expression of CD34 as a marker of tumor vascularity. The following protocol describes the immunohistochemical staining and scoring of the resected liver metastasis sections.

First, H&E-staining (hematoxylin and eosin) was performed. If viable tumor cells were present, immunohistochemistry of 5 µm paraffin embedded sections was performed.

For all immunohistochemical staining sections were deparaffinized in histosafe and rehydrated in graded ethanol solutions and kept for 30 minutes in Target Retrieval Solution. The peroxidases in the sections were blocked by keeping them in 3% H_2O_2 in methanol for 15 minutes. The sections were preincubated with 5% normal donkey serum in primary antibody diluent (PAD, Abcam, Cambridge, UK) for 30 minutes at room temperature.

For GLUT-1 staining rabbit-anti-GLUT-1 (RB-9052 P1) 1:400 in PAD was used for 45 minutes in 37 °C, followed by donkey anti-rabbit biotine 1:500 in a phosphate buffer solution (PBS) for 60 minutes at room temperature. For CA-IX staining mouse-anti-CA-IX (1:25 in PAD) was applied on the tumor sections and kept overnight at 4 °C. Sections were incubated with a second antibody, F(ab')2-Donkey-anti-mouse IgG BIOTINE (1:200 in PBS) for 60 min. at room temperature. For CD34 staining mouse-antiCD34 (1:10 in PAD) was applied to all tumor sections and kept overnight at 4 °C. The sections were incubated with a second antibody, F(ab')2-Donkey-anti-mouse IgG (1:200 in PBS) for 60 min. at room temperature.

All sections were stained with diaminobenzidine (DAB) for 10 minutes. Hematoxylin was used for counterstaining. Sections were dehydrated and mounted with KP mounting medium. Between all steps, the sections were rinsed with PBS.

All slices were digitized using a bright field light microscope equipped with a 10× magnification objective lens (Leica, Wetzlar, Germany) and Image Processing Lab software (Scanalytics Inc., Fairfax, VA, USA). A region of interest was drawn around the tumor area, excluding evident necrosis. For all slices the optimal threshold for positive staining was determined. The fraction of positive staining in the tumor area and the fraction of positive cells were calculated (18). With CD34 the relative vascular area in the tumor area was calculated and the number of vessels per square mm were scored.

Statistics

Statistical analysis were done using the PASW Statistics 18.0.2 (IBM Corporation, Armonk, New York, USA) and Prism 4.0 (GraphPad Software Inc., La Jolla, San Diego, CA, USA) software packages. For each lesion and volume matched normal liver region the 16th, 50th, and 84th percentiles of the T_2* values were calculated. The 50th percentile is also known as the median and equals the mean in a normal distribution. To provide more insight in the distribution of the T_2* values, the 16th and 84th percentile values were added, since they are one standard deviation from the mean in a normal distribution.

The Wilcoxon signed rank test was applied to indicate significant differences between the 16th, 50th, and 84th percentile values of tumor on day one and two, liver on day one and two, tumor and liver on day one, and tumor and liver on day two.

Spearman's rank correlation coefficient was applied to test for significant correlations between the 16th, 50th, and 84th percentile values and lesion size. And the same test was repeated for the normal appearing liver regions.

The repeatability was assessed using Bland Altman analyses (19,20). In the Bland-Altman plot the difference in median T_2* values measured on the first and second scan day is plotted against the mean of the two median T_2* values. The coefficient of repeatability describes, within the paired T_2* measurements, the difference that is smaller in 95% of the pairs. The coefficient of repeatability can also be seen as a boundary: changes smaller than the coefficient of repeatability could come from measurement errors and normal biological variation, while larger changes can be considered real biological changes e.g. after applying therapy. The coefficient of repeatability can be calculated by multiplying the standard deviation of the difference with 1.96. The 1.96 stems from the normal distribution where 95% of the measurements are within 1.96 times the standard deviation. The standard deviation of the difference was calculated by squaring all the differences, taking the sum and dividing it by the number of measurements and finally taking the square root. The limits of agreement were calculated by adding (upper limit) or subtracting (lower limit) the coefficient of repeatability from the mean difference. This was repeated for the normal appearing liver regions and for the 16th and 84th percentile values of the T_2* values to provide more insight in the repeatability of the distribution of the T_2* values.

Spearman's rank correlation coefficients were calculated between the average T_2*, by averaging the two median T_2* values of both the first and the second scan, and the expression of the hypoxia related markers GLUT-1 and CA-IX as well as the relative vascular area, and the vessel density. This was again repeated for the 16th and 84th percentile values of the T_2* values.

Results

A total of 22 colorectal liver metastases were analyzed in 18 patients. Median tumor size was 8.03 cm^3 (range 0.87-138 cm^3). The medians of the 16th, 50th, and 84th percentile values of T_2* are listed in table 1.

		Median T_2*		Median T_2*	Limits of agreement		Coefficient of repeatability	
		Day 1	**Day 2**	**Day 1 & 2**				
		[ms]	**[ms]**	**[ms]**	**[ms]**	**[ms]**	**[ms]**	**[% of median]**
Tumor	**P16**	19.0	16.8	17.8 ± 4.9	-8.2	7.7	7.9	44.7
	P50	24.5	24.0	25.0 ± 5.6	-13.2	9.1	11.2	44.6
	P84	31.5	32.0	30.2 ± 10.2	-18.7	14.1	16.4	54.4
Liver	**P16**	17.0	17.4	17.1 ± 4.7	-9.1	6.4	7.8	45.3
	P50	22.0	24.1	23.0 ± 4.1	-9.9	6.5	8.2	35.6
	P84	26.8	28.7	27.6 ± 4.8	-8.7	6.8	7.7	28.0

Table 1. *The median T_2* values on day one, median T_2* values on day two, the median T_2* values on day one and two (by first averaging per ROI the day one and two values) ± standard deviation, the limits of agreement, and the coefficient of repeatability of the Bland Altman analysis for the 16th, 50th and 84th percentiles*

There was no significant difference (Wilcoxon signed-rank test) between the 16th, 50th, and 84th percentile values measured on scan day one and two for tumor tissue nor for the normal appearing liver tissue. There was also no difference (Wilcoxon signed-rank test) between the 16th and 50th percentile values of tumor and normal appearing liver tissue. There was however a significant difference between the 84th percentile values of tumor and normal appearing liver for both the day one and two measurements (Wilcoxon signed-rank test (tumor – liver); day one: z=-2.99, p<0.01; day two: z=-2.88, p<0.01; both based on a positive rank). This indicates that the tumor tissue has more higher T_2* values then the normal liver tissue.

The 16th and 50th percentile values of the tumors and the size matched liver regions were not significantly correlated (Spearman's rank correlation coefficient) to their volume, calculated as the volume of the 3D ROIs. The 84th percentile values on the other hand, were significantly correlated (tumor: r=0.48, p=0.02; liver: r=0.52, p=0.01) to their volume. The standard deviation of the T_2* values of the tumors and the size matched liver regions was also significantly correlated (tumor: r=0.71, p<0.01; liver: r=0.73, p<0.01) to their volume. This indicates that larger ROIs have a larger spread and higher T_2* values.

The coefficient of repeatability for the median T_2* values was 11.2 ms for liver metastases and 8.2 ms for the normal appearing liver regions (table 1, figure 3). The limits of agreement for median T_2* values were-13.2 ms and 9.1 ms for liver metastases and-9.9 ms and 6.5 ms for the normal appearing liver regions. Small differences in the distribution are seen between

measurement day one and two. Besides the median or 50th percentile value, the Bland Altman analyses was also performed on the 16th and 84th percentile values, to provide more insight in the actual distribution of T_2* values in each lesion. The coefficient of repeatability and the range indicated by the limits of agreement, increase with increasing percentile values in tumor tissue but remains constant in normal liver tissue (table 1, figure 3). The Bland Altman plots in figure 3 show that the differences do not vary in any obvious systematic way over the range of measurement. In case the differences would be proportional to the mean for example, a cone shaped cloud of data points would be visible, and a log transform of the data would be recommended (20,21). Kendall's tau rank correlation coefficient test confirmed that there was no correlation between the difference in T_2* and the mean T_2*. The only exception was the 50th percentile of the liver which had a negative correlation of -0.38 and a p-value of 0.02. The data was however not transformed since the correlation was only minor and transformed data is often more difficult to interpret.

T_2 and the correlation with markers of hypoxia and vascularity*

Histologic material was obtained from 17 resected tumors in 16 patients. An example of the immunohistochemical stained sections is shown in figure 4. After carefully analyzing the stained sections and performing Spearman's rank correlation coefficient between the median T_2* and the expression of GLUT-1, CA-IX, the relative vascular area, and vessel density, no significant correlations were found (table 2). In addition, the 16th and 84th percentile values of T_2* also showed no significant correlation.

		Spearman's rank correlation coefficient								
		Glut-1		**CA-IX**		**RVA**		**VD**		
		r	**p-value**	**r**	**p-value**	**r**	**p-value**	**r**	**p-value**	
Tumor	**P16**	-0.03	0.90	0.15	0.55	0.30	0.24	0.12	0.65	
	P50	-0.11	0.67	-0.13	0.61	0.22	0.40	0.14	0.58	
T_2*	**P84**	0.17	0.52	-0.06	0.82	0.28	0.28	0.17	0.51	

Table 2. *The Spearman's rank correlation coefficients and p-values between the 16th, 50th and 84th percentile values of T_2* and GLUT-1, CA-IX, the relative vascular area (RVA), and the vessel density (VD).*

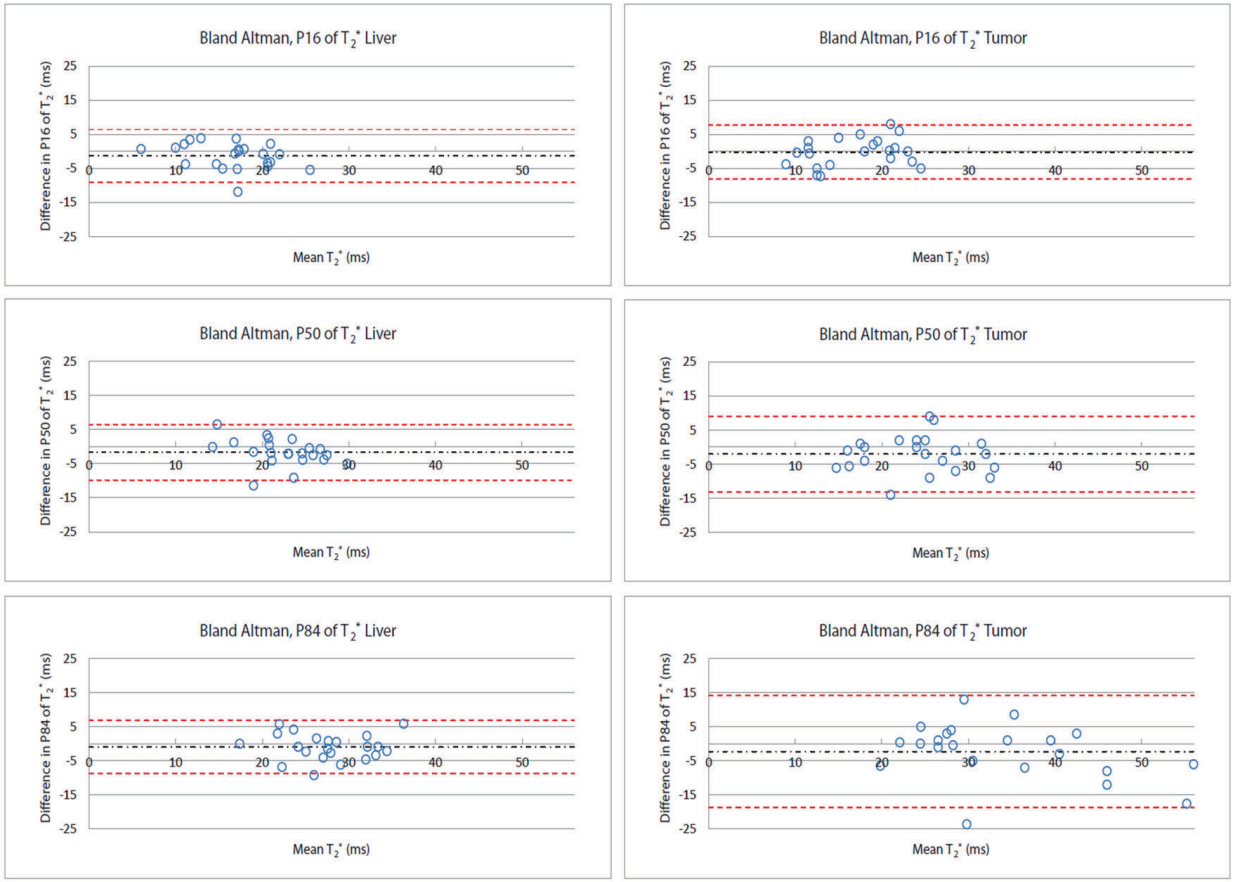

Figure 3. *Bland Altman analysis of the 16th, 50th and the 84th percentile of the T_2* values in normal appearing liver tissue (left) and tumor (right). The black dot-dashed lines indicate the mean difference and the red dashed lines indicate the limits of agreement.*

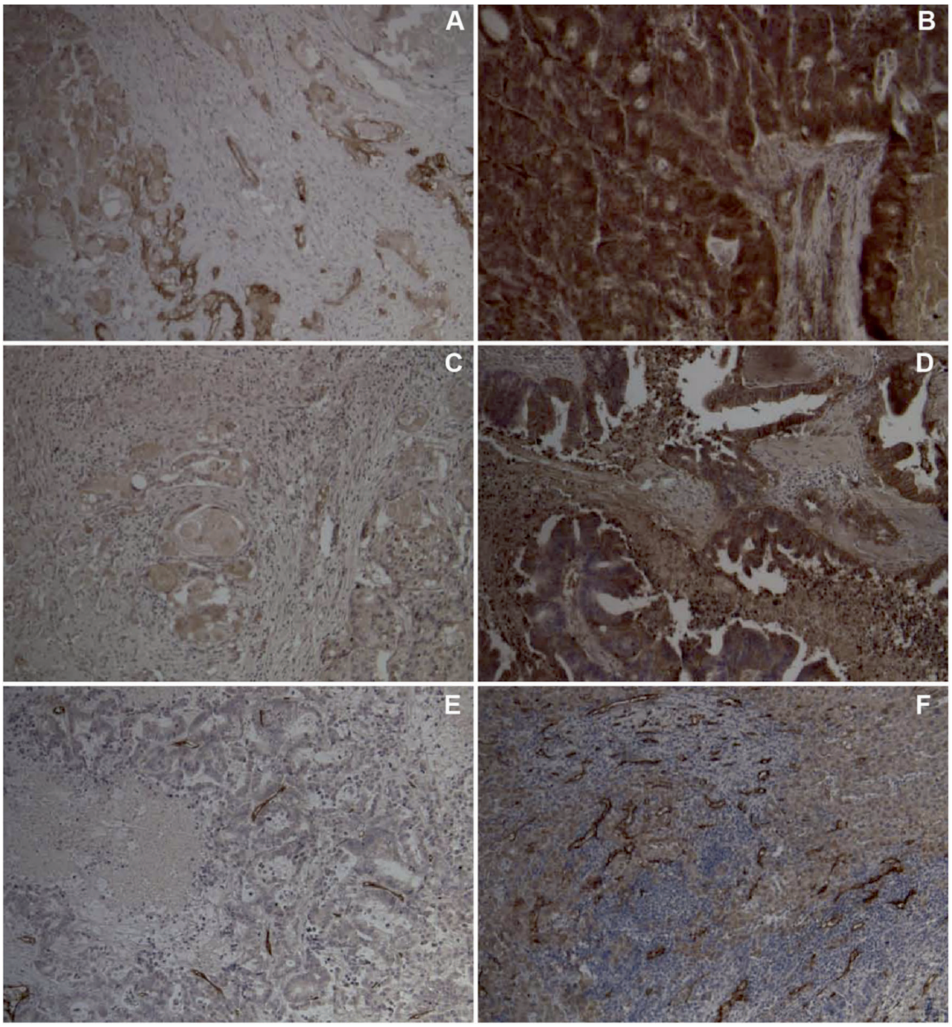

Figure 4. *Example of a tumor with low (fraction: 0.01) (A) and high (fraction: 0.42) (B) CA IX expression, an example of a tumor with low (fraction: 0.00) (C) and a tumor with high (fraction: 0.33) (D) expression of GLUT1, and an example of a tumor with a low vascular density (VD: 30/mm^2) (E) and a tumor with a high vascular density (VD:124/mm^2) (F).*

Discussion

MR imaging of T_2* relaxation provides a functional biomarker of potential value in the diagnosis of liver lesions. In this study, the repeatability of T_2* MR imaging in colorectal liver metastases was investigated and showed fair repeatability. The distribution of the lower T_2* values, the 16th and 50th percentile values, in colorectal liver metastases does not significantly differ from

surrounding normal appearing liver tissue. The colorectal liver metastases however appear to have more higher T_2* values, the 84th percentile values, than surrounding normal appearing liver tissue.

From Bland Altman analyses it can be concluded that a change due to treatment should induce at least a 45% difference in the median T_2* value to make a distinction between a true change in tumor biology and variations in the MR system or body physiology. Alonzi et al (22) investigated the R_2* (=1/T_2*) repeatability of malignant prostate tissue and found a repeatability of 64.6%. It will depend on the extent of the anticipated treatment induced changes if the current repeatability of median T_2* is sufficient to predict treatment outcome at an early stage.

The variation in T_2* values in consecutive measurements in the present study can be explained by several factors. First of all, temporary occlusions in the poor tumor vasculature can cause transient, fluctuating hypoxia in some tumor regions (23). Erythrocytes, which contain (de) oxyhemoglobin, cannot pass these temporary occlusions. Therefore temporary occlusions will influence the measured T_2* signal. Compared to other organs, T_2* imaging of the liver is challenging as there are potential field inhomogeneities and artifacts caused by respiratory movement, cardiac and aortic pulsations (24–26). Although respiratory and cardiac gating can be applied, this may increase scan time and thus patient discomfort and costs. Breath-hold acquisitions may reduce artifacts, but multiple breath-hold scans would be required to image the entire liver which is hard to perform for patients with advanced cancer. In our study we instructed patients to breath shallowly. This avoided long scanning times and difficult breath-holds, thereby increasing patients' comfort. Shallow breathing combined with liver tumor registration and motion correction could further improve repeatability. Finally, since T_2* is related to small fluctuations in local magnetic field, it is crucial for its proper application that good magnetic field homogeneity is obtained over the region of interest; especially considering the many different tissue types and air containing compartments near the liver.

Contrary to our expectations, no correlations between T_2* values, hypoxia and vascularity were observed. A study on primary rectal adenocarcinoma by Atkin et al. (27), however, also showed a lack of correlation between R_2*, CA IX and vessel density as assessed using CD31.

The Warburg effect – anaerobic glycolysis despite the presence of oxygen - could explain the lack of correlation between measured T_2* values and the expression of GLUT-1 and CA-IX (28,29). Malignant rapidly-growing tumor cells often produce energy by a high rate of glycolysis even in the presence of oxygen (30). This implies that these cells could have a high expression of GLUT-1 and CA-IX in the presence of oxygen in order to allow for the high influx of glucose and efflux of the H^+ ions. In these oxygenated areas the deoxyhemoglobin concentration will be low as less oxygen is released by hemoglobin. Therefore, these regions appear as non-hypoxic on the T_2* images, while the same region appears 'hypoxic' based on the increased expression of GLUT-1 and CA-IX.

The absence of a correlation between measured T_2* values and the RVA and VD can partially be explained by the fact that the CD34 marker attaches to both perfused and non perfused vascular endothelial cells. In contrast, T_2* only reflects oxygenation in vessels, and adjacent tissue. This difference could specifically be relevant for T_2* measurements in tumors, as the tumor microvasculature is usually less stable, more leaky and suffers more from temporary occlusions than mature microvasculature (31).

Besides the previous mentioned issues, other effects may also influence measured T_2* values. Increased blood flow may result in a lower blood desaturation if the oxygen consumption of nearby tissue remains constant. The amount of deoxyhemoglobin decreases and the measured T_2* value will therefore increase. An increased blood volume, on the other hand, could result in increased amounts of deoxyhemoglobin, if the blood desaturation remains constant. The effect of vasodilatation or vasoconstriction on T_2* is therefore difficult to predict as it will have an effect on both blood flow and volume. Hematocrit, the volume percentage of red blood cells in blood, determines the amount of hemoglobin present in the blood and it is known to decrease in smaller vessels (32,33). Since the hematocrit can vary in patients due to various reasons, the amount of deoxyhemoglobin could also change and thus influence the measured T_2* value. The blood oxygenation level is another factor that could vary. Due to the oxygen consumption of tissues adjacent to the tumor the blood oxygenation level of the blood arriving at the tumor may already be lower, thus having a higher amount of deoxyhemoglobin. A decrease in blood pH could also result in an increased oxygen release by the hemoglobin, resulting in more deoxyhemoglobin. Besides the previous mentioned blood related parameters other effects like iron accumulation can also influence the magnetic field. Since iron is ferromagnetic, it can decrease measured T_2* values.

In conclusion, the average T_2* values in colorectal liver metastases showed fair repeatability. No correlations between T_2* values, endogenous hypoxia related proteins and vascularity related markers RVA and VD were observed.

Reference List

[1] Gilbert H, Kagan A, Hintz B, Nussbaum H. Patterns of metastases. In: Weiss L, Gilbert H, editors. Liver metastases. Boston, Mass: GK Hall Medical Publishers; 1982. pp. 19–39.

[2] Pickren J, Tsukada Y, Lane W. Analysis of Autopsy Data. In: Weiss L, Gilbert H, editors. Liver metastases. Boston, Mass: GK Hall Medical Publishers; 1982. pp. 2–18.

[3] Khan AN. Liver, Metastases: eMedicine Radiology. 2009 February 10. Available from: http://emedicine.medscape.com/article/369936-overview

[4] Tofts PS, Brix G, Buckley DL, Evelhoch JL, Henderson E, Knopp MV, Larsson HBW, Lee T-Y, Mayr NA, Parker GJM, Port RE, Taylor J, Weisskoff RM. Estimating kinetic parameters from dynamic contrast-enhanced t1-weighted MRI of a diffusable tracer: Standardized quantities and symbols. Journal of Magnetic Resonance Imaging. 1999 September;10(3):223–232.

[5] Fan B, Wang X, Yang X, Zhong H, Wu C, Jiang X. Blood oxygen level-dependent MRI for the monitoring of neoadjuvant chemotherapy in breast carcinoma: initial experience. Magnetic Resonance Imaging. 2011 February;29(2):153–159.

[6] Padhani AR, Krohn KA, Lewis JS, Alber M. Imaging oxygenation of human tumours. European Radiology. 2006 October;17(4):861–872.

[7] Leach MO, Brindle KM, Evelhoch JL, Griffiths JR, Horsman MR, Jackson A, Jayson GC, Judson IR, Knopp MV, Maxwell RJ, McIntyre D, Padhani AR, Price P, Rathbone R, Rustin GJ, Tofts PS, Tozer GM, Vennart W, Waterton JC, Williams SR, Workman P. The assessment of antiangiogenic and antivascular therapies in early-stage clinical trials using magnetic resonance imaging: issues and recommendations. Br J Cancer. 0000;92(9):1599–1610.

[8] Alonzi R, Padhani AR, Maxwell RJ, Taylor NJ, Stirling JJ, Wilson JI, d' Arcy JA, Collins DJ, Saunders MI, Hoskin PJ. Carbogen breathing increases prostate cancer oxygenation: a translational MRI study in murine xenografts and humans. Br J Cancer. 2009 February 3;100(4):644–648.

[9] McPhail LD, Robinson SP. Intrinsic Susceptibility MR Imaging of Chemically Induced Rat Mammary Tumors: Relationship to Histologic Assessment of Hypoxia and Fibrosis1. Radiology. 2010 January 1;254(1):110–118.

[10] Hoskin PJ, Carnell DM, Taylor NJ, Smith RE, Stirling JJ, Daley FM, Saunders MI, Bentzen SM, Collins DJ, d' Arcy JA, Padhani AP. Hypoxia in Prostate Cancer: Correlation of BOLD-MRI With Pimonidazole Immunohistochemistry--Initial Observations. International Journal of Radiation Oncology*Biology*Physics. 2007 July 15;68(4):1065–1071.

[11] Chavhan GB, Babyn PS, Thomas B, Shroff MM, Haacke EM. Principles, Techniques, and Applications of T2*-based MR Imaging and Its Special Applications. Radiographics. 2009 September;29(5):1433–1449.

[12] Chen H, Ikeda-Saito M, Shaik S. Nature of the Fe–O2 Bonding in Oxy-Myoglobin: Effect of the Protein. Journal of the American Chemical Society. 2008 November 5;130(44):14778–14790.

[13] Pauling L, Coryell CD. The Magnetic Properties and Structure of Hemoglobin, Oxyhemoglobin and Carbonmonoxyhemoglobin. Proceedings of the National Academy of Sciences. 1936 April 1;22(4):210–216.

[14] Howe FA, Robinson SP, McIntyre DJO, Stubbs M, Griffiths JR. Issues in flow and oxygenation dependent contrast (FLOOD) imaging of tumours. NMR in Biomedicine. 2001 November 1;14(7-8):497–506.

[15] Gray LH, Conger AD, Ebert M, Hornsey S, Scott OCA. The Concentration of Oxygen Dissolved in Tissues at the Time of Irradiation as a Factor in Radiotherapy. Br J Radiol. 1953 December 1;26(312):638–648.

[16] Höckel M, Vaupel P. Tumor Hypoxia: Definitions and Current Clinical, Biologic, and Molecular Aspects. Journal of the National Cancer Institute. 2001 February 21;93(4):266 –276.

[17] Swietach P, Vaughan-Jones RD, Harris AL. Regulation of tumor pH and the role of carbonic anhydrase 9. Cancer and Metastasis Reviews. 2007 April 6;26:299–310.

[18] Rademakers SE, Rijken PF, Peeters WJ, Nijkamp MM, Barber PR, van der Laak J, van de Kogel AJ, Bussink J, Kaanders JH. Parametric mapping of immunohistochemically stained tissue sections; a method to quantify the colocalization of tumor markers. Cellular Oncology (Dordrecht). 2011 April;34(2):119–129.

[19] Altman DG, Bland JM. Measurement in Medicine: The Analysis of Method Comparison Studies. Journal of the Royal Statistical Society. Series D (The Statistician). 1983;32(3):307–317.

[20] Martin Bland J, Altman D. Statistical methods for assessing agreement between two methods of clinical measurement. The Lancet. 1986 February 8;327(8476):307–310.

[21] Galbraith SM, Lodge MA, Taylor NJ, Rustin GJS, Bentzen S, Stirling JJ, Padhani AR. Repeatability of dynamic contrast-enhanced MRI in human muscle and tumours: comparison of quantitative and semi-quantitative analysis. NMR in Biomedicine. 2002 April 1;15(2):132–142.

[22] Alonzi R, Taylor NJ, Stirling JJ, d' Arcy JA, Collins DJ, Saunders MI, Hoskin PJ, Padhani AR. Repeatability and correlation between quantitative and semiquantitative dynamic and intrinsic susceptibility-weighted MRI parameters in the benign and malignant human prostate. Journal of Magnetic Resonance Imaging. 2010 June;32(1):155–164.

[23] Brown JM. Evidence for Acutely Hypoxic Cells in Mouse Tumours, and a Possible Mechanism of Reoxygenation. British Journal of Radiology. 1979 August 1;52(620):650–656.

[24] Hanley J, Debois MM, Mah D, Mageras GS, Raben A, Rosenzweig K, Mychalczak B, Schwartz LH, Gloeggler PJ, Lutz W, Ling CC, Leibel SA, Fuks Z, Kutcher GJ. Deep inspiration breath-hold technique for lung tumors: the potential value of target immobilization and reduced lung density in dose escalation. International Journal of Radiation Oncology*Biology*Physics. 1999 October;45(3):603–611.

[25] Kitamura K, Shirato H, Seppenwoolde Y, Shimizu T, Kodama Y, Endo H, Onimaru R, Oda M, Fujita K, Shimizu S, Miyasaka K. Tumor location, cirrhosis, and surgical history contribute to tumor movement in the liver, as measured during stereotactic irradiation using a real-time tumor-tracking radiotherapy system. International Journal of Radiation Oncology*Biology*Physics. 2003 May 1;56(1):221–228.

[26] Shirato H, Seppenwoolde Y, Kitamura K, Onimura R, Shimizu S. Intrafractional tumor motion: lung and liver. Seminars in Radiation Oncology. 2004 January;14(1):10–18.

[27] Atkin G, Taylor NJ, Daley FM, Stirling JJ, Richman P, Glynne-Jones R, d' Arcy JA, Collins DJ, Padhani AR. Dynamic contrast-enhanced magnetic resonance imaging is a poor measure of rectal cancer angiogenesis. British Journal of Surgery. 2006 August;93(8):992–1000.

[28] Warburg O. On the Origin of Cancer Cells. Science. 1956 February 24;123(3191):309 –314.

[29] Warburg O, Posener E, Negelein E. Ueber den Stoffwechsel der Tumoren. Biochemische Zeitschrift. 1924;152:319–344.

[30] Busk M, Horsman MR, Kristjansen PEG, van der Kogel AJ, Bussink J, Overgaard J. Aerobic glycolysis in cancers: Implications for the usability of oxygen-responsive genes and fluorodeoxyglucose-PET as markers of tissue hypoxia. International Journal of Cancer. 2008 June 15;122(12):2726–2734.

[31] Senger DR, Water L, Brown LF, Nagy JA, Yeo K-T, Yeo T-K, Berse B, Jackman RW, Dvorak AM, Dvorak HF. Vascular permeability factor (VPF, VEGF) in tumor biology. Cancer and Metastasis Reviews. 1993 September;12(3-4):303–324.

[32] Fåhraeus R. The Suspension Stability of the Blood. Physiological Reviews. 1929 April 1;9(2):241–274.

[33] Jain RK. Determinants of Tumor Blood Flow: A Review. Cancer Research. 1988 May 15;48(10):2641–2658.

5

Repeatability of functional volume and activity concentration in ^{18}F-FDG PET/CT of liver metastases in colorectal cancer

Abstract

Background: Several studies showed potential for monitoring response to systemic therapy in metastatic colorectal cancer patients with ^{18}F-FDG PET. Before ^{18}F-FDG PET can be implemented for response evaluation the repeatability should be known. This study was performed to assess the magnitude of the changes in SUV, volume and total lesion glycolysis (TLG) in colorectal liver metastases and validate the biological basis of ^{18}F-FDG PET in colorectal liver metastases.

Methods: Twenty patients scheduled for liver metastasectomy underwent two ^{18}F-FDG PET scans within one week. Bland Altman analysis was performed to assess repeatability of SUVmax, SUVmean, volume and total lesion glycolysis. Tumors were delineated using an adaptive threshold method (PET_{SBR}) and a semi-automatic delineation (FLAB) method.

Results: Coefficient of repeatability of SUVmax and SUVmean were ~39% and ~31%, respectively, independent of the used delineation method and image reconstruction parameters. However, repeatability was worse in recently treated patients. FLAB delineation method improved the repeatability of the volume and TLG measurements compared to PET_{SBR}, from coefficients of repeatability of over 85% to 45% and 57% for volume and TLG respectively. GLUT-1 expression correlated to the SUVmean. Vascularity (CD34 expression) and tumor hypoxia (CA-IX expression) did not correlate with ^{18}F-FDG PET parameters.

Conclusion: In conclusion, repeatability of SUVmean and SUVmax was mainly affected by preceding systemic therapy. The repeatability of tumor volume and TLG could be improved using more advanced and robust delineation approaches such as FLAB, which is recommended when 18F-FDG PET is utilized for volume or TLG measurements. Improvement of repeatability of PET measurements, for instance by dynamic PET scanning protocols, is probably necessary to effectively use PET for early response monitoring.

Introduction

Colorectal cancer is a common disease and the second leading cause of cancer related death in the United States [1]. Irresectable metastatic colorectal cancer is treated with systemic therapy consisting of chemotherapy and targeted therapies, such as the angiogenesis inhibitor bevacizumab and the epidermal growth factor receptor targeting antibodies cetuximab and panitumumab. Approximately, half of the patients respond to systemic treatment, which prolongs median overall survival but is also associated with toxicity and high costs [2]. Currently, response to treatment is evaluated according to the RECIST criteria [3]. Depending on the schedule, radiological response of treatment efficacy can only be measured after 8-9 weeks of treatment. Therefore, techniques for early response monitoring are urgently warranted to facilitate patient tailored treatment. Furthermore, anatomical response evaluation may not be the optimal method to assess the efficacy of targeted therapies, because necrosis and cavitation without a reduction in tumor size may occur [4].

Several functional and molecular imaging techniques have shown potential for early response evaluation and prediction of treatment response. ^{18}F-FDG PET is one of the most described and tested imaging techniques for response evaluation in advanced colorectal cancer. The first rational for using ^{18}F-FDG PET for response prediction and treatment monitoring is the enhanced glucose metabolism in malignant tumors. High glycolysis and therefore high ^{18}F-FDG uptake is a predictor of poor prognosis [5-7]. Glycolysis is increased in oxygen deprived cells. However, most cancer cells have an increased glycolytic rate even when oxygen is abundant [8]. Due to impaired tumor vasculature, hypoxia is common in solid tumors [9] and also contributes to the increased glycolysis. The increased uptake of glucose and FDG is facilitated by the glucose uptake transporter-1 (GLUT-1), which is the main transporter of glucose over the cell membrane. GLUT-1 is overexpressed in many cancer types, including colorectal cancer [10] and in hypoxic conditions GLUT-1 is upregulated. Thus, increased uptake of FDG results from a complex interplay in the tumor microenvironment between vasculature, hypoxia, aerobic glycolysis and GLUT-1 expression.

In a recent systematic review, the role of ^{18}F-FDG PET in monitoring and predicting treatment response in advanced colorectal cancer was evaluated. Four out of five studies showed changes in standardized uptake values (SUV) of ^{18}F-FDG PET 72 hours to 2 months after start of systemic treatment [11].

Before ^{18}F-FDG PET-or other imaging techniques- can be clinically implemented for response evaluation, the repeatability should be confirmed for specific tumor types. Knowledge of repeatability is needed to determine what change in parameters between two examinations can be considered relevant in an individual patient. Assessment of repeatability becomes even more important in early response monitoring since the changes in the tumor induced by the treatment may be smaller compared to response monitoring after 2-3 cycles of treatment.

Repeatability of ^{18}F-FDG PET has been evaluated in several cancer types [12-15]. However, to the best of our knowledge repeatability of ^{18}F-FDG PET in solely colorectal liver metastases has not been assessed previously. Several factors might affect repeatability, such as methods of reconstruction and delineation. A previous study showed that an increasing number of iterations results in images with more noise and higher SUV values [16]. In fact, SUV_{max} may be influenced by outliers in the noise and, therefore, be less reproducible [17]. The effect of single outliers may be countered by assessing SUV_{max} of multiple voxels [18].
Therefore, this study was performed to assess the magnitude of the changes in SUV, volume and total lesion glycolysis (TLG, defined as the product of volume and mean SUV) that can be confidently detected in liver metastases of colorectal cancer using different image reconstruction and delineation methods. The correlation with immunohistochemistry of resected liver metastases was assessed as a secondary objective, to further understand the biological basis of ^{18}F-FDG PET parameters.

Materials and methods

Patients

Between August 2009 and January 2011, patients with one or more colorectal liver metastases, who were scheduled for metastasectomy were approached for participation in this study. Exclusion criteria were diabetes mellitus, claustrophobia and pregnancy. Prior chemotherapeutic treatment was not considered an exclusion criterion, and patients received chemotherapy up to one month prior to study participation. No chemotherapy or other anti-tumor therapy was administered between the two FDG PET scans. This study was approved by institutional review board. All patients provided written informed consent.

^{18}F-FDG-PET

All patients fasted for at least 6 hours prior to the FDG PET scans. Prior to FDG injection blood glucose levels were monitored and these were in all patients considerably below the restriction level of 10mmol/L. Approximately 3.5 MBq/kg FDG was injected intravenously 60 minutes before the scan. The intravenous cannula was flushed with 20 cc 0.9% NaCl, to avoid residual activity in the cannula. Before injection of ^{18}F-FDG, 2 ml of Furosemide (10 mg/ml) was administered. ^{18}F-FDG PET was combined with a low dose CT and performed on a PET/CT scanner (Biograph Duo, Siemens Medical Solutions USA, Inc., Knoxville, TN, USA). PET/CT scans were acquired with a hybrid PET/CT scanner (Biograph Duo, Siemens Medical Solutions USA, Inc.) containing a dual slice CT scanner. A low-dose CT scan for localization and attenuation-correction purposes was acquired in the caudocranial direction. Scanning parameters included 40 mAs (50 mAs for patient weight >100 kg and 60 mAs for >120 kg), 130 kV, 5 mm slice collimation, 0.8 seconds rotation time, and pitch of 1.5, reconstructed to 3

mm slices for smooth coronal representation. Low dose CT scans were acquired during timed unforced expiration breath-hold. For PET, a three-dimensional whole body emission scan was acquired during free breathing from proximal femora to skull base. The acquisition time per bed position was 4 minutes for emission only. Every deviation in the exact injected dose and time interval of incubation between the first and second scan has been recorded.

First, the repeatability of the maximum and mean SUV (SUV_{max} and SUV_{mean}), metabolically active volume and associated total lesion glycolysis (TLG) was assessed using the 4 iterations/16 subsets (4i/16s) OSEM2D reconstruction algorithm, being the European standard for quantitative PET [19]. Scan data were smoothed with a 5-mm full width at half maximum (FWHM) Gaussian filter. On the 4i/16s reconstruction, we also determined the repeatability of the maximized SUVmean in a size 3 sphere, containing a volume of 1.6 cm^3 (SUV_{peak}).

To assess whether repeatability of SUV_{max} was influenced by the image reconstruction parameters, the repeatability was also measured on the 2i/8s OSEM2D reconstruction. The main reason for choosing a second reconstruction method with fewer iterations was that borders may be sharper and more accurate in the 4i/16s reconstruction, but also add more noise to the data SUV_{max} may be influenced by outliers in the noise and may therefore be less reproducible [16, 17]. The 2i/8s reconstruction method gives smoother, less noisy images.

To assess the influence of the delineation method on the repeatability of PET parameters (SUV_{mean}, volume and TLG) delineations were performed on the 4i/16s reconstruction, using two different approaches. First by applying a variable threshold based on the signal-to-background ratio (PET_{SBR}), which is described as a suitable option in the PERCIST criteria [20]. The adaptive threshold was calculated with the formula: $\mathbf{threshold=SUV_{background}+0.41*(SUV_{max}-SUV_{background})}$, since the 41% isocontour generally corresponded best with the actual dimensions of the tumor for higher tumor-to-background values and homogenous backgrounds [19]. Secondly, using a semi-automatic Fuzzy Locally Adaptive Bayesian (FLAB) delineation method (software provided by the INSERM U1101 LaTIM). This delineation method does not only consider the statistical distribution of the values of the voxels within the drawn ROI, but also takes values of the nearby voxels into account and combines these in a probabilistic and fuzzy framework with iterative estimation of the parameters [21]. The technique is also able to deal with tumor heterogeneity [21, 22].

Immunohistochemistry of hypoxia, vasculature and GLUT-1 expression

To assess expression of GLUT-1 as well as CA-IX and tumor vascularity, immunohistochemistry was performed on resected liver metastases.

First, we performed H&E-staining. If viable tumor cells were present, immunohistochemistry of 5 µm paraffin embedded sections was performed for GLUT-1, CA-IX as a marker of hypoxia and CD34 expression as a marker of tumor vascularity. In total material of 19 metastases derived from 15 patients was available to be matched with ^{18}F-FDG PET parameters.

Before immunohistochemical staining procedures, sections were deparaffinized in histosafe and rehydrated in graded ethanol solutions and kept for 30 minutes in Target Retrieval Solution. The peroxidases in the sections were blocked by keeping them in 3% H_2O_2 in methanol for 15 minutes. The sections were preincubated with 5% normal donkey serum in primary antibody diluent (PAD, Abcam, Cambridge, UK) for 30 minutes at room temperature. For GLUT-1 staining rabbit-anti-GLUT-1 (RB-9052 P1) 1:400 in PAD was used for 45 minutes in 37° C, followed by biotin-labelled-F(ab')2-donkey-anti-rabbit IgG (Jackson Immuno Research) 1:500 in PBS for 60 minutes at room temperature. For CA-IX staining mouse-anti-CA-IX (1:25 in PAD) was applied on the tumor sections and kept overnight at 4° C. Sections were incubated with a second antibody, biotin-labelled-F(ab')$_2$-donkey-anti-mouse IgG (1:200 in PBS) for 60 minutes at room temperature. For CD34 staining mouse-antiCD34 (1:10 in PAD) was applied to all tumor sections and kept overnight at 4° C. The sections were incubated with a second antibody, biotin-labelled-F(ab')$_2$-donkey-anti-mouse IgG (1:200 in PBS) for 60 minutes at room temperature.

For all sections this was followed by ABC-reagent (Vector Elite kit, Vector Laboratories) incubation for 30 min. Peroxidase activity was detected with diaminobenzidine (DAB) for 10 minutes. Hematoxylin was used for counterstaining. Sections were dehydrated and mounted with KP mounting medium. Between all steps, the sections were rinsed 3 times with PBS.

All slices were digitalized using a monochrome CCD camera (Retiga SRV, 1392×1040 pixels) and a RGB filter (Slider Module; QImaging, Burnaby, BC, Canada) attached to a motorized bright field microscope (DM6000 Leica, Wetzlar, Germany) at 100X magnification and Image Processing Lab software (Scanalytics Inc., Fairfax, VA, USA) as described before (Rademakers et al. 2011). A region of interest was manually drawn around the entire tumor area, excluding evident necrosis. For all slices the optimal threshold for positive staining was determined. The fraction of positive staining was calculated relative to the total tumor area. For CD34 the number of vessels per square millimeter (vascular density- VD) was scored [23].

Statistical Analyses and Sample size considerations

Statistical analyses were performed using SPSS 16.0 (SPSS Inc, Chicago, IL) and Microsoft Office Excel 2007. Based on previous repeatability studies which included 9-26 patients we aimed to include 20 patients in our study [12-14]. Lesion-by-lesion analyses of all 24 PET-positive liver metastases was performed. To asses repeatability Bland Altman analysis was performed [24]. If the difference between the PET parameters of the first and second scan was proportional to the mean, log transformed data or percentage differences would be used [25]. The percentage differences were calculated using: **(SUV1-SUV2)/ (average SUV1,SUV2) *100**. Standard deviation of the difference (SD), coefficient of repeatability (CR) and limits of agreement (LoA) were calculated for SUV_{max}, SUV_{mean}, SUV_{peak}, volume and TLG. Coefficient of repeatability was calculated using the formula: CR= 1.96*SD. The SD was calculated by

squaring all the differences, adding them up, dividing them by the number of measurements and taking the square root [24]. The limits of agreement were calculated by adding (upper limit) or subtracting (lower limit) the coefficient of repeatability from the mean difference. Of note, after log transformation of the original data the antilog of the calculated limits of agreement are presented in a dimensionless scale [24]. To assess the relation between PET parameters and GLUT-1, CA-IX and CD34 expression, a Pearson correlation coefficient was calculated between the average of the PET-parameters measured at the two occasions and the fraction of positive staining.

Results

Patients

Twenty patients with 24 detectable liver metastases of colorectal cancer participated in this study. ^{18}F-FDG PET was performed twice in all patients with a mean interval of 5 days between the scans (range 1-7 days). Two of the patients had liver metastasis without FDG accumulation and were excluded from the analyses. The SUV_{max} in the remaining patients was 8.3 ±2.8 g/cm^3 (range 4.1-17.0). Seven of the twenty patients (with 9 FDG positive liver metastases) received chemotherapy for colorectal cancer within 3 months before the metastasectomy. Six patients received neoadjuvant chemotherapy, one received adjuvant chemotherapy for the primary tumor. There was no significant difference in the SUV-value of the tumors in recently treated patients (SUV_{max} 7.4 ±2.1 g/cm^3) compared to metastases in patients who did not receive systemic therapy for at least one year (SUV_{max} 9.0 ±3.3 g/cm^3).

Compliance to the scanning protocol

On average 63.9 minutes (range 57- 80 minutes) after FDG administration the FDG PET scan was started. The mean difference between the first and second interval was 3.5 minutes (range 0-16 minutes). In 2 patients (3 metastases) the interval difference between the first and second scan was 16 minutes, due to problems scanning earlier patients after FDG injection of the study patients. However, excluding these two patients from analysis did not significantly improve repeatability of PET parameters. Therefore, these 2 patients were included in the analyses.

On average 3.42 MBq/kg (range 3.09- 3.95) was administered. The mean difference between the first and second administration was 0.19 MBq/kg (range 0.07-0.60 MBq/kg).

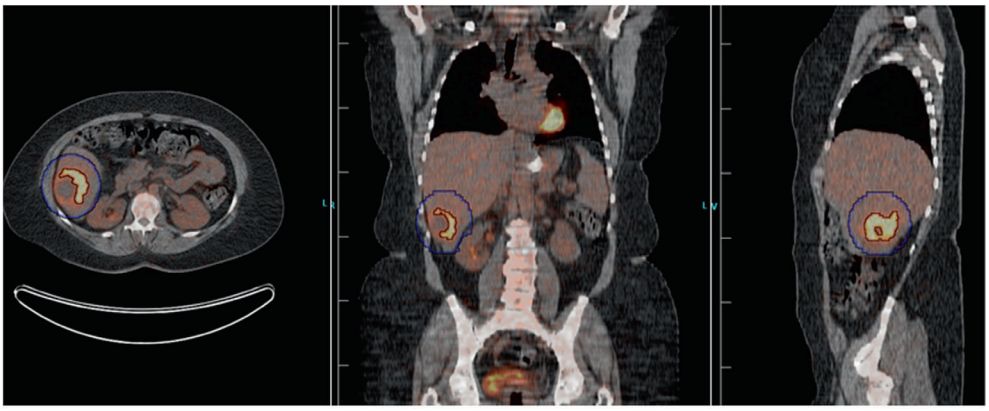

Figure 1. *Typical solitary liver metastasis of colorectal cancer. In blue the manually drawn tumor container, in red the automatically drawn ROI around the tumor (adaptive delineation method).*

Repeatability of ^{18}F-FDG PET

First, analyses were performed using ROIs drawn by the variable threshold method. An example of an ROI based on this method is shown in figure 1. The average measured volumes in all metastases by this method was 14.0 cm^3 (range 1.4- 70.0 cm^3). The average SUV_{max} and SUV_{mean} in the liver metastases on the 4i/16s PET_{SBR} analyses was 8.3 ±2.8 g/cm^3 (range 4.1-17.0). and 5.7 ±1.6 g/cm^3 (range 3.4-10.5), respectively. Resulting TLGs were 94.8 (range 6.4-480.3). The difference in SUV_{max}, SUV_{mean}, volume and TLG was proportional to the mean: the higher the mean, the larger the differences [Figure 2]. Therefore, the coefficient of repeatability (CR) was calculated after log transformation of the original data and expressed as a percentage. The CR of SUV_{max} and SUVmean was 39.0% and 31.2%, respectively [Figure 3]. The CRs of both volume and TLG were well over 85% (Table 1). The CR of the SUV_{peak} was 37.0%, comparable to the SUV_{max}.

To assess whether the reconstruction method influenced repeatability of PET-parameters, we assessed repeatability in the smoother 2i/8s reconstruction. The absolute CR decreased compared to the 4i/16s reconstruction. However, since the standardized uptake values also decreased, the CR was similar to the CR obtained with 4i/16s reconstructions. There was no significant difference in the percentage difference between the SUVmax of first and second scan in the 2i/8s versus the 4i/16s reconstruction method.

In a second step, analyses were performed using FLAB delineation software, which led to volumes measurements of 28.3 cm^3 (range 1.0-92.5 cm^3), SUV_{mean} measurements of 5.0 ±1.3 g/cm^3 (range 3.3-8.3) and resulting TLG of 163.2 (range 4.8-750.1). This method significantly improved the repeatability of the volume and TLG measurements compared to PET_{SBR}, from more than 85% to 45% and 57% for volume and TLG respectively [Table 1]. Delineation with FLAB-software did not significantly influence the CR of the SUV values. However, one small

tumor could not be automatically delineated by the software and had to be excluded from the PET_{FLAB} analyses. Therefore, the CR of maximum SUV for the PET_{SBR} (4i/16s) and PET_{FLAB} were 39.0% and 39.7% respectively. For SUV_{mean} the CR for PET_{SBR} (4i/16s) and PET_{FLAB} were 31.2% and 32.9%, respectively [Table 1].

	ABSOLUTE VALUE	PERCENTAGE	LOG-scale	
	CR (LoA)	CR (LoA)	Lower limit - Upper limit	
4i/16s (PET_{SBR})				
SUVmax	3.6 (-3.6 – 3.5)	39.0% (-40.9% – 37.1%)	0.66 (-34%)	1.45 (+45%)
SUVmean	1.9 (-1.9 – 1.8)	31.2% (-31.8% – 30.4%)	0.73 (-27%)	1.36 (+36%)
Volume in cm^3	12.8 (-14.3 – 11.3)	86.6% (-99.1% – 74.1%)	0.34 (-66%)	2.26 (+126%)
TLG	82.8 (-90.7 – 74.8)	90.8% (-103.8% – 77.8%)	0.32 (-68%)	2.35 (+135%)
4i/16s (FLAB)				
SUVmax	3.6 (-3.6 – 3.6)	39.7% (-41.4% – 38.1%)	0.66 (-34%)	1.46 (+46%)
SUVmean	1.5 (-1.7 –1.3)	32.9% (-38.0% – 27.8%)	0.68 (-32%)	1.32 (+32%)
Volume in cm^3	14.5 (-15.0 – 14.0)	45.8% (-42.7% – 49.0%)	0.65 (-35%)	1.64 (+64%)
TLG	91.9 (-94.4 – 89.4)	56.9% (-58.9% – 55.0%)	0.55 (-45%)	1.75 (+75%)
2i/8s (PET_{SBR})				
SUVmax	2.7 (-2.7 – 2.7)	38.1% (-39.0% – 37.2%)	0.67 (-33%)	1.47 (+47%)
SUVmean	1.5 (-1.6– 1. 5)	30.1% (-32.0% – 28.2%)	0.72 (-28%)	1.33 (+33%)
3 voxel cube				
SUVpeak	2.3 (-2.3 – 2.3)	37.0% (-38.5%- 35.6%)	0.68 (-32%)	1.43 (+43%)

Table 1. *Overview of coefficients of repeatability of SUVmax, SUVmean, volume and TLG in absolute value, percentage and LOG value in 4i/16s and 2i/8s reconstruction and using FLAB and PET_{SBR} delineation.*

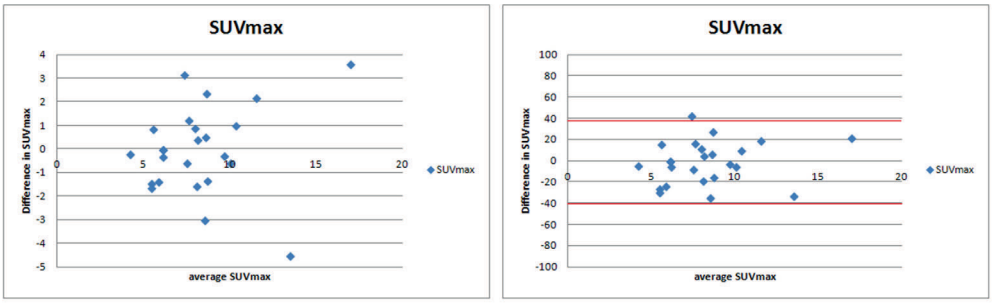

Figure 2. *Two Bland Altman analyses of the SUVmax: the x-axis shows the average SUVmax, the y-axis shows the difference between the SUVmax of the first and second scan in absolute and percentage difference. The red lines show the limits of agreement.*

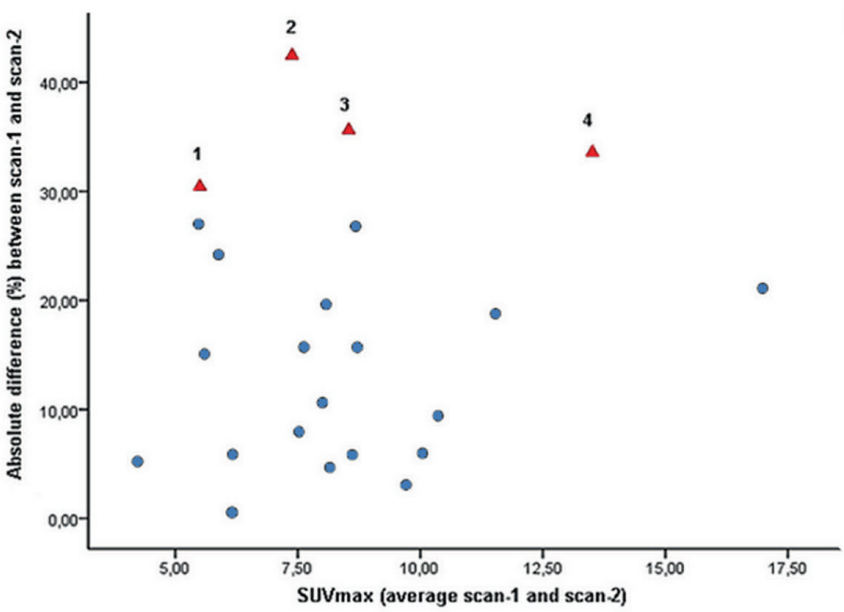

Outliers:

Number	SUVmax-1	SUVmax-2	Interval scan1(min)	Interval scan2(min)	Delay (days)	Difference injected Dose (Mbq)
1	6.34	4.66	63	61	7	11
2	5.81	8.95	64	80	4	51
3	10.06	7.02	66	69	7	9
4	15.78	11.24	63	62	4	10

Figure 3. *Scatter plot of absolute values of the difference (in percentage) versus average SUVmax. The four outliers are marked in red, representing metastases with differences over 30% between first and second SUVmax. The table provides additional data of the four outliers.*

Repeatability of 18F-FDG PET in pretreated tumors

Repeatability of SUVmax and SUVmean was worse in metastases of recently treated patient compared to metastases of untreated patients or metastases of patients who received their last therapy more than 3 months prior to study participation. In nine metastases of patients who received chemotherapy 1-3 months prior to study participation, CR of SUVmax was 47.0% and SUVmean 41.3%, compared to a CR of 33.3% and 23.1% in other metastases.

The mean (absolute) difference between the first and second scan was significantly larger in the SUVmean measurements of the recently treated tumors (19.7% vs. 8.8%, p=0.01). However, the mean difference between the first and second scan did not significantly differ between recently treated metastases and the other metastases in the SUVmax measurements (22.4% vs. 13.8%, p=0.10).

The effect of delay between the first and second scan on repeatability was assessed, both in the nine recently treated tumors and in all metastases. No significant correlation, however, has been observed between delay and absolute difference of the first and second scan.

GLUT-1 and CA-IX expression and vasculature

In two patients no metastasectomy was performed because metastases were considered irresectable during surgery. One metastasectomy was converted into radiofrequent ablation of the tumor. Thus, for 15 out of 18 PET-positive patients who participated in the study, paraffin embedded tissue of 19 liver metastases was available for analysis and correlation with ^{18}F-FDG PET.

GLUT-1, CA-IX and CD34 expression was readily visualized in all metastases [Figure 4]. The mean GLUT-1 fraction was 0.08 (range 0.00-0.33) and the mean CA-IX fraction was 0.11 (range 0.01- 0.42). Mean VD 66.7 vessels/mm^2.

The average SUVmean values positively correlated to the expression of GLUT-1 ($r = 0.51$, $p = 0.03$). Maximum SUV and TLG did no correlate to GLUT-1 expression. No correlation was observed between ^{18}F-FDG PET parameters and CA-IX expression or tumor vascularity as assessed by VD.

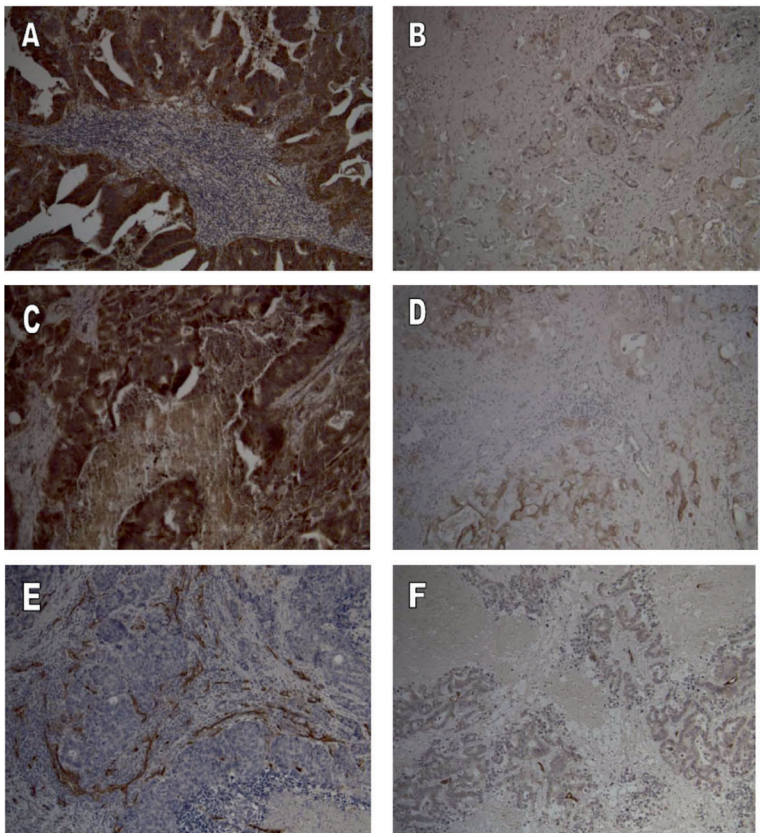

Figure 4. *Example of a tumor with high expression of GLUT1 (fraction: 0.33) (A) and a tumor with low expression of GLUT1 (fraction: 0.00) (B) ; an example of a tumor with high CA IX expression (fraction:0.42) (C) and low CA IX expression (fraction: 0.01) (D), and an example of a tumor with a high vascular density (VD:124/mm^2) (E) and a tumor with a low vascular density (VD:30/mm^2) (F).*

Discussion

Repeatability of PET imaging studies is important to assess which difference between two measurements would be significant in an individual patient. We presented the first data on the repeatability of PET imaging in solely colorectal cancer liver metastases. The coefficient of repeatability of SUV_{max} and SUV_{mean} were approximately 39% and 31% in the used PET reconstruction and delineation methods, respectively. Repeatability was less in metastases of patients who had recently been treated with chemotherapy. This could be a result of lasting cytotoxic effects, resulting in lower SUV values at the second measurement. Conversely, the recent discontinuation of systemic therapy might have led to tumor recovery in some patients and increasing SUV values on the second measurement. In both cases repeatability would be hampered.

Overall, the repeatability results are in line with reported results in studies with other tumor types or imaging methods [22, 26, 27]. Moreover, in an earlier study in patients with advanced gastrointestinal malignancies, comparable lower and upper limits of agreement for SUVmax and SUVmean measurements were reported [15].

However, two other studies assessing repeatability of ^{18}F-FDG PET reported a better repeatability of SUV_{mean} [13, 14]. In one study dynamic PET-scanning was performed with measurements using the last time frame of 60-70 minutes only. They observed that between 40 and 60 minutes FDG-uptake in lesions was still increasing by 16%, implying that in a 60-minute protocol small differences in the interval between the time of injection and start of scanning could lead to quite large differences in uptake values [14]. This could explain the excellent repeatability observed in the other study, where scanning was performed 90 minutes after FDG injection [13]. Thus, both dynamic ^{18}F-FDG PET, where time intervals are no issue-since the remote controlled intravenous injection of ^{18}F-FDG starts simultaneously with the dynamic data acquisition- and a longer interval after FDG injection might help to improve repeatability of standardized uptake values.

In the present study, the repeatability of volume and TLG in liver metastases using the variable threshold delineation method was rather poor, similarly to what was observed for various threshold-based methods previously [28]. This may be due to uptake heterogeneity within the larger volumes and the small size of some of the volumes encountered combined with the limited spatial resolution and signal-to-noise ratio in PET imaging. Using the FLAB delineation method, repeatability of volume and TLG improved, which is in line with previous findings comparing FLAB to threshold-based approaches in esophageal and breast cancer. However, the absolute repeatability values were larger relative to the previously obtained values in esophageal cancer. This might be explained by a combination of the smaller size and lower contrast levels of the delineated uptake regions encountered in this dataset with respect to what was observed in esophageal and breast lesions under investigation in the previous study [12].

In order to effectively use ^{18}F-FDG PET for response monitoring in metastatic colorectal cancer improving repeatability should be of utmost importance. Although most studies have shown a much greater change in SUV after the end of treatment in responding patients than the observed coefficient of repeatability [11], PERCIST criteria define response as 30% decrease of SUVmax. When PET is used for early response monitoring, detection of even smaller changes may be relevant. For example, Bender et al. monitored effects of 5-FU treatment in patients with irresectable colorectal cancer metastases, 72 hours after administration of 5-FU and observed an average decrease of 22% ±10% in responders. As this is within the coefficient of variation reported here, it is questionable whether depicted true early response monitoring by ^{18}F-FDG PET. In view of the abovementioned criteria for response, volume and TLG measurements would therefore only be suitable for early response prediction if the evolution of these parameters is indeed at least of this magnitude during treatment. TLG could potentially be more suitable since the magnitude of evolution of this parameter could result from both reduction of volume and mean SUV and therefore be associated with larger changes. However, to date limited data are available regarding the actual magnitude of changes of volume-based PET parameters early during treatment. Therefore, further studies are needed to establish the magnitude of change of TLG for various malignancies and treatments.

Despite the moderate results on the repeatability of FDG-PET, the SUVmean showed a significant correlation with GLUT-1 expression, underlining the biological basis of FDG-PET, since GLUT-1 facilitates the transport of FDG over the cell membrane. Vascularity and tumor hypoxia, indicated by CA-IX expression did not correlate with ^{18}F-FDG PET parameters. In contrast, an earlier study observed a positive correlation between ^{18}F-FDG uptake and microvascular density in breast cancer [29]. On the one hand, distribution of ^{18}F-FDG is dependent on the quality and density of tumor vasculature. On the other hand, it leads to a less hypoxic tumor environment, which results in a down regulation of GLUT-1 expression. Therefore, this may balance the effect of increased ^{18}F-FDG delivery, resulting in a net absence of correlation. Furthermore, we merely assessed the quantity of the vessels, not the functionality. CA-IX is a stable marker for hypoxia which is mainly upregulated in response to conditions of chronic-diffusion limited- hypoxia [30]. CA-IX should be considered as a hypoxia-*related* marker: it indicates cells that have adapted to a hypoxic stimulus [31, 32]. Due to variability in tumor perfusion, acute-perfusion limited- hypoxia may occur [33]. Acute-perfusion limited- hypoxia may also have a large effect on glycolysis, since cells switch to anaerobic glycolysis. This results in a strongly increased demand for glucose in cancer cells and thus in an increased ^{18}F-FDG uptake [34-36]. Cells switch to anaerobic glycolysis to survive short term hypoxic conditions, however, in chronic hypoxic conditions other effects may occur simultaneously that decrease ^{18}F-FDG uptake, like increased apoptosis, decreased proliferation and tumor necrosis [37]. This hypothesis may explain the absence of a correlation between CA-IX and ^{18}F-FDG uptake values.

In conclusion, repeatability of standardized uptake values of ^{18}F-FDG in colorectal liver metastases is acceptable and in line with earlier studies. Repeatability of SUVmean and SUVmax was not affected by the tested delineation methods or image reconstruction algorithms, but was affected by recent systemic therapy. The repeatability of tumor volume and TLG could be improved using a more robust delineation approach such as FLAB. When ^{18}F-FDG PET is utilized for volume or TLG measurements the use of an automatic delineation method, like the FLAB method, can be recommended. Repeatability of SUVmean and SUVmax seems sufficient for response monitoring at the end of treatment. However, improving repeatability of PET measurements -for instance by using dynamic PET scanning protocols or longer post injection intervals- may be necessary in order to effectively use PET for early response monitoring.

Reference List

[1] Jemal A, Siegel R, Xu J, Ward E. Cancer statistics, 2010. CA Cancer J Clin.60:277-300.

[2] Tol J, Koopman M, Cats A, Rodenburg CJ, Creemers GJ, Schrama JG, et al. Chemotherapy, bevacizumab, and cetuximab in metastatic colorectal cancer. N Engl J Med. 2009;360:563-72.

[3] Eisenhauer EA, Therasse P, Bogaerts J, Schwartz LH, Sargent D, Ford R, et al. New response evaluation criteria in solid tumours: revised RECIST guideline (version 1.1). EurJ Cancer. 2009;45:228-47.

[4] Desar IM, van Herpen CM, van Laarhoven HW, Barentsz JO, Oyen WJ, Van Der Graaf WT. Beyond RECIST: molecular and functional imaging techniques for evaluation of response to targeted therapy. Cancer TreatRev. 2009;35:309-21.

[5] Busk M, Horsman MR, Jakobsen S, Bussink J, van der KA, Overgaard J. Cellular uptake of PET tracers of glucose metabolism and hypoxia and their linkage. EurJ NuclMed MolImaging. 2008;35:2294-303.

[6] de Geus-Oei LF, Wiering B, Krabbe PF, Ruers TJ, Punt CJ, Oyen WJ. FDG-PET for prediction of survival of patients with metastatic colorectal carcinoma. AnnOncol. 2006;17:1650-5.

[7] Kunkel M, Reichert TE, Benz P, Lehr HA, Jeong JH, Wieand S, et al. Overexpression of Glut-1 and increased glucose metabolism in tumors are associated with a poor prognosis in patients with oral squamous cell carcinoma. Cancer. 2003;97:1015-24.

[8] Warburg O. On the origin of cancer cells. Science. 1956;123:309-14.

[9] Ruan K, Song G, Ouyang G. Role of hypoxia in the hallmarks of human cancer. J Cell Biochem. 2009;107:1053-62.

[10] Macheda ML, Rogers S, Best JD. Molecular and cellular regulation of glucose transporter (GLUT) proteins in cancer. J Cell Physiol. 2005;202:654-62.

[11] de Geus-Oei LF, Vriens D, van Laarhoven HW, Van Der Graaf WT, Oyen WJ. Monitoring and predicting response to therapy with 18F-FDG PET in colorectal cancer: a systematic review. J NuclMed. 2009;50 Suppl 1:43S-54S.

[12] Hatt M, Cheze-Le Rest C, Aboagye EO, Kenny LM, Rosso L, Turkheimer FE, et al. Reproducibility of 18F-FDG and 3'-deoxy-3'-18F-fluorothymidine PET tumor volume measurements. J Nucl Med. 2010;51:1368-76.

[13] Nahmias C, Wahl LM. Reproducibility of standardized uptake value measurements determined by 18F-FDG PET in malignant tumors. J NuclMed. 2008;49:1804-8.

[14] Weber WA, Ziegler SI, Thodtmann R, Hanauske AR, Schwaiger M. Reproducibility of metabolic measurements in malignant tumors using FDG PET. J NuclMed. 1999;40:1771-7.

[15] Velasquez LM, Boellaard R, Kollia G, Hayes W, Hoekstra OS, Lammertsma AA, et al. Repeatability of 18F-FDG PET in a multicenter phase I study of patients with advanced gastrointestinal malignancies. J Nucl Med. 2009;50:1646-54.

[16] Jaskowiak CJ, Bianco JA, Perlman SB, Fine JP. Influence of reconstruction iterations on 18F-FDG PET/CT standardized uptake values. J NuclMed. 2005;46:424-8.

[17] Boellaard R, Oyen WJ, Hoekstra CJ, Hoekstra OS, Visser EP, Willemsen AT, et al. The Netherlands protocol for standardisation and quantification of FDG whole body PET studies in multi-centre trials. Eur J Nucl Med Mol Imaging. 2008;35:2320-33.

[18] Lodge MA, Chaudhry MA, Wahl RL. Noise Considerations for PET Quantification Using Maximum and Peak Standardized Uptake Value. J Nucl Med. 2012.

[19] Boellaard R, O'Doherty MJ, Weber WA, Mottaghy FM, Lonsdale MN, Stroobants SG, et al. FDG PET and PET/CT: EANM procedure guidelines for tumour PET imaging: version 1.0. EurJ NuclMed MolImaging. 2010;37:181-200.

[20] Wahl RL, Jacene H, Kasamon Y, Lodge MA. From RECIST to PERCIST: Evolving Considerations for PET response criteria in solid tumors. J NuclMed. 2009;50 Suppl 1:122S-50S.

[21] Hatt M, Cheze Le RC, Turzo A, Roux C, Visvikis D. A fuzzy locally adaptive Bayesian segmentation approach for volume determination in PET. IEEE TransMed Imaging. 2009;28:881-93.

[22] Hatt M, Cheze Le RC, Descourt P, Dekker A, De RD, Oellers M, et al. Accurate automatic delineation of heterogeneous functional volumes in positron emission tomography for oncology applications. IntJ RadiatOncolBiolPhys. 2010;77:301-8.

[23] Rademakers SE, Rijken PF, Peeters WJ, Nijkamp MM, Barber PR, van der LJ, et al. Parametric mapping of immunohistochemically stained tissue sections; a method to quantify the colocalization of tumor markers. Cell Oncol(Dordr). 2011;34:119-29.

[24] Bland JM, Altman DG. Statistical methods for assessing agreement between two methods of clinical measurement. Lancet. 1986;1:307-10.

[25] Dewitte K, Fierens C, Stockl D, Thienpont LM. Application of the Bland-Altman plot for interpretation of method-comparison studies: a critical investigation of its practice. ClinChem. 2002;48:799-801.

[26] van Laarhoven HW, Rijpkema M, Punt CJ, Ruers TJ, Hendriks JC, Barentsz JO, et al. Method for quantitation of dynamic MRI contrast agent uptake in colorectal liver metastases. J Magn ResonImaging. 2003;18:315-20.

[27] de Langen AJ, Vincent A, Velasquez LM, van Tinteren H, Boellaard R, Shankar LK, et al. Repeatability of 18F-FDG Uptake Measurements in Tumors: A Metaanalysis. J Nucl Med. 2012.

[28] Frings V, de Langen AJ, Smit EF, van Velden FH, Hoekstra OS, van Tinteren H, et al. Repeatability of metabolically active volume measurements with 18F-FDG and 18F-FLT PET in non-small cell lung cancer. J Nucl Med. 2010;51:1870-7.

[29] Bos R, van Der Hoeven JJ, van der WE, van der GP, van Diest PJ, Comans EF, et al. Biologic correlates of (18)fluorodeoxyglucose uptake in human breast cancer measured by positron emission tomography. J ClinOncol. 2002;20:379-87.

[30] Vordermark D, Kaffer A, Riedl S, Katzer A, Flentje M. Characterization of carbonic anhydrase IX (CA IX) as an endogenous marker of chronic hypoxia in live human tumor cells. IntJ RadiatOncolBiolPhys. 2005;61:1197-207.

[31] Rademakers SE, Lok J, van der Kogel AJ, Bussink J, Kaanders JH. Metabolic markers in relation to hypoxia; staining patterns and colocalization of pimonidazole, HIF-1alpha, CAIX, LDH-5, GLUT-1, MCT1 and MCT4. BMCCancer. 2011;11:167.

[32] Rademakers SE, Span PN, Kaanders JH, Sweep FC, van der Kogel AJ, Bussink J. Molecular aspects of tumour hypoxia. MolOncol. 2008;2:41-53.

[33] Brown JM. Evidence for acutely hypoxic cells in mouse tumours, and a possible mechanism of reoxygenation. BrJ Radiol. 1979;52:650-6.

[34] Burgman P, Odonoghue JA, Humm JL, Ling CC. Hypoxia-Induced increase in FDG uptake in MCF7 cells. J NuclMed. 2001;42:170-5.

[35] Clavo AC, Brown RS, Wahl RL. Fluorodeoxyglucose uptake in human cancer cell lines is increased by hypoxia. J NuclMed. 1995;36:1625-32.

[36] Minn H, Clavo AC, Wahl RL. Influence of hypoxia on tracer accumulation in squamous-cell carcinoma: in vitro evaluation for PET imaging. NuclMed Biol. 1996;23:941-6.

[37] van Laarhoven HW, de Geus-Oei LF, Wiering B, Lok J, Rijpkema M, Kaanders JH, et al. Gadopentetate dimeglumine and FDG uptake in liver metastases of colorectal carcinoma as determined with MR imaging and PET. Radiology. 2005;237:181-8.

6

Repeatability of dynamic 18F-FDG PET compared to static ^{18}F-FDG PET in liver metastases of colorectal cancer

Abstract

Aim: The aim of this study was to validate glucose metabolic rate (MR_{glu}) obtained by dynamic FDG PET in colorectal liver metastases in terms of repeatability. Repeatability of MR_{glu} was compared to the repeatability of static FDG PET parameters.

Methods: 11 patients scheduled for metastasectomy of colorectal liver metastases participated in the study. Two 60-minute dynamic FDG PET scans per patient were performed within a week. In the last time frame (50-60 minutes) liver metastases were delineated with a background corrected threshold method and a 70% isocontour, to determine the SUV_{MAX}, SUV_{70} and $SUV_{SBR.}$ The metabolic rate map was calculated using a 50% and 70% isocontour value to determine maximum metabolic rate (MR_{glu}), MR_{glu50} and MR_{glu70}. Repeatability of static and dynamic parameters were compared. After resection, tumor volume, expression of glucose uptake transporter 1 (GLUT1), Ki67 (proliferation marker), hexokinase II (HXKII), CA-IX (hypoxia-related marker) and CD34 (vasculature) were determined.

Results: Scans of 9 patients with 15 FDG PET positive lesions were suitable for evaluation; two patients had no FDG uptake in the liver metastases. The coefficient of repeatability of MR_{glu} was superior compared to semi-quantitative PET parameters. The coefficient of repeatability was 32.5%, 33.4% and 30.1% for the maximum MR_{glu}, MR_{glu70} and MR_{glu50}. The coefficient of repeatability was 40.9% for the SUVmax, 41.6% for the SUV_{70} and 37.7% for the $SUV_{SBR.}$ There was no correlation between PET-parameters and individual histopathology results.

Conclusion: Despite smaller coefficients of repeatability of MR_{glu} compared to SUV, this difference did not reach significance. However, the metabolic rate has a higher tumor to background ratio compared to SUV and may therefore improve detections of lesions. Therefore, dynamic FDG PET may still be usefull in response monitoring studies, especially in facilitating tumor delineation and metabolic volume measurement.

Introduction

Molecular imaging techniques, like positron emission tomography (PET), can quantify molecular tumor characteristics. In the clinic, 18F-FDG PET is most commonly used for its diagnostic value to detect and characterize tumor lesions and to quantify tumor glucose metabolism. The usefulness of 18F-FDG PET for response prediction and (early) response monitoring is still subject of intensive research. In general, 18F-FDG PET shows high sensitivity to treatment induced changes [1]. In colorectal liver metastases significant decreases in standardized uptake values (SUV), were observed after systemic treatment in responding lesions [2].

However, the ability of 18F-FDG PET to monitor treatment response in individual patients does not only depend on the sensitivity of PET parameters to treatment-induced effects. A good repeatability of the PET parameters is also a prerequisite. Repeatability evaluates the normal spread in PET parameters due to measurement errors and normal variation and is, therefore, needed to determine what changes are due to real biological changes and can thus be considered clinically relevant in an individual patient. Although encouraging results of 18F-FDG PET in response monitoring studies as early as 72 hours after start of treatment have been reported [3], sufficient repeatability seems even more essential for early response monitoring as metabolic changes may still be very subtle at early time points.

The repeatability of SUV measurements reported previously might therefore not be sufficient early after start of treatment [4-6]. We hypothesize that the mediocre repeatability in these static studies performed after 60 min, is due to the fact that the steady state in colorectal carcinoma is reached beyond 60 min. post-injection. However, to our knowledge, no data on repeatability of (full) pharmacokinetic analysis in patients with colorectal liver metastases have been reported. Therefore, the objective of the present study, is to investigate whether dynamic FDG-PET can provide better results.

Dynamic PET parameters, including the metabolic rate of glucose (MRglu) assess the FDG uptake rate over time and might therefore be less influenced by the fact that the plateau phase is not yet reached. Moreover, MRglu is independent of vascular supply of nutrients and competitive uptake in other tissues [7], both factors that can influence repeatability of SUV measurements. For this reasons, dynamic PET measurements may have a superior repeatability compared to static PET measurement, while maintaining sensitive to changes in 18F-FDG uptake. Besides these advantages of dynamic PET-studies, metabolic rate of glucose (MRglu) gives a increased tumor to background ratio and smaller tumor volume than volume measurements with SUV [8, 9]. This is of increasing relevance, when background activity is high, as is the case in liver tissue. Therefore, volume measurements might be more reliable when derived from MRglu measurements than from static images (based on SUV). This may be of importance when volume or total lesion glycolysis is used for response monitoring or when PET images are used for radiotherapy planning.

On the other hand, dynamic PET imaging of the liver also comes with challenges. The dual blood supply of the liver (75% portal vein, 25% hepatic artery) means that using only the hepatic artery (or aorta) for input function, will not represent the actual blood supply to the tissue. [10]. However, since liver tumors and metastases are mainly dependent on the arterial supply, this effect might be relatively small [11, 12]. Moreover, when dynamic FDG PET is used to monitor effects of treatment over time, these effects may be clinically less relevant.

In this study, repeatability of dynamic 18F-FDG PET parameters, including full kinetic analysis, was assessed in colorectal liver metastases and compared to repeatability of SUV measurements. Volume measurements were compared to post-operative volume measurements and dynamic PET parameters were correlated to histopathology staining results.

Materials and method

Patient selection

Patients scheduled for metastasectomy of colorectal liver metastases were invited to participate in this study. In total, 11 patients were enrolled between July 2011 and October 2012. Exclusion criteria were diabetes mellitus, claustrophobia and pregnancy. Prior systemic antitumor therapy was not considered an exclusion criterion and patients could have received systemic therapy up to one month prior to study participation. The study was approved by the Institutional Review Board of the Radboud University Medical center. All patients provided written informed consent.

Dynamic PET imaging

Patients fasted for at least 6 hours before imaging. Blood glucose levels were monitored using an Accu-Check (Aviva) glucometer in whole blood. Given the scanning time of 60 minutes, no prehydration or diuretics were administered to the patients. The first four patients were scanned twice in a Biograph Duo PET/CT scanner (Siemens Medical Solutions USA, Inc., Knoxville, TN, USA). The last seven patients were scanned twice in a Biograph 40 mCT (Siemens Medical Solutions USA, Inc., Knoxville, TN, USA). Both systems were EARL-accredited [17].
Prior to each PET scan, a low dose CT was acquired during free breathing for PET attenuation correction. Approximately 3.5 MBq/kg 18F-FDG was administered intravenously with a remote controlled syringe pump at the start of the scan during 40 seconds. Afterwards the system was flushed with saline 8 mL/s for 5 s. The system was measured for residual activity in order to correct the administered activity. A plasma sample was withdrawn from a second intravenous catheter at 62-65 min (exact time point was registered) to enable correction of

the image derived arterial input function. This sample was measured together with an FDG sample as an internal standard. Analyses with and without correction of the whole blood curve for the measured activity in the plasma sample were carried out.

Data were acquired in list-mode setting, enabling retrospective time framing and image resonstruction. Images were reconstructed with the available reconstruction method. For scans from the Biograph Duo, 4 iterations / 16 subsets (4i/16s) OSEM-2D reconstruction, matrices 256x256x53, slice thickness 3mm, pixel spacing 2.65mm were used. For scans from the Biograph mCT, 3 iterations / 21 subsets (3i/21s) and using a point spread function based resolution recovery reconstruction, time of flight reconstructions, matrices 200x200x75, slice thickness 3mm, pixel spacing 4.07mm. PET data from both scanners were reconstructed into 70 time frames: 20x 5s, 5x 10s, 10x 15s, 10x 30s, 16x75s, 8x 150s, 1x600s. Images were smoothed using a 3 mm full width at half maximum (FWHM) Gaussian filter.

Dynamic PET analysis

Dynamic images were analyzed using Inveon Research Workplace (IRW 4.0, Siemens Healthcare). Patlak analyses using the data acquired between 10 and 60 minutes post-injection was performed to calculate parametric images of the metabolic rate of glucose (MR_{glu}) using the VOI of the aorta as whole blood file [13]. The lumped constant (LC) was set to 1.0. The software calculates the metabolic rate of glucose by the following formula: $\mathbf{MR_{glu} = [glu]/LC * K_i}$, while the influx constant K_i is calculated by the formula [14, 15]:

$$\frac{C_T(t)}{C_P(t)} = K_i \frac{\int_0^t C_P(\tau)d\tau}{C_P(\tau)} + intercept.$$

Pharmacokinetic rate constants (K_1,k_2,k_3,k_4 an blood volume fraction (v_b)) were calculated using an irreversible two compartment model and a reversible two compartment model, both with Poisson weighing. A correction of the time interval between the FDG concentration peak in the whole blood file and the tumor was applied.

An image derived arterial input function (IDIF) of the abdominal aorta was used, given that these IDIFs can be used as an adequate alternative to an arterial sampling derived arterial input function [16]. The IDIF was acquired by searching for the abdominal aorta with the highest SUVmax values within the first 70 seconds after FDG injection. A box was placed over the entire aorta, with the exception of the aorta visible in the borders of the field of view, because of the noise in the borders of the field of view. Voxels with a SUV >50% of the SUVmax were included in the VOI representing the aorta. An example of a typical VOI and arterial input function acquired with this method is shown in Figure 1. The arterial input was corrected for an overestimation due to partial volume effects and FDG uptake in the red blood cells, using the plasma sample taken at the end of the scan. The entire IDIF was corrected with a single factor, derived from the difference in the plasma sample and IDIF activity at 55 minutes.

MR_{glu} maps with and without plasma sample correction of the IDIF were calculated. In the MR_{glu} maps, the tumor was delineated using a border of 50% and 70% of the maximum metabolic rate and the average SUV of the voxels within the delineated area were determined (MR_{glu50} and MR_{glu70}). The tumor volume was determined by delineation of the tumor using the 50% order of the maximum MR_{glu}. The maximum MR_{glu}, MR_{glu50}, MR_{glu70} and volume were recorded.

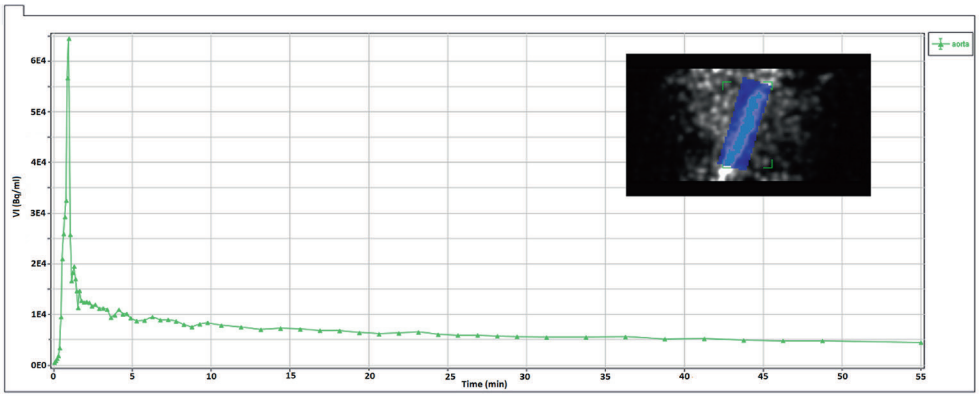

Figure 1. *Example of an image derived arterial input function. The green line shows the average activity per ml in the ROI of the aorta over time. The delineation of the aorta in an early timeframe is shown in the right upper corner.*

In the last time frame (50-60 minutes), a wide frame was drawn around each tumor, to determine the VOI. Tumors were delineated using 70% isocontours, a 50% isocontour and an adaptive threshold method of 41% of the SUVmax above background (average of the voxels in this isocontour: SUV_{SBR}):

threshold=$SUV_{background}$+0.41*(SUV_{max}-$SUV_{background}$) [17]. The average of the voxels in these isocontour resulted in the SUV_{70}, SUV_{50} and SUV_{SBR}, respectively. Furthermore, the maximal SUV (SUV_{max}), volume and total lesion glycolysis were recorded.

The 41% above background delineation method has also been used to determine the repeatability of SUVmean using static FDG PET in colorectal liver metastases [6] and therefore the SUV results (SUVmax and SUV_{SBR}) of the current study and the previous static FDG PET study could be compared. The SUV results of this and the previous study were also be combined to compare the repeatability of dynamic PET parameters with the static SUV measurements.

Immunohistochemistry

Of the 11 colorectal cancer patients who participated in the study histological material of 9 patients (10 liver metastases) was available for analysis. Before the samples were taken, the pathologist was asked to measure the tumor size in three orthogonal directions to estimate the tumor volume, by using the formula:

volume=1/6* π* h* l* b.

Immunohistochemistry of consecutive 4 µm paraffin embedded sections was performed to determine the expression of glucose uptake transporter 1 (GLUT1), Ki67 (proliferation marker), hexokinase II (HXKII), CA-IX (hypoxia-related marker) and CD34 (vasculature).
Sections were mounted on SuperFrost slides and dried overnight at 37°C. Before staining, all sections were deparaffinised in histosafe, rehydrated in graded ethanol solutions and kept for 30 minutes in Target Retrieval Solution. For another 30 minutes, the sections were preincubated with 5% normal donkey serum in primary antibody diluent (PAD, Abcam, Cambridge, UK). Staining was performed with commercially available antibodies. Between all steps, the sections were rinsed 3 times with PBS.
GLUT-1 was stained with rabbit-anti-GLUT-1 RB-9052 P1 (Labsource Inc., Illinois, USA) 1:400 in PAD 45 minutes at 37° and subsequently applying biotin-labeled-F(ab')2-donkey-anti-rabbit IgG (Jackson Immuno Research) 1:500 in PBS for 60 minutes at room temperature. Ki67 was stained with rabbit-anti-Ki67 (Abcam, Cambridge, UK) 1:100 in PAD for 30 minutes at room temperature and subsequently applying biotin-labeled-F(ab')2-donkey-anti-rabbit IgG (Jackson Immuno Research) 1:500 in PBS for 60 minutes at room temperature. For hexokinase staining 3 ug/ml goat polyclonal antibody sc-6521 (Santa Cruz Biotechnology, California, USA) was applied for 60 minutes followed by rabbit-anti-goat-biotin 1:200 (DAKO) for 30 minutes.
For CA-IX staining rabbit-anti-CAIX NB100 417B (Novus Biologicals, LCC, USA) 1:500 in PAD was applied on the tumor sections and kept overnight at 4° C. Sections were incubated with a second antibody, biotin-labeled-F(ab')$_2$-donkey-anti-mouse IgG (1:200 in PBS) for 60 minutes at room temperature. For CD34 staining mouse-anti-CD34 (Abcam, Cambridge, UK) 1:750 in PAD was applied to all tumor sections over night at 4°C. The sections were incubated with a second antibody, biotin-labeled-F(ab')$_2$-donkey-anti-mouse IgG (1:200 in PBS) for 60 minutes at room temperature.
ABC-reagent (Vector Elite kit, Vector Laboratories) was applied in all staining procedures. Peroxidase activity was detected with diaminobenzidine (DAB) and hematoxylin was used for counterstaining.
Using a monochrome CCD camera (Retiga SRV, 1392×1040 pixels) and a RGB filter (Slider Module; QImaging, Burnaby, BC, Canada) attached to a motorized bright field microscope (DM6000 Leica, Wetzlar, Germany) all slices were digitalized at 100X magnification. Image Processing Lab software (Scanalytics Inc., Fairfax, VA, USA) was utilized for the digitalization and following analyses. A region of interest was manually drawn around the entire tumor area, excluding necrotic areas. For all slices, the optimal threshold for positive staining was determined. Using Image J software, the fraction of positive staining was calculated relative to the total vital tumor area. For CD34 the number of vessels per square millimeter (vascular density) was scored. A more collaborate description of the used method is given by Rademakers et al [18].

Statistical Analyses

Statistical analyses were performed using Microsoft Office Excel 2007 and SPSS 20.0 (IBM SPSS Statistic, SPSS Inc., IBM, Chicago, IL). A lesion-by-lesion analysis of the 15 PET-positive liver metastases was performed. To asses repeatability a coefficient of repeatability (CR) was calculated. The coefficient of repeatability describes -within the paired PET measurements- the difference between the two scans that is smaller in 95% of the pairs. Therefore, changes smaller than the coefficient of repeatability could come from measurement errors and normal variation, while larger changes can be considered real biological changes. The CR is calculated by the formula: CR= 1,96* standard deviation. The differences in the measurements were proportional to the mean value. Consequently, percentual differences were used. The percentage differences were calculated using: **(parameter1-parameter2)/ average (parameter1, parameter2)*100**. The SD was calculated by taking the sum of the squared (percentage) differences, dividing them by the number of differences and taking the square root [19].

In order to compare the compare repeatability of dynamic PET parameters and static parameters the correlation coefficient R between parameter 1 and parameter 2 was calculated. The correlation coefficient R of the static parameters was compared with the coefficient R of the dynamic PET parameters using the Fisher r-to-z transformation [20]. Furthermore, Pearson correlations between the averaged imaging parameters and histopathology results were assessed.

Results

Patients

Patient characteristics are listed in table 1. Of the eleven included patients, two patients were excluded as there was no accumulation of FDG in their liver metastases, probably due to neoadjuvant chemotherapy treatment. Nine patients with 15 detectable colorectal liver metastases completed both dynamic PET scans within one week. The mean interval between the first and second scan was 2 days (range 1-5 days). An example of a tumor in the last time frame delineated with the background corrected method and the same tumor on the metabolic rate map delineated with 50% isocontour is shown in figure 2. There was a strong correlation between the MRglu and SUV measurements [figure 3]. An overview of the average values and repeatability of all parameters is given in table 2.

	Sex	Age	Neoadjuvant treatment	Glucose(1)	Glucose(2)	PET
1	F	48	+ (6 cycles)	5.0	5.0	Negative
2	F	50	-	4.6	5.2	1 liver metastasis
3	M	52	+ (3 cycles)	5.2	5.6	3 liver metastases
4	M	63	-	5.9	5.6	1 liver metastasis
5	F	65	+ (6 cycles)	5.0	5.1	2 liver metastases
6	M	70	+ (4 cycles)	6.3	7.0	Negative
7	M	57	-	6.7	6.9	1 liver metastasis
8	M	65	-	6.2	5.7	2 liver metastases
9	F	67	-	5.9	5.9	3 liver metastases
10	M	71	-	6.1	5.9	1 liver metastasis
11	M	69	-	6.0	5.8	1 liver metastasis

Table 1. *Characteristics of the participating patients.*

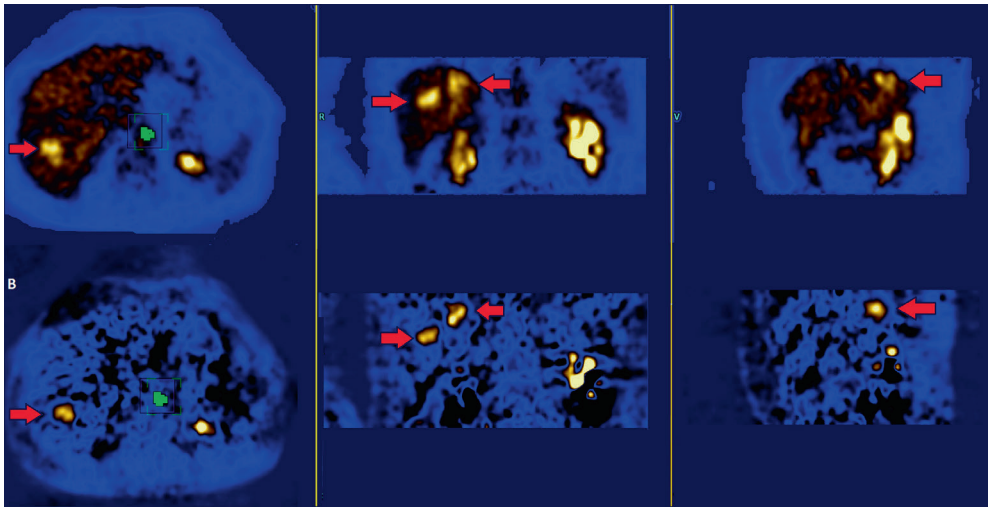

Figure 2. *Example of dynamic PET derived images of the same patient. Two liver metastases (red arrow) are shown on the last time frame (50-60 minutes) reconstruction (A) and on the metabolic rate map (B). The delineated aorta is shown in green.*

Standardized uptake values

The average SUV_{MAX}, SUV_{70}, SUV_{50} and SUV_{SBR} of the last 10-minute time frame were respectively 8.4±2.9 g/cm^3, 7.1±2.3 g/cm^3, 5.4 ±1.9 g/cm^{3}and 6.1±1.8 g/cm^3. The coefficient of repeatability was 40.9% for the SUV_{MAX}, 41.6% for the SUV_{70} and 37.7% for the SUV_{SBR}.
The repeatability of the SUV measurements derived from the last time frame of the dynamic PET were not better than the repeatability data acquired in the previous performed static PET study [6]. The coefficient of repeatability of the SUVmax and SUV_{SBR} of the dynamic PET scans (of the current study) and static PET scans (of the previous study) combined was 38.0% and 32.3%, respectively.

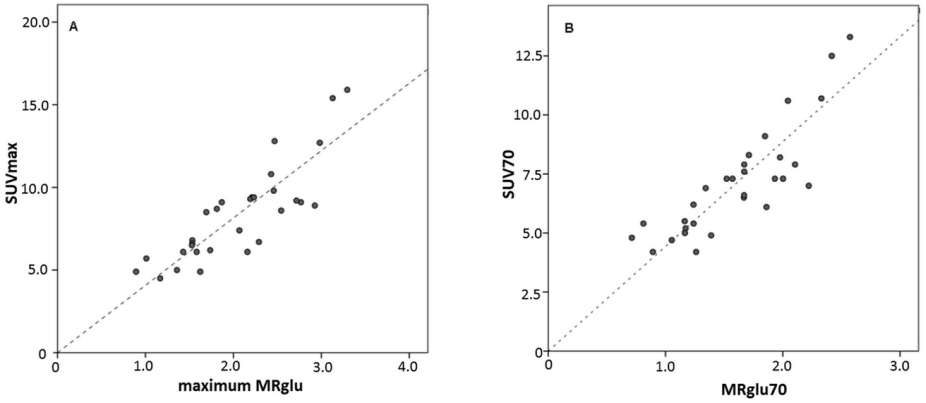

Figure 3. *Scatter plot showing the correlation between A) the SUVmax and maximum MR_{glu}, and B) the SUV_{70} and MR_{glu70}.*

Metabolic rate

The average maximum MR_{glu} in the liver metastases was 2.05±0.63 $*10^{-1}$ µmol/min/g, the MR_{glu70} in the liver metastases was 1.61±0.49 $*10^{-1}$ µmol/min/g and the MR_{glu50} in the liver metastases was 1.31±0.43 $*10^{-1}$ µmol/min/g without the correction of the IDIF for the measured activity in the plasma sample. The coefficient of repeatability was smaller in MR_{glu} measurements compared to the SUV measurements: 32.5%, 33.4% and 30.1%, respectively, for the maximum MR_{glu}, MR_{glu70} and MR_{glu50} [table 2 and figure 4].

When the whole blood file was corrected for the activity in the plasma sample taken directly after the scan, the metabolic rates in the metastases rose. The average maximum MR_{glu} increased to 3.72* 10^{-1} µmol/min/g, the average MR_{glu70} rose to 2.91* 10^{-1} µmol/min/g and the average MR_{glu50} rose to 2.39* 10^{-1} µmol/min/g. However, the repeatability deteriorated. The coefficient of repeatability was respectively 58.8%, 63.7% and 63.2% for the maximum MR_{glu}, MR_{glu70}, MR_{glu50} corrected metabolic rates.

When the correlation coefficient (R) between SUV_{MAX1} and SUV_{MAX2} (combined data, R=0.82) was compared with the correlation coefficient between the first and second maximum MR_{glu} measurements (R=0.94), there was only a trend towards a difference in correlation (p=0.09). There was no significant differences in the correlations between the SUV_{70} and MR_{70}, or SUV_{50} and MR_{70}.

Parameter		Average value	Coefficient of repeatability	R
SUV (last timeframe)		(N=15)		
	Maximum	8.4 g/cm^3	40.9%	0.83
	70% isocontour	7.1 g/cm^3	41.6%	0.79
	50% isocontour	5.4 g/cm^3	43.6%	0.85
	Background corrected threshold	6.1 g/cm^3	37.7%	0.82
MR$_{glu}$		(N=15)		
	Maximum	2.05*10^{-1} µmol/min/g	32.5%	0.94
	70% isocontour	1.61*10^{-1} µmol/min/g	33.4%	0.91
	50% isocontour	1.31*10^{-1} µmol/min/g	30.1%	0.95
Irreversible compartment model		(N=15)		
	k1	0.42 ml/g/min	59.0%	
	k2	0.67 min^{-1}	87.1%	
	k3	0.05 min^{-1}	49.7%	
	Vb	0.12	84.2%	
Reversible compartment model		(N=15)		
	k1	0.42 ml/g/min	47.7%	
	k2	0.70 min^{-1}	59.3%	
	k3	0.06 min^{-1}	63.8%	
	k4	0.018 min^{-1}	341%	
	Vb	0.11	79.6%	
SUV (data combined with previous study)		(N=39)		
	Maximum	8.1 g/cm^3	38.0%	0.82
	Background corrected threshold	5.7 g/cm^3	32.3%	0.85

Table 2. *Overview of the average value and repeatability of the quantitative and semi-quantitative PET parameters.*

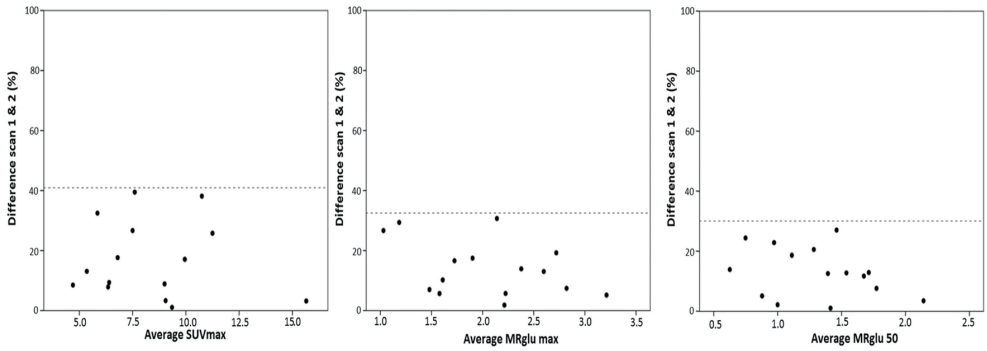

Figure 4. *Scatter plots of the percentage difference between the parameter on the first and second dynamic PET (y-axis) against the mean value (x-axis). Left: the difference in SUVmax versus the average SUV. Middle: the difference in maximum MR$_{glu}$ versus the average MR$_{glu}$. Right: the difference in MR$_{glu50}$ versus the average MR$_{glu50}$. The dotted lines indicate the coefficient of repeatability.*

Volume measurements

The average tumor volume assessed with the background corrected delineation method on the last time frame was 6.9±4.4 cm^3. The coefficient of repeatability of this volume measurement was 79.9%. The average tumor volume assessed with the SUV_{70} was 2.9±2.0 cm^3, with a poorer coefficient of repeatability of 107.3%.

The average metabolic tumor volume determined on the metabolic rate maps (50% isocontour of the maximum MR) was 6.7±3.9 cm^3. The average tumor volume assessed with the MR_{glu70} was 2.5±1.6 cm^3. The tumor-to-background ratio was on average 3.1 in the SUV measurements, while the tumor-to-background ratio was >100 fold on the MR_{glu} maps. However, despite the improved tumor-to-background ratio, only marginal improvement in the repeatability could be established: the CR of MR_{glu50} volume was 68.2%.

The volumes determined with SUV_{SBR}, SUV_{70}, MR_{glu50}, MR_{glu70} and volume estimated by 3-dimensional measurement by the pathologist were all strongly correlated. However, the larger the tumor the more the discrepancy between the PET determined volume and the volume calculated from the resection specimen. Either the PET volume showed an underestimation or the tumor volume calculated from the resection specimen showed an overestimation [figure 5].

The difference between the volume assessed with the 70% isocontours on MR_{glu} and SUV did not reach statistical significance (2.5 cm^3 vs. 2.9 cm^3, p=0.07).

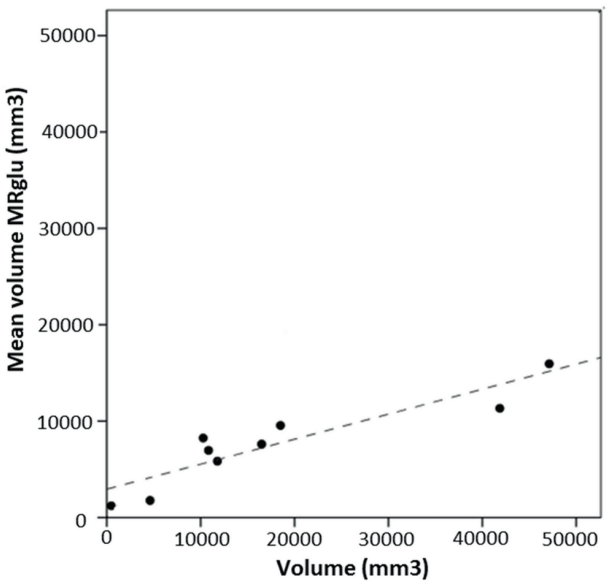

Figure 5. *Scatter plot of the average metabolic active volume on the MRguc map (y-axis) versus the tumor volume assessed by the pathologist (x-axis). MRglu volume underestimates the tumor volume mainly in larger metastases. The dotted line shows the linear fit through the scatter points.*

Pharmacokinetic rate constants

To assess the repeatability of the pharmacokinetic rate constants, the most reproducible tumor delineation method was chosen to draw the VOI: the $MR_{glu50.}$ In the irreversible two-compartment model k_1 was on average 0.42±0.20 ml/g/min, k_2 was on average 0.67±0.16 min^{-1}, k_3 was 0.05±0.03 min^{-1}, the blood volume fraction (v_b) was 0.12±0.05. When the reversible two-compartment model was used the kinetic values (k_1-k_3) hardly changed; k_1 was on average 0.42 ml/g/min, k_2 was on average 0.70 min^{-1}, k_3 was 0.06 min^{-1}, k_4 was 0.018 min^{-1}, the blood volume fraction (V_b) was 0.11.

The CR of k_1, k_2, k_3 and Vb were 59.0%, 87.1%, 49.7% and 84.2%, respectively, using the irreversible two-compartment model. The CR of respectively k_1, k_2, k_3 and V_b were 47.7%, 59.3%, 63.8%, 79.6% using the reversible two-compartment model. These are comparable repeatability values. However, the calculated dephosphorylation rate, k4, was not only insignificantly small but also poorly reproducible (CR 341%).

Immunohistochemistry

There was no correlation between GLUT1 (mean fraction 0.17±0.18), labeling index Ki67 (mean fraction 0.56±0.26), hexokinase 2 (mean fraction 0.08±0.05) or CA-IX expression (mean fraction 0.06±0.05) and SUV or MR_{glu} measurements. CD34 expression (74.5±34.6 vessels/mm^2) did not correlate to the blood volume assessed with kinetic analysis. Fraction positive hexokinase 2 staining in the tumor samples did not correlate with k_2 in the dynamic analysis of the entire tumor.

Discussion

The results of the present study show that the coefficient of repeatability in the standardized uptake values of the last time frame of the dynamic PET scans was in the same range as reported previously in static FDG PET scans of colorectal liver metastases [5]. Despite the fact that the time interval between injection and scanning in the current study was exactly the same between repetitive scans, no improvement in repeatability of the SUV measurements was established compared to the previous study [6]. Furthermore, there were no significant differences in injected doses and the mean interval between the two scans was very short, and could not explain the modest repeatability.

The repeatability of SUV measurements may have been negatively affected by the inclusion of patients who had recently received systemic therapy, as was shown in the previous study using static FDG PET scans [6]. Remaining effects of chemotherapy on the tumor cells could have influenced FDG uptake during the measurement s. Or conversely, tumor recovery (or flare-effects) might occur after therapy discontinuation and lead to increased FDG uptake during the second measurement. Both could hamper repeatability [6].

In accordance with previous reports, the current study shows a strong correlation between the SUV and MR_{glu}, [21, 22]. The repeatability of parameters of the parametric images, MR_{glu}, however, was better than of the SUV measurements. This difference did not reach statistical significance, perhaps due to the limited number of patients included in the study. We expected a more evident difference between the CR of dynamic and static PET scan parameters, as we hypothesized that in colorectal carcinoma the steady state would be reached beyond 60 min. post-injection. Other effects like vascular supply and competitive glucose may play a more important role, which would explain the better repeatability of MR_{glu} compared to SUV [7].
However, in some tumors, repeatability did not improve in MR_{glu} measurements compared to the SUV measurements. To calculate the metabolic rate, additional parameters are included in the formula, each of which has the risk of adding new potential measurement errors. For example, the whole blood file could include vessel wall tissue, which increases the amplitude of the input curve derived from later time frames and therefore could have an influence on the metabolic rate. Furthermore, noise in especially the short time frames could result in decreased accuracy of the measurements. A third variable is the plasma sample obtained at 60 min post injection, which is used to correct the IDIF for the higher activity in later time frames, due to uptake of FDG in the red blood cells en vessel wall [23]. In the present study, implementation of this plasma sample resulted in a dramatic deterioration of repeatability. The poorer repeatability may be caused by the addition of an extra variable with a potential measurement error. The repeatability of the (uncorrected) IDIFs was fairly good on visual inspection and the coefficient of the repeatability for the activity in the IDIF in the last time frame was small: 26.6%. The poor repeatability of the activity in the plasma sample is probably not due to equipment-based measurement errors, given the strict quality control program. However, given the higher FDG concentration in red blood cells compared to plasma, rupture of red blood cells during or after blood sampling could increase FDG concentration in the plasma sample. Furthermore, despite use of a precursor blood collection tube, it cannot be fully excluded that some residual normal saline in the system could have diluted the activity in some samples. Although the corrected metabolic rate values may in theory be closer to the true metabolic rate, we, therefore, advise against correction for FDG plasma levels when dynamic FDG PET is used for early response monitoring.
Despite the improved tumor-to-background ratio, the coefficient of repeatability of the metabolic volume determined with the metabolic rate map is only slightly superior to the repeatability of the metabolic volume measurements with static FDG PET. We did not observe significant smaller tumor volumes using the metabolic rate maps, as described in previous studies [8, 9]. The repeatability might be further improved by the use of automatic delineation methods, like the FLAB delineation method [4, 6, 24]. Especially in high tumor to background ratios this method might work well.

The absence of correlation between histopathology results and FDG-PET parameters may indicate that FDG uptake in tumor cells is multifactorial rather than the result of a single feature. However, the limited number of metastases available for analysis could also be a relevant factor as the low number precludes detection of weaker correlations. In the static FDG PET study (N=19) we observed a weak correlation between SUVmean and GLUT1 [6]. An additional confounding factor may be that the sample used for immunohistochemistry is not representative for the average expression in the tumor.

In conclusion, against expectations, dynamic FDG PET imaging did not significantly surpass the repeatability of static SUV measurements. Despite smaller coefficients of repeatability of MR_{glu} compared to SUV, this difference did not reach significance. However, the metabolic rate has a higher tumor to background ratio compared to SUV and may therefore improve detections of lesions. Delineation of the tumor on the parametric map also mildly improved the repeatability of tumor volume measurements. Therefore, dynamic FDG PET may still be usefull in response monitoring studies, especially in facilitating tumor delineation and metabolic volume measurement.

Reference list

[1] Weber WA. Assessing tumor response to therapy. J Nucl Med. 2009;50 Suppl 1:1S-10S.

[2] de Geus-Oei LF, Vriens D, van Laarhoven HW, Van Der Graaf WT, Oyen WJ. Monitoring and predicting response to therapy with 18F-FDG PET in colorectal cancer: a systematic review. J NuclMed. 2009;50 Suppl 1:43S-54S.

[3] Bender H, Bangard N, Metten N, Bangard M, Mezger J, Schomburg A, et al. Possible role of FDG-PET in the early prediction of therapy outcome in liver metastases of colorectal cancer. Hybridoma. 1999;18:87-91.

[4] Hatt M, Cheze-Le Rest C, Aboagye EO, Kenny LM, Rosso L, Turkheimer FE, et al. Reproducibility of 18F-FDG and 3'-deoxy-3'-18F-fluorothymidine PET tumor volume measurements. J Nucl Med. 2010;51:1368-76.

[5] de Langen AJ, Vincent A, Velasquez LM, van Tinteren H, Boellaard R, Shankar LK, et al. Repeatability of 18F-FDG Uptake Measurements in Tumors: A Metaanalysis. J Nucl Med. 2012.

[6] Heijmen L, de Geus-Oei LF, de Wilt JH, Visvikis D, Hatt M, Visser EP, et al. Reproducibility of functional volume and activity concentration in (18)F-FDG PET/CT of liver metastases in colorectal cancer. Eur J Nucl Med Mol Imaging. 2012.

[7] Vriens D, Disselhorst JA, Oyen WJ, de Geus-Oei LF, Visser EP. Quantitative assessment of heterogeneity in tumor metabolism using FDG-PET. Int J Radiat Oncol Biol Phys. 2012;82:e725-31.

[8] Cheebsumon P, van Velden FH, Yaqub M, Hoekstra CJ, Velasquez LM, Hayes W, et al. Measurement of metabolic tumor volume: static versus dynamic FDG scans. EJNMMI research. 2011;1:35.

[9] Visser EP, Philippens ME, Kienhorst L, Kaanders JH, Corstens FH, de Geus-Oei LF, et al. Comparison of tumor volumes derived from glucose metabolic rate maps and SUV maps in dynamic 18F-FDG PET. J Nucl Med. 2008;49:892-8.

[10] Keiding S. Bringing Physiology into PET of the Liver. J Nucl Med. 2012.

[11] Breedis C, Young G. The blood supply of neoplasms in the liver. The American journal of pathology. 1954;30:969-77.

[12] Brix G, Ziegler SI, Bellemann ME, Doll J, Schosser R, Lucht R, et al. Quantification of [(18)F]FDG uptake in the normal liver using dynamic PET: impact and modeling of the dual hepatic blood supply. J Nucl Med. 2001;42:1265-73.

[13] Patlak CS, Blasberg RG, Fenstermacher JD. Graphical evaluation of blood-to-brain transfer constants from multiple-time uptake data. Journal of cerebral blood flow and metabolism: official journal of the International Society of Cerebral Blood Flow and Metabolism. 1983;3:1-7.

[14] Wienhard K. Measurement of glucose consumption using [(18)F]fluorodeoxyglucose. Methods. 2002;27:218-25.

[15] Vriens D, Visser EP, de Geus-Oei LF, Oyen WJ. Methodological considerations in quantification of oncological FDG PET studies. Eur J Nucl Med Mol Imaging. 2010;37:1408-25.

[16] de Geus-Oei LF, Visser EP, Krabbe PF, van Hoorn BA, Koenders EB, Willemsen AT, et al. Comparison of image-derived and arterial input functions for estimating the rate of glucose metabolism in therapy-monitoring 18F-FDG PET studies. J Nucl Med. 2006;47:945-9.

[17] Boellaard R, O'Doherty MJ, Weber WA, Mottaghy FM, Lonsdale MN, Stroobants SG, et al. FDG PET and PET/CT: EANM procedure guidelines for tumour PET imaging: version 1.0. EurJ NuclMed MolImaging. 2010;37:181-200.

[18] Rademakers SE, Rijken PF, Peeters WJ, Nijkamp MM, Barber PR, van der LJ, et al. Parametric mapping of immunohistochemically stained tissue sections; a method to quantify the colocalization of tumor markers. Cell Oncol(Dordr). 2011;34:119-29.

[19] Dewitte K, Fierens C, Stockl D, Thienpont LM. Application of the Bland-Altman plot for interpretation of method-comparison studies: a critical investigation of its practice. ClinChem. 2002;48:799-801.

[20] Fisher RA. On the 'probable error' of a coefficient of correlation deduced from a small sample. Metron. 1921;1:3-32.

[21] Freedman NM, Sundaram SK, Kurdziel K, Carrasquillo JA, Whatley M, Carson JM, et al. Comparison of SUV and Patlak slope for monitoring of cancer therapy using serial PET scans. Eur J Nucl Med Mol Imaging. 2003;30:46-53.

[22] Cheebsumon P, Velasquez LM, Hoekstra CJ, Hayes W, Kloet RW, Hoetjes NJ, et al. Measuring response to therapy using FDG PET: semi-quantitative and full kinetic analysis. Eur J Nucl Med Mol Imaging. 2011;38:832-42.

[23] Lee JS, Su KH, Lin JC, Chuang YT, Chueh HS, Liu RS, et al. A novel blood-cell-two-compartment model for transferring a whole blood time activity curve to plasma in rodents. Computer methods and programs in biomedicine. 2008;92:299-304.

[24] Hatt M, Cheze Le RC, Turzo A, Roux C, Visvikis D. A fuzzy locally adaptive Bayesian segmentation approach for volume determination in PET. IEEE TransMed Imaging. 2009;28:881-93.

7

Monitoring hypoxia and vasculature during bevacizumab treatment in a murine colorectal cancer model

Abstract

Purpose: We assessed the effect of bevacizumab on vasculature and hypoxia in a colorectal tumor model.

Methods: Nude mice with subcutaneous LS174T tumors were treated with bevacizumab or saline. To assess tumor properties separate groups of mice were imaged using FMISO and FDG PET or MRI before and 2, 6 and 10 days after start of treatment. Tumors were harvested after imaging to determine hypoxia and vascular density immunohistochemically.

Results: T2* time increased significantly less in the bevacizumab group. FMISO uptake increased more over time in the control group. Vessel density significantly decreased in the bevacizumab-treated group. CAIX and GLUT1 fraction were higher in bevacizumab-treated tumors. However, the hypoxic fraction showed no significant difference.

Conclusion: Bevacizumab led to shorter T2* times and higher GLUT1 and CAIX expression, suggesting an increase in hypoxia and a higher glycolytic rate. This could be a mechanism of resistance to bevacizumab. The increase in hypoxia, however, could not be demonstrated by pimonidazole/ FMISO, possibly because distribution of these tracers is hampered by bevacizumab-induced effects on vascular permeability and perfusion.

Introduction

Bevacizumab (Avastin®) is an antibody against vascular endothelial growth factor (VEGF), inhibiting VEGF stimulated angiogenesis [1]. In advanced colorectal cancer bevacizumab has shown to increase progression free survival, when combined with cytotoxic treatment [2-5]. The exact mechanism of action of bevacizumab has not yet been clarified, nor are mechanisms of resistance to bevacizumab understood. It has been suggested that bevacizumab leads to vascular normalization of tumor vessels, thereby increasing delivery of cytotoxic agents to the tumor and thus improving treatment efficacy [6, 7]. Contrarily, other hypotheses claim that bevacizumab may lead to formation of inadequate tumor vessels inducing tumor hypoxia and necrosis [8]. Although inadequate vasculature and tumor hypoxia may subsequently lead to tumor necrosis, induction of hypoxia could also drive progression towards a more aggressive tumor phenotype [9, 10]. Hypoxic tumors are less responsive to systemic therapy and radiation therapy [11, 12]. This could explain the suboptimal results of bevacizumab treatment in various cancer types, including breast cancer [13-15]. The suboptimal results have recently led to withdrawal of FDA approval for the use of bevacizumab in combination with paclitaxel in metastatic breast cancer [16].

In this study we aim to assess the biological effects of bevacizumab over time in a colorectal cancer model. Functional imaging techniques were used to assess the biological effects of bevacizumab on hypoxia and functional vasculature, since these in vivo measurements provide the opportunity for repeated measurements and can also be implemented in clinical studies.

^{18}F-Fluoromisonidazole (FMISO) is a nitro-imidazole derivative, which is reduced into intermediary metabolites by intracellular enzymes at low intracellular pO2. After bioreduction FMISO (metabolites) are trapped in hypoxic cells allowing for PET imaging of hypoxic tumors [17]. Thus, FMISO PET is sensitive to hypoxia and, therefore, could probably provide an answer whether treatment with bevacizumab increases tumor hypoxia. However, no FMISO PET data after bevacizumab treatment are available.

^{18}F-Fluorodeoxyglucose (FDG) PET is sensitive to changes in tumor glucose metabolism over time. FDG uptake depends on expression of GLUT1, the main glucose and FDG transporter, and the presence and activity of the enzyme hexokinase. FDG uptake is also dependent on tumor vascularity for supply of FDG and might be influenced by tumor hypoxia due to the Pasteur effect [18, 19]. However, often tumors exhibit enhanced glycolysis under normoxic conditions (Warburg effect) for ATP production. FDG PET has been shown to have predictive value for response to several cytostatic treatments [20], including bevacizumab containing treatments [21-23].

In contrast to FDG PET, dynamic contrast enhanced MRI (DCE-MRI) is a direct measurement of functional vasculature. Various DCE-MRI parameters, such as the area under the contrast

concentration curve (AUC), blood volume, K^{trans} and k_{ep} have been shown to change after administration of antiangiogenic or antivascular drugs [21, 24, 25]. Similarly, T2* MRI can be used to assess vascular properties, without the requirement for the administration of contrast agents. T2* MR contrast arises from local inhomogeneities of the magnetic field mainly due to the tissue level of blood deoxyhemoglobin [26]. Therefore, T2* measurements are dependent on hypoxia, blood flow, and blood volume [27].
In this study, we assessed the effect of bevacizumab on functional imaging parameters with FMISO PET, FDG PET, DCE- MRI and T2* at different time points after start of treatment to assess whether bevacizumab increases hypoxia due to a disruption of tumor vasculature. Immunohistochemical analyses were used to corroborate our results.

Materials and methods

Animals

Seventy female BALB/c nu/nu mice of 19-24 gram and 6-8 weeks of age were purchased from Janvier (Uden, the Netherlands). Mice were allowed to adapt during one week after transport and were held in a controlled environment in accordance with institutional guidelines (temp. 22 °C, humidity 61%, 12 hours light-dark cycle, in individually ventilated cages). Food and water were supplied ad libitum.
Mice were injected subcutaneously, just above the right scapula, with ~$1*10^6$ cells of the bevacizumab sensitive human colon cancer cell line LS174T (CCL-188; passage 7; American Type Culture Collection, Manassas, VA, USA).. After 14 days, tumors had grown to a maximum diameter of 0.4-0.8 cm and treatment was started. Animals were divided into four groups: an experimental group undergoing MR imaging; an experimental group undergoing PET imaging; a control group undergoing MR imaging and a control group undergoing PET imaging. For each day of imaging a separate group of mice was used, except for the sequential PET imaging days. In order to reduce the burden of repetitive anesthesia for each mouse, to make sure overall drop out was low and measurements were reliable, separate groups of 5 mice were used for PET and MR-imaging on each day [Figure 1].
All experiments were approved by the Animal Welfare Committee of the Radboud University Medical Centre.

Treatment

In the experimental group, bevacizumab (Avastin®, Roche Pharma, Germany) was administered twice a week (during 10 days) by intraperitoneal injection in a dose of 5 mg/kg. The control group received an intraperitoneal injection with 0.9% saline at the same time points.

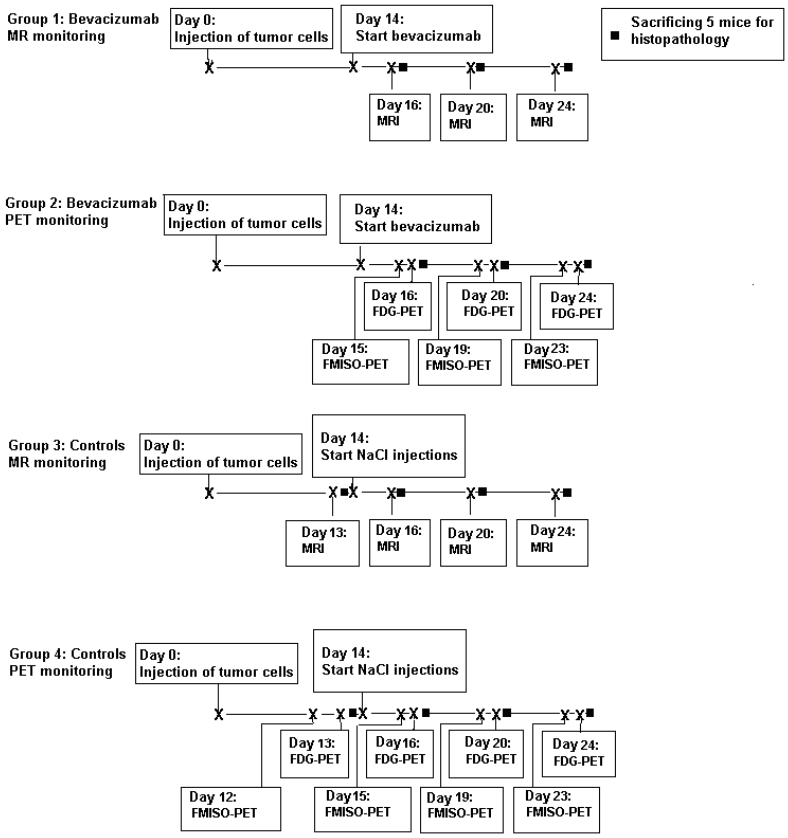

Figure 1. *Schedule of imaging and sacrificing of the mice.*

Imaging

PET imaging was performed on an Inveon preclinical PET scanner (Inveon, Siemens USA, Inc., Knoxville, TN). FMISO PET imaging was performed before treatment and 1, 5 and 9 days after start of bevacizumab therapy. FDG PET imaging was performed before treatment and 2, 6 and 10 days after start of bevacizumab therapy [Figure 1]. Before FDG PET imaging, mice fasted for 12 hours. Ten minutes before administration of FDG mice were anaesthetized with Isoflurane 4% for induction and 1.5-2% for maintenance. A 60 minute interval between injection of FDG an FMISO and start of the PET scan was used. All PET scans were a 20 minute single bed position measurements. Mice were injected intravenously in an inserted tail vein cannula with a solution of approximately 10 MBq of the radiotracer in 0.2 ml NaCl 0.9%. Images were reconstructed using OSEM-3D-MAP reconstruction. The highest standardized uptake values (SUVmax) for both FMISO and FDG PET were recorded for each tumor, by drawing a ROI around the entire tumor. In general, SUVmax has a larger change after start of treatment than SUVmean. Therefore the SUVmax values are reported.

MR imaging was performed on a 7 Tesla small animal MR scanner (Clinscan, Bruker Biospin, Ettlingen, Germany) using a Bruker rat brain receiver coil. Imaging was performed at baseline and 2, 6 and 10 days after start of therapy.
DCE-MRI was performed using a T1 weighted fast low-angle shot (FLASH) sequence. Sequence parameters: repetition time (TR) 90ms, echo time 1.82 ms, flip angle 15 degrees, 16 slices with a thickness of 1 mm, field of view 30 mm, matrix size 64x64.
After approximately 6 seconds, 0.2 ml (0.02 mmol/ml) of the contrast agent Gadomer-17 (Schering AG, Berlin, Germany) was injected in the tail vein cannula. Before and after DCE-MRI proton density images were recorded with the same sequence parameters as the DCE-MRI except for the flip angle 20 degrees and TR 1500 ms. Data from these images were combined with the DCE-MRI data to calculate the concentration of Gadomer-17, using the method described by Hittmair et al.[28] area under the concentration peak (AUC) was calculated for 0- 90 seconds and 0-180 seconds after contrast injection.
T2* imaging was performed with a gradient echo sequence, with a TR of 1000 ms and 6 different TE-times: 2.78, 4.86, 6.89, 8.92, 10.95 and 12.98 ms. Eighteen 1mm slices were obtained with 2 averages. T_2* calculated maps were generated using in-house built software based on Matlab (MathWorks, Natick, MA, USA). The data was fitted pixel by pixel to a mono-exponential curve $SI = A\ \rho\ exp(- TE / T_2^*) + B$ where ρ is the proton density, TE is the echo time, and the parameter of interest T_2^*, the relaxation time. The ROI for the MR images were manually drawn on T2 images and copied onto the T2* map and contrast concentration images.

Immunohistochemistry

To correlate in vivo hypoxia and vasculature measurements with ex vivo measurements, all mice were euthanized immediately after the last scan. Respectively 50-80 minutes and 2 minutes before death, the hypoxic marker pimonidazole (80 mg/kg in 0.1 ml) ((1-[(2-hydroxy-3-piperidinyl) propyl]-2-nitroimidazole hydrochloride; Natural Pharmacia International, Research Triangle Park, NC 80 mg/kg in 0.1 ml) and the perfusion marker Hoechst 33342 (Sigma Chemical Co., St Louis, MO) were administered. Tumors were removed and snap-frozen in liquid nitrogen. Tumors were stored at-80°C.
Tumor sections (4 µm) were fixed in acetone at 4°C for 10 minutes and washed with phosphate buffered saline (PBS). The sections were incubated overnight at 4°C with a rabbit anti-pimonidazole (gift from J.A. Raleigh, Department of Radiation Oncology, University of North Carolina School of Medicine, Chapel Hill, NC, USA) in primary antibody diluent (1:1000) (PAD, Abcam, Cambridge, UK). Sections were rinsed 3 times with PBS. To stain the vasculature, undiluted 9F1 (rat anti-mouse endothelium, dept Pathology Radboud University Medical Center) was applied to the slides for 45 minutes at 37°C.

To extend our data concerning hypoxia and functionality of the vessels after bevacizumab treatment, all tumors harvested on day 10 were stained for carbonic anhydrase IX (CAIX) and glucose uptake transporter 1 (GLUT1). Sections were pre-incubated for 30 minutes in 5% normal donkey serum (NDS) in primary antibody diluent (PAD). CAIX was stained by applying rabbit anti-CAIX-biotin (Novus Biologicals NB100-417B) (1:500 in PAD) overnight at 4°C followed by mouse anti-biotin-Alexa4888 (1:200 in PAD) for 30 minutes at 37°C. GLUT1 was stained using rabbit anti-GLUT1 (Neomarkers) (1:100 in PAD) overnight at 4°C and goat anti-rabbit-Cy3 (1:600 in PBS), 30 min at 37 °C. In between, sections were rinsed 3 times with PBS. Sections were mounted in Fluorostab.
Using a fluorescence microscope (Axioskop, Zeiss, Göttingen, Germany) all stained sections were digitalized using a computer-controlled motorized stepping stage system. By means of Image Processing Lab software (Scanalytics Inc., Fairfax, VA, USA), the tumor area was drawn, excluding necrotic areas. The fraction of positive staining in the total tumor area was calculated, providing the hypoxic fraction (fraction of pimonidazole positive staining) and vascular density (number of vessels within 1 mm^2) [29].

ELISA procedure for Bevacizumab

Bevacizumab concentration in plasma was measured with a 1-site enzyme-linked immunosorbent assay (ELISA). In short, 96-well plates (Greiner Bio-One, Alphen a/d Rijn, The Netherlands) were coated overnight at 4°C with 100 µl VEGF (0.50 µg/ml, Genentech Inc, San Francisco, CA), washed (96PW plate washer, Tecan Group Ltd., Männedorf, Switzerland), and then blocked with 150 µl Superblock (Pierce, Rockford, IL) during 30 minutes at ambient temperature, washed and further blocked with 300 µl bovine serum albumin (BSA) (Sigma Chemical, St. Louis, MO) for 4 hours at ambient temperature. Subsequently, the plate was washed and standards (range 0-10 ng/ml Avastin, Roche, Basel, Switzerland), study samples and a reference sample were put into the wells and the plate was incubated overnight at 4°C. After washing, the plate was incubated with 100 µl Mouse anti-Human IgG (Fc) peroxidase, (dilution 1:25,000, SouthernBiotech, Birmingham, U.K.) for 2 hours at ambient temperature, again washed and incubated with 100 µl ready-to-use tetramethyl benzidine (TMB) solution (Kem-En-Tec, Taastrup, Denmark) for 15-20 minutes for color development. The reaction was terminated by addition of 0.5 M H_2SO_4 and optical density was measured at 450 nm in a Multiskan Ascent plate reader (Lab Systems, Oy, Helsinki, Finland). The analytical sensitivity, defined as the minimum bevacizumab concentration evoking a response significantly different from that of the zero calibrator, was 16 pg/ml. Plasma samples, diluted 4,000 – 24,000 fold, exhibited excellent linearity. To six plasma samples known quantities of bevacizumab were added. The recoveries in the plasma samples ranged from 87% to 110% with a mean recovery of 98%. In each run the reference preparation, prepared from a pool of plasma from animals treated with bevacizumab, was used to monitor the long-term performance of the assay. The

concentration in the reference preparation was 1670 ng/ml, the within-run coefficient of variation (CV) and the between-run CV were 7.0% and 10.0%, respectively.

Statistical analyses

To compare the course of changes in the parameters over time between the bevacizumab and control group, linear regression analysis was used. Linear regression analysis assessed the effect of treatment over time on hypoxia and vasculature. We assessed the interception of the lines of the bevacizumab and control groups at day 0. When the lines did not intercept at day 0, we started linear regression analyses from day 1 (start of treatment). This method of analysis was used to accommodate a flare-up in (PET) parameters directly after start of treatment. This flare-up has directly after start of treatment has been described before by Findlay et al [30].If the lines did intercept, the regression analyses were started at the baseline measurements. The difference in the course of the measurement parameters over time in the bevacizumab and control group was expressed in a standard coefficient beta. Linear regression analysis was also used to assess whether parameters changed in time independent of treatment. A Student *t*-test was used to test for differences between control and treatment groups at the last time point, since the differences were expected to be largest at the last measurement. Furthermore, a Student *t*-test was used to compare CAIX and GLUT1 staining at the same time point. A Pearson correlation was used to assess correlations between image parameters and histopathology results. *P* values <0.05 were considered to be statistically significant. All data were analyzed using SPSS 16.0 (SPSS inc, Chicago, IL, USA).

Results

Tumors

In 69 of the 70 mice subcutaneous tumor growth was observed. Therefore, 34 mice were imaged with FMISO and FDG PET and 35 mice with MRI, leaving only 4 mice in the intervention group at day 9 and 10 measured with PET. All other groups contained 5 mice. Tumor volume (measured with MR) increased over time (r=0.46 p<0.01). The average tumor volume before the start of treatment was 310 ±156 mm^3, while the average volume 10 days after the start of treatment was 420 ±137 mm^3 for the intervention group and 783 ±179 mm^3 for the control group. The increase in tumor volume was significantly larger in the untreated control group compared to the bevacizumab group (standardized coefficient beta-0.62, p=0.01) [Figure 2].

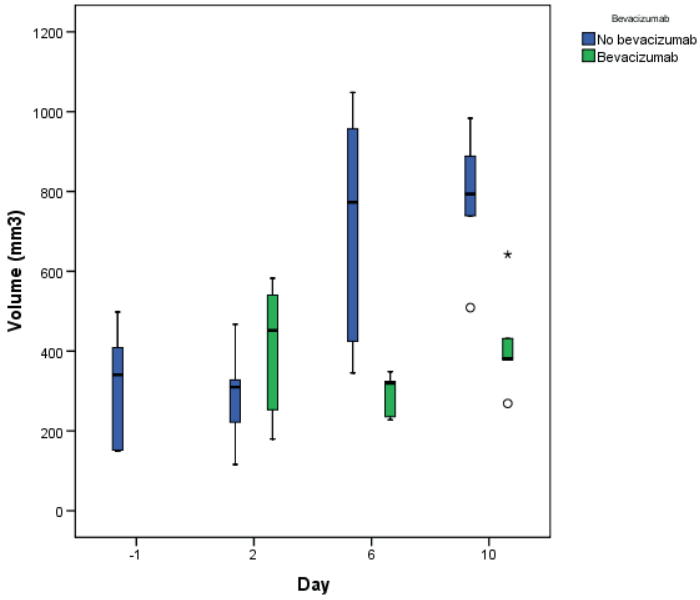

Figure 2. *Box plot of the mean tumor volume. The increase in tumor volume was significantly less pronounced in the bevacizumab group (beta -0.62 p<0.01).*

Imaging

FMISO particularly accumulated in the centre of the tumor, while FDG uptake was mainly observed at the tumor rim [Figure 3]. FMISO uptake in the tumor as measured by SUVmax steadily increased over time from 0.67 g/cm^3 before treatment to 1.43 g/cm^3 at day 9 in the control group. In the bevacizumab group the SUVmax increased from 0.67 g/cm^3 before treatment to 1.25 g/cm^3 at day 1, but thereafter decreased to 0.91 g/cm^3 and 0.88 g/cm^3 at days 5 and 9, respectively [Figure 4A]. Regression analysis starting from start of treatment showed a significant difference in the course of FMISO uptake between the treated group and the control group, with less hypoxia in the treated group (standardized coefficient beta -0.85, p=0.04). At day 10 there was a trend towards a difference between the bevacizumab-treated and control group (0.88 versus 1.43 g/cm^3, p=0.07)

In the control group the average SUVmax of FDG increased from 0.53 g/cm^3 before treatment to 1.08 g/cm^3 at day 2 and then remained stable. In contrast, in the bevacizumab treated group SUVmax of FDG increased on day 2 (1.22 g/cm^3), but decreased again at day 6 and at day 10 (day 6: 1.04 g/cm^3, day 10: 0.88 g/cm^3) [Figure 4B]. With linear regression analysis no significant difference was observed in the course of FDG uptake between the two groups. However, after 10 days the FDG uptake was significantly lower in the bevacizumab-treated group (average SUVmax 0.88 g/cm^3 versus 1.10 g/cm^3, p=0.05). A positive correlation between FDG PET SUVmax and FMISO PET SUVmax values was observed (r=0.52, p=<0.01).

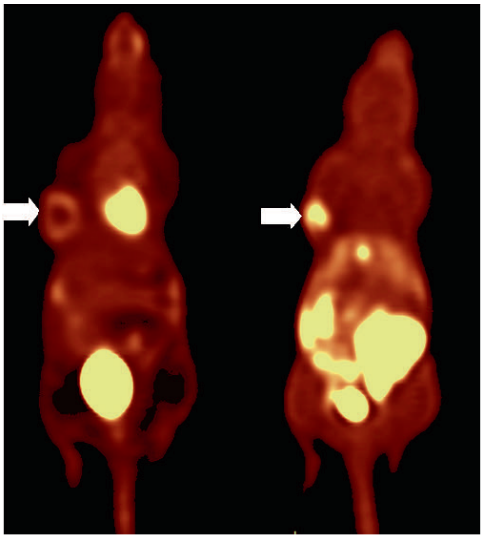

Figure 3. *An example of an FDG PET scan showing a tumor with the highest uptake in the rim and an FMISO PET showing uptake in the center of the tumor.*

On DCE-MRI, the AUC90 and the AUC180 decreased over time in both the bevacizumab treated and the control group. No significant differences were observed between the two groups, either in course over time (linear regression analysis) or at the last measurement (Student t-test) [Figure 4C]. However, the area under the contrast concentration curve was significantly lower in larger tumors (for AUC 180 r=-0.45, p=0.02, for AUC90 r=-0.44, p=0.02). The T2* value of the tumors increased over time from an average of 3.9 ms before treatment to 7.0 ms on day 10. The rise was more prominent in the control group than in the bevacizumab group (standardized coefficient-0.45, p=0.01). However, there was a large spread in the measurements [fig 4 D]. After 10 days a trend for a lower average T2* value was observed in the bevacizumab-treated mice compared to the control group (T2* at day 10: 5.14 ms versus 8.94 ms p=0.09). The T2* value correlated to the size of the tumor (r=0.68 p<0.01) in both the treated and untreated tumors.

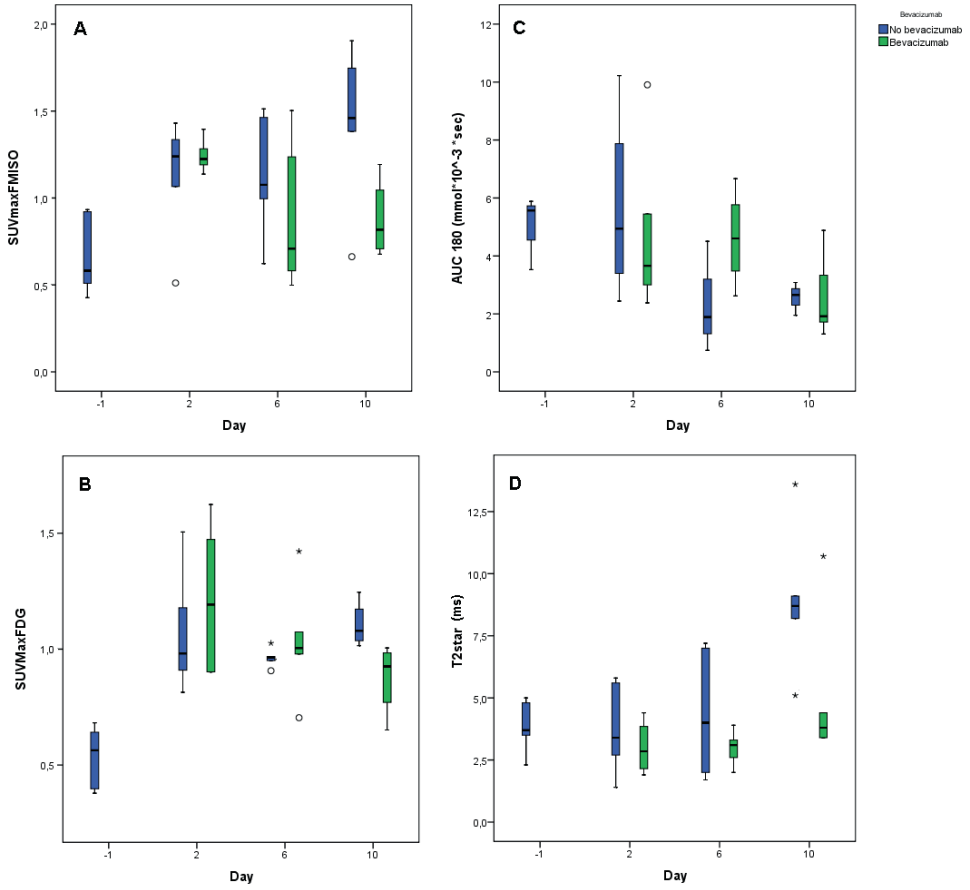

Figure 4. *(A) Maximum uptake values of FMISO (y-axis) versus the day of treatment (x-axis). (B) the maximum uptake values of FDG (y-axis) versus the day of treatment (x-axis). Maximum FDG uptake at day 10 was significantly lower in the bevacizumab group (green) than in the control group (blue) (p=0.01). (C) AUC180 values (y-axis) versus the day of treatment (x-axis). The AUC180 values decreased over time in both treatment and control group. (D) Boxplot of the mean T2* values (y-axis) versus the day of treatment (x-axis). The T2* values increased over time. The rise was more pronounced in the control group (-0.45, p=0.01).*

Immunohistochemical assessment of tumor hypoxia and vascular density

A typical image of the hypoxia, perfusion and vessels in the colorectal tumor is shown in figure 5. The hypoxic areas are widespread and shown in green (pimonidazol staining). The non-hypoxic areas were generally well perfused with Hoechst (blue) and high vascular density (red), but areas are overlapping indicating regions with acute hypoxia (perfused, Hoechst positive areas that are hypoxic (pimonidazol positive, green). The average hypoxic fraction in the LS174T tumors was 0.38 and did not significantly change over time. Furthermore, no difference in hypoxic fraction was observed between the treated and the control group.

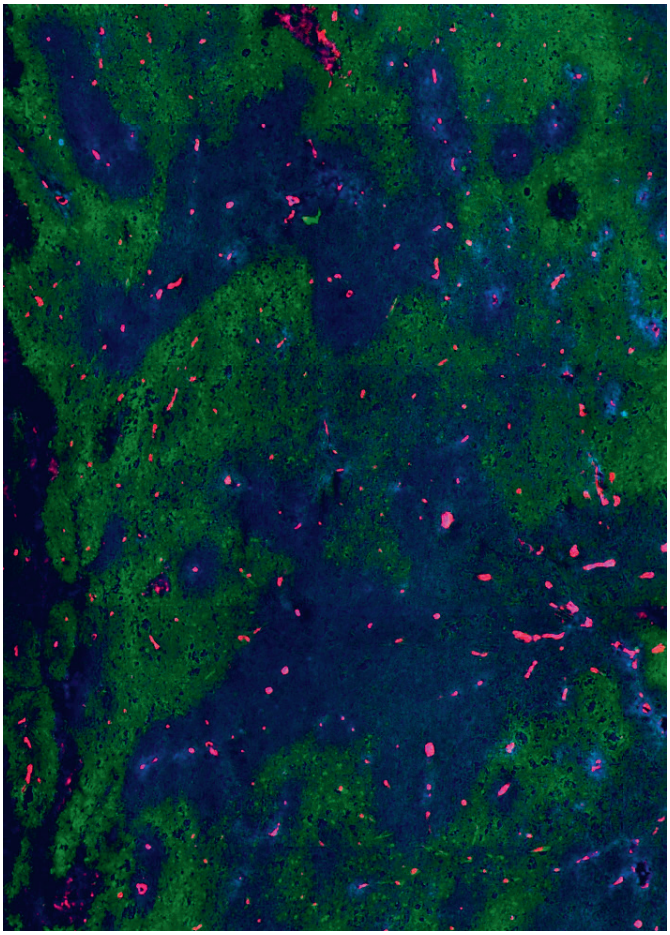

Figure 5. *Example of a vital non-necroltic area of an untreated tumor 10 days after start of treatment showing the combined image of hypoxia (pimonidazole, green), perfused vessels (hoechst, blue) and vessels (9F1, red).*

In contrast, CAIX and GLUT1, metabolic markers that are associated with hypoxia, were significantly higher in bevacizumab-treated tumors 10 days after start of treatment (0.22 versus 0.09, $p<0.01$ and 0.10 versus 0.05, $p=0.05$) [Figure 6]. Before start of treatment the average vascular density was 100.7 vessels/mm^2. Vascular density significantly decreased over time in the bevacizumab-treated group compared to the control group (beta -0.25, $p=0.05$). After 10 days of treatment the vascular density was 74.5±25.4 vessels/mm^2 in the bevacizumab-treated group and 110±36.0 vessels/mm^2 in the control group. There was a significant negative correlation between vascular density and CAIX expression ($r=-0.56$, $p=0.02$) and a significant positive correlation between CAIX and GLUT1 expression ($r=0.57$, $p=0.01$).

Vascular density was positively correlated to AUC180 (r=0.41 p=0.03). The average perfused fraction in the tumors was 0.41 and this parameter was unaffected by time or treatment. The perfused fraction did not significantly correlate with vascular density.

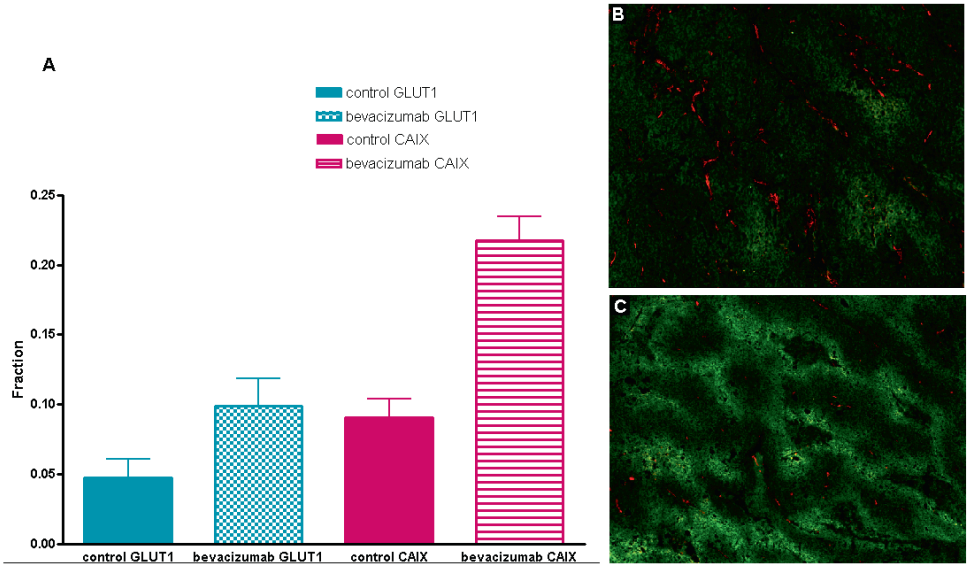

Figure 6. *Figure 6.A) Mean GLUT1 and CAIX staining in the control group and bevacizumab group at day 10. The difference in GLUT1 and CAIX expression differed significantly. (B) An example of an untreated tumor in the control group with low CAIX expression (green) and a high vascular density (red) and (C) an example of a treated tumor in the bevacizumab group of a tumor with a high CAIX expression and a low vascular density.*

Bevacizumab plasma levels

In the control group no bevacizumab was detectable. Plasma bevacizumab concentrations increased in the treatment group from an average of 30.2±15.0 µg/ml on day 2 to 56.4±2.3 µg/ml on day 6 and 61.5±16.6 µg/ml on day 10. Bevacizumab concentrations were inversely correlated with the immunohistochemically determined vascular density (r=-0.45 p=0.01) and positively correlated with CAIX expression in the tumor (r=0.77, p=0.02). Bevacizumab levels did not correlate to imaging parameters.

Discussion

In this study, functional imaging techniques were used to assess tumor hypoxia and vascularity after bevacizumab treatment. The FMISO PET imaging technique indicating hypoxia did not show an increase in hypoxia after bevacizumab treatment. In fact, FMISO PET even showed a trend towards a lower FMISO uptake in bevacizumab treated tumors, suggesting a decrease

in hypoxia. However, the lower T2* values measured with MRI in the bevacizumab-treated group pointed towards a higher deoxyhemoglobin concentration and thus hypoxia or a lower blood volume. Also, although pimonidazole binding in bevacizumab-treated tumor did not increase significantly, we observed a marked increase in the hypoxia-related metabolic parameters CAIX and GLUT1 in bevacizumab treated tumors. Furthermore, the level of bevacizumab in the blood of the mice was inversely correlated to CAIX expression, suggesting a stronger effect with longer and higher dose exposition. Finally, we observed an inverse correlation between CAIX and vascular density. Thus, these data suggest that bevacizumab treatment increases hypoxia in the tumor, which, however, could not be detected by FMISO PET or pimonidazole.

The question is how the conflict of data should be interpreted. It is relevant to note that all the techniques that used injected tracers to measure tumor hypoxia failed to show an increase in tumor hypoxia after bevacizumab treatment, while techniques based on intrinsic tumor properties did show an increase in hypoxia. It could be hypothesized that tracer distribution in the tumor is affected by the effect of bevacizumab on the number of functional vessels and vascular permeability. Previously, anti-VEGF has been shown to diminish accumulation of several macromolecules (trastuzumab, anti-EGFR and anti-IGF-1R antibodies) and of chemotherapy [31-33]. Moreover, to the combination of chemotherapy, cetuximab and bevacizumab led to detrimental outcome in colorectal cancer patients [34], which in part might be due to this phenomenon. The effect of bevacizumab on tumor accumulation of small molecules, such as FMISO, FDG and pimonidazole is unknown. However, our data suggest that also the uptake of small molecules may be hampered by bevacizumab treatment as well. therefore, the interval of 60 minutes for FMISO scanning may have been too short to reliably detect hypoxia. FMISO imaging in patients generally requires a 2-3 hours interval after injection [35]. Although metabolism and uptake in mice is generally faster than humans and shorter intervals have been described [36], our FMISO results may not only reflect tumor hypoxia, but also tumor vascular supply. In our study, higher blood levels of bevacizumab were associated with lower tumor vascular density. Similarly, in a study monitoring the vascular effects of the vascular disrupting agent (5,6-dimethylxanthenone-4-acetic acid, DMXAA) a marked decrease in FMISO uptake was observed in several tumors together with a decreased perfusion [36].

In the literature contradictory results have been reported concerning the effect of bevacizumab on tumor hypoxia. In various studies it has been reported that bevacizumab treatment resulted in vascular normalization. In two studies in murine melanoma and glioma models, treatment with bevacizumab decreased the hypoxic fraction measured with pimonidazole, and increased radiosensitivity [37, 38]. A study in patients with hepatic liver metastases of colorectal cancer who were treated with neoadjuvant chemotherapy and bevacizumab also showed that bevacizumab treatment resulted in tumor vessel stabilization,

leading to more mature, stable vessels with an increased diameter, while decreasing the vascular density and increasing necrosis [39]. In contrast, several studies showed an increase in pimonidazole positive areas after bevacizumab [40-42]. In the literature, hypoxic areas indicated by pimonidazole and CAIX seem to increase after bevacizumab administration, although pimonidazole staining gave some conflicting results (35-40). The conflicting results using pimonidazole staining support the hypothesis that intravascular tracers might be less reliable after administration of bevacizumab, because delivery of the tracer might be affected: pimonidazole does not increase while hypoxia indeed increases due to bevacizumab treatment.

However, we did not observe a drop in the perfusion marker Hoechst in the bevacizumab treated group. In line with this interpretation, DCE-MRI parameters AUC90 and AUC180 were not significantly different between the treated and untreated group, despite the observed decrease in vascular density in the immunohistochemical analysis of the bevacizumab treated tumors. These data oppose to the theory that bevacizumab significantly hampered the vascular supply of systemically administered tracers.

Alternative explanations for the conflicting results between HIF-1 upregulated markers GLUT1 and CAIX, and pimonidazole and FMISO, is the difference at which pO2 level CAIX is upregulated and nitroimidazoles are reduced. CAIX and GLUT1 up regulation likely starts at a higher pO2 level than nitromidazoles are reduced [43]. Therefore a small reduction in pO2 levels caused by bevacizumab treatment might increase CAIX expression without affecting pimonidazole and FMISO uptake. Furthermore, bevacizumab might cause tumor cells to switch towards a more glycolytic, anaerobe metabolism, decreasing the aerobe metabolism and need for oxygen. This implies that these cells could have a high expression of GLUT-1 and CA-IX, in order to allow for the high influx of glucose and efflux of the H+ ions needed for glycolysis, without an increase in hypoxia. Enhanced expression of the endogenous hypoxia marker CAIX was observed after bevacizumab administration in previous studies and is believed to be a mechanism of resistance to bevacizumab treatment [44]. Two studies showed bevacizumab efficacy increased by inhibiting CAIX or the HIF-1 pathway [41, 45].

In conclusion, in this study, bevacizumab treatment induced shorter T2* times on MR imaging, a higher fraction of the intrinsic hypoxia markers GLUT1 and CAIX on immunohistochemical staining, and a decreased vascular density, suggest an increase in tumor hypoxia -and glycolysis- mediated by a decrease in tumor vascularity. This could be a mechanism of resistance to bevacizumab. The increase in hypoxia, however, could not be demonstrated by pimonidazole or FMISO, possibly because the distribution of these tracers is hampered by the effects of bevacizumab on vascular permeability and perfusion.

Reference list

[1] Hicklin DJ, Ellis LM. Role of the vascular endothelial growth factor pathway in tumor growth and angiogenesis. J Clin Oncol. 2005;23:1011-27.

[2] Hurwitz H, Fehrenbacher L, Novotny W, Cartwright T, Hainsworth J, Heim W, et al. Bevacizumab plus irinotecan, fluorouracil, and leucovorin for metastatic colorectal cancer. N Engl J Med. 2004;350:2335-42.

[3] Kabbinavar FF, Schulz J, McCleod M, Patel T, Hamm JT, Hecht JR, et al. Addition of bevacizumab to bolus fluorouracil and leucovorin in first-line metastatic colorectal cancer: results of a randomized phase II trial. J Clin Oncol. 2005;23:3697-705.

[4] Saltz LB, Clarke S, Diaz-Rubio E, Scheithauer W, Figer A, Wong R, et al. Bevacizumab in combination with oxaliplatin-based chemotherapy as first-line therapy in metastatic colorectal cancer: a randomized phase III study. J Clin Oncol. 2008;26:2013-9.

[5] Tebbutt NC, Wilson K, Gebski VJ, Cummins MM, Zannino D, van Hazel GA, et al. Capecitabine, bevacizumab, and mitomycin in first-line treatment of metastatic colorectal cancer: results of the Australasian Gastrointestinal Trials Group Randomized Phase III MAX Study. J Clin Oncol. 2010;28:3191-8.

[6] Jain RK. Normalization of tumor vasculature: an emerging concept in antiangiogenic therapy. Science. 2005;307:58-62.

[7] Ma J, Waxman DJ. Combination of antiangiogenesis with chemotherapy for more effective cancer treatment. Mol Cancer Ther. 2008;7:3670-84.

[8] Leite de OR, Hamm A, Mazzone M. Growing tumor vessels: more than one way to skin a cat - implications for angiogenesis targeted cancer therapies. MolAspects Med.32:71-87.

[9] Conley SJ, Gheordunescu E, Kakarala P, Newman B, Korkaya H, Heath AN, et al. Antiangiogenic agents increase breast cancer stem cells via the generation of tumor hypoxia. Proc Natl Acad Sci U S A. 2012;109:2784-9.

[10] Yuan X, Qin L, Xiao-Yu L, Qiu-Ya Y, Wei-Wei X, Gao-Lin L. Short-term anti-vascular endothelial growth factor treatment elicits vasculogenic mimicry formation of tumors to accelerate metastasis. J Exp Clin Cancer Res. 2012;31:16.

[11] Brown JM, Wilson WR. Exploiting tumour hypoxia in cancer treatment. Nat Rev Cancer. 2004;4:437-47.

[12] Tredan O, Galmarini CM, Patel K, Tannock IF. Drug resistance and the solid tumor microenvironment. J Natl Cancer Inst. 2007;99:1441-54.

[13] Kindler HL, Niedzwiecki D, Hollis D, Sutherland S, Schrag D, Hurwitz H, et al. Gemcitabine plus bevacizumab compared with gemcitabine plus placebo in patients with advanced pancreatic cancer: phase III trial of the Cancer and Leukemia Group B (CALGB 80303). J Clin Oncol. 2010;28:3617-22.

[14] Ohtsu A, Shah MA, Van Cutsem E, Rha SY, Sawaki A, Park SR, et al. Bevacizumab in combination with chemotherapy as first-line therapy in advanced gastric cancer: a randomized, double-blind, placebo-controlled phase III study. J Clin Oncol. 2011;29:3968-76.

[15] Robert NJ, Dieras V, Glaspy J, Brufsky AM, Bondarenko I, Lipatov ON, et al. RIBBON-1: randomized, double-blind, placebo-controlled, phase III trial of chemotherapy with or without bevacizumab for first-line treatment of human epidermal growth factor receptor 2-negative, locally recurrent or metastatic breast cancer. J Clin Oncol. 2011;29:1252-60.

[16] Proposal to withdraw approval for the breast cancer indication for Avastin (bevacizumab). http://www.fda.gov/downloads/NewsEvents/Newsroom/UCM280546.pdf: FDA; 2011.

[17] Mees G, Dierckx R, Vangestel C, Van de Wiele C. Molecular imaging of hypoxia with radiolabelled agents. Eur J Nucl Med Mol Imaging. 2009;36:1674-86.

[18] Pauwels EK, Ribeiro MJ, Stoot JH, McCready VR, Bourguignon M, Maziere B. FDG accumulation and tumor biology. Nucl Med Biol. 1998;25:317-22.

[19] Busk M, Horsman MR, Jakobsen S, Bussink J, van der Kogel A, Overgaard J. Cellular uptake of PET tracers of glucose metabolism and hypoxia and their linkage. Eur J Nucl Med Mol Imaging. 2008;35:2294-303.

[20] Contractor KB, Aboagye EO. Monitoring predominantly cytostatic treatment response with 18F-FDG PET. J Nucl Med. 2009;50 Suppl 1:97S-105S.

[21] de Langen AJ, van dBV, Lubberink M, Backes WH, Marcus JT, van TH, et al. Monitoring response to antiangiogenic therapy in non-small cell lung cancer using imaging markers derived from PET and dynamic contrast-enhanced MRI. J NuclMed.52:48-55.

[22] Goshen E, Davidson T, Zwas ST, Aderka D. PET/CT in the evaluation of response to treatment of liver metastases from colorectal cancer with bevacizumab and irinotecan. Technol Cancer Res Treat. 2006;5:37-43.

[23] Vriens D, de Geus-Oei LF, Heerschap A, van Laarhoven HW, Oyen WJ. Vascular and metabolic response to bevacizumab-containing regimens in two patients with colorectal liver metastases measured by dynamic contrast-enhanced MRI and dynamic 18F-FDG-PET. Clin Colorectal Cancer. 2011;10:E1-5.

[24] Hirashima Y, Yamada Y, Tateishi U, Kato K, Miyake M, Horita Y, et al. Pharmacokinetic parameters from 3-Tesla DCE-MRI as surrogate biomarkers of antitumor effects of bevacizumab plus FOLFIRI in colorectal cancer with liver metastasis. Int J Cancer. 2011.

[25] Ungersma SE, Pacheco G, Ho C, Yee SF, Ross J, van BN, et al. Vessel imaging with viable tumor analysis for quantification of tumor angiogenesis. Magn ResonMed. 2010;63:1637-47.

[26] Chavhan GB, Babyn PS, Thomas B, Shroff MM, Haacke EM. Principles, techniques, and applications of T2*-based MR imaging and its special applications. Radiographics. 2009;29:1433-49.

[27] Howe FA, Robinson SP, McIntyre DJ, Stubbs M, Griffiths JR. Issues in flow and oxygenation dependent contrast (FLOOD) imaging of tumours. NMR Biomed. 2001;14:497-506.

[28] Hittmair K, Gomiscek G, Langenberger K, Recht M, Imhof H, Kramer J. Method for the quantitative assessment of contrast agent uptake in dynamic contrast-enhanced MRI. Magnetic resonance in medicine: official journal of the Society of Magnetic Resonance in Medicine / Society of Magnetic Resonance in Medicine. 1994;31:567-71.

[29] Hendriksen EM, Span PN, Schuuring J, Peters JP, Sweep FC, van der Kogel AJ, et al. Angiogenesis, hypoxia and VEGF expression during tumour growth in a human xenograft tumour model. Microvasc Res. 2009;77:96-103.

[30] Findlay M, Young H, Cunningham D, Iveson A, Cronin B, Hickish T, et al. Noninvasive monitoring of tumor metabolism using fluorodeoxyglucose and positron emission tomography in colorectal cancer liver metastases: correlation with tumor response to fluorouracil. Journal of clinical oncology: official journal of the American Society of Clinical Oncology. 1996;14:700-8.

[31] Van der Veldt AA, Lubberink M, Bahce I, Walraven M, de Boer MP, Greuter HN, et al. Rapid decrease in delivery of chemotherapy to tumors after anti-VEGF therapy: implications for scheduling of anti-angiogenic drugs. Cancer Cell. 2012;21:82-91.

[32] Pastuskovas CV, Mundo EE, Williams SP, Nayak TK, Ho J, Ulufatu S, et al. Effects of anti-VEGF on pharmacokinetics, biodistribution, and tumor penetration of trastuzumab in a preclinical breast cancer model. Mol Cancer Ther. 2012;11:752-62.

[33] Heskamp S, Boerman OC, Molkenboer-Kuenen JDM, Oyen WJG, van der Graaf WTA, van Laarhoven HWM. The effect of bevacizumab on targeting of anti-epidermal growth factor receptor and anti-insulin-like growth factor 1 receptor antibodies. J Clin Oncol 30. 2012;(suppl; abstr 3035).

[34] Tol J, Koopman M, Cats A, Rodenburg CJ, Creemers GJ, Schrama JG, et al. Chemotherapy, bevacizumab, and cetuximab in metastatic colorectal cancer. N Engl J Med. 2009;360:563-72.

[35] Lee ST, Scott AM. Hypoxia positron emission tomography imaging with 18f-fluoromisonidazole. Seminars in nuclear medicine. 2007;37:451-61.

[36] Oehler C, O'Donoghue JA, Russell J, Zanzonico P, Lorenzen S, Ling CC, et al. 18F-fluromisonidazole PET imaging as a biomarker for the response to 5,6-dimethylxanthenone-4-acetic acid in colorectal xenograft tumors. J Nucl Med. 2011;52:437-44.

[37] Masunaga S, Liu Y, Tanaka H, Sakurai Y, Suzuki M, Kondo N, et al. Reducing intratumour acute hypoxia through bevacizumab treatment, referring to the response of quiescent tumour cells and metastatic potential. Br J Radiol. 2011;84:1131-8.

[38] McGee MC, Hamner JB, Williams RF, Rosati SF, Sims TL, Ng CY, et al. Improved intratumoral oxygenation through vascular normalization increases glioma sensitivity to ionizing radiation. Int J Radiat Oncol Biol Phys. 2010;76:1537-45.

[39] Weisshardt P, Trarbach T, Durig J, Paul A, Reis H, Tilki D, et al. Tumor vessel stabilization and remodeling by anti-angiogenic therapy with bevacizumab. Histochem Cell Biol. 2012;137:391-401.

[40] Paez-Ribes M, Allen E, Hudock J, Takeda T, Okuyama H, Vinals F, et al. Antiangiogenic therapy elicits malignant progression of tumors to increased local invasion and distant metastasis. Cancer Cell. 2009;15:220-31.

[41] Rapisarda A, Hollingshead M, Uranchimeg B, Bonomi CA, Borgel SD, Carter JP, et al. Increased antitumor activity of bevacizumab in combination with hypoxia inducible factor-1 inhibition. Mol Cancer Ther. 2009;8:1867-77.

[42] Ren Y, Fleischmann D, Foygel K, Molvin L, Lutz AM, Koong AC, et al. Antiangiogenic and radiation therapy: early effects on in vivo computed tomography perfusion parameters in human colon cancer xenografts in mice. Invest Radiol. 2012;47:25-32.

[43] Airley RE, Loncaster J, Raleigh JA, Harris AL, Davidson SE, Hunter RD, et al. GLUT-1 and CAIX as intrinsic markers of hypoxia in carcinoma of the cervix: relationship to pimonidazole binding. Int J Cancer. 2003;104:85-91.

[44] Mehta S, Hughes N, Jubb A, Turley H, Han C, Li S, et al. Early changes in angiogenesis and hypoxia following bevacizumab therapy in primary breast cancer. J Clin Oncol 30, 2012 (suppl; abstr 1066).

[45] McIntyre A, Patiar S, Wigfield S, Li JL, Ledaki I, Turley H, et al. Carbonic Anhydrase IX Promotes Tumor Growth and Necrosis In Vivo and Inhibition Enhances Anti-VEGF Therapy. Clin Cancer Res. 2012;18:3100-11.

8

Monitoring the effects of bevacizumab beyond progression in a murine colorectal cancer model: a functional imaging approach

Abstract

Background: Clinical studies have shown that bevacizumab beyond progression to first line therapy is beneficial for overall survival in advanced stage colorectal cancer. We studied the utility of several functional imaging modalities to assess the efficacy of bevacizumab beyond progression (BBP).

Methods: All BALB/c mice with s.c. LS174T xenografts were treated with capecitabine, oxaliplatin and bevacizumab combination therapy. Tumor volume was assessed using caliper measurements. Increase of 1.5 times the initial volume on two subsequent measurements, was considered progression. In half of the mice bevacizumab treatment was continued (n=13) after progressive disease was established, while the others received saline injections (n=12). Within 3 days after progression, multi-modal imaging was performed using FDG-PET, diffusion weighted imaging, T2* and dynamic contrast enhanced MRI. Measurements were repeated 7 and 10 days after the first measurements. Afterwards, tumors were analyzed for expression of carbonic anhydrase IX, glucose transporter 1, 9F1 to stain the vasculature and Ki67 to assess proliferation.

Results: In the BBP group tumor growth after progression was reduced compared to the control group ($p<0.01$). FDG-PET showed a trend towards lower FDG uptake in the BBP group ($p=0.08$). DWI, T2* and DCE-MRI parameters were not significantly different between both groups. The immunohistochemical analyses showed higher CAIX-positive fraction ($p<0.01$) and lower Ki67 expression ($p=0.06$) in the BBP group. The relative vascular area was significantly lower in the BBP group ($p=0.03$). GLUT-1 expression and vascular density did not significantly differ between both groups.

Conclusion: Bevacizumab after progression resulted in significant changes in the tumor proliferation and microenvironment compared to discontinuation of bevacizumab. FDG-PET may be sensitive to BBP-induced effects.

Introduction

Addition of bevacizumab, a monoclonal antibody against vascular endothelial growth factor (VEGF), to regular first line chemotherapy treatment has increased progression free survival in metastasized colorectal cancer patients [1-4]. It has been suggested that bevacizumab leads to normalization of the architecture of vessels, leaving more mature, stabile and functional vessels, while decreasing the vascular density by inhibiting formation of new chaotic or non-functional vessels. Thereby enhancing delivery of chemotherapeutics the to the tumor cells [5, 6]. However, the working mechanism of bevacizumab is not fully understood, nor is the emergence of resistance. In fact, progression on first-line chemotherapy does not necessarily imply that continuation of bevacizumab would no longer be effective, as the angiogenic signal remains beyond progression, VEGF suppression might still be useful [7]. Moreover, vascular normalization may lead to an improved delivery of cytotoxic treatment to the tumor [5] and could, therefore, also be of added value after a switch in cytotoxic treatment. The BRiTE study retrospectively analyzed data of all patients that received bevacizumab in first-line treatment. Patients who had progression on first line bevacizumab containing therapy and who received chemotherapy in combination with bevacizumab in second-line treatment had a significant survival benefit compared to patients who had received chemotherapy without bevacizumab in second-line (median overall survival 31.8 months vs. 19.9 months) [8]. These data were confirmed in the more recent observational cohort study, ARIES [9]. Moreover in a recent prospective randomized controlled study (TML study), again a benefit of bevacizumab beyond progression was described. After progression patients were randomized between chemotherapy with or without bevacizumab and the overall survival data were significantly better for the group with bevacizumab (median overall survival 11.2 months vs. 9.8 months) [10].

However, given the costs and toxicity of bevacizumab, continuation of an ineffective therapy is undesirable. Functional imaging techniques might offer information on the effectiveness of bevacizumab beyond progression. In a previous study in the same murine colorectal cancer model, we observed changes in fluorodeoxyglucose positron emission tomography (FDG-PET) and in the MRI measurable relaxation time T2* induced by bevacizumab and at 10 days after start of treatment [11]. FDG-PET monitors tumor glucose metabolism [12]. The T2* is influenced by blood flow, blood volume, hypoxia and hematocrit level, as it is sensitive to the paramagnetic effect of deoxyhemoglobin, which shortens the T2* time [13, 14]. Dynamic contrast-enhanced MRI (DCE-MRI), a tool to measure functional vasculature, has previously shown to be sensitive to bevacizumab-induced changes [15, 16] and could monitor this effect as early as 48 hours after start of treatment [17]. Diffusion weighted imaging (DWI), which measures the water mobility and therefore is inversely related to cellular density, has also shown potential to monitor bevacizumab effects: several studies have shown a significant

increase in the mean ADC after antiangiogenic therapy-containing treatment [18, 19]. This probably results from bevacizumab-induced cell death. The predictive value of all these functional imaging parameters in relation to the effects of bevacizumab beyond progression, however, is still unknown.
In this study, FDG-PET, T2*, DCE-MRI and DWI were performed and bevacizumab levels were determined to measure effects of bevacizumab beyond progression in a bevacizumab-sensitive human colorectal cancer mouse model. Furthermore, we measured the effect of bevacizumab beyond progression on tumor proliferation, vascular density and hypoxia assessed as by immunohistochemistry.

Material and methods

Animals

Twenty-six female BALB/c nu/nu mice between 6 and 8 weeks old, weighing between 18-23 gram, were purchased from Janvier (Uden, the Netherlands). Mice were allowed to acclimatize to the new housing conditions for one week. Food and water were supplied ad libitum. The mice were kept in a controlled environment in accordance with the institutional guidelines (temp. 22 °C, humidity 61%, 12 hours light-dark rhythm, individually ventilated cages, nesting material in each cage).
Mice were injected subcutaneously with ~$1*10^6$ LS174T tumor cells (human colon cancer cell line sensitive to bevacizumab (CCL-188; passage 7; American Type Culture Collection, Manassas, VA, USA)) just above the right scapula. The Animal Welfare Committee of the Radboud University Nijmegen Medical Centre approved all experiments.

Treatment

Tumor growth was assessed daily by measuring tumor diameter in three dimensions. Treatment was started once the tumor had reached a diameter of at least 0.4 cm in at least one dimension. A suboptimal (lower dose) chemotherapy regimen was chosen, in order to promote progression to therapy. According to the literature, the Maximum Tolerated Dosage (MTD) of Capecitabine in mice is 400 mg/kg/day in a 14/7 schedule and of Oxaliplatin 10 mg/kg once a week [20]. To promote tumor progression, we decided to use suboptimal doses of Capecitabine and Oxaliplatin. According to Kollinsky et al. 67% of the MTD was almost as effective as the MTD. Furthermore, addition of Oxaliplatin (67% of the MTD) and bevacizumab to the Capecitabine treatment (67% of the MTD) resulted in a tumor growth inhibition of >100% [20]. Therefore, in two pilot studies we used 50% of the MTD for Capecitabine and 30% of the MTD for Oxaliplatin. Treatment consisted of weekly Oxaliplatin (Oxalisin®, Pharmachemie B.V., Haarlem, the Netherlands) 3 mg/kg i.p., daily oral administration of 200 mg/kg Capecitabine solution (Xeloda®, Roche Pharma, Germany) and

bevacizumab (Avastin®, Roche Pharma, Germany) 5 mg/kg i.p. twice a week. Tumor volume was calculated using the formula 4/3π *0.5 length *0.5 width *0.5 height. Once the tumor volume had grown to ≥1.5 times the initial volume on two subsequent measurements, mice were considered progressive. Subsequently, 50% of mice continued bevacizumab treatment (bevacizumab beyond progression group = BBP group), while the control group received 0.9% saline injections i.p twice a week.

Imaging

In a pilot study (n=10) the growth rate of the tumors in the BBP and in the control group was assessed, to decide when the measurements should take place. Tumor volume and the condition of the mice were generally evaluated as acceptable until 12-15 days after tumor progression.

The first measurements with MRI and FDG-PET were performed early after tumor progression (1-3 days). Seven and ten days after the first measurements, the second and third measurements took place. After the third measurement mice were euthanized, tumors were snap-frozen in liquid nitrogen and stored at -80°C. All measurements included FDG-PET scanning, diffusion weighted imaging, T2* imaging and DCE-MRI.

Mice were fasted before FDG-PET imaging (Inveon preclinical PET scanner) over night by supplying a minimal amount of 2g food per mice for the night. They were anaesthetized with Isoflurane 4% for induction and 1.5-2% for maintenance starting 10 minutes before administration of FDG. Mice were kept anesthetized during FDG PET and subsequent DWI and were anesthetized again (following the same protocol using isoflurane) a few hours later for the T2* and DCE-MRI. Body heat was kept constant during anesthesia (before the PET scan) with a heat lamp and during PET imaging with a heat mattress (with warm water of 38°C). During MR imaging the body temperature was controlled with a heat blower that kept the body temperature at 37.5°C.

One hour before scanning, approximately 10 MBq FDG in 0.2 ml 0.9% NaCl was injected intravenously via an inserted tail vein cannula. Images were reconstructed using OSEM-3D reconstruction. Matrices 256x256; 159 slices, resulting in a voxel volume of 0.28mm^3.The highest standardized uptake value (SUVmax) of each tumor was recorded.

MR for T2* and DCE imaging was performed on a 7T MR-system (ClinScan, Bruker Biospin, Ettlingen, Germany). A 'rat brain' quadrature receiver coil (Bruker Biospin, Ettlingen, Germany) was used for signal acquisition. Images for T2* values were acquired with a gradient echo sequence, with a TR of 1,000 ms and 6 TE-times: 2.78, 4.86, 6.89, 8.92, 10.95 and 12.98 ms. Eighteen slices of 1 mm were obtained with 2 averages. T2* maps were reconstructed using in-house built software based on Matlab.

For DCE-MRI a single shot SE sequence with a low flip angle (15°) was applied. Sixteen slices with a thickness of 1 mm were obtained with TR 90 ms, TE 1.82 ms, 3.4 seconds time

resolution and FOV 30x30 mm. After 6-8 seconds, 0.2 ml of the contrast agent Gadomer-17 (Schering AG, Berlin, Germany) was administered via the tail vein cannula. Before and after DCE-MRI proton density images were recorded. Image-derived contrast concentrations were computed and an area under the concentration curve (AUC) was calculated for the first 180 seconds after contrast injection.

DWI was performed using an EPI sequence with five b-values: 0-100-200-500-1000 on a 11.7 T horizontal bore MR system (Biospec, Bruker Biospin, Ettlingen, Germany) using a mouse brain surface receive coil (Bruker Biospin, Ettlingen, Germany). Nine slices of 1 mm were obtained. Slices with evident ghosting artifacts were discarded. Ghosting is the displaced reduplication of images in the phase encoding direction. This is caused by (respiratory) movement and the artifacts could influence the calculated ADC values. ADC maps were created using the ISA-tool on the Bruker scanner software and were exported as dicom files. A region of interest was drawn around the tumor and data of the values per voxel were exported to excel in order to facilitate histogram analyses. Mean ADC, 25th and 75th percentile values were calculated.

Immunohistochemistry

Four µm tumor sections were fixed in acetone at 4°C for 10 minutes and rehydrated in phosphate buffered saline (PBS). Sections were pre-incubated for 30 minutes in 5% normal donkey serum in primary antibody diluent (PAD). Ki67 was stained using rabbit anti-Ki67 (Abcam ab833-500) (1:100 in PAD) overnight at 4°C and donkey anti-rabbit-Fab-Alexa488 (1:200 in PAD) 30 minutes at 37°C. CAIX was stained by applying rabbit-anti CAIX-biotin (Novus Biologicals NB100-417B) (1:500 in PAD) overnight at 4°C, followed by applying mouse anti- biotin-Alexa488 (1:200 in PAD) for 30 minutes at 37°C. For vessel staining an undiluted anti-murine vessel antibody 9F1 (rat anti-mouse endothelium, dept Pathology Radboud University Medical Center) was applied for 45 minutes at 37°C followed by chicken anti-rat-Alexa647 (1:100 in PBS) for 45 minutes at 37°C.

All sections were digitalized using a fluorescent microscope (Axioskop, Zeiss, Göttingen, Germany) and a computer-controlled motorized stepping stage system. Sections were scanned for each signal separately. Using Image Processing Lab software (Scanalytics Inc., Fairfax, VA, USA), the tumor areas were drawn, excluding evident necrotic areas and artifacts. The grey scale images were converted to binary images for further analysis. The positively stained fractions of the total tumor area were calculated using ImageJ software [21, 22].

ELISA procedure for Bevacizumab levels in plasma

Bevacizumab concentration was measured with a 1-site enzyme-linked immunosorbent assay (ELISA). In short, 96-well plates (Greiner Bio-One, Alphen a/d Rijn, The Netherlands) were coated overnight at 4°C with 100 µl VEGF (0.50 µg/ml, Genentech Inc, San Francisco, CA), washed (96PW plate washer, TecanGroup Ltd., Männedorf, Switzerland), and then blocked

with 150 µl Superblock (Pierce, Rockford, IL) during 30 minutes at ambient temperature, washed and further blocked with 300 µl bovine serum albumin (BSA) (Sigma Chemical, St. Louis, MO) for 4 hours at ambient temperature. Subsequently, the plate was washed and standards (range 0-10 ng/ml Avastin, Roche, Basel, Switzerland), study samples and a reference sample were pipetted into the wells and the plate was incubated overnight at 4°C. After washing, the plate was incubated with 100 µl Mouse anti-Human IgG (Fc) peroxidase, (dilution 1:25,000, SouthernBiotech, Birmingham, U.K.) during 2 hours at ambient temperature and again washed. Thereafter incubation with 100 µl ready-to-use tetramethyl benzidine (TMB) solution (Kem-En-Tec, Taastrup, Denmark) for 15-20 minutes took place for color development. The reaction was stopped by addition of 0.5 M H_2SO_4 and optical density was measured at 450 nm in a Multiskan Ascent plate reader (Lab Systems, Oy, Helsinki, Finland). The analytical sensitivity, defined as the minimum bevacizumab concentration evoking a response significantly different from that of the zero calibrator, was 16 pg/ml. Plasma samples, diluted 4,000 – 24,000 fold, exhibited excellent linearity. To six plasma samples known quantities of bevacizumab were added. The recoveries in the plasma samples ranged from 87% to 110% with a mean recovery of 98%. In each run the reference preparation, prepared from a pool of plasma from patients treated with bevacizumab, was used to monitor long-term performance of the assay. The concentration in reference preparation was 1670 ng/ml, and the within-run coefficient of variation (CV) and the between-run CV amounted to 7.0% and 10.0%, respectively.

Statistical analyses

Values of the measurements in both groups and there standard deviation are reported. Linear mixed models were used to assess differences between the BBP and the control group over time. Given the fact that the repeated measurements are linked over time, it was necessary to take random effects into account. Linear mixed models assessed the trend in changes of imaging parameters over time in the BBP and control group, while taking into account the random effect of each mouse. Time point, treatment (BBP or control) and interaction between time and treatment were chosen as fixed variables. Each mouse was a random variable in the linear mixed model.

To assess differences in immunohistochemical results between the BBP and the control group an independent sample Student *t*-test was used. Correlations between immunohistochemistry and imaging parameters of the last measurement were assessed using a Pearson correlation coefficient.

P-values below 0.10 were considered a trend, and *p*-values below 0.05 were considered significant. Data were analyzed using SPSS 16.0 (SPSS inc, Chicago, IL, USA).

Results

Tumors

Tumors reached a diameter of at least 0.4 cm on average 13.6 days after s.c. inoculation of the tumor cells (range 11-21 days). On average 4.6 days after start of therapy, progressive disease was observed and imaging measurements were started. In the control group tumor growth after progression was more pronounced than in the BBP group (p<0.01) [Figure 1]. When progressive disease was esthablished (just before measurement 1), the tumor volume in the BBP group was 154±125 mm^3 and 256±184 mm^3 in the control group. Six to seven days after progression-before measurement 2- the tumor volume in the BBP group was 208±127 mm^3 in the BBP group (relative change since progression 1.52 times the initial volume) and 459±423 mm^3 (relative change 1.82) for the control group. Nine to ten days after progression -before measurement 3- the tumor volume in the BBP group was 311±200 mm^3 (relative change since progression 2.03) and 572±263 mm^3 (relative change 2.74) for the controle group. Due to tumor growth and poor condition of the mice (due to chemotherapy, repeated anesthesia and fastening) 10 mice had to be euthanized before the third measurement. The tumors of these mice were included in the immunohistochemical analysis and in the analysis of the growth rate.

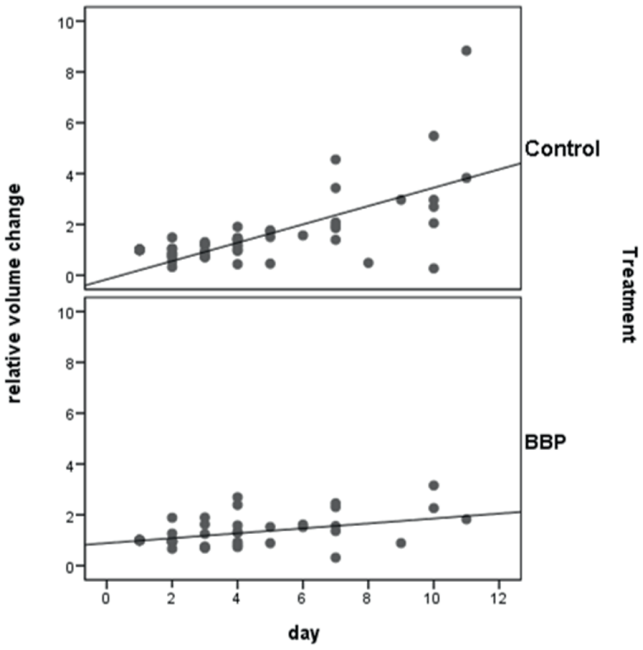

Figure 1. *Relative volume change in the control group (above) and BBP (below) since progression was established. The volume change was significantly larger in the control group.*

Bevacizumab levels

Bevacizumab levels, as determined in the serum from the blood samples drawn after the last imaging measurement, were significantly higher in the BBP group (86±39 ng/ml vs. 22±19 ng/ml, $p<0.01$), but bevacizumab was still detectable in the control group.

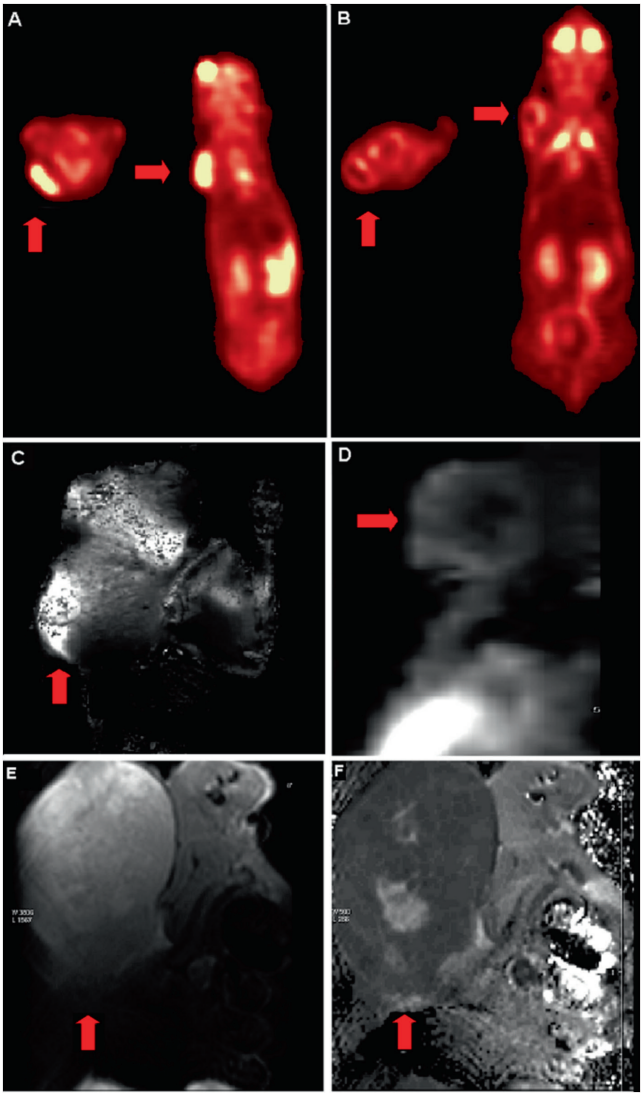

Figure 2. *Arrows point towards the subcutaneous tumors in (A) transverse and coronal FDG-PET images of a mouse from the control group at the third measurement (SUV max = 1.69) and (B) a mouse from the BBP group at the third measurement (SUV max = 1.36). (C) Calculated T2* image showing a large tumor. (D) A dynamic contrast enhanced image showing more contrast agent in the tumor margin. (E) Diffusion weighted image of the subcutaneous tumor and the calculated ADC map (F) of the same tumor.*

FDG-PET

FDG-PET showed a trend towards higher FDG uptake in the control group compared to the BBP group (p=0.08). At the first measurement, no difference was observed between the BBP group and the control group (1.22±0.20 versus 1.14±0.26, respectively). One week later, at the second measurement, SUVmax values were significantly higher in the control group, while the values were approximately the same in the BBP group (1.13±0.22 versus 1.48±0.43, p=0.05). At the third measurement SUVmax values were still lower in the BBP group as compared to the control group, although this difference did not reach statistical significance (1.18±0.32 versus 1.36±0.48, p=0.40) [Figure 3A and 2].

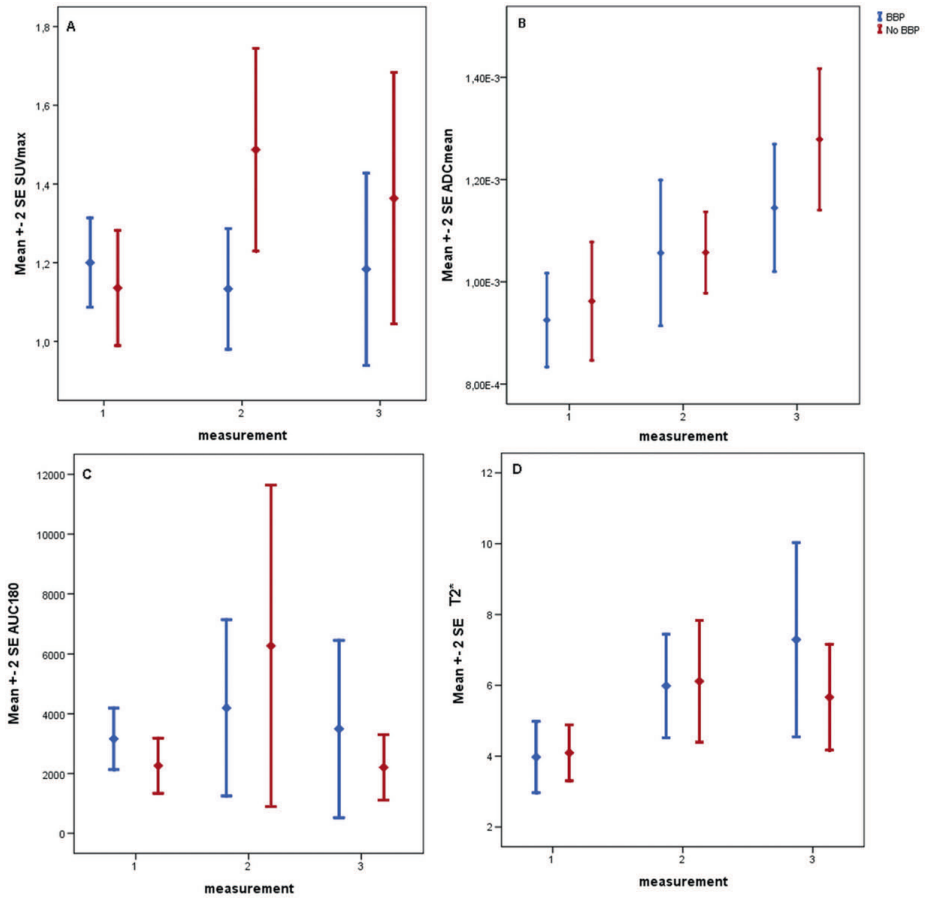

Figure 3. *Plots showing the mean and 2 standard errors of the mean (SEM): (A) SUVmax value at the first, second and third measurement of the BBP (blue) and control group (red). At day two the SUV values differ significantly. (B) ADCmean values at the first, second and third measurement, showing no difference between the BBP (blue) and control group (red). (C) AUC180 (in mmol*sec) at the first, second and third measurement of the BBP (blue) and control group (red). There was no significant difference between BBP group and control group. (D) Error bars showing 2 standard errors of the mean T2* at the first, second and third measurement of the BBP (blue) and control group (red). There was no significant difference between BBP group and control group.*

Magnetic resonance imaging

Mean T2* time in the tumors increased over time, however, these values were not significantly different between the BBP and the control group [Figure 3B]. Neither a significant change over time of the area under the contrast curve during the first 180 seconds after contrast administration was observed, nor a difference between the BBP and the control group. A large variation in the area under the contrast curve in both groups was detected. [Figure 3C] The apparent diffusion coefficient (ADC) values did not significantly differ between the BBP and control group. Mean tumor ADC-values increased over time in both the BBP and control group [Figure 3D]. Also in the lower (p25) and higher (p75) percentiles of the ADC values, no difference between the BBP and control group were observed.

Histopathology

The immunohistochemical analyses showed a higher CAIX-positive fraction (0.21±0.09 vs. 0.10±0.06, p<0.01) and a trend towards lower labeling index of Ki67 (0.14±0.05 vs. 0.23±0.15, p=0.06) in the BBP group compared to the control group. [Figure 4] GLUT-1 expression (0.08±0.03 vs. 0.11±0.11, p=0.48) and vascular density (104±18 vs. 127±52 vessels/mm^2, *p*=0.16) did not significantly differ between the BBP and control group. However, the relative vascular area was significantly lower in the BBP than in the control group (0.029±0.010 vs. 0.042±0.017, *p*=0.03). The vascular density and relative vascular area were inversely correlated to the CAIX fraction (r=-0.50 p=0.01, r=-0.45 p=0.02 respectively). The bevacizumab levels correlated with the CAIX fraction (r=0.59, p=0.008) and inversely correlated to the labeling index of Ki67 (r=-0.47, p=0.04). The labeling index of Ki67 did not significantly correlate to the last measured ADCmean (r=-0.30, p=0.20). Also other immunohistochemical analyses did not correlate significantly with functional imaging results.

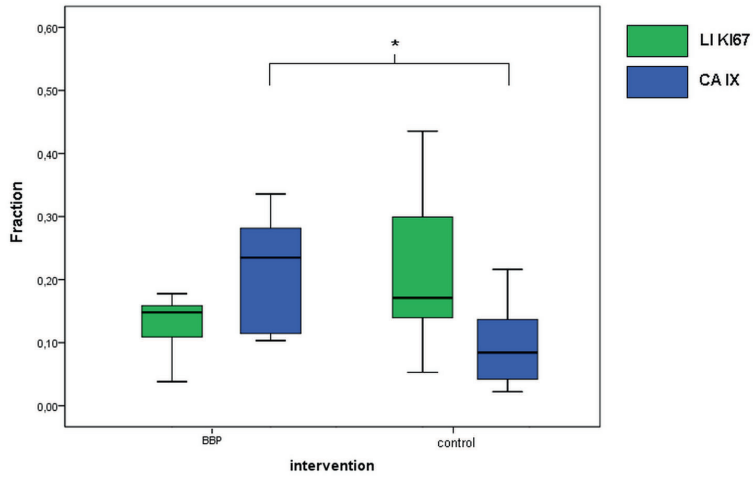

Figure 4. *Box plot of the labeling index of Ki67 (green) and the fraction positive CAIX staining (blue). The CAIX fraction is significantly higher in the BBP group, while there is a trend towards a lower labeling index of Ki67 in the BBP group.*

Discussion

Since the survival benefit of BBP is of borderline clinical significance [10], a selection of patients that benefit most is warranted. We investigated in a murine model whether the effects of BBP could be monitored with functional imaging techniques. In this study, continuation of bevacizumab inhibited tumor growth even after progression. This indicates that discontinuation of bevacizumab may not be desirable upon progressive tumor growth during bevacizumab-containing combinations of chemotherapy. This also implies that imaging techniques merely based on anatomical hallmarks will be insufficient to monitor the efficacy of continued bevacizumab treatment in patients.

Of course, in the human situation bevacizumab beyond progression would always be given in combination with second line chemotherapy, because bevacizumab monotherapy has proven to be unsuccessful in humans [23]. However, bevacizumab monotherapy is effective in xenografts [24]. Furthermore, the effect of second line chemotherapy could be of far greater influence on the functional imaging results than the continuation of bevacizumab and thus second line chemotherapy could be a major confounder to measure effects of bevacizumab beyond progression. Therefore, we decided to measure the effects of bevacizumab monotherapy beyond progression. In this study, FDG-PET was sensitive to bevacizumab-induced changes beyond progression and may therefore be a sensitive marker to monitor bevacizumab efficacy.

FDG uptake depends on glycolytic activity and may be regarded as a marker for metabolic activity of the tumor. Glycolysis in normal tissue is increased in hypoxic conditions. However, cancer cells have an increased glycolytic rate even at normoxic conditions [25]. Several theories have been suggested as an explanation why aerobic glycolysis is increased in tumors. Such as the theory that selection due to periodic hypoxia early in carcinogenesis, gives a proliferative advantage to highly glycolytic, acid-resistant cells. An advantage of high glycolysis -even in later aerobic conditions- might come from the by-products of the glycolytic process: acid, to provide a selective advantage to invading tumor cells, and essential anabolic substrates for proliferation deriving from glucose [26-28]. Previous studies showed a positive correlation between Ki67 expression, proliferation and FDG uptake in several malignancies [28-30].

The decreased growth rate and Ki67 expression observed in our study are in agreement with the observed decreased in FDG uptake in the BBP group. It should be noted that bevacizumab might influence the distribution of systemically administered tracers, including FDG. Therefore, additional information from immunohistochemistry is of great importance to get more insight in the specific bevacizumab induced changes in tumor microenvironment that might cause the alterations in metabolism detected with FDG-PET.

The levels of hypoxia measured with the intrinsic hypoxia marker CAIX were higher in tumors of mice that continued bevacizumab beyond progression. Given the decrease in relative

vascular area in the BBP group, the increase in tumor hypoxia is most likely mediated by decreased vascularity. CAIX is a hypoxia related marker sensitive to current or previous chronic hypoxia, but influenced by nonhypoxic stimuli [31]. Also GLUT1 may be upregulated in hypoxic conditions. However, in our study GLUT1 expression was similar in both groups. This may be explained by the fact that GLUT1 expression also increases with higher proliferative activity [32]. Since proliferative activity is higher in the control group, whilst the hypoxia level is higher in the BBP group, both effects may balance out in terms of GLUT1 expression.

An increase in tumor hypoxia of animals treated with bevacizumab beyond progression would imply higher levels of deoxyhemoglobin and thus lower T2* times as measured with MRI. However, in our study T2* times increased in both groups. Possibly, an increase in size of necrotic, non-perfused areas can explain these results. There is a lack of blood in non-perfused areas, and therefore deoxyhemoglobin is absent, resulting in high T2* values. Both high tumor growth rate, resulting in central necroses by shortcoming of vasculature in the center of the tumor and treatment effect, might cause necrotic non-perfused areas increasing the T2* times. Given the complete overlap in T2* times at the first, second and third time point, T2* is not an adequate imaging tool to evaluate effectiveness of bevacizumab beyond progression in this tumor type.

Tumors treated with bevacizumab beyond progression demonstrated a significantly lower relative vascular area than tumors in the control group. In addition, a lower vascular density was observed in the BBP treated tumors, although not significant. Thus, even after progression bevacizumab continued to (modestly) exert effects on tumor vasculature. However, the effect of bevacizumab on the number of vessels and functional vasculature might have been too subtle to be detected with DCE-MRI.

Given the effect of bevacizumab beyond progression on tumor proliferation, DWI would be expected to be a sensitive tool for response monitoring. Proliferation and apoptotic processes influence cell density and thus the ADC value. Correlations between ADC and proliferation and apoptotic markers have been shown in an animal model before [33], but unfortunately no significant correlations were observed in this study. However, the lack of difference in ADC value between the two groups might be due to technical reasons. In this study, DWI was acquired during free breathing. Given the sensitivity of DWI for movement, breathing movement could influence ADC measurements. In addition, selection of the slices without ghosting may have affected the measured ADC value per tumor: the rim of the tumor may have far lower ADC values than a necrotic centre. If more slices from the rim or from the centre of the tumor are selected (by the random effect of ghosting) this might influence the measured average ADC for that tumor. Both the effect of movement on the measured ADC value and selection of slices decrease the accuracy of the ADC measurement and therefore decrease the sensitivity to measure treatment effects.

In conclusion, bevacizumab after progression induced significant changes in tumor proliferation and tumor microenvironment, decreasing the relative vascular area in and increasing CAIX expression. FDG-PET may be a sensitive functional imaging technique to assess effects of bevacizumab beyond progression.

Reference list

[1] Hurwitz H, Fehrenbacher L, Novotny W, Cartwright T, Hainsworth J, Heim W, et al. Bevacizumab plus irinotecan, fluorouracil, and leucovorin for metastatic colorectal cancer. N Engl J Med. 2004;350:2335-42.

[2] Kabbinavar FF, Schulz J, McCleod M, Patel T, Hamm JT, Hecht JR, et al. Addition of bevacizumab to bolus fluorouracil and leucovorin in first-line metastatic colorectal cancer: results of a randomized phase II trial. J Clin Oncol. 2005;23:3697-705.

[3] Saltz LB, Clarke S, Diaz-Rubio E, Scheithauer W, Figer A, Wong R, et al. Bevacizumab in combination with oxaliplatin-based chemotherapy as first-line therapy in metastatic colorectal cancer: a randomized phase III study. J Clin Oncol. 2008;26:2013-9.

[4] Tebbutt NC, Wilson K, Gebski VJ, Cummins MM, Zannino D, van Hazel GA, et al. Capecitabine, bevacizumab, and mitomycin in first-line treatment of metastatic colorectal cancer: results of the Australasian Gastrointestinal Trials Group Randomized Phase III MAX Study. J Clin Oncol. 2010;28:3191-8.

[5] Weisshardt P, Trarbach T, Durig J, Paul A, Reis H, Tilki D, et al. Tumor vessel stabilization and remodeling by anti-angiogenic therapy with bevacizumab. Histochem Cell Biol. 2011.

[6] Jain RK. Normalization of tumor vasculature: an emerging concept in antiangiogenic therapy. Science. 2005;307:58-62.

[7] Gridelli C, Bennouna J, de Castro J, Dingemans AM, Griesinger F, Grossi F, et al. Randomized phase IIIb trial evaluating the continuation of bevacizumab beyond disease progression in patients with advanced non-squamous non-small-cell lung cancer after first-line treatment with bevacizumab plus platinum-based chemotherapy: treatment rationale and protocol dynamics of the AvaALL (MO22097) trial. Clin Lung Cancer. 2011;12:407-11.

[8] Grothey A, Sugrue MM, Purdie DM, Dong W, Sargent D, Hedrick E, et al. Bevacizumab beyond first progression is associated with prolonged overall survival in metastatic colorectal cancer: results from a large observational cohort study (BRiTE). J Clin Oncol. 2008;26:5326-34.

[9] Cohn A, Bekaii-Saab T, Bendell J, Hurwitz H, Kozloff M, Roach N, et al. Clinical outcomes in bevacizumab-treated patients with metastatic colorectal cancer: results from ARIES observational cohort study and confirmation of BRiTE data on bevacizumab beyond progression.. J Clin Oncol 2010 ASCO Annual Meeting Proceedings. 2012;Vol 28, No 15_suppl (May 20 Supplement), 2010: 3596.

[10] Arnold D, Andre T, Bennouna J, Sastre J, P.J. O, Greil R, et al. Bevacizumab (BEV) plus chemotherapy (CT) continued beyond first progression in patients with metastatic colorectal cancer (mCRC) previously treated with BEV plus CT: Results of a randomized phase III intergroup study (TML study). J Clin Oncol 30, 2012 (suppl; abstr CRA3503). 2012.

[11] Heijmen L, Boerman OC, Punt CJA, Ter Voert E.E.G, Oyen WJG, Bussink J, et al. Tumor hypoxia as a mechanism of resistance to bevacizumab in a murine model. J Clin Oncol 30, 2012 (suppl; abstr e13111). 2012.

[12] Busk M, Horsman MR, Jakobsen S, Bussink J, van der KA, Overgaard J. Cellular uptake of PET tracers of glucose metabolism and hypoxia and their linkage. EurJ NuclMed MolImaging. 2008;35:2294-303.

[13] Chavhan GB, Babyn PS, Thomas B, Shroff MM, Haacke EM. Principles, techniques, and applications of T2*-based MR imaging and its special applications. Radiographics. 2009;29:1433-49.

[14] Howe FA, Robinson SP, McIntyre DJ, Stubbs M, Griffiths JR. Issues in flow and oxygenation dependent contrast (FLOOD) imaging of tumours. NMR Biomed. 2001;14:497-506.

[15] de Langen AJ, van dBV, Lubberink M, Backes WH, Marcus JT, van TH, et al. Monitoring response to antiangiogenic therapy in non-small cell lung cancer using imaging markers derived from PET and dynamic contrast-enhanced MRI. J NuclMed.52:48-55.

[16] Hirashima Y, Yamada Y, Tateishi U, Kato K, Miyake M, Horita Y, et al. Pharmacokinetic parameters from 3-Tesla DCE-MRI as surrogate biomarkers of antitumor effects of bevacizumab plus FOLFIRI in colorectal cancer with liver metastasis. Int J Cancer. 2011.

[17] Ungersma SE, Pacheco G, Ho C, Yee SF, Ross J, van BN, et al. Vessel imaging with viable tumor analysis for quantification of tumor angiogenesis. Magn ResonMed.63:1637-47.

[18] Anzidei M, Napoli A, Zaccagna F, Cartocci G, Saba L, Menichini G, et al. Liver metastases from colorectal cancer treated with conventional and antiangiogenetic chemotherapy: evaluation with liver computed tomography perfusion and magnetic resonance diffusion-weighted imaging. J Comput Assist Tomogr. 2011;35:690-6.

[19] Fenchel M, Konaktchieva M, Weisel K, Kraus S, Claussen CD, Horger M. Response assessment in patients with multiple myeloma during antiangiogenic therapy using arterial spin labeling and diffusion-weighted imaging: a feasibility study. Acad Radiol. 2010;17:1326-33.

[20] Kolinsky K, Zhang YE, Dugan U, Heimbrook D, Packman K, Higgins B. Novel regimens of capecitabine alone and combined with irinotecan and bevacizumab in colorectal cancer xenografts. Anticancer Res. 2009;29:91-8.

[21] Rademakers SE, Rijken PF, Peeters WJ, Nijkamp MM, Barber PR, van der LJ, et al. Parametric mapping of immunohistochemically stained tissue sections; a method to quantify the colocalization of tumor markers. Cell Oncol(Dordr).34:119-29.

[22] Rademakers SE, Lok J, van der Kogel AJ, Bussink J, Kaanders JH. Metabolic markers in relation to hypoxia; staining patterns and colocalization of pimonidazole, HIF-1alpha, CAIX, LDH-5, GLUT-1, MCT1 and MCT4. BMC Cancer. 2011;11:167.

[23] Giantonio BJ, Catalano PJ, Meropol NJ, O'Dwyer PJ, Mitchell EP, Alberts SR, et al. Bevacizumab in combination with oxaliplatin, fluorouracil, and leucovorin (FOLFOX4) for previously treated metastatic colorectal cancer: results from the Eastern Cooperative Oncology Group Study E3200. J Clin Oncol. 2007;25:1539-44.

[24] Gerber HP, Ferrara N. Pharmacology and pharmacodynamics of bevacizumab as monotherapy or in combination with cytotoxic therapy in preclinical studies. Cancer Res. 2005;65:671-80.

[25] Warburg O. On the origin of cancer cells. Science. 1956;123:309-14.

[26] Langbein S, Zerilli M, Zur Hausen A, Staiger W, Rensch-Boschert K, Lukan N, et al. Expression of transketolase TKTL1 predicts colon and urothelial cancer patient survival: Warburg effect reinterpreted. British journal of cancer. 2006;94:578-85.

[27] Gillies RJ, Gatenby RA. Adaptive landscapes and emergent phenotypes: why do cancers have high glycolysis? Journal of bioenergetics and biomembranes. 2007;39:251-7.

[28] Shou Y, Lu J, Chen T, Ma D, Tong L. Correlation of fluorodeoxyglucose uptake and tumor-proliferating antigen Ki-67 in lymphomas. J Cancer Res Ther. 2012;8:96-102.

[29] Higashi K, Ueda Y, Yagishita M, Arisaka Y, Sakurai A, Oguchi M, et al. FDG PET measurement of the proliferative potential of non-small cell lung cancer. J Nucl Med. 2000;41:85-92.

[30] Nguyen XC, Lee WW, Chung JH, Park SY, Sung SW, Kim YK, et al. FDG uptake, glucose transporter type 1, and Ki-67 expressions in non-small-cell lung cancer: correlations and prognostic values. Eur J Radiol. 2007;62:214-9.

[31] Vordermark D, Kaffer A, Riedl S, Katzer A, Flentje M. Characterization of carbonic anhydrase IX (CA IX) as an endogenous marker of chronic hypoxia in live human tumor cells. Int J Radiat Oncol Biol Phys. 2005;61:1197-207.

[32] Younes M, Brown RW, Mody DR, Fernandez L, Laucirica R. GLUT1 expression in human breast carcinoma: correlation with known prognostic markers. Anticancer Res. 1995;15:2895-8.

[33] Zhang XY, Sun YS, Tang L, Xue WC, Zhang XP. Correlation of diffusion-weighted imaging data with apoptotic and proliferation indexes in CT26 colorectal tumor homografts in balb/c mouse. JMagn ResonImaging.33:1171-6.

9

Multimodality imaging to predict response to systemic treatment in patients with advanced colorectal cancer

Abstract

Background: Aim of this study was to investigate the potential of 18F-FDG PET, diffusion weighted imaging (DWI) and susceptibility-weighted (T2*) MRI to predict response to systemic treatment in patients with colorectal liver metastases. The predictive values of pretreatment measurements and of early changes one week after start of therapy, were evaluated.

Patients and methods: Imaging was performed prior to and one week after start of first line chemotherapy in 39 patients with colorectal liver metastases. 18F-FDG PET scans were performed on a PET/CT scanner and DWI and T2* were performed on a 1.5T MR scanner. The maximum standardized uptake values (SUV), total lesion glycolysis (TLG), apparent diffusion coefficient (ADC) and T2* value were assessed in the same lesions. Up to 5 liver metastases per patient were analyzed. Outcome measures were progression free survival (PFS), overall survival (OS) and size response.

Results: At pretreatment, high SUVmax, high TLG, low ADC and high T2* were associated with a shorter OS. Low pretreatment ADC value was associated with shorter PFS. After 1 week a significant drop in SUVmax and rise in ADC were observed. The drop in SUV was correlated with the rise in ADC (r=-0.58, p=0.002). Neither change in ADC nor in SUV was predictive of PFS or OS. T2* did not significantly change after start of treatment.

Conclusion: Pretreatment SUVmax, TLG, ADC, and T2* values in colorectal liver metastases are predictive of patient outcome. Despite sensitivity of DWI and 18F-FDG PET for early treatment effects, change in these parameters was not predictive of long term outcome.

Introduction

The liver is the most frequently affected organ in disseminated colorectal cancer and most patients with metastatic disease rely on palliative systemic treatment (1). Depending on the schedule, response is commonly evaluated 8-9 weeks after start of treatment. Currently, response to treatment is monitored by size response evaluation according to the RECIST criteria (2). A reliable tool that predicts response early after start of therapy is desirable, as this would prevent unnecessary toxicity and costs.

Size response evaluation may be a suboptimal method to assess efficacy of targeted therapies, since necrosis or fibrosis without reduction in tumor size may occur (3, 4). The outcome of palliative systemic therapy has improved in recent years by the addition of targeted agents to cytotoxic treatment. The addition of bevacizumab, a monoclonal antibody which targets the vascular endothelial growth factor has resulted in significant benefits in progression free survival and overall survival (5).

Several functional imaging techniques have shown potential for prediction of response as well as early response monitoring. In a systematic review, the role of 18F-FDG PET in treatment response prediction and monitoring in advanced stage colorectal cancer was evaluated. Four out of five studies showed changes in standardized uptake values (SUV) of 18F-FDG PET after start of systemic treatment (6) and two of these four studies showed a correlation with long term outcome (7, 8). In the palliative setting, metabolic response after one cycle of chemotherapy was a stronger predictor for survival than RECIST evaluation after 3 cycles of chemotherapy (9). However, combined with other functional imaging techniques 18F-FDG-PET might be an earlier and stronger predictor of response to therapy.

Diffusion weighted imaging (DWI) is another promising functional imaging tool for tissue characterization, pretreatment response prediction and response evaluation in cancer (10, 11). From the diffusion weighted MR images an apparent diffusion coefficient (ADC) can be calculated, which is a measure for the mobility of water. The ADC is inversely correlated to the cell density, since cellular membranes inhibit water movement (12). Changes in ADC may precede changes in tumor size, since early after start of treatment changes in cellularity and necrosis may already occur. It has been demonstrated that ADC increased within days after chemotherapy in colorectal cancer metastases (13, 14). These studies investigated the correlation between ADC change and response in metastases. However, to be implemented in clinic, changes in ADC should predict response or (progression free) survival in the patient. Vascular changes induced by bevacizumab and chemotherapeutic treatment may also be indicative of response. Furthermore, vascular status by itself may predict response, since hypoxia and vascular supply of the chemotherapy influence treatment efficacy. T2* MRI, also called intrinsic susceptibility-weighted MRI or BOLD, is investigated as an alternative to (dynamic) contrast enhanced imaging (15, 16). The transverse relaxation time, T2*, is

dependent on magnetic field inhomogeneity and is therefore significantly affected by the presence of paramagnetic deoxyhemoglobin. The higher the deoxyhemoglobin concentration, the lower the T2* value (17). To our knowledge, thus far no studies using T2* for response prediction of metastatic colorectal cancer have been published.
The aim of this prospective study was to assess the predictive value of 18F-FDG PET, DWI and T2* MRI for response to first line chemotherapy and outcome in advanced stage colorectal cancer patients.

Material and methods

Patients

Between August 2009 and September 2012 patients of 18 years and older with histologically confirmed colorectal cancer and non-resectable colorectal liver metastases starting first line palliative or neoadjuvant chemotherapy were approached for participation in this study. Exclusion criteria were: Karnofsky performance status <70, (adjuvant) chemotherapy <6 months before study participation, renal function impairment (MDRD <60 ml/min/1.73 m2) or pregnancy. Specific contra-indications for 18F-FDG PET (including diabetes mellitus) or MRI only excluded patients for either the PET or MRI part of the study protocol. In total, 39 patients were enrolled, 28 males and 11 females (mean age 62 years, range 29-77 years). The study was approved by the institutional review board (CMO region Arnhem-Nijmegen). All patients provided written informed consent before entering the study.

Imaging methods

Before start of chemotherapy 18F-FDG PET, contrast CT and MRI were performed. These scans were performed median 5 days before start of treatment. One week after start of chemotherapy (range 6-8 days), 18F-FDG PET and MRI were repeated. After 3 cycles of chemotherapy an 18F-FDG PET and contrast CT were performed to assess treatment response.
PET CT-scans were performed on a PET/CT scanner: a Biograph Duo (Siemens Medical Solutions USA, Inc., Knoxville, TN, USA) for the first 26 patients and a Biograph mCT PET/CT scanner for the 13 most recently enrolled patients. Both PET/CT-scanners were accredited by the EANM-EARL QA/QC program for quantitative PET (18). Images of the Biograph Duo scanner were reconstructed using the 4 iterations/16 subsets (4i/16s) OSEM-2D reconstruction algorithm, smoothed with a 5-mm FWHM Gaussian filter. Images of the Biograph mCT scanner were reconstructed using TrueX, time of flight and the 3i/21s reconstruction algorithm, smoothed with an 8-mm FWHM Gaussian filter. All PET scans were corrected with a low dose CT for attenuation correction (19).

Contrast enhanced CT using ioversol (125ml Optiray 350) was performed. Scanning parameters for contrast-enhanced CT imaging were care dose referenced at 80 mAs for the thorax and 130mAs for the abdomen, 110 kV, rotation time 0.8s, slice 3 mm, slice collimation 2.5mm, feed/rotation 10mm for thorax and 6.3mm for the abdomen on the Biograph duo. A delay of 40s after injection of ioversol was applied for thorax imaging and a delay of 10s was set to automatically shift to the abdominal imaging. The scanning parameters for CT on the Biograph mCT were set as follows: 200 mAs, 120 kV, pitch 1.2, slice 1 mm, delay of 40s after contrast injection and bolus tracking.

DWI and gradient echo measurements to obtain ADC and T2* values were performed on a 1.5T MR system (Magnetom Avanto, Siemens Medical Solutions, Erlangen, Germany) using a body coil for excitation and a body matrix coil combined with spine matrix coil for signal reception. DWI was performed with an EPI sequence and diffusion weighted images were obtained in three orthogonal directions with b-values of 50, 300, and 600 s/mm2. A 2D- Prospective Acquisition CorrEction navigator triggering was used to avoid respiratory motion artifacts. Parallel imaging was combined with Generalized Autocalibrating Partially Parallel Acquisition and an acceleration factor of 2. Spectrally Adiabatic Inversion Recovery was included to suppress the fat signal. Other scan parameters were as follows: TR 2000 ms; TE 82 ms; 30 transversal slices of 6.0 mm thickness separated by 1.2 mm; field of view 400x400 mm; matrix size 192x192; bandwidth 1736 Hz/px; 3 averages; anterior-posterior phase encoding direction.

To obtain T2* images a spoiled gradient-recalled echo, FLASH 2D, sequence was employed. Each slice was obtained with multiple TE values (4.76, 9.53, 14.29, 19.06, 23.82, 28.58, 33.35, 38.11, 42.88, 47.64, 52.40 ms) and a TR of 225 ms. Other parameters were as follows: flip angle 25 degrees; field of view 400x400mm; slice thickness 6.0 mm; matrix size 128x128. Parallel acquisition (GRAPPA) with an acceleration factor of 2 was used. Patients continued normal breathing during the T2* scans.

Image analysis

The maximum and mean SUV (SUVmax and SUVmean) of the liver lesions with a maximum of 5 liver lesions per patient were assessed by applying a variable threshold delineation method based on the signal-to-background ratio (20). The liver lesions were selected based on good visible separation from other metastases and the right kidney on the PET images. The SUV was corrected for total body weight. The adaptive threshold was calculated with the formula: **threshold=SUVbackground+0.41*(SUVmax-SUVbackground** (21). All tumors were delineated using Inveon Research Workplace (IRW 3.0, Siemens Medical Solutions, USA). A volume weighted average of the SUVmax over the assessed liver lesions was calculated. A total lesion glycolysis (TLG) was calculated by multiplying the metabolic volume with the SUVmean. The sum of the total lesion glycolysis of the assessed tumors was calculated.

The ADC images were calculated automatically by the Syngo VB17 scanner software using a noise level of 10. ROI's were manually drawn on the diffusion weighted b=50s/mm2 images for optimal tumor-background contrast and were drawn around the entire metastasis (on all slices). ROI's were drawn around the same lesions as delineated on the PET scans. Inveon Research Workplace overlays the ADC map on diffusion weighted b=50s/mm2 image. The mean ADC value in each metastasis was calculated.
T2* maps were generated using in-house built software based on Matlab (MathWorks, Natick, MA, USA). The echo time data was fitted pixel by pixel to a mono-exponential curve. ROIs drawn on diffusion weighted b=50s/mm2 image were copied on the T2* map, to calculate the mean T2* values. Baseline images and the images one week after start of treatment were analyzed by before the outcome after 3 cycles was evaluated. To evaluate CT response, the maximum lesion diameters after 3 and 6 cycles were compared to lesion size before start of treatment.

Statistics

All data were imported in SPSS 20.0 (IBM SPSS Statistic, SPSS Inc., IBM, Chicago, IL). To assess the predictive value of the pretreatment SUVmax, TLG, ADC and T2* measurement to progression free and overall survival a Cox proportional regression analysis was used. A multivariate Cox proportional regression analysis was used to assess predictive value of combined parameters. Given the limited number of patients in this study, no multivariate analysis to correct for (other) prognostic parameters was performed. Progression free survival was defined as the time from start of therapy to disease progression on CT (defined according to RECIST criteria) or death by any cause. Overall survival was defined as time from start of treatment to death by any cause.
A paired sample T-test was performed to assess whether the measured SUV, T2* and ADC one week after start of therapy significantly differed from the values before start of therapy. Cox regression analysis was performed to assess the predictive value for PFS and OS, if the parameters showed a statistically significant change after a week.
Furthermore, we assessed the correlation between the pretreatment values and early changes on PET and MRI with the changes on CT after 3 cycles of chemotherapy in a lesion-by-lesion and patient-by-patient analysis.

Results

Patients

Thirty-nine patients participated in the study. In total, 154 liver metastases were assessed. Patient characteristics are summarized in Table 1. Two patients underwent MRI only. In two patients only an 18F-FDG PET/CT was performed. The first follow-up scan (one week after start of treatment) was not completed by eight patients. Side effects of chemotherapy was the main reason for protocol deviations. The final follow-up scans (after 3 treatment cycles) were not completed by 7 patients [Table 2 and 3]. Median follow-up was 65.5 weeks (range 2 - 221 weeks). After three cycles 43.6% (N=17) of the patients showed partial response, 41.0% (N=18) of the patients had stable disease and 12.8% (N=5) of the patients died or had severe progression clinically.

Patient characteristics	*N*=39
Sex	• 71.8% male (*N*=28) • 28.2% female (*N*=11)
Mean age	• 62 years (range 29-77)
Localization primary tumor	• 41.0% Right hemicolon (*N*=16) • 28.2% Left hemicolon, including sigmoid (*N*=11) • 23.1% Rectal cancer (*N*=9) • 7.7% Unknown location in colon (*N*=3)
Treatment	• CAPOX+ bevacizumab (*N*=32) • Capecitabine+ bevacizumab (*N*=4) • CAPOX (*N*=1) • UFT (*N*=1) • FOLFOX with hyperthermia (*N*=1)
Intention of treatment	• Neoadjuvant (*N*=5) o 4 resected • Palliative (*N*=35)

Table 1. *Characteristics of participating patients. CAPOX= capecitabine and oxaliplatin; UFT= tegafur-uracil ; FOLFOX= fluorouracil and oxaliplatin*

Predictive value of pretreatment 18F-FDG PET and MRI parameters

An example of a pretreatment 18F-FDG PET, DWI, ADC map and T2* image of a patient with multiple liver metastases is shown in Figure 1. In general, high uptake of FDG was visible in the liver metastases on the PET-images. On the ADC-map, there was a dark signal (low ADC) in the rim of all tumors and high signal in the centre of most tumors, indicating central necrosis. There was little contrast between liver and tumor on the T2*-map.

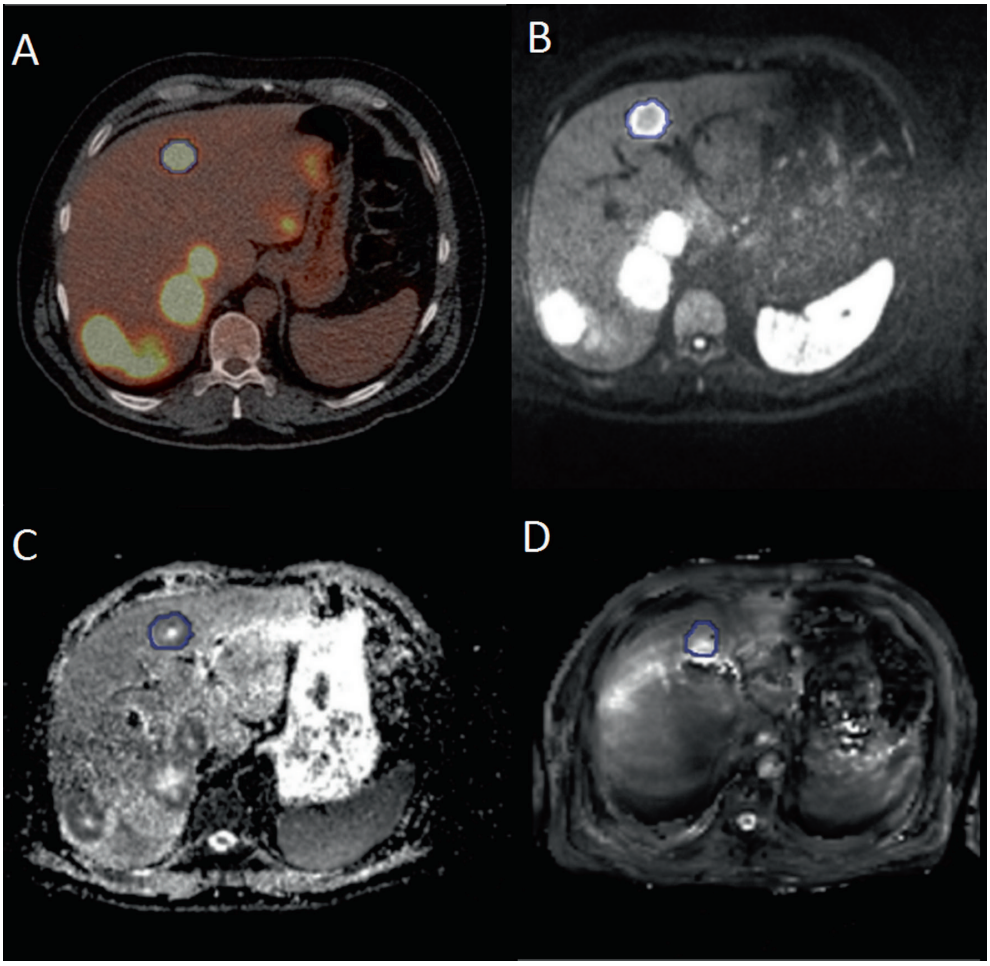

Figure 1. *Typical images acquired with FDG PET, DWI and T2* of a patient with multiple liver metastases. One liver metastasis is delineated with a blue line on A) FDG-PET/CT B) a diffusion weighted image (b-value 50 s/mm2), C) ADC-map and D) T2*-map.*

The mean SUVmax in the liver lesions was 11.3 g/cm3 (range 5.8-20.5 g/cm3) and the mean sum of the TLG in the assessed liver lesions was 1084g (range 12.8-4845g). The SUVmax value was not a significant predictor of PFS, but was predictive of OS. Each 1.0 increase in SUVmax was associated with a 1.125 higher risk of death (95% CI 1.020-1.241, p=0.02). Although TLG was not predictive of PFS, it did show predictive value for OS: each 100g increase in pretreatment TLG value was associated with a 1.047 increased hazard of dying (95% BI 1.010-1.085, p=0.01).

The average pretreatment ADC value was 1.21 *10-3 mm2/s and the average pretreatment T2* value was 30.2 ms. The pretreatment ADC value was a significant predictor of both PFS

and OS: a 0.1 *10-3 mm2/s higher pretreatment ADC value provided a hazard ratio of 0.749 for progression (95% CI 0.561-1.000, p=0.05) and a decreased risk of dying (HR 0.667, 95% CI 0.466-0.955, p=0.03). Kaplan Meier survival plots for the patients with higher and lower than median ADC are shown in figure 2.

Pretreatment T2* value was a significant predictor for OS, but not for PFS. A 1 ms higher average T2* time was associated with an increased risk of dying (HR 1.118, 95% CI 1.023-1.222, p=0.01).

Combining the pretreatment ADC values and SUVmax in a multivariate model showed a higher predictive value for survival, p<0.01. Adding T2* or TLG parameters did not increase the predictive value of the model.

Pretreatment SUVmax, ADC and T2* were not correlated to the size change on CT after three cycles of chemotherapy, neither in the patient-by-patient analysis nor in the lesion-by-lesion analysis.

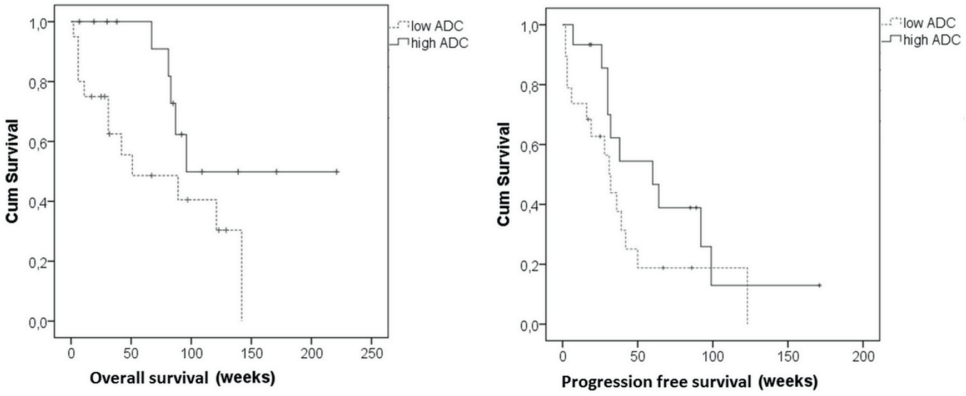

Figure 2. *Kaplan Meier Survival curve for a higher or lower than mean ADC value (1.21 mm2/s) at pretreatment, showing a significant difference in overall survival (p=0.022) and progression free survival (p=0.001).*

9

Predictive value of early changes in 18F-FDG PET and MRI parameters

SUVmax significantly decreased one week after start of treatment (SUVmax: 11.3 to 6.3, p<0.01). SUVmax decreased on average with 18.0% ±19.1% (range 66.1% decrease-14.8% increase).TLG decreased on average 19% ±35.0% after one week of treatment (1084 to 726, p=0.07). The ADC values significantly increased after one week of treatment from 1.20 to 1.27 *10-3 mm2/s (p=0.01). The average increase was 0.0710-3 mm2/s ± 0.13*10-3 mm2/s. The T2* values were on average 30.2ms before treatment and 26.7ms one week after start of treatment. This was not a significant decrease (p=0.17).

The change in ADC value was inversely correlated to the change in SUVmax, r=-0.58, p<0.01 [figure 3]. No correlation with changes in T2* was observed. The degree of change in SUVmax, TLG and ADC were not predictive of either PFS or OS. Also combined changes in SUVmax, TLG and ADC did not predict PFS or OS.

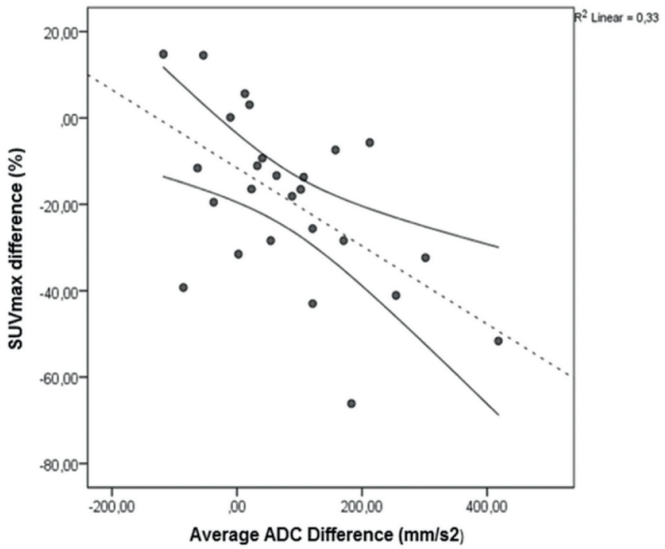

Figure 3. *Regression analysis of the changes in SUVmax on differences in ADC one week after start of treatment (r=-0.58, p=0.002). The fit line (red) and 95% confidence interval (black) are shown.*

Furthermore, the change in SUVmax, TLG and ADC after one week did not correlate to size change on CT after 3 cycles in a lesion by lesion analyses or patient-by-patient analysis. As shown in figure 4, there is no difference between CT responders and non responders in change in SUVmax or ADC. Of note, in only 23 metastases an increase in SUV after one week of treatment was observed, of which 16 metastases had a reduced diameter after 3 cycles.
In previous studies the reproducibility of FDG PET and DWI in liver metastases was assessed. (22). When patients with a increase in ADC over 0.20 *10-3 mm2/s (twice the standard deviation of normal variation) and decrease in SUVmax over 40% were classified as responder, there was still no significant difference in CT response, PFS or OS.

	Pretreatment Average (SD)	1 week Average (SD)	3 cycles Average (SD)
FDG PET			
SUVmax (g/cm3)	11.4 (4.7)	8.8 (3.7)	5.0 (3.3)
	1084 (1244)	726 (1145)	144 (212)
TLG (g)	*N*=37	*N*=30	*N*=29
MRI			
DWI (ADC)	1.21 (0.17)	1.27 (0.20)	
T2* (ms)	30.2 (7.0)	26.7 (8.1)	
	N=36	*N*=29	
CT (RECIST)			
Sum of diameters (mm)	153 (90)		104 (74)
	N=39		*N*=31

Table 2. *Average ^{18}F-FDG PET, MRI and CT parameters at pretreatment, one week after start of therapy and after 3 cycles of therapy.*

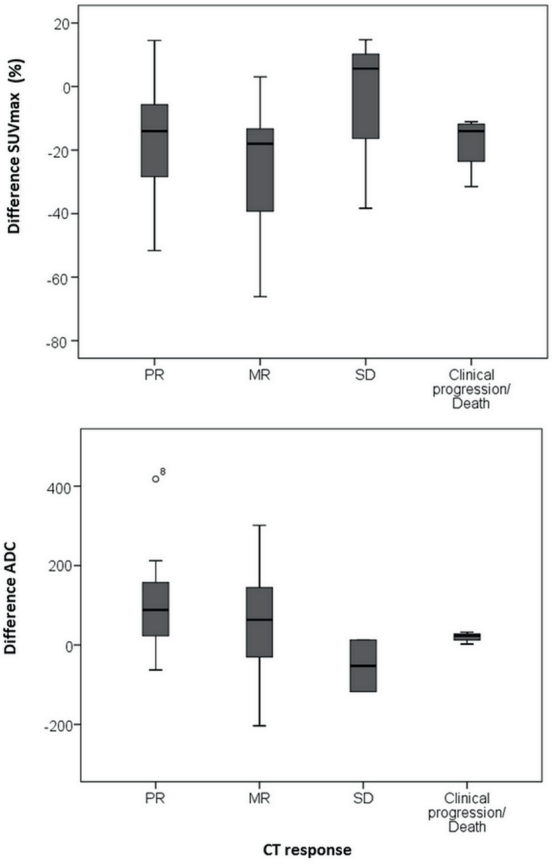

Figure 4. *Boxplots showing the change in SUV_{max} and ADC in patients with partial response, minor response, stable disease and in patient unable to perform the scan after 3 cycles due to clinical progression or death. There was no relation between response and changes in SUV_{max} or ADC.*

Discussion

Pretreatment 18F-FDG PET and MRI parameters

Combining the pretreatment ADC values and SUVmax in a multivariate model showed a higher predictive value for survival. Also, a correlation between SUVmax and survival was observed. This is in line with previous studies, performed in patients with both primary resectable and irresectable colorectal liver metastases, in which significantly higher pretreatment SUV was associated with poorer outcome (7, 23).

In this study, lower pretreatment ADC values predicted poorer outcome, which may be related to the association between ADC values and histological grade. In breast and prostate cancer lower ADC values were correlated with higher histological grade and higher Gleason score (24-26). In colorectal cancer, a higher histological grade is correlated with an adverse outcome (27, 28).

A low T2* value, indicating higher concentration of deoxyhemoglobin, was favorable for longer OS, but did not correlate with PFS. However, the deoxyhemoglobin is not only dependent on hypoxia. In very poor vascular supply and necrotic areas, there may be also very little deoxyhemoglobin present.

Early changes in 18F-FDG PET and MRI parameters

Both 18F-FDG PET and DWI showed therapy induced changes one week after start of treatment. The changes in 18F-FDG PET and DWI were correlated, suggesting an association between treatment effects leading to decreased cellular density and metabolic response.

Unfortunately, the measured treatment effects were not predictive of survival or CT-response. The lack of relation between changes in 18F-FDG PET and MRI parameters and treatment outcome can be attributed to several factors. In contrast to comparable previous studies, bevacizumab was part of the standard treatment regimen in the present study. Antiangiogenic treatments, such as bevacizumab, may alter the distribution of intravenously injected tracers or contrast agents in the tumor (29). Decrease in SUV might therefore, in part, reflect alterations in tumor blood supply, rather than metabolic changes. This might obscure the association between metabolic response and treatment outcome. The use of a variable threshold to delineate the tumor on 18F-FDG-PET may have resulted in an underestimation of the effect of treatment on TLG, since SUVmax decreased as an effect to treatment and therefore the threshold was lower for the second scan. However, the use of a fixed threshold is also problematic due to high background activity in liver tissue.

DWI and T2* are not dependent on administration of intravenous contrast agents. However, the observed increase in ADC and reduction in T2* may be a reflection of therapy induced necrosis, related to a favorable outcome, as well as to bevacizumab induced reduction in vascularization and hypoxia, related to therapy resistance and a dismal outcome. Thus, the

relation between outcome and changes in DWI and T2* are obscured by differential effects on the tumor. T2* did not significantly alter after start of treatment. Therefore, this parameter may be less suitable as a predictor of response to therapy.
Finally, the interval between start of treatment and the first evaluation may be of crucial importance for response monitoring with 18F-FDG PET and ADC. An interval of one week after start of targeted therapy containing treatment might be too short for 18F-FDG PET. 1-2 weeks after start of treatment a flare-up phenomenon has been described, defined by an initial rise in metabolic activity in lesions that would respond later on (30). This phenomenon might also interfere with the measured parameters.
Conversely, changes in ADC cannot only precede changes in tumor size, but may even disappear after a certain time due to activated repair mechanisms (31). In a previous study an increase in ADC in colorectal and gastric liver metastases (of 23 patients) was described after 3 and 7 days of treatment. However, only a weak correlation between change in ADC on day 3 and final change in size could be established, whereas no significant correlation between changes at day 7 and final lesion size was observed (13). Therefore, it might be more effective to measure ADC at a shorter time interval after start of treatment. Finally, we can only speculate on the optimal interval for early response prediction using T2* in the present study. In a breast cancer study after 2 cycles of chemotherapy, however, a significant increase in T2* was observed (32), suggesting that longer time intervals may benefit.

Study limitations

Although the number of included patients and evaluated metastases is limited, it is reasonably compared to other imaging studies. Given the burden of imaging procedures and associated costs, acceptable sample size is in the range of 30-70 patients. For a hazard ratio of 0.85 (power 80% and α 0.05) 40 patients would be sufficient to demonstrate this association with a standard deviation of 2.5. Therefore, with this number of patients hazard ratio's can be calculated, but not with high prognostic performance.
The patients with the poorest treatment outcome could not complete all scans which limits correlation with changes in size after 3 cycles. The use of two different PET-CT scanners should not have influenced the predictive value of the pretreatment SUV and TLG measurements as both scanners were EANM-EARL accredited for quantitative PET.

Conclusion

Pretreatment SUVmax, TLG values, ADC and T2* in colorectal liver metastases are predictive of patient survival. In the future, this could provide the opportunity to select patients who could benefit from chemotherapy prior to start of treatment. Early effects after one week of treatment with chemo- and targeted therapy can be measured with 18F-FDG PET and DWI, however, these effects were not predictive of long term outcome in this study.

Reference List

[1] Manfredi S, Lepage C, Hatem C, Coatmeur O, Faivre J, Bouvier AM. Epidemiology and management of liver metastases from colorectal cancer. AnnSurg. 2006;244(2):254-9.

[2] Therasse P, Arbuck SG, Eisenhauer EA, et al. New guidelines to evaluate the response to treatment in solid tumors. European Organization for Research and Treatment of Cancer, National Cancer Institute of the United States, National Cancer Institute of Canada. J Natl Cancer Inst. 2000;92(3):205-16.

[3] Desar IM, van Herpen CM, van Laarhoven HW, Barentsz JO, Oyen WJ, van der Graaf WT. Beyond RECIST: molecular and functional imaging techniques for evaluation of response to targeted therapy. Cancer Treat Rev. 2009;35(4):309-21.

[4]. Gruenberger T, Arnold D, Rubbia-Brandt L. Pathologic response to bevacizumab-containing chemotherapy in patients with colorectal liver metastases and its correlation with survival. Surgical oncology. 2012;21(4):309-15.

[5]. Tol J, Punt CJ. Monoclonal antibodies in the treatment of metastatic colorectal cancer: a review. Clin Ther. 2010;32(3):437-53.

[6] de Geus-Oei LF, Vriens D, van Laarhoven HW, Van Der Graaf WT, Oyen WJ. Monitoring and predicting response to therapy with 18F-FDG PET in colorectal cancer: a systematic review. J NuclMed. 2009;50 Suppl 1:43S-54S.

[7] de Geus-Oei LF, Wiering B, Krabbe PF, Ruers TJ, Punt CJ, Oyen WJ. FDG-PET for prediction of survival of patients with metastatic colorectal carcinoma. Ann Oncol. 2006;17(11):1650-5.

[8]. Dimitrakopoulou-Strauss A, Strauss LG, Burger C, et al. Prognostic aspects of 18F-FDG PET kinetics in patients with metastatic colorectal carcinoma receiving FOLFOX chemotherapy. J Nucl Med. 2004;45(9):1480-7.

[9] Hendlisz A, Golfinopoulos V, Garcia C, et al. Serial FDG-PET/CT for early outcome prediction in patients with metastatic colorectal cancer undergoing chemotherapy. Ann Oncol. 2012;23(7):1687-93.

[10] Koh DM, Collins DJ. Diffusion-weighted MRI in the body: applications and challenges in oncology. AJR AmJ Roentgenol. 2007;188(6):1622-35.

[11] Heijmen L, Verstappen MCHM, ter Voert EEGW, et al. Tumour response prediction by diffusion-weighted MR imaging: ready for clinical use? Critical Reviews in Oncology/Hematology. 2012.

[12] Yablonskiy DA, Sukstanskii AL. Theoretical models of the diffusion weighted MR signal. NMR Biomed;23(7):661-81.

[13] Cui Y, Zhang XP, Sun YS, Tang L, Shen L. Apparent diffusion coefficient: potential imaging biomarker for prediction and early detection of response to chemotherapy in hepatic metastases. Radiology. 2008;248(3):894-900.

[14] Koh DM, Scurr E, Collins D, et al. Predicting response of colorectal hepatic metastasis: value of pretreatment apparent diffusion coefficients. AJR Am J Roentgenol. 2007;188(4):1001-8.

[15] Padhani AR, Krohn KA, Lewis JS, Alber M. Imaging oxygenation of human tumours. European radiology. 2007;17(4):861-72.

[16] Fan B, Wang XY, Yang XD, Zhong H, Wu CX, Jiang XX. Blood oxygen level-dependent MRI for the monitoring of neoadjuvant chemotherapy in breast carcinoma: initial experience. Magnetic resonance imaging. 2011;29(2):153-9.

[17] Chavhan GB, Babyn PS, Thomas B, Shroff MM, Haacke EM. Principles, techniques, and applications of T2*-based MR imaging and its special applications. Radiographics: a review publication of the Radiological Society of North America, Inc. 2009;29(5):1433-49.

[18] Boellaard R, O'Doherty MJ, Weber WA, et al. FDG PET and PET/CT: EANM procedure guidelines for tumour PET imaging: version 1.0. European journal of nuclear medicine and molecular imaging. 2010;37(1):181-200.

[19] Ter Voert EE, van Laarhoven HW, Kok PJ, Oyen WJ, Visser EP, de Geus-Oei LF. Comparison of liver SUV using unenhanced CT versus contrast-enhanced CT for attenuation correction in 18F-FDG PET/CT. Nuclear medicine communications. 2014.

[20] Wahl RL, Jacene H, Kasamon Y, Lodge MA. From RECIST to PERCIST: Evolving Considerations for PET response criteria in solid tumors. J NuclMed. 2009;50 Suppl 1:122S-50S.

[21] Frings V, de Langen AJ, Smit EF, et al. Repeatability of metabolically active volume measurements with 18F-FDG and 18F-FLT PET in non-small cell lung cancer. J Nucl Med. 2010;51(12):1870-7.

[22] Heijmen L, de Geus-Oei LF, de Wilt JH, et al. Reproducibility of functional volume and activity concentration in 18F-FDG PET/CT of liver metastases in colorectal cancer. European journal of nuclear medicine and molecular imaging. 2012;39(12):1858-67.

[23] De Bruyne S, Van Damme N, Smeets P, et al. Value of DCE-MRI and FDG-PET/CT in the prediction of response to preoperative chemotherapy with bevacizumab for colorectal liver metastases. British journal of cancer. 2012;106(12):1926-33.

[24] Hambrock T, Somford DM, Huisman HJ, et al. Relationship between Apparent Diffusion Coefficients at 3.0-T MR Imaging and Gleason Grade in Peripheral Zone Prostate Cancer. Radiology. 2011.

[25] Nakajo M, Kajiya Y, Kaneko T, et al. FDG PET/CT and diffusion-weighted imaging for breast cancer: prognostic value of maximum standardized uptake values and apparent diffusion coefficient values of the primary lesion. European journal of nuclear medicine and molecular imaging. 2010;37(11):2011-20.

[26] Woodfield CA, Tung GA, Grand DJ, Pezzullo JA, Machan JT, Renzulli JF, 2nd. Diffusion-weighted MRI of peripheral zone prostate cancer: comparison of tumor apparent diffusion coefficient with Gleason score and percentage of tumor on core biopsy. AJR Am J Roentgenol. 2010;194(4):W316-22.

[27] Liu CJ, Lin JK, Chen WS, et al. The efficacy of chemotherapy in patients with high-grade metastatic colon cancer. Hepato-gastroenterology. 2011;58(110-111):1495-501.

[28] Nanni O, Volpi A, Frassineti GL, et al. Role of biological markers in the clinical outcome of colon cancer. British journal of cancer. 2002;87(8):868-75.

[29] Heijmen L, Voert EGWt, C.J.A. Punt AH, et al. Monitoring hypoxia and vasculature during bevacizumab treatment in a murine colorectal cancer model Contrast Media and molecular imaging. accepted.

[30] Findlay M, Young H, Cunningham D, et al. Noninvasive monitoring of tumor metabolism using fluorodeoxyglucose and positron emission tomography in colorectal cancer liver metastases: correlation with tumor response to fluorouracil. J Clin Oncol. 1996;14(3):700-8.

[31] Desar IM, van Laarhoven HW, Hambrok T, et al. Assessment of early vascular effects of the angiogenesis inhibitor sunitinib (SU) in renal cell carcinoma (RCC) by dynamic contrast enhanced MRI (DCE-MRI) and diffusion weight MRI (DWI) at 3 tesla (T). ASCO.

[32] Li SP, Taylor NJ, Makris A, et al. Primary human breast adenocarcinoma: imaging and histologic correlates of intrinsic susceptibility-weighted MR imaging before and during chemotherapy. Radiology. 2010;257(3):643-52.

10

Summary

Introduction

Functional and molecular imaging techniques might be able to effectively monitor therapy response in cancer at an earlier stage than the current techniques for response evaluation using volumetric response criteria. There are numerous functional imaging techniques that each measures a distinctive tumor aspect. **Chapter 1** explains the need for response prediction in advanced colorectal cancer and provides a short overview of the functional imaging techniques discussed in this thesis.

Colorectal cancer is the second most common cause of cancer related death in the Netherlands. Most patients with (liver) metastases have to rely on palliative systemic therapy for treatment. Despite improvement of palliative treatment with targeted therapies, disease stabilization is not reached in a considerable percentage of patients (5.4-14.6%). Response prediction would prevent toxicity and reduce costs in these patients. Furthermore, volumetric response evaluation seems suboptimal for targeted therapies. The effect of targeted therapies might be more successfully assessed by functional imaging.

Using MRI, diverse tumor properties can be assessed. Diffusion weighted imaging (DWI) measures the diffusion rate of water molecules (apparent diffusion coefficient, ADC). Since the diffusion movement is inhibited by cellular structures, the diffusion rate is inversely related to the cell density. T2* and dynamic contrast enhanced MRI (DCE-MRI) are two techniques to assess the tumor vasculature. T2* depends on local field inhomogeneities that are mainly caused by deoxyhemoglobin molecules, while DCE-MRI monitors the perfusion and permeability of tumor vessels by monitoring the infusion of a contrast agent over time.

FDG PET is one of the most frequently used functional imaging techniques. It monitors the uptake and phophorylation of glucose analog FDG. Since cancer cells are dependent of glycolysis for most of their energy supply, tumors in general have a high uptake of glucose and FDG. Dynamic FDG PET monitors the FDG uptake over time-from the time of injection of FDG- and therefore is also able to correct for vascular supply and competitive uptake.

Chapter 2 discusses the role of DWI in tissue characterization and (early) response monitoring. The literature reviewed demonstrated that DWI has the potential to differentiate benign from malignant lesions based on a lower ADC value in malignant lesions. Furthermore, most articles showed that a lower ADC value, and thus higher cell density, is associated with a poorer differentiation grade and outcome. However, in different studies, both high and low pretreatment ADC were found to be associated with response rate. A high pretreatment ADC was in most cases hypothesized to correspond to a poorer response; necrotic tumor areas, with high ADC values, are often surrounded by hypoxic tissue that is more aggressive and therapy resistant.

In the course of treatment, an increase in ADC, and thus decrease in cell density, was associated with response in most cases. The changes in ADC seemed even more lucid in studies using DWI for early response monitoring. The potential of DWI for (early) response monitoring of anticancer therapies has been demonstrated. However, validation is hampered by the lack of repeatability and standardization. We recommended that these issues should be properly addressed prior to further testing the clinical use of DWI in the assessment of treatments.

Repeatability of the functional imaging techniques

Before functional imaging techniques can be implemented in standard clinical practice for response monitoring, data on repeatability are needed to assess which differences outside the range of normal variation can be detected in an individual patient. In this thesis the repeatability of several functional imaging techniques in colorectal liver metastases were assessed. The coefficient of repeatability is an important tool to validate the repeatability: it describes-within the paired measurements- the difference between the two measurements that is smaller in 95% of the pairs. Furthermore, to provide a biological basis for the measurements, their relation with histopathology was assessed.

Chapter 3 describes the repeatability of DWI in colorectal liver metastases and the correlation with histopathology. DWI was performed twice within one week in 18 patients scheduled for metastasectomy of colorectal liver metastases. We assessed the repeatability of the ADC values in 21 colorectal liver metastases. A good repeatability of the mean ADC (coefficient of repeatability 0.20 *10-3 mm2/s) was observed in colorectal liver metastases. The mean ADC value was 1.17 *10-3 mm2/s. To provide a biological basis for these values, the correlation with histopathology was also assessed. Correlation between ADC values and apoptosis marker p53, anti-apoptotic protein BCL-2 and proliferation marker Ki67 were assessed. The ADC value was related to the proliferation index and BCL-2 expression of the metastases. Furthermore, in metastases recently treated with systemic therapy, the ADC was significantly higher (1.27 *10-3 mm2/s vs. 1.05 *10-3 mm2/s, P=0.02). The good repeatability, correlation with histopathology and implied sensitivity for systemic treatment-induced antitumor effects suggested that DWI might be an excellent tool to monitor response in metastatic colorectal cancer.

Chapter 4 reports the repeatability of T2* MR imaging in colorectal liver metastases and correlated T2* values with the expression of the hypoxia related markers GLUT1 and CAIX as well as the relative vascular area, and the vessel density in resected tumors. The repeatability of T2* was analyzed in 18 patients with in total 22 colorectal liver metastases by repeating two T2* measurements within a week. The repeatability was analyzed using the Bland & Altman method for the mean, the 16th, 50th, and 84th percentile values. The average T2* of all liver metastases was 25.9±7.1 ms vs. 22.4±4.5 ms in normal liver. The coefficient of

repeatability was 11.2 ms and the limits of agreement were-12.4 ms and 10.0 ms for mean T2* values. On average T2* showed reasonable repeatability. Immunohistochemical staining was performed on 17 resected tumors obtained from 16 patients. No correlations between T2* values, hypoxia and vascularity related markers were observed.

Chapter 5 describes the repeatability of functional volume and activity concentration in ^{18}F-FDG PET/CT of liver metastases in colorectal cancer. Twenty patients scheduled for liver metastasectomy underwent two ^{18}F-FDG PET scans within one week. Bland Altman analysis was performed to assess repeatability of SUV_{MAX}, SUV_{MEAN}, volume and total lesion glycolysis. Tumors were delineated using an adaptive threshold method (PET_{SBR}) and a semi-automatic delineation (FLAB) method. Coefficient of repeatability of SUV_{MAX} and SUV_{MEAN} were ~39% and ~31%, respectively, independent of the used delineation method and image reconstruction parameters. However, repeatability was worse in recently treated patients. FLAB delineation method improved the repeatability of the volume and TLG measurements. GLUT1 expression correlated to the SUVmean. Vascularity (CD34 expression) and tumor hypoxia (CAIX expression) did not correlate with ^{18}F-FDG PET parameters.

Chapter 6 reports on the repeatability of dynamic ^{18}F-FDG PET and compares the results to the repeatability of static ^{18}F-FDG PET in liver metastases of colorectal cancer. 11 patients scheduled for metastasectomy of colorectal liver metastases participated in the study and underwent two 60-minute dynamic FDG PET scans within a week. In the last time frame (50-60 minutes) the tumors were delineated with a background corrected threshold method and a 70% isocontour, to determine the SUV_{MAX}, SUV_{SBR} and SUV_{70}. Metabolic rate maps were calculated and the tumors were delineated using a 50% and 70% isocontour to determine maximum metabolic rate (MR_{glu}), MR_{glu50} and MR_{glu70}. Nine patients had 15 FDG PET positive lesions; two patients had no FDG uptake in the liver metastases. The coefficient of repeatability of MR_{glu} was superior compared to semi-quantitative PET parameters. The coefficient of repeatability was 32.5%, 33.4% and 30.1% for the maximum MR_{glu}, MR_{glu70} and MR_{glu50}. The coefficient of repeatability of 40.9% for the SUV_{MAX}, 41.6% for the SUV_{70} and 37.7% for the $SUV_{BGC.}$ In conclusion, repeatability of MR_{glu} was superior to the repeatability of SUV parameters.

Measurement of treatment effects

In **chapter 7** the effect of bevacizumab monotherapy on vasculature and hypoxia in a colorectal tumor model is assessed. Nude mice with subcutaneous LS174T tumors were treated with bevacizumab or saline. To assess tumor properties, separate groups of mice were imaged using FMISO and FDG PET or MRI, before and 2, 6 and 10 days after start of treatment. Tumors were harvested after imaging to determine hypoxia and vascular density immunohistochemically. T2* time increased significantly less in the bevacizumab group. FMISO uptake increased more over time in the control group compared to the bevacizumab

group. Vessel density significantly decreased in the bevacizumab-treated group. CAIX and GLUT1 fraction were higher in bevacizumab-treated tumors. However, the hypoxic fraction showed no significant difference.

Bevacizumab led to shorter T2* times and higher GLUT1 and CAIX expression, suggesting an increase in hypoxia and a higher glycolytic rate. This could be a mechanism of resistance to bevacizumab. The increase in hypoxia, however, could not be demonstrated by pimonidazole/FMISO, possibly because distribution of these tracers is hampered by bevacizumab-induced effects on vascular permeability and perfusion.

Chapter 8 reports on the utility of several functional imaging modalities to assess the efficacy of bevacizumab beyond progression (BBP). Clinical studies have shown that bevacizumab beyond progression to first line therapy is beneficial for overall survival in advanced stage colorectal cancer. However, there is no effective means to monitor effectiveness of bevacizumab beyond progression.

BALB/c mice with s.c. LS174T xenografts were treated with capecitabine, oxaliplatin and bevacizumab. Tumor volume was assessed using caliper measurements. Increase of 1.5 times the initial volume on two subsequent measurements, was considered progression. In half of the mice bevacizumab treatment was continued (n=13), while the others received saline injections (n=12). Within 3 days after progression, multi-modal imaging was performed using FDG-PET, diffusion weighted imaging, T2* and dynamic contrast enhanced MRI. Measurements were repeated 7 and 10 days after the first measurements. Afterwards, tumors were analyzed for expression of carbonic anhydrase IX, glucose transporter 1, 9F1 and Ki67. In the BBP group tumor growth after progression was reduced compared to the control group ($p<0.01$). FDG-PET showed a trend towards lower FDG uptake in the BBP group ($p=0.08$). DWI, T2* and DCE-MRI parameters were not significantly different between both groups. The immunohistochemical analyses showed higher CAIX-positive fraction ($p<0.01$) and lower Ki67 expression ($p=0.06$) in the BBP group. The relative vascular area was significantly lower in the BBP group ($p=0.03$). GLUT-1 expression and vascular density did not significantly differ between both groups. Bevacizumab after progression resulted in significant changes in the tumor proliferation and microenvironment compared to discontinuation of bevacizumab. FDG-PET may be sensitive to BBP-induced effects.

In **chapter 9** the potential of FDG-PET, DWI and T2* MRI to predict response to systemic treatment in patients with colorectal liver metastases is assessed. The predictive value of baseline measurements, as well as the predictive value of early changes one week after start of therapy, were evaluated.

FDG-PET, DWI and T2* MRI were performed prior and 1 week after start of first line chemotherapy. The FDG PET scan was performed 60 minutes post injection on a hybrid PET/CT scanner and DWI and T2* were performed on a 1.5T MR scanner. Lesions on the FDG PET scan were delineated using a background corrected variable threshold method. The mean and

maximum standardized uptake values (SUV) were assessed. By multiplying the SUVmean with the volume, the total lesion glycolysis (TLG) was calculated. The same lesions on DWI were evaluated by ROIs drawing ROIs around the metastases to examine the apparent diffusion coefficient (ADC) value. The ROIs of the DWI were copied on the T2* maps. A maximum of 5 liver metastases per patient were analyzed. Primary outcome measure was progression free survival (PFS). Predictive value for overall survival (OS), as secondary outcome measure, was also assessed.

A low baseline ADC value was associated with a poorer PFS and OS. A higher baseline T2*, SUVmax and TLG were associated with a poorer OS. After 1 week a significant drop in SUVmax and a significant rise in ADC were observed. The drop in SUV was correlated with the rise in ADC. However, neither change in ADC nor SUV were predictive of PFS or OS. T2* did not significantly change after start of treatment. In conclusion, baseline ADC values in colorectal liver metastases are predictive of the outcome. Despite sensitivity of DWI and FDG PET for early effects of therapy, the extents of change in the parameters were not predictive of long term outcome. T2* did not show changes early after start of treatment.

10

Nederlandse samenvatting

Introductie

Functionele en moleculaire beeldvormende technieken zijn mogelijk in staat om op een eerder tijdpunt respons op therapie in tumoren te meten, dan de traditionele technieken die gebruik maken van volume veranderingen in de tumor. Er zijn verschillende functionele beeldvormende technieken die ieder een specifiek aspect van de tumor meten.

Hoofdstuk 1 beschrijft waarom het vroegtijdig voorspellen van de respons op therapie bij uitgezaaide colorectale tumoren nuttig is en geeft een kort overzicht van de gebuikte beeldvormende technieken in dit proefschrift.

Colorectaal carcinoom is de op een na meest voorkomende oorzaak van kanker gerelateerde sterfte in Nederland. De meeste patiënten met levermetastasen zijn afhankelijk van palliatieve systeemtherapie voor hun behandeling. Ondanks verbeteringen in de palliatieve behandeling door het toevoegen van “targeted therapies” wordt in een aanzienlijk deel van de patiënten (5.4-14.6%) geen stabilisatie van de ziekte bereikt. Vroege voorspelling van respons zou deze patiënten een onsuccesvolle behandeling, en dus onnodige toxiciteit en kosten, kunnen besparen. Verder lijkt bepalen van de respons op basis van volume verandering, minder geschikt voor de “targeted therapies”, omdat deze behandelingen niet altijd leiden tot een afname van tumorgrootte. Functionele beeldvormende technieken zijn mogelijk gevoeliger voor de effecten van “targeted therapies”.

FDG PET is een van de meest gebruikt functionele beeldvormende technieken. Het meet de opname en fosforylatie van de glucose analoog, FDG. Doordat de kankercellen vooral van glycolyse afhankelijk zijn voor hun energievoorziening, nemen tumoren over het algemeen veel glucose en FDG op. Dynamische FDG PET meet de opname van FDG in de tijd vanaf het moment dat FDG wordt geïnjecteerd. Daardoor kan bij dynamische PET, de opname van FDG in de tumor gecompenseerd worden voor de beschikbare FDG in de vaten en competitieve opname in andere weefsels.

Met MRI kunnen diverse tumor eigenschappen worden afgebeeld, diffusie gewogen MRI (DWI) meet de mate van beweging van water moleculen (apparent diffusion coefficient, ADC). Omdat de waterbeweging ingeperkt wordt door de aanwezigheid van celstructuren, zoals celmembranen, is de ADC waarde negatief gecorreleerd met de celdichtheid. T2* en dynamische contrast MRI (DCE-MRI) zijn twee MRI technieken om de tumorvasculatuur in kaart te brengen. T2* is afhankelijk van de inhomogeniteit van het magnetisch veld. De inhomogeniteit van het magnetisch veld wordt sterk beïnvloed door de aanwezigheid van deoxyhemoglobine. DCE-MRI meet de perfusie en permeabiliteit van de tumorvaten door de infusie van een contrastmiddel over de tijd te volgen.

In **hoofdstuk 2** wordt de rol van DWI in de karakterisatie van weefsel en in het meten van (vroege) therapie respons bediscussieerd. De besproken literatuur laat zien dat DWI veel

potentie heeft in het differentiëren tussen goedaardige en kwaadaardige afwijkingen. Verder laten de meeste artikelen zien dat een lage ADC waarde, en dus hoge celdichtheid, geassocieerd zijn met een slechtere differentiatiegraad en slechtere uitkomst. Echter, in verschillende tumoren en studies zijn er resultaten over ADC en respons op therapie tegenstrijdig. In de meeste gevallen is een hoge ADC waarde voor start van de behandeling geassocieerd met een slechtere respons op therapie. De hypothese hierachter is dat necrotisch weefsel met een hoge ADC waarde vaak omgeven is door hypoxisch weefsel, dat vaak agressiever en meer therapieresistent is. Na start van de behandeling is een stijging van de ADC waarde, en dus lagere celdichtheid, meestal geassocieerd met respons. De stijging in de ADC waarden leken zelfs sterker vroeg na start van de behandeling.
De potentie van DWI is dus in meerdere studies getoond. De validatie van de techniek is echter beperkt, doordat standaardisatie van de protocollen en reproduceerbaarheiddata voor veel tumoren en locaties ontbreken. We raden aan deze zaken aan te pakken, alvorens de techniek uitgebreid te testen voor klinische doeleinden.

Reproduceerbaarheid van functionele beeldvormende technieken
Voordat functionele beeldvormende technieken in de klinische praktijk gebruikt kunnen worden zijn data over de reproduceerbaarheid nodig om vast te stellen welke veranderingen buiten de normale variatie liggen en dus in een individuele patiënt gedetecteerd kunnen worden. In dit proefschrift wordt de reproduceerbaarheid van een aantal functionele beeldvormende technieken beschreven. Een belangrijke maat voor de reproduceerbaarheid is de Coefficient van Reproduceerbaarheid (CR): het beschrijft –binnen de gepaarde metingen- het verschil dat kleiner is in 95% van de paren. Verder wordt de correlatie met de histopathologie beschreven om een biologische basis voor de parameters te geven.
In **hoofdstuk 3** wordt de reproduceerbaarheid van DWI in colorectale levermetastasen en de correlatie van ADC met de histologie beschreven. DWI is tweemaal binnen een week uitgevoerd in 18 patiënten, die gepland stonden voor een metastasectomie. We hebben de reproduceerbaarheid in 21 lever metastasen bepaald. Een goede CR van de gemiddelde ADC (0.20 *10-3 mm2/s) werd waargenomen. De ADC werd gecorreleerd met apoptose marker p53, anti-apoptotisch eiwit BCL-2 and proliferatie marker Ki67. De ADC was gecorreleerd met de proliferatie index en met BCL-2 expressie in de metastasen.
Verder werd geobserveerd dat metastasen in recent systemisch behandelde patiënten en significant hogere ADC waarde hadden (1.27 *10-3 mm2/s vs. 1.05 *10-3 mm2/s, P=0.02).
De goede reproduceerbaarheid, correlatie met histologie en de geïmpliceerde gevoeligheid voor systemische behandeling suggereren dat DWI mogelijk een heel goede techniek is om respons te meten in gemetastaseerd colorectaal carcinoom.
Hoofdstuk 4 rapporteert over de reproduceerbaarheid van T2* MRI in colorectale lever metastasen en correleert T2* waarden met de hypoxie gerelateerde markers GLUT1 en

CAIX en met de vaatdichtheid in de gereseceerde tumoren. De reproduceerbaarheid van T2* werd bepaald in 18 patiënten met in totaal 22 lever metastasen, door binnen een week twee T2* metingen uit te voeren. De reproduceerbaarheid werd met behulp van de Bland & Altman methode bepaald voor de gemiddelde, 16^{e}, 50ste en 85ste percentiel waarden bepaald. De gemiddelde T2* van alle lever metastasen was 25.9 ± 7.1 ms ten opzichte van 22.4 ± 4.5 ms in normaal leverweefsel. De CR was 11.2 ms en limits of agreement -12.4 ms en 10.0 ms voor de gemiddelde T2* waarden. Over het algemeen vertoonde de T2* een redelijke reproduceerbaarheid. Immunohistochemische kleuringen werd uitgevoerd op 17 gereseceerde tumoren verkregen uit 16 patienten. Er werd geen correlatie gezien tussen de T2* waarden, hypoxie markers en vaatdichtheid.

Hoofdstuk 5 beschrijft de reproduceerbaarheid van metabool actief volume en de activiteitsconcentratie in de colorectale levermetastasen op ^{18}F-FDG PET/CT. Twintig patiënten, die gepland stonden voor een resectie van colorectale lever metastasen, werden twee keer met ^{18}F-FDG PET gescand. Twee patiënten hadden PET-negatieve metastasen. Vierentwintig laesies werden waargenomen in de overige 18 patiënten. Reproduceerbaarheid werd bepaald met behulp van de Bland & Altman analyse, voor de maximale SUV (waarde voor gestandaardiseerde opname), gemiddelde SUV, volume en TLG (total lesion glycolysis). Delineatie van de tumoren werd gedaan middels een adaptieve grenswaarde methode en een semi-automatische delineatie (FLAB) methode. De CR van de maximum en gemiddelde SUV was ~39% and ~31%, respectievelijk, onafhankelijk van de gebruikte delineatie methode en reconstructie parameters.

In **hoofdstuk 6** wordt de reproduceerbaarheid van dynamische FDG PET analyse vergeleken met statische PET parameters. Daarvoor is in 11 patiënten, die gepland stonden voor een metastasectomie van colorectale levermetastasen, binnen een week tweemaal een 60 minuten durende dynamische FDG PET verricht. Van de elf patiënten waren er negen met PET positieve lever metastasen (N=15).

In het laatste tijdframe (50-60 minuten) van de dynamische PET werden de tumoren gedelinieerd met een achtergrond gecorrigeerde grenswaarde methode en een 70% isocontour om de SUV_{MAX}, SUV_{SBR} en SUV_{70} te bepalen. Een map van de stofwisselingssnelheid (MR_{glu}) werd berekend en de tumoren werden gedelinieerd met een 50% en 70% isocontour om de maximale MR_{glu}, MR_{glu50} en MR_{glu70} vast te stellen. De reproduceerbaarheid van MRglu was beter dan de reproduceerbaarheid van de SUV metingen. De Coefficient van Reproduceerbaarheid was 32.5%, 33.4% en 30.1% voor respectievelijk de maximale MR_{glu}, MR_{glu70} en MR_{glu50}. De Coefficient van Reproduceerbaarheid was 40.9%, 41.6% en 37.7% voor respectievelijk de SUV_{MAX}, SUV_{70} en SUV_{BGC}.

De reproduceerbaarheid van de SUV metingen verbeterde niet door het dynamische PET protocol, maar de dynamische PET parameters hebben wel een betere reproduceerbaarheid dan SUV metingen. Dit verschil was echter niet statistisch significant.

Monitoren van behandeleffecten

In **hoofdstuk 7** wordt het effect van monotherapie bevacizumab op de vasculatuur en hypoxie in een colorectaal tumor model geëvalueerd. Naakte muizen met een subcutane tumor (LS174T) werden behandeld met bevacizumab of fysiologisch zout. Om de tumoreigenschappen te meten werden muizen in aparte groepen afgebeeld met ofwel FMISO en FDG PET, ofwel MRI voor start van behandeling en op 2, 6 en 10 dagen na start van de behandeling. De tumoren werden onmiddellijk na de laatste scan ingevroren om hypoxie en vasculatuur in de tumor met immunohistochemie te kunnen bepalen.

De T2* tijd steeg significant minder in de behandel groep ten opzichte van de controlegroep. Ook de FMISO opname steeg in de tijd meer in de controlegroep dan in de behandelgroep. De vaatdichtheid daalde significant in de behandelde groep, terwijl de hypoxie gerelateerde markers CAIX en GLUT1 significant hoger waren.

Echter de hypoxische fractie, bepaald met pimonidazol, liet geen verschil tussen de behandelde en controlegroep.

De kortere T2* tijden, hogere GLUT1 en CAIX expressie duiden op een toename van hypoxie en glycolyse door bevacizumab behandeling. Dit is mogelijk een resistentiemechanisme tegen bevacizumab. De toename van hypoxie kon echter niet worden waargenomen in de pimonidazol en FMISO opname. Een mogelijke verklaring hiervoor is dat de distributie van FDG beperkt is door de effecten van bevacizumab op de vasculatuur.

Hoofdstuk 8 rapporteert over het nut van verschillende beeldvormende technieken om de effectiviteit van bevacizumab na progressie (BBP) te meten. Aanleiding is dat klinische studies een overlevingsvoordeel hebben laten zien van patiënten die na progressie op eerste lijn therapie met bevacizumab, continueerden met bevacizumab behandeling.

Om in te schatten welke beeldvormende techniek gevoelig is voor effecten van bevacizumab na progressie, werden naakte muizen met subcutane tumoren (LS174T) behandeld met bevacizumab en een suboptimale dosis capecitabine en oxaliplatin. Met een schuifmaat werd de tumorgroei in drie richtingen gemeten om het tumor volume te bepalen. Als bij twee achtereenvolgende metingen anderhalf keer het uitgangsvolume wordt gemeten, dan wordt de tumor als progressief beschouwd. De helft van de muizen continueerden met bevacizumab terwijl de andere helft injecties met fysiologisch zout kreeg. Binnen drie dagen nadat progressie werd vastgesteld werden de muizen voor de eerste keer gescand met FDG PET, DWI, T2* en DCE-MRI. Metingen werden 7 en 10 dagen na de eerste scans herhaald.

CAIX, GLUT1, 9F1 (vaten) en Ki67 (proliferatie) werden gekleurd op het tumormateriaal verzameld na de laatste scan. In de BBP groep was er significante reductie van de tumorgroei ($p<0.01$). FDG PET liet een trend zien voor lagere opname in de BBP groep ($p=0.08$). De overige scans lieten geen significante verschillen zien tussen beide groepen.

Immunohistochemische analyse liet een hogere CAIX-positieve fractie ($p<0.01$) en een lagere Ki67 expressie ($p=0.06$) zien in de BBP groep. Het relatieve vaatoppervlakte was significant

lager in de BBP groep (p=0.03). GLUT1 expressie en de vaatdichtheid waren niet significant verschillend.
De belangrijkste conclusie is dat bevacizumab na progressie een significant effect heeft op de proliferatie van de tumor en de micro-omgeving, vergeleken met het staken van de therapie. FDG PET is mogelijk gevoelig voor de effecten van bevacizumab na progressie.
In **hoofdstuk 9** worden de resultaten besproken van een klinische studie waarbij in patiënten met naar de lever gemetastaseerd colorectaal carcinoom die starten met systemische behandeling, gekeken is naar de voorspellende FDG PET, DWI en T2* MRI voor de uitkomst van de therapie en de ziekte.
39 patiënten werden geïncludeerd voor studiedeelname. FDG PET, DWI en T2* MRI werden voor start en een week na start van de eerste lijn behandeling met chemotherapie uitgevoerd. Een FDG PET-CT werd na 3 kuren chemotherapie herhaald.
De FDG PET werd 60-minuten na injectie van FDG op een PET/CT scanner uitgevoerd. De DWI en T2* MRI werden uitgevoerd op een 1.5T MRI scanner. Per patiënt werden maximaal 5 levermetastasen geanalyseerd. De gestandaardiseerde FDG opname waarden (SUV), totale lesie glycolyse (TLG), gemiddelde T2* tijden en ADC waarden per patiënt weden geanalyseerd. De predictieve waarde voor de progressie vrije overleving en algehele overleving werd onderzocht.
De belangrijkste uitkomsten waren dat een lagere ADC waarde bij de uitgangsscan geassocieerd was met een slechtere progressie vrije overleving en algehele overleving. Een hogere T2*, SUVmax en TLG bij de uitgangsscan waren geassocieerd met een slechtere overleving. Een week na start van de behandeling was er een significante daling in de SUV en een significante stijging in de SUV. De daling in SUV was gecorreleerd met een stijging in de ADC. Echter ondanks de gevoeligheid voor de therapie-effecten, was noch de verandering in de SUV, noch de verandering in de ADC voorspellend voor de uitkomst op de lange termijn. T2* liet een week na start van de therapie geen significante verandering zien. Na 3 kuren was het resterende TLG voorspellend voor de progressie vrije en algehele overleving.

11

General discussion and future prospects

Response evaluation

The potential of functional and molecular imaging techniques to predict and monitor response in malignancies has been widely recognized and is subject of intensive research. However, compared to response evaluation based on tumor size, there is little consensus about the optimal settings, timing of response monitoring and cut-off values when using functional and molecular imaging techniques [1]. Despite the limitations of anatomical imaging, there is vast clinical evidence for volumetric response evaluation. Most clinical trials have been performed using volumetric response evaluation (RECIST) and clinicians understand the implications of changes in tumor size for the clinical results of a treatment. Thus, volumetric evaluation is still the golden standard that drives most decisions on continuation or discontinuation of antitumor treatment. Nevertheless, due to the development of therapies that might not directly affect tumor size, like targeted therapies and new local treatments such as local tumor ablation or transarterial (chemo-) embolization, the need for other ways of response evaluation increases [2-4]

Ideally, (imaging) biomarkers should be evaluated and used from the moment a new drug or treatment is pre-clinically evaluated. An effective means to evaluate treatment effect would help to select potentially successful drugs more quickly. Furthermore, an effective biomarker might help to determine the optimal dosing and duration of treatment. Unfortunately, for currently used targeted treatments, in many cases no effective biomarker is available. For example, recently it has been shown that that continuation of the anti-VEGF agent bevacizumab beyond disease progression prolongs survival in advanced colorectal cancer patients [5-7]. Since by definition all patients were progressive on RECIST response evaluation, this implies that volumetric evaluation is inadequate to determine in which patients bevacizumab treatment is successful. As a consequence, all patients may need to continue a therapy that might be effective in only a subset of patients [3, 4].

Functional and molecular imaging may become the next gold standard for response evaluation as it can repetitively assess the tumor characteristics (in contrast to biopsy), reveals intratumoral heterogeneity and is generally applicable in almost all tumor types. However, validation is essential for each functional and molecular imaging technique and each tumor type and location. To achieve this, correlation of imaging results with clinical outcome needs to be established. Furthermore, repeatability of the technique and the correlation with histopathology need to be determined. Repeatability and validation are, among others, dependent on the tumor heterogeneity and location of the tumor in the body.

Liver imaging

Imaging of liver lesions, as is discussed in this thesis, comes with some additional challenges. First of all, the liver moves up to 4 cm during a breathing cycle [8]. For DWI, that monitors the diffusion movement of water this is of particular importance, since the movement

induced by breathing far exceeds the effects of the random water movement. However, as reported in chapter 3, using respiratory triggered DWI, fairly good repeatability in colorectal liver metastases can be achieved. A significant difference in ADC-value and repeatability was observed, when free-breathing ADC was compared to respiratory triggered ADC [9].
Part of the moderate repeatability of PET imaging in liver lesions presented in this thesis, can also be explained by blurring caused by respiratory movement, as well as mismatches between respiratory phase on CT and PET, as discussed in chapter 5. This may be especially true for tumors in the liver dome. Repeatability of static FDG PET imaging, as currently performed without respiratory gating, might not be sufficient to measure small changes, early after start of treatment in an individual patient.
Respiratory gating technology, i.e. only including data acquired on exhalation, has (recently) become available for FDG-PET. Respiratory gating helps to improve the accuracy of measurements. In lung tumors respiratory gating resulted in an increased signal to noise and more accurate delineation of lesion volumes [10, 11]. Additional studies are needed to determine whether respiratory-gated PET indeed will improve repeatability of PET parameters in liver (and lung) lesions.
In order to compare the results of different studies, image acquisition protocols and timing of imaging should be harmonized. For FDG-PET consensus on optimal scanning protocols and reconstruction settings were the first to be published: the EANM procedure guideline [12]. A consensus guideline for the optimal setting for DWI, depending on the tumor localization also appeared in 2009 [13]. For now, widely accepted guidelines for response monitoring are only available for FDG-PET imaging in form of the PERCIST criteria [14], although solid data correlating imaging responses to clinical outcome are still pending for many tumor types. Guidelines and consensus protocols should be regularly updated to incorporate the technical improvements in the functional and molecular imaging modalities.

Functional and molecular imaging not described in this thesis

Other functional and molecular imaging techniques also have shown potential for response prediction in other tumor types, but also remain challenging in liver metastases. PET with 3′-deoxy-3′-[^{18}F] fluorothymidine (FLT) is a molecular imaging tool. FLT is trapped inside the cells after phosphorylation by thymidine kinase-1 (TK1), an enzyme in the salvage pathway of DNA synthesis. It is generally assumed that the trapping of FLT is a representation of thymidine incorporation into DNA and therefore is a marker of cell proliferation. FLT-PET is widely investigated as an early marker for response to anticancer treatment. However, FLT-PET for response monitoring in metastatic colorectal cancer comes with two important challenges. Firstly, due to high background activity in normal liver, approximately only a third of all colorectal liver metastases are detectable using FLT-PET [15]. Since the liver is the most common site for colorectal metastases, this is an important drawback. The second problem is

an interaction between fluoropyrimidines (fluorouracil and capecitabine) and the FLT-uptake pathway. Fluoropyrimidines inhibit the function of thymidylate synthase, an enzyme needed for required for the de novo synthesis of thymidylate. Inhibition of thymidylate synthase, leads to an upregulation of thymidine kinase 1 (TK1) activity and nucleoside transporter expression as a salvage pathway and therefore leads initially to an increased uptake of FLT [16]. This interaction could potentially be employed to determine treatment effect, however, the data are more difficult to interpret as an increase in FLT could be a sign of effective therapy as well as increased proliferation, indicating treatment failure.

^{19}F MR spectroscopy (MRS) is a technique that is totally dependent on the intake of fluoropyrimidines, which are a standard component of the systemic treatment of colorectal cancer. As ^{19}F is not a naturally occurring compound in our body, all ^{19}F signals in the MR spectrum come from the administered fluor-containing drug or its metabolites. Previously it has already been suggested that trapping of fluorouracil is beneficial for treatment outcome [17]. Furthermore, the conversion of fluorouracil to the cytotoxic anabolites and catabolites can be monitored. Catabolites have been associated with toxicity [18]. However, ^{19}F MRS also has some practical limitations. The signal to noise ratio is limited even when measured in a large volume. The (required) large volume and respiratory movement lead to partial volume effects during tumor measurements. Possibly due to these limitations, ^{19}F MRS parameters could not be related to tumor response [19]. The utility of ^{19}F MRS appears limited for response evaluation in the liver at present, but could be assessed again when spectroscopic imaging with small voxels can be achieved in the liver, e.g. by better RF coils, higher fields and motion correction.

Increased choline content is a hallmark in many tumors such as in brain, prostate and breast [20]. Choline content as quantified by ^{1}H MRS is related to tumor aggressiveness [21, 22] and a decrease in the choline signal was observed after successful treatment [23-25]. However, in the liver the situation is different as healthy liver already has a relatively high choline content. In a pilot study we observed a lower choline signal in ^{1}H MR spectra of tumors in the liver and the largest tumors appeared to have the lowest choline signal [manuscript in preparation]. This might be caused by contamination of the voxel signal in small tumors with signal from healthy liver tissue (partial volume effect) or by the fact that the larger tumors often have central necrosis, decreasing the choline signal. Therefore, measuring choline content by ^{1}H MRS to evaluate liver metastasis currently is problematic. However, like with^{19}F MRS, when ^{1}H MR spectroscopic imaging with small voxels can be achieved in liver tissue in the future, new opportunities may arise. This may also require higher magnetic field together with motion correction.

Theranostics

Theranostics is the combination of diagnostics and therapy in patients. The theranostic field develops strategies for visualization of drug delivery, drug release and therapy response monitoring [26]. This will help treatment effectiveness, predict adverse effects and help personalize medicine. Molecular imaging is particularly suitable for theranostics. For example, the expression of receptors or other drug targets can be assessed by a radiolabeled antibody, thereby selecting only the patients with (high) expression of the target. But also, imaging of the distribution of a drug (by radiolabeling of the drug) or combining imaging with radio-immunotherapy are possible [27].

The use of monoclonal antibodies for PET imaging is also called immuno-PET. Isotopes with long half-lives, like ^{89}Zr and ^{124}I, are generally used for immuno-PET. Feasibility of ^{89}Zr-bevacizumab, ^{89}Zr-cetuximab and ^{89}Zr-trastuzumab PET imaging has already been shown in clinical studies [28-30]. Immuno-PET enables direct imaging of the distribution of the drug and therefore could help select patients with high tumor targeting and help determine optimal dosing.

MRI is also suited for theranostics, with the development of nanoparticles such as (targeted) liposomes loaded with contrast agents. Small particles of ironoxide or gadolinium, which decrease longitudinal and transverse relaxation times, can be incorporated in liposomes. Due to increased permeability and retention in tumors, these liposomes could be used for tumor imaging. However, by incorporating a targeting ligand (antibody, peptide or phospholipid), not only (tumor) vascularisation, but also specific receptors can be imaged. When drugs are incorporated in the paramagnetic liposomes, MRI could be used for image guided drug delivery. These techniques are still in the preclinical phase [31].

For almost all currently available therapies more effective ways are warranted to evaluate their efficacy, which may be provided by functional imaging. In this respect the development and implementation of a PET/MRI machine is of interest as it is a combination of optimal anatomical imaging with the most advanced functional and molecular imaging techniques that can be achieved in a single imaging session. This expensive hybrid technique still needs to prove its value in terms of response monitoring. As is also shown in this manuscript combined parameters of functional imaging modalities may be a stronger predictor of response. The results of our studies as presented in this thesis support that data of PET and MRI provide complementary tumor information.

Reference list

[1] Desar IM, van Herpen CM, van Laarhoven HW, Barentsz JO, Oyen WJ, van der Graaf WT. Beyond RECIST: molecular and functional imaging techniques for evaluation of response to targeted therapy. Cancer treatment reviews. 2009;35:309-21.

[2] Eisenhauer EA. Response evaluation: beyond RECIST. Annals of oncology: official journal of the European Society for Medical Oncology / ESMO. 2007;18 Suppl 9:ix29-32.

[3] Chun YS, Vauthey JN, Boonsirikamchai P, Maru DM, Kopetz S, Palavecino M, et al. Association of computed tomography morphologic criteria with pathologic response and survival in patients treated with bevacizumab for colorectal liver metastases. JAMA: the journal of the American Medical Association. 2009;302:2338-44.

[4] Shindoh J, Loyer EM, Kopetz S, Boonsirikamchai P, Maru DM, Chun YS, et al. Optimal morphologic response to preoperative chemotherapy: an alternate outcome end point before resection of hepatic colorectal metastases. J Clin Oncol. 2012;30:4566-72.

[5] Grothey A, Sugrue MM, Purdie DM, Dong W, Sargent D, Hedrick E, et al. Bevacizumab beyond first progression is associated with prolonged overall survival in metastatic colorectal cancer: results from a large observational cohort study (BRiTE). J Clin Oncol. 2008;26:5326-34.

[6] Cohn A, Bekaii-Saab T, Bendell J, Hurwitz H, Kozloff M, Roach N, et al. Clinical outcomes in bevacizumab-treated patients with metastatic colorectal cancer: results from ARIES observational cohort study and confirmation of BRiTE data on bevacizumab beyond progression. J Clin Oncol 2010 ASCO Annual Meeting Proceedings. 2012;Vol 28, No 15_suppl (May 20 Supplement), 2010: 3596.

[7] Arnold D, Andre T, Bennouna J, Sastre J, P.J. O, Greil R, et al. Bevacizumab (BEV) plus chemotherapy (CT) continued beyond first progression in patients with metastatic colorectal cancer (mCRC) previously treated with BEV plus CT: Results of a randomized phase III intergroup study (TML study). J Clin Oncol 30, 2012 (suppl; abstr CRA3503). 2012.

[8] Kirilova A, Lockwood G, Choi P, Bana N, Haider MA, Brock KK, et al. Three-dimensional motion of liver tumors using cine-magnetic resonance imaging. International journal of radiation oncology, biology, physics. 2008;71:1189-95.

[9] Larsen NE, Haack S, Larsen LP, Pedersen EM. Quantitative liver ADC measurements using diffusion-weighted MRI at 3 Tesla: evaluation of reproducibility and perfusion dependence using different techniques for respiratory compensation. Magma. 2013;26:431-42.

[10] Lupi A, Zaroccolo M, Salgarello M, Malfatti V, Zanco P. The effect of 18F-FDG-PET/CT respiratory gating on detected metabolic activity in lung lesions. Annals of nuclear medicine. 2009;23:191-6.

[11] Nehmeh SA, Erdi YE, Ling CC, Rosenzweig KE, Schoder H, Larson SM, et al. Effect of respiratory gating on quantifying PET images of lung cancer. Journal of nuclear medicine: official publication, Society of Nuclear Medicine. 2002;43:876-81.

[12] Boellaard R, O'Doherty MJ, Weber WA, Mottaghy FM, Lonsdale MN, Stroobants SG, et al. FDG PET and PET/CT: EANM procedure guidelines for tumour PET imaging: version 1.0. European journal of nuclear medicine and molecular imaging. 2010;37:181-200.

[13] Boellaard R, O'Doherty MJ, Weber WA, Mottaghy FM, Lonsdale MN, Stroobants SG, et al. FDG PET and PET/CT: EANM procedure guidelines for tumour PET imaging: version 1.0. EurJ NuclMed MolImaging. 2010;37:181-200.

[14] Wahl RL, Jacene H, Kasamon Y, Lodge MA. From RECIST to PERCIST: Evolving Considerations for PET response criteria in solid tumors. J NuclMed. 2009;50 Suppl 1:122S-50S.

[15] Francis DL, Visvikis D, Costa DC, Arulampalam TH, Townsend C, Luthra SK, et al. Potential impact of [18F]3'-deoxy-3'-fluorothymidine versus [18F]fluoro-2-deoxy-D-glucose in positron emission tomography for colorectal cancer. European journal of nuclear medicine and molecular imaging. 2003;30:988-94.

[16] Lee SJ, Kim SY, Chung JH, Oh SJ, Ryu JS, Hong YS, et al. Induction of thymidine kinase 1 after 5-fluorouracil as a mechanism for 3'-deoxy-3'-[18F]fluorothymidine flare. Biochemical pharmacology. 2010;80:1528-36.

[17] Zhang RW, Soong SJ, Liu TP, Barnes S, Diasio SB. Pharmacokinetics and tissue distribution of 2-fluoro-beta-alanine in rats. Potential relevance to toxicity pattern of 5-fluorouracil. Drug metabolism and disposition: the biological fate of chemicals. 1992;20:113-9.

[18] Presant CA, Wolf W, Waluch V, Wiseman C, Kennedy P, Blayney D, et al. Association of intratumoral pharmacokinetics of fluorouracil with clinical response. Lancet. 1994;343:1184-7.

[19] van Laarhoven HW, Klomp DW, Rijpkema M, Kamm YL, Wagener DJ, Barentsz JO, et al. Prediction of chemotherapeutic response of colorectal liver metastases with dynamic gadolinium-DTPA-enhanced MRI and localized 19F MRS pharmacokinetic studies of 5-fluorouracil. NMR in biomedicine. 2007;20:128-40.
[20] Glunde K, Bhujwalla ZM, Ronen SM. Choline metabolism in malignant transformation. Nature reviews Cancer. 2011;11:835-48.
[21] Steffen-Smith EA, Shih JH, Hipp SJ, Bent R, Warren KE. Proton magnetic resonance spectroscopy predicts survival in children with diffuse intrinsic pontine glioma. J Neurooncol. 2011;105:365-73.
[22] Zakian KL, Shukla-Dave A, Ackerstaff E, Hricak H, Koutcher JA. 1H magnetic resonance spectroscopy of prostate cancer: biomarkers for tumor characterization. Cancer Biomark. 2008;4:263-76.
[23] Mueller-Lisse UG, Swanson MG, Vigneron DB, Hricak H, Bessette A, Males RG, et al. Time-dependent effects of hormone-deprivation therapy on prostate metabolism as detected by combined magnetic resonance imaging and 3D magnetic resonance spectroscopic imaging. Magn Reson Med. 2001;46:49-57.
[24] Alexander A, Murtha A, Abdulkarim B, Mehta V, Wheatley M, Murray B, et al. Prognostic significance of serial magnetic resonance spectroscopies over the course of radiation therapy for patients with malignant glioma. Clin Invest Med. 2006;29:301-11.
[25] Bathen TF, Heldahl MG, Sitter B, Vettukattil R, Bofin A, Lundgren S, et al. In vivo MRS of locally advanced breast cancer: characteristics related to negative or positive choline detection and early monitoring of treatment response. Magma. 2011;24:347-57.
[26] Terreno E, Uggeri F, Aime S. Image guided therapy: the advent of theranostic agents. Journal of controlled release: official journal of the Controlled Release Society. 2012;161:328-37.
[27] Lee DY, Li KC. Molecular theranostics: a primer for the imaging professional. AJR American journal of roentgenology. 2011;197:318-24.
[28] Wright BD, Lapi SE. Designing the magic bullet? The advancement of immuno-PET into clinical use. Journal of nuclear medicine: official publication, Society of Nuclear Medicine. 2013;54:1171-4.
[29] Zhang Y, Hong H, Cai W. PET tracers based on Zirconium-89. Current radiopharmaceuticals. 2011;4:131-9.
[30] Gaykema SB, Brouwers AH, Lub-de Hooge MN, Pleijhuis RG, Timmer-Bosscha H, Pot L, et al. 89Zr-bevacizumab PET imaging in primary breast cancer. Journal of nuclear medicine: official publication, Society of Nuclear Medicine. 2013;54:1014-8.
[31] Langereis S, Geelen T, Grull H, Strijkers GJ, Nicolay K. Paramagnetic liposomes for molecular MRI and MRI-guided drug delivery. NMR in biomedicine. 2013;26:728-44.

List of publications

About the author

Dankwoord

List of publications

L. Heijmen, J. Vehof, and H. W. van Laarhoven. Case report: Blistering of the Hand in a Breast Cancer Patient. Extravasation. Neth J Med 69, no. 2 (Feb 2011): 82, 85.

E.G. ter Voert, **L. Heijmen**, H.W.M. van Laarhoven, and A. Heerschap. In Vivo Magnetic Resonance Spectroscopy of Liver Tumors and Metastases. World J Gastroenterol 17, no. 47 (Dec 21 2011): 5133-49

L. Heijmen, H.W.M. van Laarhoven, C.J.A. Punt, D. van den Hurk, M.A. van der Drift, P.B. Ottevanger, and J.N. Timmer-Bonte. Encouraging Results in Older Patients Receiving Chemotherapy: A Retrospective Analysis of Treatment Guideline Adherence in Daily Practice. Geriatr Gerontol Int 12, no. 1 (Jan 2012): 80-5.

L. Heijmen, M.C.H.M. Verstappen, E.G.W. ter Voert, C.J.A. Punt, W.J.G. Oyen, L.F. de Geus-Oei, J.J. Hermans, Arend Heerschap, H.W.M. van Laarhoven, Tumor response prediction by diffusion -weighted MR imaging: ready for clinical use? Critical Reviews in Oncology/ Hematology 83, no. 2 (Aug 2012): 194-207.

L. Heijmen, J.J. Futterer, and H.W.M. van Laarhoven. Case report: Intra-Thoracic Mass on Ct in a Breast Cancer Patient. Neth J Med 70, no. 6 (Aug 2012): 283, 86.

L. Heijmen, L.F. de Geus-Oei, J.H.W. de Wilt, D. Visvikis, M. Hatt, E.P. Visser, J. Bussink, C.J.A. Punt, W.J.G. Oyen, H.W.M. van Laarhoven, Repeatability of functional volume and activity concentration in 18F-FDG PET/CT of liver metastases in colorectal cancer, European Journal of Nuclear Medicine and Molecular Imaging 39, no. 12 (Dec 2012): 1858-67.

L. Heijmen, E.J. van Dijk, B. Goraj, and H.W.M. van Laarhoven. Case report: Moyamoya Disease Misdiagnosed as Leptomeningeal Metastases. J Clin Oncol 30, no. 36 (Dec 20 2012): e382-5.

L. Heijmen, E.G.W. ter Voert, I. D. Nagtegaal MD, P.N. Span, J. Bussink, C.J.A. Punt, J.H.W. de Wilt, F.C.G.J. Sweep, A. Heerschap, H.W.M. van Laarhoven, Diffusion weighted imaging in liver metastases of colorectal cancer: repeatability and biological validation, European Radiology 23, no. 3 (Mar 2013): 748-56.

L. Heijmen, C.J.A. Punt, E.G.W. ter Voert, L.F. de Geus-Oei, A. Heerschap, J. Bussink, C.G.J. Sweep, V. Zerbi, W.J.G. Oyen, P.N. Span, O. Boerman, H.W.M. van Laarhoven, Monitoring the effects of bevacizumab beyond progression in murine colorectal cancer: a functional imaging approach, Investigational New Drug 31, no. 4 (Aug 2013): 881-90.

H. Prinsen, G. Bleijenberg, **L. Heijmen**, M.J. Zwarts, J.W. Leer, A. Heerschap, M.T. Hopman, and H.W.M. van Laarhoven. The Role of Physical Activity and Physical Fitness in Postcancer Fatigue: A Randomized Controlled Trial. Support Care Cancer 21, no. 8 (Aug 2013): 2279-88.

E.G.W. ter Voert, **L. Heijmen**, J.H.W. de Wilt, J. Bussink, C.J.A. Punt, H.W.M. van Laarhoven, A. Heerschap, Repeatability and biological basis of in vivo T2* magnetic resonance imaging of liver metastasis of colorectal cancer, Magnetic Resonance in Medicine 70, no. 4 (Oct 2013): 1145-52.

N. Grebenchtchikov., A.J. Geurts-Moespot, **L. Heijmen**, H. W. van Laarhoven, C.M. van Herpen, A.M. Thijs, P.N. Span, and F.C. Sweep. "Quantification of Patient Specific Assay Interference in Different Formats of Enzyme Linked Immunoassays for Therapeutic Monoclonal Antibodies. Ther Drug Monit (May 9 2014).

L. Heijmen, E.G.W. ter Voert, C.J.A. Punt, A. Heerschap, W.J.G. Oyen, J. Bussink, C.G.J Sweep, P. Laverman, P.N. Span, L.F. de Geus-Oei, O.C. Boerman, H.W.M. van Laarhoven, Monitoring hypoxia and vasculature during bevacizumab treatment in a murine colorectal cancer model, Contrast Media and Molecular Imaging 9, no. 3 (May-Jun 2014): 237-45.

L. Heijmen, E.G.W. ter Voert, W. Oyen, C.J.A. Punt, D.J. van Spronsen, A. Heerschap, L.F de Geus- Oei, H.W.M. van Laarhoven, Multimodality imaging to predict response to systemic treatment in patients with advanced colorectal cancer, submitted

L. Heijmen, E.A. Usmanij, C. Brouwer, B.F. Bulten, M.J.R. Janssen, Case report: 131-iodine uptake in metastatic gallbladder cancer, tijdschrift voor nucleaire geneeskunde, accepted.

About the author

Linda Heijmen was born in Zevenaar on April 11, 1985. In 2003 she graduated from the Liemers college (gymnasium) in Zevenaar. The same year she started her study Medicine at the Radboud University Nijmegen. After the last medical internship at the Medical Oncology department, she started her research internship at the department Medical Oncology were she assessed the effect of age on the administered chemotherapy schedule. In April 2010 she received her medical degree at the Radboud University and started working on her PhD project, which resulted in this thesis. During her research, her work brought her in contact with several departments and there she discovered a preference for the field of nuclear medicine.
Currently she is specializing to become a nuclear medicine physician at the department of Radiology and Nuclear Medicine at the Radboud University medical center.

Dankwoord

Geen proefschrift komt tot stand zonder de medewerking, handreikingen en ondersteuning van mensen. Mensen die je helpen met kennis, een kritische blik en een luisterend oor. Ook voor dit boekje geldt dat het zonder de intensieve betrokkenheid van anderen niet voor u zou liggen. Bij deze zou ik er graag enkelen bedanken.

Mijn grootste dank gaat uit naar mijn meest directe begeleiders, mijn co-promotoren, Hanneke en Lioe-Fee, ondertussen professor dr. H.W.M. van Laarhoven en professor dr. L.F. de Geus- Oei. Bedankt voor alle suggesties, opmerkingen, aanmerkingen en denkrichtingen. Of het nu het becommentariëren van een eerste concept of een scherpe, kritische revisie van de zesde versie van een manuscript betrof, ik werd altijd geholpen en voelde me gehoord. Jullie hebben inmiddels beiden de titel van professor verdiend en ik kan vanuit mijn ervaringen geen collega's bedenken die deze eer meer toe zou komen. Ik weet zeker dat ook toekomstige promovendi zeer blij mogen zijn met jullie als promotor.
Hanneke, ook alle dank dat je me de kans hebt gegeven om kennis te maken met onderzoek. In eerste instantie met mijn onderzoekstage en later dankzij jou ook de kans om dit promotieonderzoek te mogen doen.
Lioe-Fee, je hebt me heel enthousiast weten te maken over nucleaire geneeskunde en de kans gegeven om nu hier in te specialiseren. Heel fijn dat ik de komende jaren ook nog van je mag leren als AIOS!
Beste Kees, prof. Dr. C.J.A. Punt, de grote lijn blijven doorzien en andere helpen die lijn vast te houden is denk ik een van je beste kwaliteiten als promotor. Het is heel fijn geweest dat iemand vanuit een andere invalshoek naar de artikelen en naar het boekje als geheel kon kijken. Dat is het eindresultaat wat mij betreft zeer ten goede gekomen.
Beste Arend, prof. A. Heerschap, bedankt voor je geduld bij het toelichten en verhelderen van de technische kant van dit onderzoek. Je bent als geen ander in staat om je inhoudelijke kennis over MRI over te dragen aan medici zoals ik.
Beste Wim, prof. Dr. W.J.G. Oyen, zoals de voorgaand genoemde mensen heb je een belangrijke rol gespeeld in het onderzoek. Vooral je kennis over waar, op welke manier en wanneer de inhoud van artikelen het beste tot zijn recht komt was zeer waardevol. Het maakt de artikelen scherper en doelgericht en is daarmee onmiskenbaar één van de zaken geweest waardoor ik met trots dit boekje kan presenteren.

Beste Edwin, fijn om jou als medestander te hebben in dit onderzoek! Ik heb bewondering voor je geduld om alle problemen tot op de bodem uit te zoeken en oplossingen te blijven zoeken. De data van de DCE-MRI en de uitdagingen van de fluor-spoel maakte je onderzoek niet altijd makkelijk. Ik ben blij dat jij voor onze gezamenlijke studies veel technische

uitdagingen al had opgelost. Ik hoop dat je binnenkort ook je proefschrift mag verdedigen, maar ondertussen veel plezier met de PET-MRI uitdagingen in Zurich.
Mijn verschillende kamergenootjes, zowel bij de oncologie als later bij de nucleaire geneeskunde, dank voor de gezelligheid en een luisterend oor bij voor sommige herkenbare frustraties aan onderzoek doen. Voor alle collega's van de afdeling nucleaire geneeskunde: dankzij jullie is er een gezelligheid en sfeer op deze afdeling die ik nog nergens anders ben tegen gekomen! Ik ben blij dat ik hier voorlopig mag blijven werken.
Mijn dank aan de PET-laboranten, in het bijzonder Peter en Jurrian, voor alle hulp bij het plannen van de PET-scans. Het was soms erg lastig om met de vaak beperkte tijd alle scans te plannen en ook nog te combineren met de MRI! Zonder jullie medewerking waren er veel minder patiënten gescand.
Aan de (oud-)onderzoekers bij de radiotherapie en radiologie, waar ik ook af en toe mocht verblijven voor stukjes van mijn onderzoek, heel fijn dat jullie me wegwijs hebben willen maken op de afdelingen en me altijd welkom hebben laten voelen.
Beste Bianca, Kitty en Iris, het proefdieronderzoek liep niet altijd helemaal zoals gepland en het was soms zwaarder dan verwacht. Dankzij jullie kundigheid en inzet is het toch gelukt de experimenten tot een goed einde te brengen. Fijn dat jullie altijd wilden meedenken om de belasting van de dieren te verminderen en daarmee ook het slagen van het onderzoek zeker te stellen.

Tot slot wil ik graag de mensen uit mijn persoonlijke omgeving niet vergeten. Zij zijn degenen die me in staat hebben gesteld om de benodigde tijd en energie in dit onderzoek te steken. Van mijn ouders die mijn studie hebben moeten financieren en altijd belangstelling hadden in mijn onderzoek, tot mijn zus die mijn koppigheid (haar hele leven) heeft moeten tolereren, tot mijn vriendinnen die me hebben weten te inspireren, tot mijn vriend die me met emotionele (en gastronomische) ondersteuning altijd heeft bijgestaan.